



UNIVERSITY OF KWAZULU-NATAL

**SYNTHESIS, CHARACTERIZATION AND APPLICATION OF NOVEL
COMPOSITE NANO-MATERIALS FOR THE ELECTROCHEMICAL DETECTION
OF MRSA AND RELATED DRUGS**

2020

BY: ATAL ANUDEEP SINGH GILL

(STUDENT No: 216076933)

Submitted in fulfillment of the requirements for the degree of
Doctor of Philosophy in Pharmaceutical Chemistry
Discipline of Pharmaceutical Science, College of Health Science,
University of KwaZulu-Natal, Durban, South Africa.

PREFACE

The experimental work described in this thesis was conducted at the Medicinal Chemistry laboratory at the School of Pharmaceutical Sciences, University of KwaZulu-Natal, Westville, South Africa, from August 2017 to December 2019, under the supervision of Prof. Rajshekhar Karpoomath.

This thesis has been prepared according to Format 4 (Thesis by publications) as outlined in the guidelines of College of Health Sciences, University of KwaZulu-Natal. The chapters consist of a general introduction, chapters in discrete research papers and a final discussion. Two chapters have been published and the remaining chapter has been submitted in peer-reviewed internationally accepted journal.

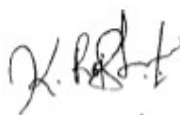
This work has not been submitted in any form for any degree or diploma to any tertiary institution, where use has been made of the work of others, it is duly acknowledged in the text.



Atal Anudeep Singh Gill

Date: 08 / 07 / 2020

As the candidate's supervisor I agree to the submission of the thesis:



Prof. Rajshekhar Karpoomath

Date: 9th July 2020

As the candidate's co-supervisor I agree to the submission of the thesis:



Dr. Neeta B Thapliyal

Date: 08.07.2020

© Copyright by Atal Anudeep Singh Gill 2020

All Rights Reserved.

DECLARATION 1 – PLAGIARISM

I, **Atal Anudeep Singh Gill**, declare that

- i. The research reported in this thesis, except where otherwise indicated, is my original work.
- ii. This thesis has not been submitted for any degree or examination at any other university.
- iii. This thesis does not contain other person's data, pictures, graphs or other information, unless specifically acknowledged as being sourced from other persons.
- iv. This thesis does not contain other persons' writing, unless specifically acknowledged as being sourced from other researchers. Where other written sources have been quoted, then:
 - a. Their words have been re-written but the general information attributed to them has been referenced
 - b. Where their exact words have been used, then their writing has been placed in italics and inside quotation marks, and referenced.
- v. Where I have reproduced a publication of which I am an author, co-author or editor, I have indicated in detail which part of the publication was actually written by
- vi. This thesis does not contain text, graphics or tables copied and pasted from the internet, unless specifically acknowledged, and the source being detailed in the thesis and in the References sections.



Signed

Date: 08/ 07 / 2020

DECLARATION 2 – PUBLICATION

DETAILS OF CONTRIBUTION TO PUBLICATIONS that form part and/or include research presented in this thesis (include publications in preparation, submitted, in press and published and give details of the contributions of each author to the experimental work and writing of each publication)

Publications

Gill, Atal AS, Sima Singh, Neeta Thapliyal, and Rajshekhar Karpoomath. "Nanomaterial-based optical and electrochemical techniques for detection of methicillin-resistant *Staphylococcus aureus*: a review." *Microchimica Acta* 186, no. 2 (2019): 114. (IF: 6.232)
Contributions: I did the literature review and original draft and further was assisted in compiling the manuscript under the supervision of Dr. Sima Singh and Prof. Rajshekhar Karpoomath. Rest all the co-authors assisted me in improvisation, writing up and proof reading.

Atal A.S. Gill, Sima Singh, Nikhil Agrawal, Zondi Nate, Tirivashe E. Chiwunze, Neeta Bachheti Thapliyal, Ruchika Chauhan, Rajshekhar Karpoomath. "A poly(acrylic acid)-modified copper-organic framework for electrochemical determination of vancomycin." *Microchimica Acta*. 2020 Jan 2; 187(1):79.

Contributions: I did the experimental part and made the original draft. The computational studies were carried out by Dr. Nikhil Agrawal. Rest all the co-authors assisted me in improvisation, writing up and proof reading. The manuscript was prepared under the supervision of Prof. Rajshekhar Karpoomath.

Atal Anudeep Gill, sima singh, Zondi Nate, Ruchika Chauhan, Nissar Sayyad, Neeta Thapliyal, Rajshekhar Karpoomath, Rajkumar Patel. One pot synthesis of β -cyclodextrin modified silver nanoparticles for highly sensitive detection of ciprofloxacin. *Mircochimica acta*. (Under review)

Contributions: Majority of the work was carried out by me. Rest all the co-authors assisted me in improvisation, writing up and proof reading. The manuscript was prepared under the supervision of Prof. Rajshekhar Karpoomath.

Ruchika Chauhan, **Atal Gill**, Zondi Nate, Rajshekhar Karpoormath. Highly selective electrochemical detection of ciprofloxacin using reduced graphene oxide/poly(phenol red) modified glassy carbon electrode. Journal of Electroanalytical Chemistry. Available online 19 May 2020, 114254 (IF: 3.807)

Contributions: The idea and rational of the study was designed by me. The material synthesis and characterization was also carried out by me. Finally, the corrections and the proof reading of the manuscript was carried by me. The manuscript was prepared under the supervision of Prof. Rajshekhar Karpoormath.

Atal A.S. Gill, Sima Singh, Zondi Nate, Ruchika Chauhan, Neeta B. Thapliyal, Rajshekhar karpoormath. A novel copper-based 3D porous nanocomposite for electrochemical detection and inactivation of pathogenic bacteria. Sensors and Actuators B: Chemical Available online 13 June 2020, 128449. (IF 7.1)

Contributions: Synthesis, characterization and detection was carried out by me. The bacterial inactivation studies were carried out by Dr. Sima Singh. The manuscript was prepared under the supervision of Prof. Rajshekhar Karpoormath.

DEDICATION

I dedicate this thesis to my parents, my
mom (Anoop Kaur)
and
dad (Amardjeep Singh Gill).

ACKNOWLEDGEMENTS

First of all, I want to thank God for his grace that has brought me this far. I want to thank my parents Mrs. Anoop Kaur and Mr. Amardeep Singh Gill for their support, encouragement and the belief they had in me. I would not be here if it wasn't for them. I would also like to thank my grandparents for supporting me and for keep pushing me to do better.

I also wish to express my sincere gratitude to my supervisors Dr Rajshekhar Karpoomath and Dr. Neeta B. Thapliyal for giving me the opportunity of carry out my Ph.D research under their guidance. I sincerely thank Dr Sima Singh for mentoring me through my whole Ph.D and always encouraging me to keep on going and guiding me on writing up my manuscripts, you are always a voice of encouragement.

I also would like to thank:

My fellow colleagues, Zondi Nate, Tirivashe E. Chiwunze, Francis Kayamba, Cleopus Mavela, Dr. Ruchika and the rest of SMCRG for being my family in Africa and for providing me the right advice.

My friends Jagriti Sethi, Himanshu Kapoor, Sonali Verma and Nikhil Agrawal for being there for me during the times I was under pressure and needed someone to talk and for always being available when I needed someone by my side.

Funding

Acknowledgment

The authors would like to thank the College of Health Sciences, University of Kwazulu-Natal (UKZN), Nanotechnology platform-UKZN and the National Research Foundation of South Africa (NRF-SA) for funding (Grant No.103728 and 112079)

Table of contents

PREFACE	iii
DECLARATION 1 – PLAGIARISM.....	iiv
DECLARATION 2 – PUBLICATION	v
DEDICATION	vii
ACKNOWLEDGEMENTS	viii
TABLE OF CONTENTS.....	ix
LIST OF FIGURES	ixiv
LIST OF TABLES.....	xix
LIST OF ABBREVIATIONS	xxi
ABSTRACT	xxvi
CHAPTER 1.....	xxviii
1.1 Introduction.....	xxviii
1.2 Backgroud.....	xxviii
1.3 <i>Staphylococcus aureus</i> (<i>S. aureus</i>) and methicillin-resistant <i>S. aureus</i> (MRSA).....	xxix
1.4 Mechanism of development of methicillin-resistance	xxx
1.5 Approved antibiotic therapy for MRSA.....	xxx
1.6 Relevance and importance of this study	xxxi
1.7 Aim and Research Objectives	xxxii
1.8 Thesis Outline.....	xxxiii
CHAPTER 2.....	xxxix
Introduction.....	xlii
Key problems of resistance in hospitals and communities	xliii
Biomarkers for MRSA.....	xliv
Conventional detection techniques for MRSA	xlvi

Traditional cell culturing.....	xlvi
Automated culturing	xlvi
Enzyme-linked immunoassay (ELISA)	xlix
Polymerase chain reaction (PCR) based techniques	l
Nanomaterials and their role	li
Electrochemical sensors.....	lii
Cyclic voltammetry (CV)	liii
Square wave voltammetry (SWV)	liv
Electrical impedance spectroscopy (EIS)	lv
Differential pulse voltammetry (DPV).....	lvi
Luminescence-based sensors.....	lvii
Fluorescence.....	lvii
Luminescence resonance energy transfer (LRET).....	lx
Surface-enhanced Raman spectroscopy (SERS).....	lxiii
Colorimetric sensing.....	lxiv
Surface plasmon resonance (SPR) based on colorimetric sensing.....	lxvi
Polymerase chain reaction (PCR) based sensing.....	lxvii
Other techniques.....	lxviii
Conclusions and outlook.....	lxxii
 CHAPTER 3	 xciv
1. Introduction.....	xcvii
2. Method	xcix
2.1 Chemicals, reagents and instrumentation.....	xcix
2.2 Synthesis of HKUST-1 and P-HKUST-1	xcix
2.3 Preparation of complexes with vancomycin	c
2.4 Preparation of electrode	c

2.5	Preparation of urine and serum samples	ci
3.	Results and discussion	ci
3.1	Choice of material	ci
3.2	Detection mechanism	cii
3.3	Electrochemical response of MOFs	ciii
3.4	Performance of diagnostic assay	civ
3.5	Selectivity studies	cvii
3.6	Real Sample analysis	cix
4.	Conclusions and Perspectives	cxii
CHAPTER 4		cxvii
1.	Introduction	cxix
2.	Method	cxx
2.1.	Chemicals, reagents and instrumentation	cxx
2.2.	Synthesis of β -cyclodextrin modified silver nanoparticle composite	cxxi
2.3.	Preparation of electrode	cxxi
2.4.	Preparation of serum sample and waste water sample	cxxii
3.	Results and discussion	cxxii
3.1	Choice of material	cxxii
3.2	Characterization of β -cyclodextrin modified silver nanoparticle composite	cxxiii
3.3	Electrochemical characterization	cxxix
3.4	Electrochemical detection of ciprofloxacin	cxix
3.5	Analytical performance	cxixii
4.	Conclusion	cxixvi
CHAPTER 5		cxli
1.	Introduction	cxliv
2.	Materials and method	cxlvi
2.1	Chemicals, reagents, and instrumentation	cxlvi

2.2	Synthesis of β -cyclodextrin modified copper nanoparticle composite.....	cxlvii
2.3	Synthesis of Cu- β -CD-GO nanocomposite.....	cxlvii
2.4	Preparation of electrode	cxlvii
2.5	In vitro antibacterial activity.....	cxlviii
3.	Results and discussion	cxlix
3.1.	Electrochemical characterization	cxlix
3.2.	Morphological characterization	cli
3.3.	Spectral characterization	cliii
3.4.	Electrochemical properties of composites	clvii
3.5.	Electrochemical response and optimization of conditions.....	clix
3.6.	Analytical performance for bacterial detection.....	clx
3.7.	In vitro antibacterial activity	clxii
4.	Conclusion	clxiii
CHAPTER 6.....		clxx
1.	Introduction.....	clxxiii
2.	Experimental	clxxiv
2.1	Materials	clxxiv
2.2	Apparatus	clxxv
2.3	Preparation of PPR.....	clxxv
2.4	Preparation of rGO/PPR/GCE	clxxvi
2.5	Preparation of blood sample.....	clxxvi
3.	Results and discussion	clxxvii
3.1	FT-IR spectroscopic studies.....	clxxvii
3.2	FE-SEM Analysis	clxxviii
3.3	Electrochemical characterization of modified electrodes	clxxix
3.4	Electrochemical Detection of Cfx.....	clxxxi
3.4.1	Effect of scan rate	clxxx
3.4.2	Effect of solution pH.....	clxxxiii

3.4.3 Electrochemical determination of ciprofloxacin	clxxxiii
3.5 Interference study.....	clxxxvi
3.6 Reproducibility and Stability.....	clxxxviii
3.7 Real sample analysis.....	clxxxviii
4. Conclusion.....	clxxxix
 CHAPTER 7	 cxcv
1. Summary and Conclusion.....	cxcv
2. Future works.....	cxcviii
APPENDEX I (Chapter 3- Supplementary information).....	cc

LIST OF FIGURES

Chapter 1:

Fig. 1 Mechanism of development of resistance by microbes to antimicrobials drugs..... xxix

Fig. 2 Factors linked to transmission of MRSA in hospitals and health-care workxxx

Chapter 2:

Fig. 1 Schematic presentation of transmission of MRSA in community and hospitals.....xliv

Fig. 2 Schematic illustrates the structure of SCCmec. SCCmec is composed of two essential gene complexes. One is *mec*-gene complex, encoding methicillin resistance (*mecA* gene) and its regulators (*mecI* and *mecRI*), and the other is *ccr*-gene complex that encodes the movement, of the entire SCC element. Abbreviations: IR, inverted repeat; DR, direct repeat xlvi

Fig. 3 Schematic of the fabrication of the electrochemical biosensor.....lvi

Fig. 4 Schematic presentation of fluorescence resonance energy transfer process between the dye and GO..... lxiii

Fig 5. Schematic presentation of enhancements in the signals due to the bacterial and nanocomposite interactions for detection.....lxiv

Fig 6. Schematic presentation of ClearRead procedure.....lxxii

Chapter 3:

Fig. 1 (a) CV of P-HKUST-1 at different pH [4.0 (a), 7.0(b), 8.5(b)]. R1, R2 are the reduction peaks and O1, O2 are the oxidation peaks of copper ion core of P-HKUST-1. **(b)** CV in 0.1 M phosphate buffers at pH 4 of GCE (a), HKUST-1 (b) and P-HKUST-1 (c) **(c)** CV in 0.1 M phosphate buffers at pH 7 of GCE (a), HKUST-1 (b) and P-HKUST-1 (c) **(d)** CV in 0.1 M phosphate buffers at pH 8.5 of GCE (a), HKUST-1 (b) and P-HKUST-1 (c)..... civ

Fig. 2 (a) Cyclic voltammograms in 2.5 mM $[\text{Fe}(\text{CN})_6]^{3-/4-}$ in 1 M KCl at different modified electrodes (i.e. (a) HKUST-1/GCE, (b) Van-HKUST-1/GCE, (c) P-HKUST-1/GCE, (d) Van-P-HKUST-1/GCE) **(b)** pH plot for P-HKUST-1/GCE in 2.5 mM $[\text{Fe}(\text{CN})_6]^{3-/4-}$ in 1 M KCl and phosphate buffer in (1:1),

with varying pH from 5.5 to 8.5 at a scan rate of 0.1 V.s⁻¹. [Inset- pH vs current (I_p) plot] (c) Control studies carried out for P-HKUST-1/GCE in pH 7 phosphate buffer at a scan rate of 0.1 V.s⁻¹ with three consecutive voltammograms.....cv

Fig. 3 (a) Cyclic voltammograms of 2.5 mM [Fe(CN)₆]^{3-/4-} in 1 M KCl and phosphate buffer (0.1 M) at pH of 7.0 using Van-P-HKUST-1/GCE (scan rate 0.1 V.s⁻¹) with varying concentration of vancomycin from 0 nM to 500 nM, **(b)** calibration plot of [vancomycin] vs I_p. The readings were carried out in triplicates and the standard deviation was calculated and the calibration plot was plotted as the average the three readings.....cvii

Fig. 4 Cyclic voltammograms in 2.5 mM [Fe(CN)₆]^{3-/4-} (1 M KCl, at 0.1 V.s⁻¹) of Van-P-HKUST-1 modified electrode in presence of **(a)** other drugs (ciprofloxacin and gentamicin). **(b)** Metal ions such as (Na, Mg, K), with varying concentrations of vancomycin (0 nM, 1 nM, 100 nM, 250 nM, 500 nM) **(c)** Stability test for P-HKUST-1/GCE over the period of 5 weeks was also carried out.....cix

Fig. 5 (a) CV curves of P-HKUST-1 in 2.5 mM [Fe(CN)₆]^{3-/4-} in 1 M KCl as the redox couple and electrolyte (scan rate of 0.1 V.s⁻¹) at different concentration spikes of vancomycin in human urine sample (0 nM, 1 nM, 100 nM, 250 nM, 500 nM) **(b)** CV curves in animal serum sample (Vancomycin concentration: 0 nM, 1 nM, 100 nM, 250 nM, 500 nM).....cxi

Chapter 4:

Fig. 1. (a) ¹H NMR spectra's of Ibuprofen, β-cyclodextrin and silver nanoparticles modified β-cyclodextrin (Ag-β-CD). (b) NMR showing the peak shifts that occur in the β-cyclodextrin structure at the -OH functional groups.....cxxv

Fig. 2. (a) FTIR spectrum of β-cyclodextrin and Ag-β-CD. (b) FTIR of a) Ag-β-CD (w), b) Ag-β-CD (mw) and c) Ag-β-CD. (c) UV-absorbance curve of Ag-β-CD in water. (d) UV-absorbance curves of a) Ag-β-CD (w), b) Ag-β-CD (mw) and c) Ag-β-CD in water (1 mg.mL⁻¹).....cxxvii

Fig. 3. (a) FE-SEM image of Ag-β-CD. (b) EDX analysis of Ag-β-CD. (c) Elemental mapping of Ag-β-CD composite showing equal distribution of silver nanoparticles on β-cyclodextrin sheets. (d) HR-TEM analysis of Ag-β-CD at 100 nm, with silver nanoparticles. (e) HR-TEM at 2 μm showing the sheets and silver nanoparticles separately. (f) N₂ adsorption and desorption isotherms obtained from BET analysis of Ag-β-CD. (g) XRD of Ag-β-CD with characteristic peaks of silver nanoparticles and β-cyclodextrin.....cxxix

Fig. 4. (a) Scan rate studies of Ag- β -CD /GCE from (0.01 to 0.10 V s⁻¹) carried out in 2.5 mM [Fe(CN)₆]^{3-/4-} in 1 M KCl, Inset- calibration plot for anodic peak current vs root of scan rate. **(b)** EIS spectra in 2.5 mM [Fe(CN)₆]^{3-/4-} in 1 M KCl at GCE, Ag- β -CD/GCE. Inset- Randles equivalent circuit model.....cxxx

Fig. 5. (a) Cyclic voltammograms in 0.1 mM ciprofloxacin in 0.1 M phosphate buffer (pH 7.0) at different modified electrodes (i.e. GCE, Ag- β -CD/GCE) Scan rate = 0.1 V.s⁻¹. (b) Cyclic voltammograms between current density vs potential, showing the high sensitivity of electrode towards electrooxidation of ciprofloxacin. (c) Scan rate studies at Ag- β -CD/GCE in 0.1 mM ciprofloxacin+0.1 M phosphate buffer (pH 7.0) by varying scan rates from 0.01 V.s⁻¹ to 0.1 V.s⁻¹. (d) Calibration plot of scan rate vs current plotted for the scan rate studies in ciprofloxacin. (e) pH studies in 0.1 mM ciprofloxacin in 0.1 M phosphate buffer at Ag- β -CD/GCE with varying pH, at scan rate = 0.1 V.s⁻¹. (f) pH vs current vs potential plot for variations in potentials and peak currents in different pH buffers.....cxxxii

Fig. 6. (a) DPV in 0.1 M phosphate buffer (pH 7.5) at Ag- β -CD/GCE at varying concentration of ciprofloxacin from 0.1 nM [a] to 50 nM [i]. (b) Calibration plot of [ciprofloxacin] vs peak currents. (c) DPV at Ag- β -CD/GCE in 0.1 mM ciprofloxacin in 0.1 M phosphate buffer (pH 7.5), by adding (1 mL of 1 mM) each interfering agent separately and DPVs are recorded. (d) Stability of Ag- β -CD/GCE to 0.1 mM ciprofloxacin in 0.1 M phosphate buffer (pH 7.5) by DPV for four days. (e) DPV curve of Ag- β -CD/GCE in animal serum sample spiked with increasing concentrations of ciprofloxacin from a to e. (f) Calibration plot for [ciprofloxacin] vs peak currents in serum sample. (g) CV curve of run-off water sample spiked with increasing concentrations of ciprofloxacin from a to e. (h) Calibration plot for [ciprofloxacin] vs peak currents in run-off water sample.....cxxxvi

Chapter 5:

Fig. 1 (a) Scan rate studies of Cu- β -CD-GO(ii)/GCE from (0.01 to 0.10 V s⁻¹) carried out in 1 mM [Fe(CN)₆]^{3-/4-} in 1 M KCl, Inset- calibration plot for anodic peak current vs root of scan rate. **(b)** EIS spectra in 1 mM [Fe(CN)₆]^{3-/4-} in 1 M KCl at GCE, Cu- β -CD-GO(i)/GCE, Cu- β -CD-GO(ii)/GCE, Van-Cu- β -CD-GO(ii)/GCE. Inset- Randles equivalent circuit model.....cl

Fig. 2 (a) FE-SEM image of Cu- β -CD (b) Backscatter (FE-SEM) image of Cu- β -CD (c) FE-SEM image of Cu- β -CD-GO(i) (d) FE-SEM image of Cu- β -CD-GO(ii) (e) HR-TEM image of Cu- β -CD showing distinct nanoparticles in β -CD sheets. (f) HR-TEM image of Cu- β -CD-GO(i) showing distinct nanoparticles in clustered β -CD and GO composite (g) HR-TEM image of Cu- β -CD-GO(ii) showing

distinct smaller and distinct nanoparticles in a condense β -CD and GO composite. (h) N_2 adsorption and desorption isotherms obtained from BET analysis of Cu- β -CD and Cu- β -CD-GO(ii).....cliii

Fig 3 (a) FTIR spectrum of Cu- β -CD and Cu- β -CD-GO(ii). (b) FTIR spectrum of Cu- β -CD-GO(ii) and Van-Cu- β -CD-GO(ii). (c) UV-absorbance curve for Cu- β -CD and Cu- β -CD-GO(ii). (d) Tauc plot for Cu- β -CD and Cu- β -CD-GO(ii) which provides the band gap for each composite. (e) XRD analysis for Cu- β -CD and Cu- β -CD-GO(ii), which confirm the presence of both Cu_2O and Cu nanoparticles in the composite.....clvii

Fig. 4 CV of Cu- β -CD and Cu- β -CD-GO(ii) at pH 7.5 phosphate buffer (0.1 M), R1, R2 are the reduction peaks and O1, O2 are the oxidation peaks of copper nanoparticles in the composite. **(b)** CV in 0.1 M phosphate buffers at pH 4.5 of Cu- β -CD and Cu- β -CD-GO(ii). **(c)** CV in 0.1 M phosphate buffers at pH 4.5, 7.5 of Cu- β -CD. **(d)** CV in 0.1 M phosphate buffers at pH 7.5 of Cu- β -CD-GO(ii)..clix

Fig. 5 . (a) DPV in 1 mM $[Fe(CN)_6]^{3-/4-}$ in 0.01 M phosphate buffer saline (pH 7.4) at different modified electrodes to confirm the detection of MRSA. (b) calibration curve for the optimal concentration of vancomycin that can be immobilized over the modified electrode. (c) DPV of electrode for varying incubation time in 1 mM $[Fe(CN)_6]^{3-/4-}$ in 0.01 M phosphate buffer saline (pH 7.4).....clx

Fig. 6 DPV 1 mM $[Fe(CN)_6]^{3-/4-}$ in 0.01 M phosphate buffer saline (pH 7.4) at Van-Cu- β -CD-GO(ii) at varying concentration of MRSA from 10 to 10^7 CFU mL^{-1} . (b) Calibration plot for peak currents vs concentration of MRSA [inset- peak currents vs log[concentration]]. (c) Repeatability checked by recording the current response at different modified electrodes. (d) Specificity carried out using *E.coli*, shows that there is no change in the peak current of the Van-Cu- β -CD-GO(ii)/GCE after incubation with *E.coli*.....clxii

Chapter 6:

Fig. 1 Proposed structure and redox reaction of PPRclxxiv

Fig. 2 Successive cyclic voltammograms during the polymerization of phenol red at surface of GC..clxvi

Fig. 3 ATR-FTIR results of the modified GCE electrodes by PPR and rGO/PP.....clxxviii

Fig. 4 (a, b) Illustrate the FE-SEM of PPR at low and high magnification respectively and (c, d) illustrates rGO/PPR composite at low and high magnification respectively under FE-SEM.....clxxix

Fig. 5 (A) Cyclic voltammograms of (a) GCE, (b) PPR/GCE, (c) rGO/GCE, (d) rGO/PPR/GCE (B) linear plot of the anodic peak current density vs. scan rate. (Inset- Cyclic voltammograms at various

scan rates (0.01 to 0.14 V sec⁻¹). (C) EIS spectra of 0.1 M KCl containing 2.5mM [Fe (CN)₆]^{3-/4-} at modified and bare GCEs. (Inset- Randles equivalent circuit model). (D) linear plot of the peak potential vs. log scan rate (V sec⁻¹).....clxxx

Fig. 6 (a) Cyclic voltammograms at scan rates from A to K (0.01-0.14 V s⁻¹) of rGO/PPR/GCE electrode in 1mM ciprofloxacin (0.1 M PB at pH 5.5).inset (a) linear plot between peak current density and scan rate Vsec⁻¹ inset (b) linear plot between potential vs log scan rate.....clxxxiii

Fig. 7 Plots of peak current I_p vs. pH from differential pulse voltammograms of 1mM solutions of ciprofloxacin at rGO/PPR/GCE electrode in different buffer electrolytes as a function of pH. Scan rate: 100mVsec⁻¹clxxxiii

Fig. 8 Differential pulse voltammograms of ciprofloxacin with the different concentrations of ciprofloxacin in 0.1M PB of pH 5.5. (b) Calibration plot of I_{pa} vs different concentration of ciprofloxacin at pH 5.5 with a scan rate of 100 mV s⁻¹; inset (a) for linear range 1-400 µML⁻¹ (b) for linear range 0.002-0.1 µML⁻¹clxxxv

Fig. 9 (A) DPV at optimum conditions for interference studies of non-target agents in 0.1M PB buffer. (Inset – graph showing linear plots of peak current vs concertation of ciprofloxacin for lower and higher range 0.002-0.1 and 1-400 µML⁻¹ respectively , (B) DPV at optimum conditions for interference studies of other drug in 0.1M PB buffer. (Inset – graph showing linear plots of peak current vs concertation of ciprofloxacin for lower and higher range 0.002-0.1 and 1-400 µML⁻¹ respectively.....clxxxvii

Fig. 10 DPV at optimum conditions for animal serum studies in 0.1M PB buffer. (Inset – graph showing linear plots of peak current vs concertation of ciprofloxacin for lower and higher range 0.002-0.1 and 1-400 µML⁻¹ respectively.....clxxxviii

LIST OF TABLES

Chapter 1:

Table 1. List of antibiotics effective against MRSA.....	xxx
---	-----

Chapter 2:

Table 1. Genetic and protein-based biomarker currently used for MRSA detection.....	xlvi
--	------

Table 2. Number of swabs testing positive for MRSA by anatomical site (detected on chromogenic agar) and percentage positive compared with the gold standard.....	xlvi
--	------

Table 3. Nanomaterials used in various electrochemical techniques for detection of MRSA.....	lii
---	-----

Table 4. Nanomaterials used in various luminescence-based techniques for detection of MRSA.....	lix
--	-----

Table 5. Novel techniques and methods developed for detection of MRSA using nanomaterials.....	lxx
---	-----

Chapter 3

Table 1. Comparison of other techniques with the proposed sensor for vancomycin determination...	cvii
---	------

Chapter 4:

Table 1. Components of Randles equivalent circuit for GCE and Ag- β -CD/GCE.....	cxxx
---	------

Table 2. Comparison of previous modified electrodes for detection of ciprofloxacin.....	cxxxi
--	-------

Chapter 5:

Table 1. Components of Randles equivalent circuit for GCE and Ag- β -CD/GCE.....	cl
---	----

Table 2. Comparison of previous methods for detection of MRSA.....	clxii
---	-------

Table 3. Comparative in vitro antibacterial activity of Cu- β -CD, Cu- β -CD-GO, Van-Cu- β -CD-GO, and powdered Van again MRSA bacteria.....	clxiii
---	--------

Chapter 6:

Table 1: Components of randles equivalent circuit for GCE and all modified electrodes.....	clxxxi
Table 2: Comparison of previous modified electrodes for detection of ciprofloxacin.....	clxxxv
Table 3: Results of analysis of blood samples.....	clxxxix

LIST OF ABBREVIATIONS

ABSSSIs: Acute bacterial skin and skin structure infections

ACME: Arginine catabolic mobile element

AdTS SWV: Adsorptive transfer stripping square wave voltammetry

AgNps: Silver nanoparticles

Ag- β -CD: Beta-cyclodextrin modified with silver nanoparticles

APTES: Aminopropyl triethoxy silane

AuNps: Gold nanoparticles

BSA: Bovine serum albumin

BTC: Benzene tricarboxylic acid

CA-MRSA: Community-associated methicillin-resistant *Staphylococcus aureus*

CdTe QDs: Cadmium telluride quantum dots

CFU: Colony forming unit

CNT's: Carbon nanotubes

Cu- β -CD-GO: Copper, β -cyclodextrin, and graphene oxide based nanocomposite

CV: Cyclic voltammetry

DIS: Dielectric impedance spectroscopy

DNA: Deoxyribonucleic acid

DPV: Differential pulse voltammetry

dsDNA: Double stranded DNA

EIS: Electrical impedance spectroscopy

EIS: Electrical impedance spectroscopy

ELISA: Enzyme-linked immunosorbent assay

FITC: Fluorescein isothiocyanate

FTO: Fluorine-doped tin oxide

GCE: Glassy carbon electrode

GO: Graphene oxide

H₂O₂: Hydrogen peroxide

HA-MRSA: Hospital associated MRSA

HSA: Human serum albumin

HIV: Human immunodeficiency virus

HRP: Horseradish peroxidase

IgG: Immunoglobulin G

ISAM: Ionic self-assembled multilayer

LAMP: Loop-mediated isothermal amplification

LEDs: Light emitting diodes

LFB: Lateral flow biosensor

LFI: Lateral flow immunoassay

LOD: Limit of detection

LPG: Long-period grating

LRET: Luminescence resonance energy transfer

MAB: Monoclonal antibodies

MCDA: Multiple cross displacement amplification

ME: Magneto-elastic

MGEs: Mobile genetic elements

MIC: Minimum inhibitory concentration

MOF: Metal organic framework

MPA: Mercapto acetic acid

MR-CoNS: Methicillin-resistant coagulase-negative staphylococcus

MRSA: Methicillin-resistant *Staphylococcus aureus*

MSP: Multiple signal probes

NIRF: Near-infrared fluorescence

PAA: Poly acrylic acid

PAAPEG-Van: Polyethylene glycol and vancomycin-conjugated poly(acrylic acid)

PBP2A: Penicillin-binding protein 2A

PCBS: Poly-1-[p-(3'-carboxy-4'-hydroxyphenylazo) benzene sulfonamido-1,2-ethandiyl

PCR: Polymerase chain reaction

PPR: Poly(phenol red)

PTT: Photothermal therapy

PVL: Pantan-Valentine leukocidin

RCTs: Randomized controlled trials

rGO: reduced graphene oxide

RNA: Ribonucleic acid

RPA: Recombinase polymerase amplification

RPS: Resistive pulse sensing

rRNA: Ribosomal ribonucleic acid

RT-PCR: Real-time PCR

S. aureus: *Staphylococcus aureus*

SA-DNPs: Streptavidin-coated polymer nanoparticles

SCCmec: Staphylococcal cassette chromosome mec

SE: Staphylococcal enterotoxins

SERS: Surface-enhanced Raman spectroscopy

SiO₂/PAH-cy: Poly (allylamine) coated silica-cypate

SPR: Surface plasmon resonance

ssDNA: Single stranded DNA

SWV: Square wave voltammetry

TLA: Total Laboratory Automation

TSP: Tetrahedral nanostructure-based capture probe

UCNs: Up-conversion nanoparticles

Van: Vancomycin

Van-Cu- β -CD-GO: Vancomycin conjugated Cu- β -CD-GO

VRSA: Vancomycin resistance *S. aureus*

WASP: Walk away specimen processor

WHO: World health organization

ABSTRACT

This thesis reports the development of electroanalytical methods applicable for detection of MRSA and selected antibacterial drugs; vancomycin and ciprofloxacin. The detection techniques used to carry out all electrochemical measurements involved Ag/AgCl (3 M KCl) as reference electrode, platinum wire as the counter electrode and the glassy carbon electrode (GCE) as the working electrode. Firstly, to carry out the detection of vancomycin as single shot detection assay comprising of poly acrylic acid modified copper tricarboxylic acid based metal organic framework was employed. Cyclic voltammetry was used to carry out the highly sensitive detection of vancomycin. Ciprofloxacin was detected by modification of the GCE by beta cyclodextrin modified silver nanoparticles (Ag- β -CD/GCE) and by modifying another electrode with poly(phenol red)/reduced graphene oxide (rGO/PPR/GCE). Differential pulse voltammetry (DPV) was used to carry out the detection of the drug in various analytes such as animal blood serum, urine and domestic waste water samples. Finally, the electrode was modified with copper-beta-cyclodextrin-graphene oxide composite conjugated with vancomycin to act as a thernostic tool for detection and treatment of MRSA bacterial strains. DPV and impedance spectroscopy was used to carry out optimization and further the detection of MRSA. The designed sensors provided good sensitivity and low LOD for detection of the respective analytes with good specificity. Thus, the present study demonstrates a promising and alternative approach for clinical analysis and quality control of vancomycin and ciprofloxacin.

CHAPTER ONE

1.1. Introduction

This chapter consist of a brief background to the study, indicating infectious diseases status with various antibiotics therapies problems. The chapter further provides details on several strategies remedies to detect drug of choice for methicillin-resistant *Staphylococcus aureus* (MRSA) (vancomycin) and restricted drug (ciprofloxacin). Further, MRSA detection using nanomaterials based electrochemical biosensors technique is discussed. Finally, chapter concludes by demonstrating the aims and objectives of the study along with the novelty and the structure of following chapters.

1.2. Background

Bacterial resistance to the largely accessible anti-microbial drugs poses one of the most significant risks to human health and can cause tremendous healthcare and economic burden [1]. In recent years, antimicrobial resistance against antibiotics has become a serious health issue, posing a global threat. The lack of development of new antibiotics for treating illnesses, as well as the appearance of multidrug-resistant strains, have worsened the scenario. To date, only two new classes of antibiotics have appeared in the last four decades In fact, it is estimated that by 2050 antibiotic resistance will have caused approximately 300 million deaths, with an economic loss of \$100 trillion, and according to the World Health Organization antibiotic resistance is one of the major health problems of the century [2]. Medications such as penicillin and methicillin are commonly prescribed for anti-microbial therapy. However, after a certain administration period, it was reported to result in anti-microbial drugs resistance. Antibiotic resistance occurs when bacteria change in response to the use of these medicines. These bacteria then infect humans and are harder to treat than non-resistant bacteria. Antimicrobial resistance (AMR) is a broader term, encompassing resistance to drugs to treat infections caused by other microbes as well, such as parasites (e.g. malaria), viruses (e.g. HIV) and fungi (e.g. Candida). AMR is the ability of a microorganism (like bacteria, viruses, and some parasites) to stop an antimicrobial action of antibiotics and antivirals against target organism. As a result, standard treatments become ineffective, infections persist and may spread to others [3]. **Figure 1** showed the mechanistic approach by which microbes develop resistance to the most of the antimicrobials drugs.

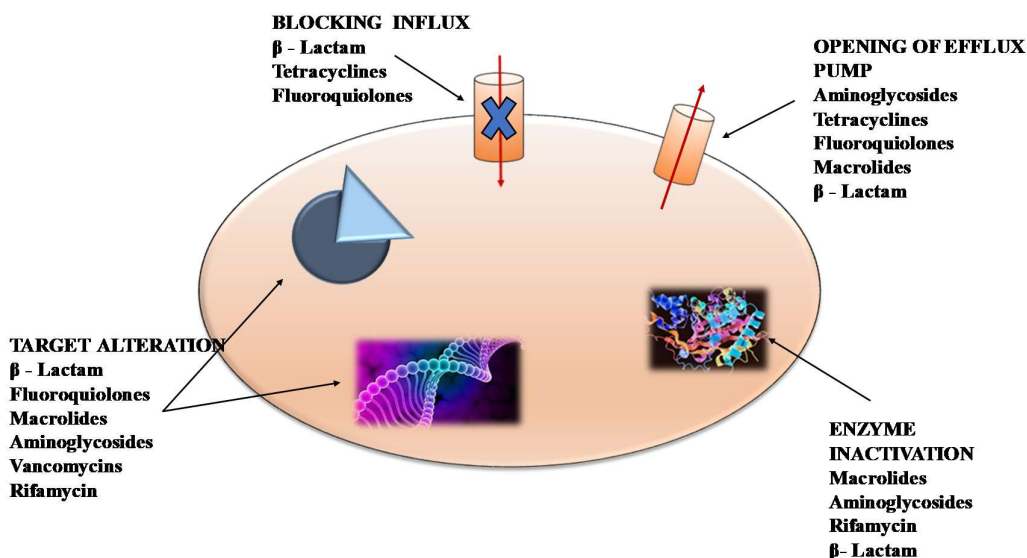


Figure 1. Mechanism of development of resistance by microbes to antimicrobials drugs.

1.3. *Staphylococcus aureus* (*S. aureus*) and methicillin-resistant *S. aureus* (MRSA)

Staphylococcus aureus (*S. aureus*) has been key human pathogen and causes several serious infection syndromes in both community-and healthcare-associated settings. *S. aureus* possesses a remarkable number of factors of resistance and virulence with a unique ability to adapt and survive under different host conditions, making it a dangerous pathogen [4]. It is responsible for a number of human diseases, from mild skin infections to severe sepsis disease conditions, which further result in multiple organ failure and other complications. For example, if the cutaneous and mucosal defense are compromised due to chronic skin conditions, injuries or surgical intervention, *S. aureus* may enter the underlying tissues or bloodstream and cause infections in other parts of the body [5]. One of the most widely used and clinically important group of antibiotics as a treatment therapy is the β -lactam family of antibiotics (penicillins, cephalosporins, carbapenems and monobactams) [6]. While Staphylococci were normally resistant to penicillin G, in the 1950s there was a rapid resistance to the distribution of penicillinase-encoding plasmids. The development of penicillinase has become a species-related trait of most staphylococcal strains [7].

Further, methicillin is used as the therapy to combat the resistance due to β -lactamases. But sadly after a few methicillin doses, *S. aureus* developed resistance [8]. Resistant strains of *S. aureus*, including methicillin-resistant *S. aureus* (MRSA), have been identified by use of antibiotics [9]. MRSA is one of the most successful modern pathogens that clinically causes life-threatening disorders like sepsis and severe endocarditis [10]. In the last two decades, it has increased the burden on the healthcare system globally, with high mortality rate 64%. High mortality rates associated with MRSA infections are the result of the increase in drug-resistance via natural selection. With the ever-increasing number

of MRSA patients reported, it imposes a serious economic burden on scarce healthcare resources worldwide [11]. In Europe, data from the European Antimicrobial Resistance Surveillance System (EARSS) reported that prevalence of HA-MRSA in acute care and long-term settings ranged between 1% and 24% with considerable intracountry and intercountry variation [12]. The average excess costs per MRSA-positive patient ranged from 5,700 to 10,000 Euros [13]. World Health Organisation (WHO) first global report on antibiotic resistance published in 2014 noted that in the African region, there exists a major gap in monitoring and tracking antibiotic resistance, with data gathered in only limited number of countries across the continent [14]. The WHO report also noted that in some parts of Africa as many as 80% of *S. aureus* infections are resistant to methicillin (MRSA), rendering treatment with standard antibiotics ineffective [15]. **Figure 2** shows the various factors linked to transmission of MRSA in hospitals and health-care worker.

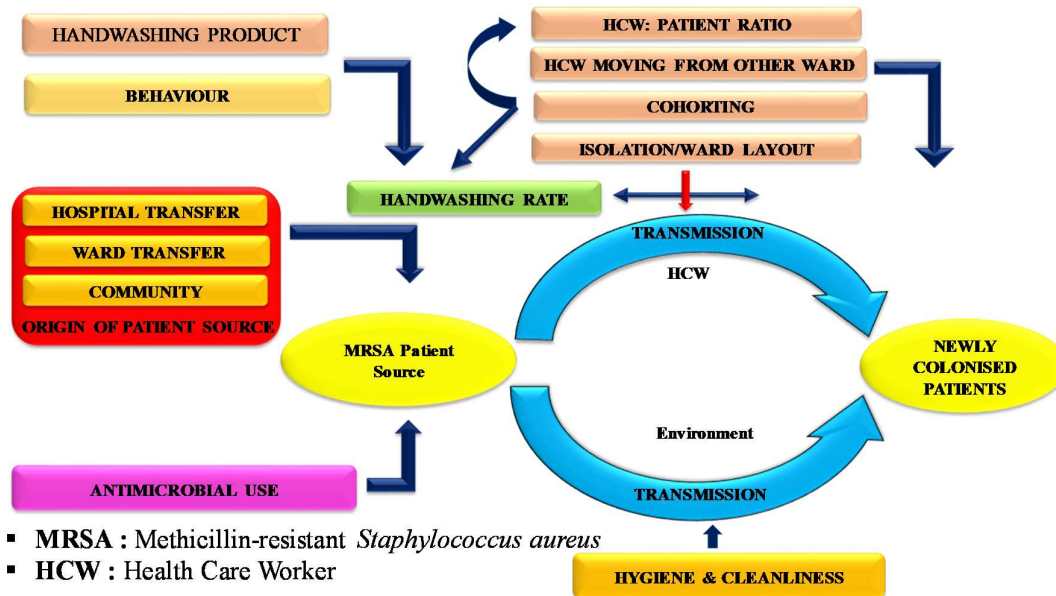


Figure 2. Factors linked to transmission of MRSA in hospitals and health-care worker.

1.4 Mechanism of development of methicillin-resistance

The main challenge being depicted by methicillin-resistance (MR) is mediated by the acquisition of the penicillin-binding protein 2A (PBP2A), which is encoded by the *mecA* gene. This resistance is due to limited accessibility of the antibiotics to the active site. In contrast to the low accessibility of the PBP2a active site to β -lactam antibiotics, the native peptidoglycan substrate is still able to access the active site, believed to be a result of conformational changes brought about by allosteric binding of peptidoglycan to the enzyme, resulting in effective peptidoglycan cross-linking and subsequent cell-wall viability [16]. Mutations acquired by individual bacteria or horizontal gene transfer leads to the

decrease in effectiveness of antibiotics and thus resistant traits proliferate. Resistance to β -lactam antibiotics predominantly occurs through one of two mechanisms: 1) the production of β -lactamases, which is the most common resistance mechanism in Gram-negative bacteria, or 2) the production of an altered PBP with a lower affinity for most β -lactam antibiotics [17].

MRSA strains also harbor other mobile genetic elements (MGEs), including plasmids, pathogenicity islands, transposons, integrons and prophages, which comprise 15-25% of the genome. MGEs carry the majority of the genes, through which strains of staphylococcal vary from each other, such as resistance and virulence genes [18]. MGEs play a significant role in bacterial survival and adaptability, as they encode many antibiotic resistance determinants and virulence factors, hence understanding their composition will broaden our knowledge on their genetic determinants [19].

1.5 Approved antibiotic therapy for MRSA

Approved MRSA antibiotics are medically adjustable and it varies from condition of patient's clinical disease indication. Given the prevalence and importance of MRSA infections, the relative lack of high quality randomized controlled trials (RCTs) to direct the treatment of all indications except acute bacterial skin and skin structure infections (ABSSSIs) has been noted [20]. The number of therapeutic choices has been declining over time, as Glycopeptide vancomycin is currently used as primary treatment for MRSA. The increase in use of vancomycin has, unsurprisingly, caused resistance to appear with a consequent decrease in its effectiveness in MRSA. Reports of strain resistance infections to the newest available drugs (daptomycin, vancomycin, teicoplanin) and their rapid spread are of major concern as they introduce new therapeutic and diagnostic challenges [21]. The latest clinical data for antibiotics with MRSA activity are summarized in **Table 1**.

Table 1. List of antibiotics effective against MRSA

Name of the antibiotics	FDA-approved indications	Comments	References
Vancomycin	Bacteraemia, pneumonia, osteoarticular infection, ABSSSI	It remains the first- line therapy for MRSA.	[22]
Daptomycin	Bacteremia, ABSSSI	In activation of the drug is caused by lung surfactant and therefore not recommended during pneumonia treatment. Can lead to increased levels of creatine kinase.	[23], [24]
Linezolid	Pneumonia, ABSSSI	Cause of prolonged therapy due to neurotoxicity and myelosuppression.	[25]
Tedizolid	ABSSSI	Lower incidence of thrombocytopenia and gastrointestinal side effects compared to linezolid.	[26]
Ceftaroline	Pneumonia (only for community-acquired pneumonia — not MRSA pneumonia)	This drug shows side effect profile similar to other cephalosporins.	[27]
Telavancin	Pneumonia ABSSSI	The drug caused high creatinine levels on clinical level in ASSURE trail than standard therapy. The trail was discontinued for bacteraemia.	[28], [29]
Dalbavancin	ABSSSI	Use the drug once a week. The trail was discontinued for bacteraemia by sponsor.	[30]
Oritavancin	ABSSSI	Use the drug once a week.	[31]
Delafloxacin	ABSSSI	Well tolerated, minimal effect on cytochrome P450 enzyme and QTc interval.	[32]

1.6. Relevance and importance of this study

A delay in initiation of appropriate therapy is associated with increased mortality. Therefore, an assay to detect MRSA infection and its related drugs rapidly with high specificity and sensitivity is highly desirable to initiate appropriate antibiotic therapy. MRSA detection strategies vary substantially in terms of the duration, sensitivity, sophistication and the infrastructure requirements [33]. Additionally, the prescribed drugs in accumulate in the body and can lead to various toxic side effects if not administered properly and in time. Further, the discharge of these drugs in the environment can lead to emergence of novel drug resistant strains. This can further increase infection of new bacterial strains, therefore making it necessary to detect drug in biological as well as in environmental matrices. Earlier reported methodologies for the detection of more frequently prescribed medicine vancomycin, restricted antibiotics i.e. ciprofloxacin and MRSA bacterial detection have a few constraints. These techniques require large capital requirement for installation and instrumentation, trained professionals and are time consuming. Therefore, to avoid such a financial burden and carry out the rapid detection of MRSA, nanomaterial-based detection techniques have been developed. Nanomaterials such as graphene, CNT's, molecularly imprinted polymers, carbon black etc. have been used as transduction element or detection element to carry out detection through electrochemical, fluorescence, optical fibres and many others. These nanomaterials provide high sensitivity, specificity, easy and accessible method for detection of analytes. Therefore, on basis of these characteristics, we employ novel synthesized nanomaterials to carry out the electrochemical detection of vancomycin, ciprofloxacin and MRSA bacterial strain. The integration of nanostructured materials on the surface of the working electrode introduces diversity in the physical (electronic, photonic and catalytic) properties [34]. These variations can be exploited to optimize the performance of the working electrode. The nanostructured particles also have a very high surface to volume ratio. The larger active surface area allows more biomolecules to be immobilized at or near the electrode surface. This reduces the distance for electron transfer between the biomolecule and the metal/metal oxide particles facilitating the charge transfer to the electrodes. These nanomaterials can be conjugated Conducting polymers are redox-active, can be modified to bind bio-molecules to itself as well as tuned as per requirement [35]. The ease of fabrication and functionalization of organic molecule with nanoparticles accompanied by their catalytic synergistic effect make them very useful for the development of modified electrodes with specific detection of molecules of biological interest. Therefore, electrochemical sensors based on novel nanomaterials and nanocomposites have been synthesized to

provide a rapid, sensitive, inexpensive, and user-friendly analytical method for the detection of MRSA, vancomycin and ciprofloxacin.

Novel nanocomposite materials were synthesized as a potential electrode modifier to carry out detection. The present thesis focuses majorly on novel organo-metallic nanomaterials. These materials were chosen due to their higher surface area and porous nature. Further, these nanomaterials exhibit lower toxicity as compared to their inorganic counterparts due to the presence of organic component. We used copper and silver nanoparticles for synthesizing the organo-metallic nanomaterials due to their antibacterial nature and good electro catalytic properties.

The electrochemical studies were carried out using a potentiostat which provides the required potential difference for the three electrode electrochemical cell. The system uses a reference electrode (Ag/AgCl), a counter electrode (platinum wire) and working electrode (glassy carbon electrode) which are supported by an electrolyte to provide a medium for the electron transportation. The supporting electrolyte can act as a redox active couple which can provide an output response to detect in a particular range of applied potential. Further, electrochemical techniques such as cyclic voltammetry (CV), differential pulse voltammetry (DPV) and electrical impedance spectroscopy (EIS) have been employed to carry out the characterization of the nanomaterials modified electrode and also the detection of analytes, which were vancomycin, ciprofloxacin and MRSA bacterial strains.

1.7 Aim and Research Objectives

The current thesis focuses on synthesis of novel nanomaterials for electro-catalytic and electrochemical bio-sensing applications. The characterization of the synthesized materials was carried out. Further, their applicability was tested by electrochemical detection of vancomycin, ciprofloxacin and MRSA bacterial strains.

Specific objectives of the studies are:

1. To synthesize and characterize poly(acrylic) acid modified HKUST-1 metal organic framework (MOF) to carry out the detection of vancomycin.
2. To synthesize β -cyclodextrin modified by silver nanoparticles and its characterization follow by the detection of ciprofloxacin.

3. To synthesize and characterize β -cyclodextrin capped on copper nanoparticles via hydrothermal route for detection of MRSA and check the MIC values of the composite against MRSA.
4. To synthesize reduce graphene oxide (rGO)/poly(phenol red)/GCE and characterize the electrode. Further, to carry out the detection of ciprofloxacin.
5. Finally, the prepared nanomaterials were used to detect the respective analytes in real samples to check the practical applicability of the proposed methods.

1.8. Thesis Outline

The thesis is compiled in seven chapters. These seven chapters are presented as four experimental manuscripts and one review article

- **Chapter one** briefs about the topic of thesis and give a short outline about the problems along with the outline of the thesis.
- **Chapter two** consists of the literature review about the various biomarkers for MRSA along with their detection techniques using novel nanomaterials.
- **Chapter three** involves a poly(acrylic) acid (PAA) modified copper benzene-1,3,5-tricarboxylic acid (BTC) metal-organic framework (MOF) as a single shot assay for electrochemical detection of vancomycin.
- **Chapter four** shows one pot synthesis of silver nanoparticles modified β -cyclodextrin for highly sensitive detection of ciprofloxacin.
- **Chapter five** reports a beta cyclodextrin modified with copper nanoparticles for detection of MRSA bacterial strains.
- **Chapter six** reports detection of ciprofloxacin using rGO/PPR/GCE electrode.
- **Chapter seven** provides the summary and concludes the major findings of the present work along with future prospective.

References

- [1] Gradmann C. Magic bullets and moving targets: Antibiotic resistance and experimental chemotherapy, 1900-1940. *Dynamis* 2011. doi:10.4321/S0211-95362011000200003.
- [2] de Kraker MEA, Stewardson AJ, Harbarth S. Will 10 Million People Die a Year due to Antimicrobial Resistance by 2050? *PLoS Med* 2016. doi:10.1371/journal.pmed.1002184.

- [3] The Review on Antimicrobial Resistance. The Review on Antimicrobial Resistance. 2016. doi:10.1016/j.jpha.2015.11.005.
- [4] Koch G, Yepes A, Förstner KU, Wermser C, Stengel ST, Modamio J, et al. Evolution of resistance to a last-resort antibiotic in staphylococcus aureus via bacterial competition. *Cell* 2014. doi:10.1016/j.cell.2014.06.046.
- [5] Deurenberg RH, Stobberingh EE. The evolution of *Staphylococcus aureus*. *Infect Genet Evol* 2008. doi:10.1016/j.meegid.2008.07.007.
- [6] Poole K. Resistance to β -lactam antibiotics. *Cell Mol Life Sci* 2004. doi:10.1007/s00018-004-4060-9.
- [7] Chambers HF, DeLeo FR. Waves of resistance: *Staphylococcus aureus* in the antibiotic era. *Nat Rev Microbiol* 2009. doi:10.1038/nrmicro2200.
- [8] Gill AAS, Singh S, Thapliyal N, Karpoormath R. Nanomaterial-based optical and electrochemical techniques for detection of methicillin-resistant *Staphylococcus aureus*: a review. *Microchim Acta* 2019. doi:10.1007/s00604-018-3186-7.
- [9] Paterson GK, Harrison EM, Holmes MA. The emergence of *mecC* methicillin-resistant *Staphylococcus aureus*. *Trends Microbiol* 2014. doi:10.1016/j.tim.2013.11.003.
- [10] Vicetti Miguel CP, Mejias A, Leber A, Sanchez PJ. A decade of antimicrobial resistance in *Staphylococcus aureus*: A single center experience. *PLoS One* 2019. doi:10.1371/journal.pone.0212029.
- [11] Kahn JG, Jiwani A, Gomez GB, Hawkes SJ, Chesson HW, Broutet N, et al. The cost and cost-effectiveness of scaling up screening and treatment of syphilis in pregnancy: A model. *PLoS One* 2014. doi:10.1371/journal.pone.0087510.
- [12] Dulon M, Peters C, Schablon A, Nienhaus A. MRSA carriage among healthcare workers in non-outbreak settings in Europe and the United States: A systematic review. *BMC Infect Dis* 2014. doi:10.1186/1471-2334-14-363.
- [13] Robotham J V., Graves N, Cookson BD, Barnett AG, Wilson JA, Edgeworth JD, et al. Screening, isolation, and decolonisation strategies in the control of meticillin resistant

Staphylococcus aureus in intensive care units: Cost effectiveness evaluation. *BMJ* 2011. doi:10.1136/bmj.d5694.

- [14] Högberg LD, Muller A, Zorzet A, Monnet DL, Cars O. Antibiotic use worldwide. *Lancet Infect Dis* 2014. doi:10.1016/S1473-3099(14)70987-9.
- [15] WHO. Antimicrobial resistance. Global report on surveillance. World Heal Organ 2014. doi:10.1007/s13312-014-0374-3.
- [16] Fuda C, Hesek D, Lee M, Morio KI, Nowak T, Mobashery S. Activation for catalysis of penicillin-binding protein 2a from methicillin-resistant *Staphylococcus aureus* by bacterial cell wall. *J Am Chem Soc* 2005. doi:10.1021/ja0434376.
- [17] Lindsay JA. Hospital-associated MRSA and antibiotic resistance-What have we learned from genomics? *Int J Med Microbiol* 2013. doi:10.1016/j.ijmm.2013.02.005.
- [18] Lindsay JA, Moore CE, Day NP, Peacock SJ, Witney AA, Stabler RA, et al. Microarrays reveal that each of the ten dominant lineages of *Staphylococcus aureus* has a unique combination of surface-associated and regulatory genes. *J Bacteriol* 2006. doi:10.1128/JB.188.2.669-676.2006.
- [19] Lindsay JA, Holden MTG. *Staphylococcus aureus*: Superbug, super genome? *Trends Microbiol* 2004. doi:10.1016/j.tim.2004.06.004.
- [20] Turner NA, Sharma-Kuinkel BK, Maskarinec SA, Eichenberger EM, Shah PP, Carugati M, et al. Methicillin-resistant *Staphylococcus aureus*: an overview of basic and clinical research. *Nat Rev Microbiol* 2019;17:203–18. doi:10.1038/s41579-018-0147-4.
- [21] Tucker EC, Roberts MB, Sweeney NA, Gordon DL. Miscellaneous Antibacterial Drugs. *Side Eff. Drugs Annu.*, 2018. doi:10.1016/bs.seda.2018.07.019.
- [22] Coia JE, Duckworth GJ, Edwards DI, Farrington M, Fry C, Humphreys H, et al. Guidelines for the control and prevention of methicillin-resistant *Staphylococcus aureus* (MRSA) in healthcare facilities. *J Hosp Infect* 2006. doi:10.1016/j.jhin.2005.10.014.
- [23] Fowler VG, Boucher HW, Corey GR, Abrutyn E, Karchmer AW, Rupp ME, et al. Daptomycin versus standard therapy for bacteremia and endocarditis caused by

Staphylococcus aureus. N Engl J Med 2006. doi:10.1056/NEJMoa053783.

- [24] Bartlett JG. The safety and efficacy of daptomycin for the treatment of complicated skin and skin-structure infections. Infect Dis Clin Pract 2004. doi:10.1097/01.idc.0000144912.27311.19.
- [25] Wunderink RG, Niederman MS, Kollef MH, Shorr AF, Kunkel MJ, Baruch A, et al. Linezolid in methicillin-resistant *Staphylococcus aureus* nosocomial pneumonia: A randomized, controlled study. Clin Infect Dis 2012. doi:10.1093/cid/cir895.
- [26] Shorr AF, Lodise TP, Corey GR, De Anda C, Fang E, Das AF, et al. Analysis of the phase 3 ESTABLISH trials of tedizolid versus linezolid in acute bacterial skin and skin structure infections. Antimicrob Agents Chemother 2015. doi:10.1128/AAC.03688-14.
- [27] Ramani A, Udeani G, Evans J, Jandourek A, Cole P, Smith A, et al. Contemporary use of ceftaroline fosamil for the treatment of community-acquired bacterial pneumonia: CAPTURE study experience. J Chemother 2014. doi:10.1179/1973947814Y.00000000184.
- [28] Rubinstein E, Lalani T, Corey GR, Kanafani ZA, Nannini EC, Rocha MG, et al. Telavancin versus vancomycin for hospital-acquired pneumonia due to gram-positive pathogens. Clin Infect Dis 2011. doi:10.1093/cid/ciq031.
- [29] Stryjewski ME, Graham DR, Wilson SE, O’Riordan W, Young D, et al. Telavancin Versus Vancomycin for the Treatment of Complicated Skin and Skin-Structure Infections Caused by Gram-Positive Organisms. Clin Infect Dis 2008. doi:10.1086/587896.
- [30] Boucher HW, Wilcox M, Talbot GH, Puttagunta S, Das AF, Dunne MW. Once-weekly dalbavancin versus daily conventional therapy for skin infection. N Engl J Med 2014. doi:10.1056/NEJMoa1310480.
- [31] Corey GR, Kabler H, Mehra P, Gupta S, Overcash JS, Porwal A, et al. Single-Dose oritavancin in the treatment of acute bacterial skin infections. N Engl J Med 2014. doi:10.1056/NEJMoa1310422.
- [32] O’Riordan W, McManus A, Teras J, Poromanski I, Cruz-Saldariagga M, Quintas M, et al. A Comparison of the Efficacy and Safety of Intravenous Followed by Oral Delafloxacin with Vancomycin Plus Aztreonam for the Treatment of Acute Bacterial Skin and Skin Structure

Infections: A Phase 3, Multinational, Double-Blind, Randomized Study. Clin Infect Dis 2018. doi:10.1093/cid/ciy165.

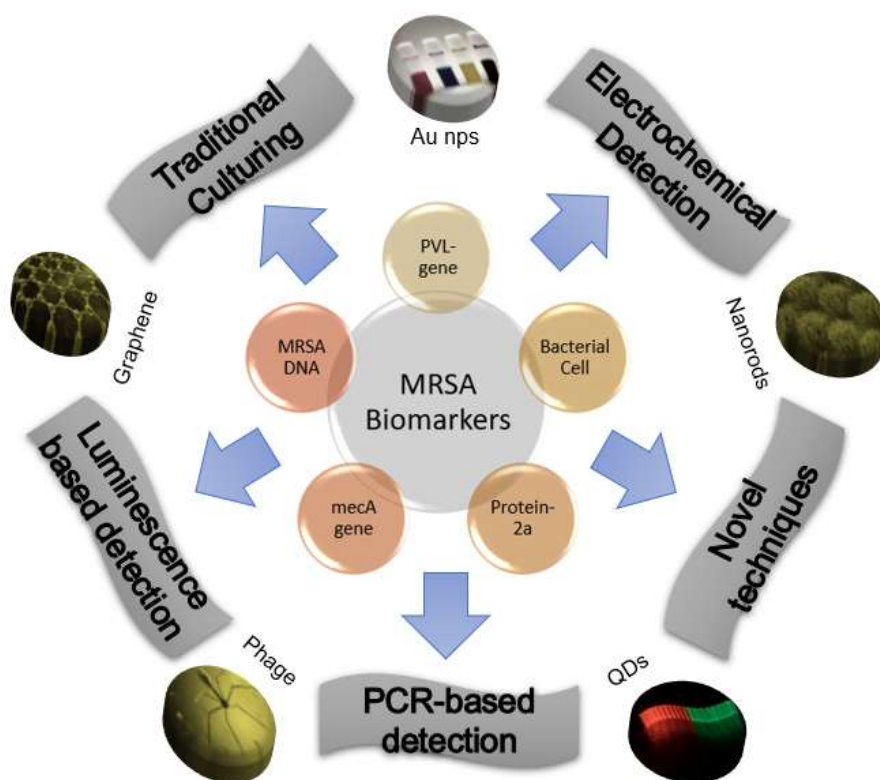
- [33] Hadi M, Mollaei T. Electroanalytical Determination of Vancomycin at a Graphene-modified Electrode: Comparison of Electrochemical Property Between Graphene, Carbon Nanotube, and Carbon Black. Electroanalysis 2018. doi:10.1002/elan.201800497.
- [34] Lestner JM, Hill LF, Heath PT, Sharland M. Vancomycin toxicity in neonates: A review of the evidence. Curr Opin Infect Dis 2016. doi:10.1097/QCO.0000000000000263.
- [35] Korposh S, Chianella I, Guerreiro A, Caygill S, Piletsky S, James SW, et al. Selective vancomycin detection using optical fibre long period gratings functionalised with molecularly imprinted polymer nanoparticles. Analyst 2014. doi:10.1039/c3an02126b.

CHAPTER TWO

Nanomaterial-based optical and electrochemical detection techniques for Methicillin-resistant

Staphylococcus aureus: A review

Graphical Abstract



Nanomaterial-based optical and electrochemical techniques for detection of methicillin-resistant *Staphylococcus aureus*: a review

Atal A. S. Gill, Sima Singh, Neeta Thapliyal & Rajshekhar Karpoormath 

Microchimica Acta **186**, Article number: 114 (2019) | [Cite this article](#)

719 Accesses | 10 Citations | 1 Altmetric | [Metrics](#)

Abstract

Methicillin-resistant *Staphylococcus aureus* (MRSA) is responsible for a number of life-threatening complications in humans. Mutations in the genetic sequence of *S. aureus* due to the presence of certain genes results in resistance against β -lactamases. Thus, there is an urgent need for developing highly sensitive techniques for the early detection of MRSA to counter the rise in resistant strains. This review (142 refs.) extensively covers literature reports on nanomaterial-based optical and electrochemical sensors from the year 1983 to date, with particularly emphasis on recent advances in electrochemical sensing (such as voltammetry and impedimetric) and optical sensing (such as colorimetry and fluorometry) techniques. Among the electrochemical methods, various nanomaterials were employed for the modification of electrodes. Whereas, in optical assays, formats such as enzyme linked immunosorbent assay, lateral flow assays or in optical fiber systems are common. In addition, novel sensing platforms are reported by applying advanced nanomaterials which include gold nanoparticles, nanotitania, graphene, graphene-oxide, cadmium telluride and related quantum dots, nanocomposites, upconversion nanoparticles and bacteriophages. Finally, closing remarks and

Abstract

Methicillin-resistant *Staphylococcus aureus* (MRSA) is responsible for a number of life-threatening complications in humans. Mutations in the genetic sequence of *S. aureus* due to the presence of certain genes results in resistance against β -lactamases. Thus, there is an urgent need for developing highly sensitive techniques for the early detection of MRSA to counter the rise in resistant strains. This review (142 refs.) extensively covers literature reports on nanomaterial-based optical and electrochemical sensors from the year 1983 to date, with particularly emphasis on recent advances in electrochemical sensing (such as voltammetry and impedimetric) and optical sensing (such as colorimetry and fluorometry) techniques. Among the electrochemical methods, various nanomaterials were employed for the modification of electrodes. Whereas, in optical assays, formats such as enzyme linked immunosorbent assay, lateral flow assays or in optical fiber systems are common. In addition, novel sensing platforms are reported by applying advanced nanomaterials which include gold nanoparticles, nanotitania, graphene, grapheneoxide, cadmium telluride and related quantum dots, nanocomposites, upconversion nanoparticles and bacteriophages. Finally, closing remarks and an outlook conclude the review.

Keywords: Methicillin-resistant *Staphylococcus aureus* (MRSA); Biosensors; Nanomaterials; Electrochemical sensing; Luminescence-based techniques; Polymerase chain reaction (PCR),

Introduction

Gram-positive *Staphylococcus aureus* (*S. aureus*) is the most commonly isolated bacterium known for its serious pathogenic nature [1], is responsible for numerous diseases in humans from mild skin infection to fatal sepsis resulting in multiple organ failure [2]. It is accountable for the high rate of morbidity and mortality globally and is known to spread at an alarming rate, thus posing a challenging task for healthcare professionals. It has been reported, that four out of five bacterial infections in patients with implants are due to the staphylococci bacterial strains especially *S. aureus* and *S. epidermidis* [3] and is estimated that ten million people will die by 2050 [4].

An era before, when the accessibility to antibiotics was not easy, infections caused by *S. aureus* were often disastrous especially in patients who had undergone surgical interventions or prolonged hospitalizations. Introduction of penicillin significantly developed the prognosis for patients with severe staphylococcal infections. However, regular or overuse of penicillin in clinical practice led to the development of resistance in bacteria owing to the production of β -lactamases [5]. The *S. aureus* bacteria possess a special defensive mechanism to protect itself against the immune system of the human body. This characteristic is due to the spread of unicellular organism, rapid and fast proliferation, colonizes body forming surfaces, and persistent against stress conditions in tissues as multicellular aggregates called the matrix [6].

To counter the resistance due to β -lactamases [5], methicillin was introduced for the treatment. But in a few years' time, methicillin-resistant forms of pathogenic *Staphylococcus aureus* (MRSA) strains were isolated, which were resistant to all β -lactam antibiotics [5]. In a short span, MRSA spread as an extensively nosocomial pathogen found mainly in hospitalized patients leading to hospital-acquired infections. Currently, these resistant strains have been progressively isolated from community-acquired infections as well. The emergence of methicillin-resistant forms of

Staphylococcus aureus (MRSA) has further complicated the diagnosis and management of infection in the medical world, resulting in a constant rise in mortality [7].

Key problems of resistance in hospitals and communities

MRSA is the most common microorganism linked with healthcare-associated infections [8], typically confined to hospitals, nursing homes and poverty-stricken areas. Despite that, it does not affect the hospital staff or the family members of the affected person by maintaining good hygiene and covering wounds [9]. In spite of current advanced therapy, there has been a constant rise in the number of multi-drug resistant cases reported either in hospitals or in hyper-virulent community-associated MRSA (CA-MRSA), as presented in Figure 1.

In the past three decades, MRSA strains have been prominent in hospital settings and hospital-acquired MRSA (HA-MRSA) has become a major cause of infection. Recent reports indicate that MRSA developed resistance very quickly, creating many challenging problems in the clinical world [10]. The major risk factors responsible for complicating the treatment of MRSA infections are patients with chronic illness, elderly people and weak immunity [11]. The MRSA infection spreads either by direct contact with uncovered wounds/ulcers containing pus cells or infected invasive medical devices such as intravenous lines and catheters. These provide a gateway for the bacteria leading to secondary infections like pneumonia, surgical site infections, bacteremia, and other nosocomial infections. Thus, increasing the burden on the whole health system with a rise in morbidity and mortality along with hospitalization overheads [12].

In the mid-1990s, new MRSA strains appeared in the community setting as community-acquired (CA-MRSA), infecting healthy people including students, athletes and even military personnel. The major risk factors included overuse or abuse of antibiotics, direct skin contact especially in sports like wrestling and crowded places with poor sanitation [13]. On the other hand,

in hospital settings, the infection spread to other patients with a history of recent discharge, dialysis, chronic diseases, human immunodeficiency virus (HIV) infection, and by intravenous route of drug administration [14]. CA-MRSA strains cause inflammation of the skin, severe necrotizing pneumonia, furunculosis, and shock resulting in death. Researchers have suggested that CA-MRSA strains have arisen from changed genetic backgrounds rather from the worldwide spread of a single clone [15]. Thus, to counter the rapid spread of MRSA infection it is essential to detect the infection at an early stage with the help of biomarkers to fill the gap between occurrence and treatment of MRSA in patients.

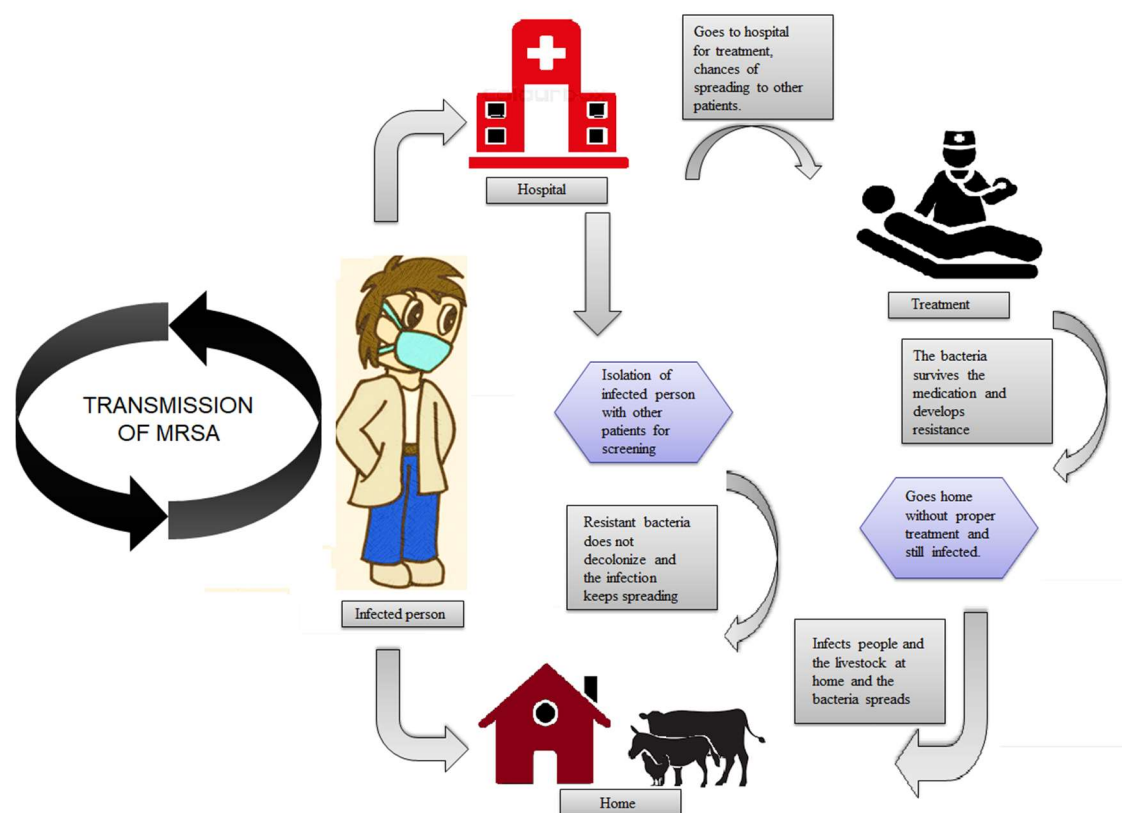


Fig. 1 Schematic presentation of transmission of MRSA in community and hospitals.

Biomarkers for MRSA

Scientifically, biomarkers refer to the quantity that can be measured in a certain biological state or disease conditions. According to WHO, a biomarker is described as any structure, process or substance or their respective products that can be measured to predict or influence the onset of a disease or an outcome [16].

In the case of MRSA bacterial strains, PBP2a protein is a major biomarker which is responsible for developing resistance against methicillin antibiotics. This protein is produced by *mecA* gene present as an element in staphylococcal cassette chromosome mec (SCCmec) [17] as shown in Figure 2 and is known to produce resistance against drugs by facilitating the transpeptidase action, which alters the bacterial cell wall structure, preventing drugs from disrupting the cell wall synthesis [18]. The major bacterial strains with SCCmec I, II and III are known to be associated with HA-MRSA while SCCmec IV and V strains are generally associated with CA-MRSA. In the case of SCCmec IV and V strains, an additional Pantone-Valentine leukocidin (PVL) gene element was found which can be considered as a biomarker for the detection of CA-MRSA bacterial strains [19,20]. Another genetic element as a biomarker that has not been explored for the screening of MRSA is the arginine catabolic mobile element (ACME) which is known to be present in MRSA but not in the MSSA bacterial strains [21]. The ACME marker is generally associated with CA-MRSA bacterial strain, particularly USA300 clone, which is extensively being studied by various researchers [22,23]. The USA300 clone is a SCCmec type IV strain which has a PVL-positive strain of bacteria [22]. ACME I element of ACME gene has been known to increase the virulence factor of bacterial strains [24]. Sean et al. conducted a study and revealed that most of the strains that had both PVL and ACME were a new polymorphed *S. aureus pbp3* strains [25]. Furthermore, studies are being carried out on the same and its role in the bacterial infection. Various biomarkers for MRSA are enlisted in Table 1.

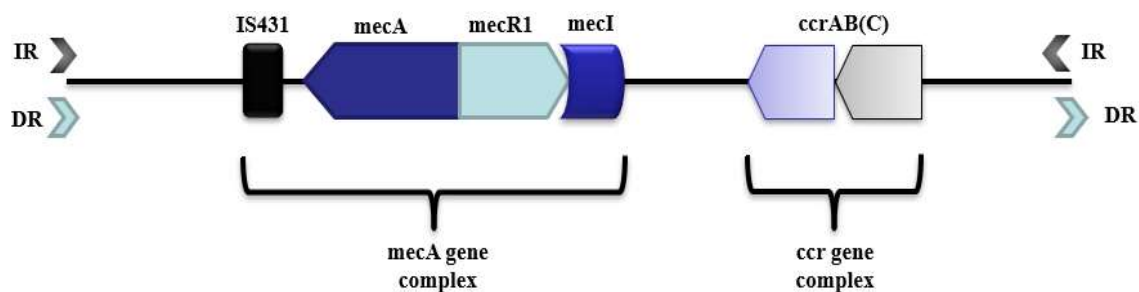


Fig 2. Schematic illustrates the structure of SCCmec. SCCmec is composed of two essential gene complexes. One is *mec*-gene complex, encoding methicillin resistance (*mecA* gene) and its regulators (*mecI* and *mecR1*), and the other is *ccr*-gene complex that encodes the movement, of the entire SCC element. Abbreviations: IR, inverted repeat; DR, direct repeat

Table 1 Genetic and protein-based biomarker currently used for MRSA detection

Genetic biomarkers	SSCmec I, II and III for HA-MRSA, SSCmec IV and V for CA-MRSA, <i>mecA</i> gene, PVL-gene, genomic DNA, ssDNA.
Protein biomarkers	PBP2a (penicillin binding protein)

Conventional detection techniques for MRSA

There are different types of analytical techniques available for the quantitative or qualitative detection of bacteria. Among these, the bacterial culture is one of the widely used technique but suffers from several drawbacks involving time-consuming steps such as sample pre-enrichment, selective enrichment, and bacterial colony isolation on selective agar plates. Further, these time-consuming practices may also undesirably lead to false results in the absence of typical colonies. The bacterial detection is also performed with other methods, e.g., immunological assays (ELISA, agglutination test, etc.) and nucleic acid amplification (polymerase chain reaction (PCR), Colony-PCR, RT-PCR, etc.) [26-30].

Traditional cell culturing

Traditional cell culturing generally involves isolation of patients to prevent the spread of bacterial infection and then collecting samples from isolated patients. The samples are collected from skin or nasal cavity and from other inorganic surfaces such as metals or plastic, using regular fibre or nylon swabs [31]. For clinical screening, E-swabs are employed for the collection of samples as they recover more amount of sample from the subject as compared to traditional swabs. For example, the amount of colony forming units of bacteria obtained from screening is 3.6 to 9 times higher with E-swabs as compared to traditional swabs [32]. Further, the sample conditions of urine, blood, pus, sputum, and bodily fluids can vary significantly on container size and mode of transport [33].

Until the late 1990's, the utilization of oxacillin and methicillin chromogenic agars was prominent in conventional techniques to distinguish MRSA and MSSA bacterial strains. Presently cephamycin and cefoxitin agars are utilized for MRSA as they show better selectivity towards PBP2a protein [34-38]. Kumar et al. reviewed the specificity and selectivity of commercially available chromogenic agars towards MRSA bacterial strains and highlighted the positive and negative sides of each agars [39]. To check the practical applicability of traditional swabbing a broad national cross-sectional study, which screened more than 10 000 patients for MRSA, wherein the samples were collected from nose, throat, axilla, perineum, and wound or device sites found that a nasal swab identified only 66% of MRSA carriers using the traditional culturing technique [40]. Addition of second and further swabs increased the detection rate, with nose and perineum swabs identifying 82% of the cases. The axilla site had the minimum value for identifying carriers (8% detection rate as given in Table 2). Thus, common screening methods should include a minimum of two swabs (a nasal swab plus a perineal or throat swab) to detect infection. This illustrated the lack of effective extraction of swabs for detection purposes and further complicates the detection process.

Table 2 Number of swabs testing positive for MRSA by anatomical site (detected on chromogenic agar) and percentage positive compared with the gold standard* [40]

Anatomical sites	No of samples positive for MRSA (n=298)	Percentage (95% CI) detection (versus gold standard*)	Percentage (95% CI) extra detection with extra sites used (versus nasal alone)
Nasal + throat + axilla + perineum	273	91.6 (87.9 to 94.3)	25.2 (20.3 to 30.5)
Nasal + throat	228	76.5 (71.4 to 81.0)	10.1 (6.9 to 14.1)
Nasal alone	198	66.4 (60.9 to 71.6)	-
Perineum alone	107	35.9 (30.7 to 41.5)	-
Nasal + perineum	245	82.2 (77.5 to 86.1)	15.8 (11.8 to 20.4)
Nasal + throat + perineum	269	90.3 (86.3 to 93.4)	23.8 (19.1 to 29.1)
Axilla alone	23	7.7 (5.2 to 11.3)	-
Nasal + axilla + perineum	250	83.9 (79.3 to 87.6)	17.5 (13.3 to 22.2)
Nasal + throat + axilla	234	78.5 (73.5 to 82.8)	12.1 (8.6 to 16.3)
Throat alone	103	34.6 (29.4 to 40.1)	-
Nasal + axilla	205	68.8 (63.3 to 73.8)	2.4 (0.95 to 4.8)

*Gold standard was all anatomical swab sites combined, pooled in nutrient broth and cultured on chromogenic agar.

Automated culturing

A big step forward in reducing diagnostic time was the automation of inoculation procedures developed by Vista technology (Edmonton, Alberta, Canada) and the instrument was known as Isoplater [41]. It is a fully automated system that allows for liquid handling to inoculating plates saving up to 30 mins of hands-on time per 100 cultures, thus drastically reducing detection time. Further such systems improved distribution and colony quality in comparison to manual streaking [42]. Another automated inoculation technique developed by BD Kiestra Total Laboratory Automation (TLA) known as walk away specimen processor unit (WASP) enables real-time

monitoring of the samples and uses any one of three metal loops (1 μL , 10 μL , and 30 μL) with magnetic beads in liquid samples for inoculation and streaking [43]. Further to check the compatibility of automated systems with E-swabs, Faron et al. conducted a study by screening 57,000 subjects and concluded high compatibility with 100% sensitivity and specificity between 90.0% and 96.0% across all sites [44]. A recent review published by Rajendran et al. highlighted the advantages of automated techniques for rapid MRSA detection [45].

Enzyme-linked immunoassay (ELISA)

The recent developments in non-labelled and labelled based optical immunoassays have been exploited for the detection of MRSA. The various assays such as competitive, direct and sandwich assays were utilized to detect secreted enterotoxins and/or complete MRSA cells [46]. Furthermore, 23 enterotoxins of staphylococcal origin have been identified with distinct serological existence [47]. A review by Wu et al. described various methods for the detection of *S. aureus* enterotoxins in clinical media and food products [48]. The most commonly known staphylococcal enterotoxins (SE) are labelled as SE-A and SE-B and were detected at 0.05 to 1 $\text{ng}\cdot\text{mL}^{-1}$ in the human urine sample and buffer solutions [49]. Templeman et al. and Goldman et al. employed enzyme-linked immunosorbent assay (ELISA) that rendered results in < 3 hours saving significant time and resources [50,51]. Primarily ELISA tests are performed to identify *S. aureus* and vancomycin resistance *S. aureus* (VRSA) strains, if the results are negative then alternative tests are carried out to detect Pantone-Valentine Leukocidin (PVL-S) toxin and PBP2a protein [52], where PVL-S is generally associated with CA-MRSA and not with nosocomial MRSA. However, the PVL-S is not multidrug resistant gene element and act as carriage of type IV SCCmec gene [53]. In 2014, Poojary NS et al. reported a highly sensitive detection technique for PVL-S using three monoclonal antibodies employing dot ELISA test [54].

Polymerase chain reaction (PCR) based techniques

The amplification of nucleic acid is done by PCR techniques along with simultaneous quantification and identification of bacterial DNA and RNA. The sensitivity of traditional PCR was reported to decrease during proteinous background with detection time of 24 to 48 hours [55]. On the other hand, real-time PCR (RT-PCR) monitors PCR products in real time and is utilized for detection of resistant bacteria [55]. Njihuis et al. applied two RT-PCR assays for screening 13,387 samples of MRSA and obtained reliable results in 24 hours [56]. Another low-cost alternative to RT-PCR is multiplex-PCR (M-PCR), which targets more than two sequences of MRSA and was recently utilized to differentiate between methicillin-resistant coagulase-negative staphylococcus (MR-CoNS) isolates and MRSA by the amplification of *mecA*, *nuc* and 16S RNA specimens [57]. Further, the sensitivity, accuracy and selectivity of M-PCR are enhanced by the increase in the number of targets/biomarkers.

The screening of antibiotic resistance *S. aureus* strains is efficiently carried out using traditional PCR technique, however, some studies have concluded that this method fails to detect genetically distant SCCmec (CoNS) subtypes [58]. An alternative to traditional PCR technique is a new technique called loop-mediated isothermal amplification (LAMP), which proceeds by the strand displacement of Bst DNA polymerase and a set of primers which folds into a dumbbell-shaped DNA structure that triggers cyclic isothermal amplification. Another technique, similar to the LAMP that utilizes isothermal amplification is recombinase polymerase amplification (RPA). Shen et al. carried out quantitative detection at a single molecular level for the nucleic acid sequences, utilizing a microfluidic digital recombinase polymerase amplification (RPA) SlipChip for monitoring 1000 nL scale reactions. In addition, the validation of results was carried out via counting amplified single molecules of genomic bacterial strains [59].

In spite of recent technology advances, it is still very challenging for early detection of MRSA infection in patients. This was attributed to the fact that some patients are chronic carriers of MRSA [60], hence, do not lose the infection easily and lead to further spread of infection in community and hospitals. So, for effective screening, more efficient and rapid sensing techniques are required. Hence, this challenging gap is addressed effectively by developing nanomaterial-based biosensors for rapid and early detection of MRSA.

Nanomaterials and their role

A nanomaterial is a combination of many nanoparticles which are less than 100 nm in at least one dimension. The tunable morphology and properties of the nanomaterials make them useful in many fields such as chemistry, electronics, biology and engineering etc. [61-67]. Recent advances in nanotechnology have found its application in the healthcare sector, one such application is the fabrication of nanomaterial based-biosensors, for early, rapid and accurate diagnosis of diseases. A biosensor consists of four parts: bioreceptor, transducer, signal processor and interface display. A number of samples such as cell cultures, body fluids and food samples have been used as an analyte for detection using nanomaterial biosensors. The tailored nanomaterials provide better conducting, optical and mechanical properties with higher surface areas which result in amplified signals, better efficiency and higher compatibility with biomolecules. This makes them an excellent bioreceptor and transducer for these biomaterials [68]. However, miniaturization and automation still pose a challenge for the researchers. Huang and co-workers described the use of graphene oxide (GO) to selectively adsorb single-stranded DNA from the mixture of single- and double-stranded material [69]. Table 3 shows various nanomaterial-based biosensors for detection of MRSA bacterial strains and its respective biomarkers.

Table 3 Nanomaterials used in various electrochemical techniques for detection of MRSA

Technique	Nanoparticles	LOD	Detection target	Time for Detection	Ref.
Cyclic Voltammetry	Titania nanotubes	1–10 ng · μl^{-1}	Protein 2a (PBP2a)	-	[72]
Cyclic Voltammetry	Gold and magnetic	10 pM	Genomic DNA	-	[74]
Cyclic Voltammetry	DNA nano-tetrahedron probe	10 fM ssDNA and 57 fM gDNA	ssDNA and genomic DNA (gDNA)	4 hours	[75]
SWV	Gold and magnetic	2×10^7 CFU · mL^{-1}	MRSA culture	-	[79]
EIS	Graphene Oxide (GO)	100 fM	ssDNA	-	[98]
EIS	ZnO and Ag	330 CFU · mL^{-1}	MRSA culture	50 mins	[99]
DPV	Gold	23 pM	mecA gene	2 hours	[104]

Electrochemical sensors

Electrochemical sensors provide an insight about the system/reaction in a real-time and consists of a chemically selective layer coupled with a transducer, which converts the obtained signal into an electrochemical signal, further processed to a readable analytical output. The ease of using this setup and minimal instrumentation requirement make them one of the most extensively used methods for detection purposes [70]. Electrochemical sensor possesses other advantages such as quick response, low interference and good selectivity. Various techniques that make up electrochemical sensors are characterized on the basis of electrical magnitude which is provided to the electroactive layer connected with the transducer. The different techniques used are: conductometric (variation in conductance); potentiometric (varying membrane potential); amperometric or voltammetric

(variation in current with fixed potential in the first case and current varying with applied voltage in the latter) and impedimetric (variation in the impedance) [70].

Cyclic voltammetry (CV)

In cyclic voltammetry, technique potential is applied to the working electrode, which is swept across electrode twice in both positive and negative directions with a constant rate of scan. This technique measures the current as the output as a function of the potential. This technique also helps in the determination of diffusion coefficients and area of modified electrodes for any reaction using the Randles-Sevcik equation [71]. At low amplitude currents, noise interferes in the output signals obtained during the analyte detection. This can be overcome by modification of the working electrode by nanomaterials. Mandal et al. reported an electrochemical biosensor for the detection of PBP2a protein using working electrode modified by titania nanotubes. These nanotubes were conjugated with anti-PBP2a antibody as biorecognition element. This technique provided better sensitivity as compared to conventional ELISA-based techniques [72]. However, single probe-based detection does not restrict background current in the absence of target [73]. Therefore, restrict the interference of background currents in the output signal. Suye and co-workers developed a dual probe sandwich system to detect MRSA DNA. Magnetic nanoparticles conjugated to a complementary DNA was used as the first probe. For the second probe, gold nanoparticles (AuNps) were conjugated to another complementary DNA sequence, which was further conjugated with ferrocene derivative. These probes were then incubated with the target DNA sequence, forming a complex which was separated by magnetic separation. Finally, the complex was then used for detection using cyclic voltammetry. For amplification of the output signal L-proline dehydrogenase and L-proline were employed, which on reaction provides electrons to the ferrocene derivative providing an enhanced oxidation peak, with a limit of detection (LOD) at 10 pM [74]. To further increase the sensitivity of sandwich hybridization method Liu and co-workers employed a multi labelled probe for enhancing the output signal. They

synthesized a multiple signal probes (MSP) using seven biotin-labelled system to hybridize the target gene or DNA. The detection of *mecA* gene and synthetic ssDNA by employing a sandwich like a strategy was carried out. The probes consisted of a tetrahedral nanostructure-based capture probe (TSP) which is deposited on a gold electrode through self-assembly, further modified with a *mecA* specific capture probe. Meanwhile, biotinylated reporter probe is conjugated with the target gene to produce detectable signal using polymerized streptavidin-HRP (horseradish peroxidase) conjugate. After, hybridization of the target gene with the modified gold electrode, a detectable signal is obtained in a solution of H_2O_2 and TMB. The length of the detection probes used was 12-15 nucleotides and the cyclic voltammetry technique was employed resulting in two well-defined redox peaks. The proposed sandwich probe helped to achieve LOD at 57 fM [75]. Therefore, exploring novel probes and sandwich systems that can provide an enhanced output signal should be targeted to achieve better sensitivity and higher peak currents for CV based detection methods.

Square wave voltammetry (SWV)

Square wave voltammetry (SWV) combines staircase potential with a square wave to a stationary electrode forming a linear potential sweep voltammetry. SWV technique involves a reference electrode at a constant potential with respect to which change in current at the working electrode is measured linearly in time [76]. SWV is extensively used in electrochemistry for multiple reasons such as significant time evolution between potential reversal, current sampling and high sensitivity screening [77]. These properties help to work at nanomolar analyte concentrations, providing an added advantage over CV. Although, SWV technique is widely used but kinetic studies limit its application [78]. Adam along with his co-workers (2016) developed a sandwich of two nanoparticle-based probes for the detection of MRSA. One of the probes was prepared by conjugating magnetic nanoparticles with immunoglobulin G (IgG) and the second probe was conjugated AuNPs with anti-MRSA antibody. These probes were incubated with target MRSA bacterial strains resulting in a

sandwiched product that is the fixation of MRSA between the two probes. The sandwiched product was purified and electrochemically detected using the adsorptive transfer stripping square wave voltammetry (AdTS SWV) technique with a LOD of 2×10^7 colony forming units per milliliters (CFU·mL⁻¹) for MRSA [79]. This was the first report where the detection of whole MRSA cell via an electrochemical method was carried out but failed to provide high sensitivity. In addition, they also demonstrated the affinity of IgG towards MRSA bacterial cells, which can be utilized by researchers for their future research work.

Electrical impedance spectroscopy (EIS)

This technique involves measurement of change in impedance of working electrode and helps to study surface characteristics of a material. This technique is majorly divided into electrochemical (EIS) and dielectric impedance spectroscopy (DIS). In EIS mainly materials that exhibit ionic conduction are analyzed; where as in DIS involves the analysis of dielectrics [80]. Some of the materials used are glasses [81–83], polymers [84–86] and solid or liquid electrolytes [87–89]. However, this technique also has its uses in other fields such as fuel cells [90–92], solar cells [93,94] and batteries [95–97]. Wang et al. developed an electrochemical sensor for the detection of MRSA-DNA, wherein a glassy carbon electrode (GCE) was modified by aminopropyl triethoxy silane (APTES), drop coated with GO and later reduced electrochemically. The final electrode was prepared by conjugating ssDNA, which is complementary to target DNA as shown in Figure 3. Prior and after hybridization, electrodes' EIS measurements were taken and the difference was recorded and noted, enabling determination of target DNA with 100 fM LOD [98]. The obtained result was good with low LOD, but there is chance of unwanted background currents or interfering agents leading to false signals due to single probe system. To avoid the unwanted false signals a sandwich-based probe can be a good alternative to carry out the detection. Later in 2017, Zhang and co-workers utilized vancomycin as the sensing probe to detect the target bacteria. They fabricated a fluorine-doped tin oxide (FTO) based

electrode by coating zinc oxide nanorods (ZnO) with silver nanoparticles (AgNps). Finally, vancomycin was conjugated to modified FTO electrode with the help of mercapto acetic acid (MPA) by incubation of electrode in their respective solutions. The detection was carried out via electrical impedance spectroscopic technique with a limit of detection found to be $330 \text{ CFU} \cdot \text{mL}^{-1}$ [99]. As a bioreceptor, vancomycin provided better result with higher sensitivity as compared to previous reported electrochemical technique to detect MRSA cells. The only drawback of using vancomycin as a bioreceptor is the lack of specificity. This can be attributed to the affinity of vancomycin towards gram-positive bacteria due to its glycopeptide in nature [100]. So, a better alternative to vancomycin is phages or aptamers which are highly specific and provide excellent results as well.

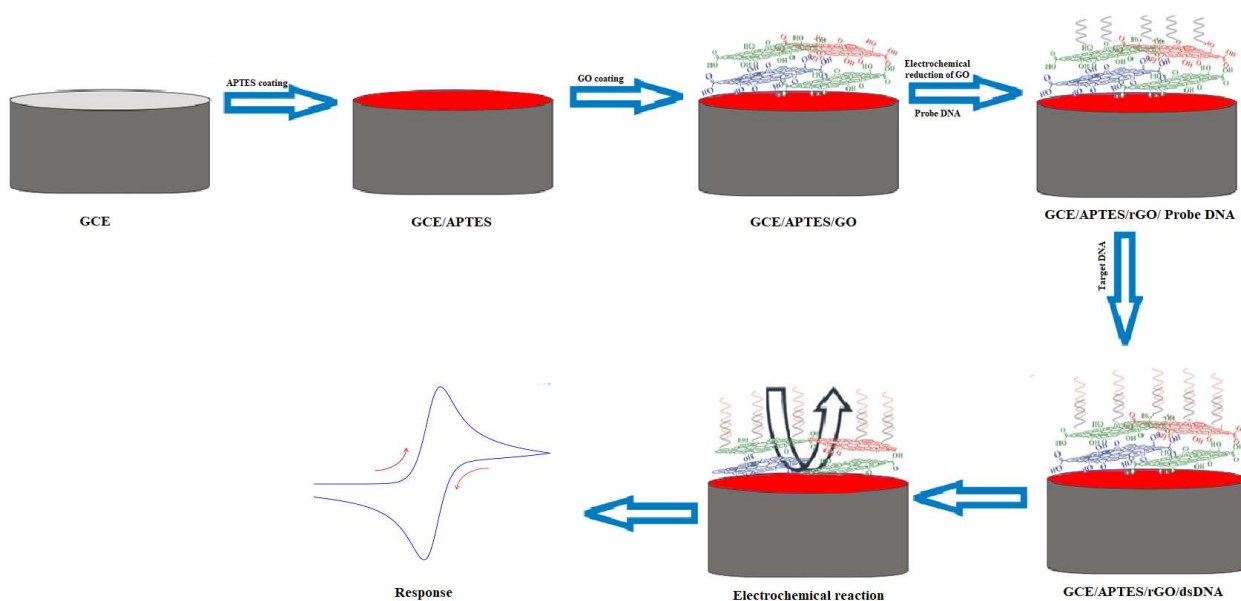


Fig 3. Schematic of the fabrication of the electrochemical biosensor.

Differential pulse voltammetry (DPV)

This voltammetry technique is a derivative of the staircase voltammetry. This involves a series of voltage pulses superimposed on potential linear sweep [101-103]. As potential changes, current is

measured along with plotting the difference. This measurement is used to study the redox properties of analytes with very low concentration values. This is achieved due to low charging currents which provide high sensitivity. Also, due to the extraction of only faradaic current, reactions at the working electrode are analyzed effectively. Liu et al. also utilized single probe system to carry out the detection of *mecA* gene. Where working electrode was modified with au-nps conjugated with a capture probe and an alkaline phosphatase to produce electrochemical signal [104]. The use of single probe resulted in 30 mins incubation time of working electrode in target gene solution to achieve hybridization. The incubation time can be reduced by using a multi-probe which would aid in faster hybridization of gene and yielding faster results.

Table 1 compiles the LOD, detection time, technique used and nano-material utilized to carry out the detection of MRSA via electrochemical techniques. It is clear from the table that sandwich probe-based detection provided better LODs. Further, IgG and vancomycin were used as biorecognition elements for detection of whole MRSA cells and it can be concluded that vancomycin was a better bioreceptor as it provided lower sensitivity.

Luminescence-based sensors

Fluorescence

Fluorescence is a phenomenon involving emission of light upon absorption of light of any wavelength or electromagnetic radiation. Generally, light emitted during fluorescence has a longer wavelength than absorbed light. The high sensitivity and selectivity of the photo- or chemifluorescence is imparted to the electronic excitation is due to luminophore or fluorophore selected, resulting in tailored wavelengths for excitation and emission [105-107]. A nanolaterns based chips [108] and cadmium telluride quantum dots (CdTe QDs) [109] conjugated with PCR amplified products for fluorescence-based detection of bacterial gene were carried out. The amplification of genes via PCR

is tedious and requires a trained professional to carry out the task. However, after hybridization the fluorescent signal obtained from nanolanters was not quantified, whereas major advantage of cadmium telluride quantum dots (CdTe QDs) was single wavelength excitation of these quantum dots using 250 nm radiation. The output signal for quantum dots was quantified and LOD at 10^2 CFU·mL⁻¹ was achieved. Quantum dots provided better fluorescent response for the detection of MRSA gene as compared to nanolanters.

A visual detection technique was developed by Chan et al. for carrying out the detection of MRSA utilizing human serum albumin (HSA) as the sensing probe. In this study, gold nanocomposites (AuNCs) were synthesized and further conjugated with HSA to test the binding affinity of HSA towards MRSA bacterial strains. HSA is known to be a carrier protein and which has proven to show a binding affinity towards various ions and species as a reducing group or chelating group. AuNCs synthesized using HSA are known to show a special affinity towards *S. aureus* and MRSA bacterial strains and hence making them a suitable probe for sensing of these bacterial strains. The aptamer sequence of HSA that was binding to MRSA bacterial strains was not found, which is still needed to be explored [110]. In another example, Chen and group synthesized silica nanoparticles based nanoprobe for specific binding and detection of bacterial strains. They created an activatable theranostic nanoprobe for sensitive near-infrared fluorescence (NIRF) imaging and photothermal therapy (PTT) of MRSA infections. This was based on poly (allylamine) coated silica-cypate (SiO₂/PAH-cy) nanosystems modified with polyethylene glycol and vancomycin-conjugated poly(acrylic acid) molecules (PAAPEG-Van). Generally, obtained nanoprobe (SiO₂-Cy-Van) are nonfluorescent in aqueous environments due to the aggregation of hydrophobic cypate (cy) fluorophores on silica nanoparticles to induce ground-state quenching. Yet in presence of MRSA, interactions between Van and MRSA were stronger than binding between PAH and silica nanoparticles. Activated fluorescence was found after incubation with MRSA cultures (10^7 CFU) for

4 hours [111]. The use of vancomycin for the detection of MRSA reduces its specificity, however, vancomycin is a good bioreceptor for whole MRSA cells which provide good sensitivity. [100].

Fluorescence based detection is considered better than electrochemical methods due to the visible response that can be attained using this technique. However, it is not able to match the low detection limits that electrochemical techniques can achieve. Therefore, using other optical methods and novel fluorescent nanomaterials can help in enhancing the response even at lower concentrations as shown in table 4.

Table 4 Nanomaterials used in various luminescence-based techniques for detection of MRSA

Technique	Nanoparticles	LOD	Detection target	Time for Detection	Ref.
Fluorescence	Nanolanterns	-	DNA	-	[108]
Fluorescence	CdTe QDs	$10^2 \text{CFU} \cdot \text{mL}^{-1}$	mecA gene	-	[109]
Fluorescence (Naked eye)	Gold composite	$10^6 \text{cells} \cdot \text{mL}^{-1}$	mecA	2 hours	[110]
Fluorescence	Silica	$10^7 \text{CFU} \cdot \text{mL}^{-1}$	MRSA bacteria	Immediate	[111]
LRET	NaYF ₄ :Yb, Er UCNs,	0.18 nM	MRSA DNA	-	[113]
FRET	GO	$0.5\text{-}40 \text{nmol} \cdot \text{L}^{-1}$	mecA gene	-	[115]
FRET	GO	$30 \text{CFU} \cdot \text{mL}^{-1}$	16 rDNA	-	[116]
SERS	Gold nanopopcorn and GO	$10 \text{CFU} \cdot \text{mL}^{-1}$	MRSA bacterial strains	-	[120]
Colorimetric	Gold nanoparticles	66 pg/ μl	Genomic DNA	-	[123]

SPR	Gold nanoparticles and rods	-	MRSA cells	-	[124]
PCR-Colorimetric	Gold	~100 ng target DNA	mecA gene	-	[125]
PCR-Colorimetric	Gold nanopartilces	500 ng and 50 ng respectively	MRSA and mecA gene	-	[126]
Colorimetric	Nano magnetic beads	-	MRSA bacterial strains	1 min.	[127]
SPR	Bacteriophages	$10^3 \text{ CFU} \cdot \text{mL}^{-1}$	MRSA culture	20 mins	[129]
LAMP-SPR	Lamp amplicons and gold	10 copies $\cdot \text{mL}^{-1}$	mecA gene	1 hour	[130]
RT-PCR	Polystyrene beads and metallic nps	~0.5 pM	PVL gene	2 hours	[132]

Luminescence resonance energy transfer (LRET)

Luminescence resonance energy transfer (LRET) is majorly employed for luminescence-based applications such as in medical diagnostics, sensing properties, DNA analysis, and optical imaging. LRET phenomenon involves energy transfer between two molecules, which helps in understanding certain biological systems and application in thin film devices and optoelectronics which helped gain it a sizeable interest of researchers in various fields [112]. A variety of new nano-chemical sensors and biosensors based on LRET phenomenon have been developed. Liu et al. prepared up-conversion nanoparticles (UCNs) based on LRET to detect MRSA DNA sequence [113]. However, major disadvantage of LRET or FRET systems is that with the change in distance between donor and

acceptor which leads to decrease in the efficiency. This was overcome by conjugating UCNs (energy donors) with oligonucleotides and TAMRA (a dye) was conjugated with nanoparticles, as the energy acceptor. No spectral overlap is observed due to the difference in the excitation wavelength of TAMRA and the UCNs. Therefore, upon the interaction with target DNA sequence, an effective LRET signal was observed with limit of detection at 0.18 nM. While, UCNs provide low LODs and act as a very good energy donor to carry out LRET, synthesis of desired UCNs is a complex procedure and requires the use of costly precursors. UCNs are generally synthesized using heavy metals which are expensive and involve complex synthesis procedures, which can be overcome by using other cheap alternative dyes or fluorescent nanomaterials such as quantum dots and GO [114]. A similar fluorescence energy transfer method was used by Chen and group using economical materials and achieved a comparable detection limit. They fabricated a GO-based sensing platform which followed the principle of strain displacement polymerization and synchronous fluorescent signal amplification for the detection of *mecA* gene. A probe labelled with FAM (carboxy-fluorescein fluorophore) over GO was prepared. The probes consisted of 2 regions, one made up of a complementary probe which would bind with the target gene and the other region was a primer which was responsible for amplification of fluorescent signals after the SYBR Green I dsDNA is formed as depicted in Figure 4. The fluorescent emission peaks were recorded at 514 nm for SYBR Green I. FAM also emitted light of the same wavelength, resulting in the amplification of the fluorescent signal with a clear response. The range of concentration of target DNA for which the fluorescent signal was obtained at 0.5-40 nmol·L⁻¹ [115]. Another system prepared by Ning et al. provided better selectivity, repeatability and removed any interference caused due to other DNAs that may be present in the system. This experimental bioassay study was carried out using FAM labelled probe with two sections over GO for FRET based detection of 16 rRNA of MRSA bacterial strain. They employed deoxyribonuclease I (DNase I) for amplification of output signal and recycling target sequence. The FAM labelled probe is attached to the GO by π -stacking, quenching its fluorescence. After

introduction of the target sequence, cleavage of FAM took place producing a target induced fluorescence signal. This signal was recorded using fluorescence spectroscopy and a detection limit of $30 \text{ CFU} \cdot \text{mL}^{-1}$ with high selectivity [116]. This technique provided a unique method to recycle the target sequence using DNase I leading to improved output signals and better repeatability. The only shortcoming of the procedure was the digestion time taken by DNase I and quenching time, which would delay the results for an hour.

LRET or FRET is a better technique as compared to fluorescence which provides better LODs and brighter output response. Even single molecule can be detected using this technique leading to lower consumption of sample reducing the amount of DNA or RNA required to extract and lowering the overall cost by reducing associated extraction process of the target molecules from cells for detection.

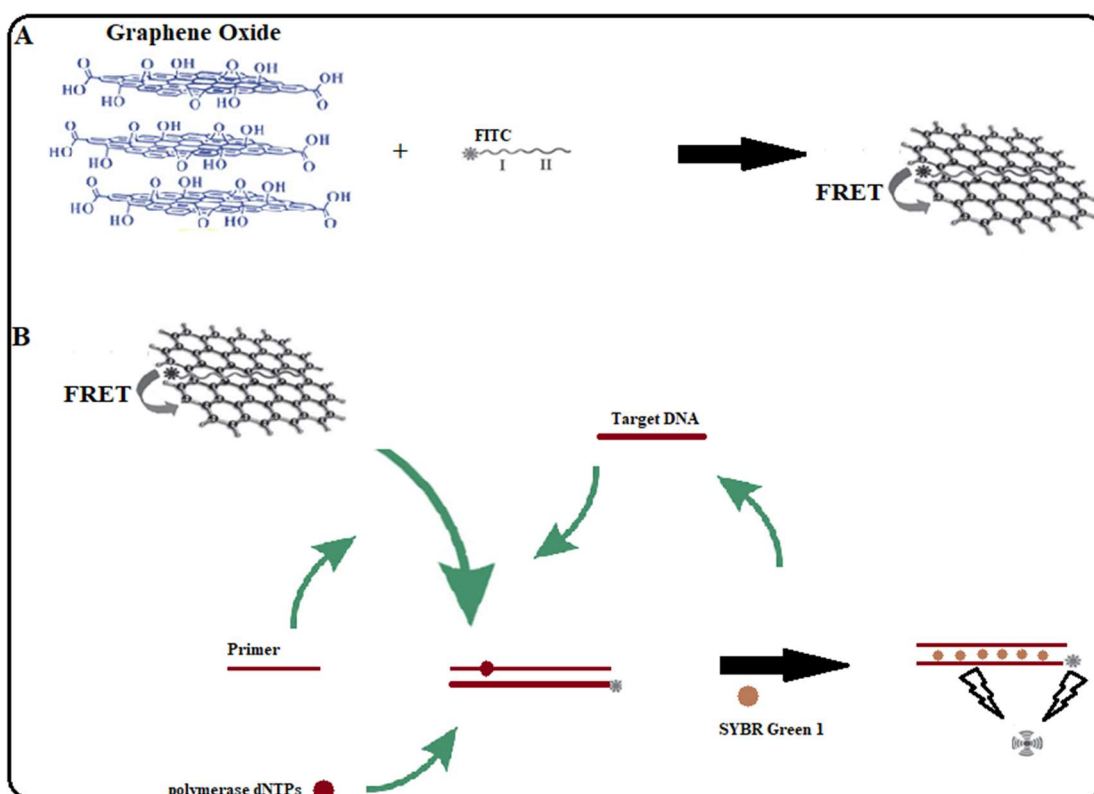


Fig 4. Schematic presentation of fluorescence resonance energy transfer process between the dye and GO

Surface-enhanced Raman spectroscopy (SERS)

Surface-enhanced Raman spectroscopy is a surface-sensitive technique that enhances Raman scattering of light by molecules adsorbed on rough metal surfaces or by nanostructures such as plasmonic-magnetic silica nanotubes [117]. The signal enhancement factor can be as much as 10^{10} to 10^{11} [118], which means this technique detected even a single molecule [119]. However, the mechanism of this technique is still not clear. It is assumed to be on the basis of either of the two theories one being electromagnetic theory and other chemical theory. The major disadvantage of this method is the requirement of labelling probe to be attach to target, which can block the reactive binding sites. To remove the interference caused by labelling probe Ray and group developed a novel SERS probe. This probe was synthesized by a four-step process based on gold nano popcorn attached to GO. This hybrid probe provided good affinity and high surface area for the attachment of complementary DNA or aptamer and removed the requirement of labelling probe to carry out detection. An aptamer known as APT^{SEBI} was chosen and immobilized on the GO hybrid for selective detection of the bacteria. Figure 5 shows the chemical (CM) enhancement in the signal by GO and the electrochemical (EM) signal enhancement due to gold nano popcorn. To study SERS signal capabilities of the prepared GO-based hybrids, Rh6G a Raman active dye was used for enhancing signals at various concentrations to study emitted SERS data and optimize the hybrid. To test the hybrid SERS probe a selective and a label-free bacterial detection was carried out for the sensing of MRSA [120]. SERS is a very effective technique with an inherent property of detection at molecular levels. Further, optofluidic devices have been fabricated as a lab-on-a-chip sensor utilizing SERS as a detection technique [121], providing a wide scope to explore in this field for the researchers.

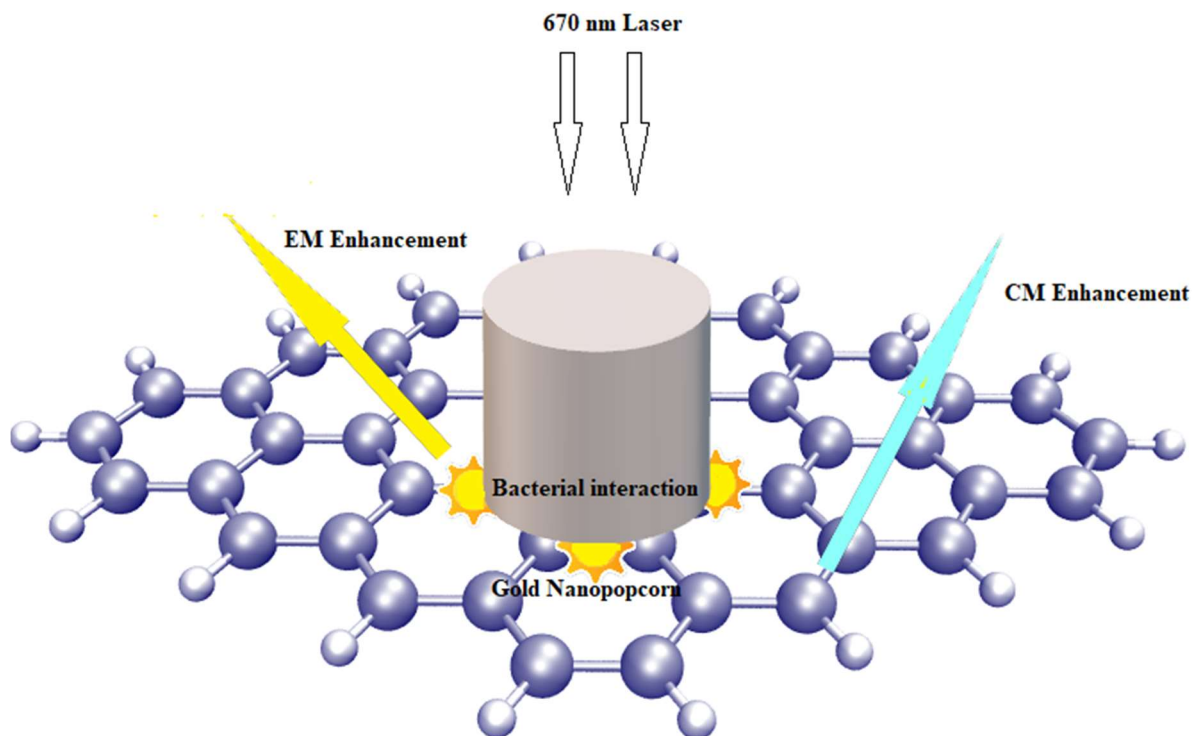


Fig 5. Schematic presentation of enhancements in the signals due to the bacterial and nanocomposite interactions for detection.

Colorimetric sensing

Colorimetric Sensing is used to determining the concentration of a certain analyte in a particular solution by a color indicator. This method can be used for all types of compounds either organic or inorganic in nature [122], with or without enzyme platform. Colorimetric detection method generally provides high detection limits due to base mismatches, insertions or deletions in the assays. However, Storhoff et al. countered this by utilizing snap freeze hybridization technique to achieve picomolar concentration of probes and femtomolar concentrations of the target sequence to carry out the detection process. They used two oligonucleotides complementary to the target sequence of the *mecA* gene as the sensing probes [123], without any amplification of the target gene sequence. The oligonucleotides were conjugated to two AuNps of different sizes having different absorption bands.

The hybridized DNA-AuNp probes immobilized on a glass slide and illuminated by white light. The change in the color indicated the detection of target DNA. Negative test control studies were also carried out successfully using the methicillin-susceptible *S. aureus*. Testing of clinical samples was also carried out and acceptable results were obtained. Another technique utilized AuNps and nanorods conjugated with target specific aptamer for detection of MRSA via surface plasmon resonance [124]. The aptamer makes for a robust sensor and is a cheaper alternative for other bioreceptors. The attachment of aptamer was carried out by “Cell-SELEX” method, which is the laborious process involved and unpredictable efficiencies they provide for the sensing platform. To carry out efficient attachment a sulphide terminated group can be attached to the aptamer which will easily conjugate with gold nanoparticles through gold-sulphur interactions.

Later, nanomaterials were introduced in PCR assays to provide an enhanced colorimetric response. Eldin and group carried out the specific detection of the *mecA* gene using AuNps conjugated with complementary ssDNA strands for the detection [125]. However, in this case, probes were amplified for better sensitivity using the PCR technique and was found compatible with the target gene sequence. This method produced visible color changes, which was confirmed using UV-spectroscopy and provided high sensitivity of 90.9% at 10 μ l of DNA target per 200 μ l of the total volume of the reaction mixture. A similar PCR-based colorimetric assay was developed by Leung and co-workers [126]. They used AuNps conjugated with *mecA* and 23rRNA specific oligonucleotides as sensing probes. However, they used AuNps to make a PCR-based colorimetric assay for detection of *mecA* gene and 23rRNA. This assay used two nanoparticle probes hybridized with *mecA* and 23rRNA genes to bring about observable color change with just 1.39% error compared to other conventional methods. Further, this method presented good results when clinical samples such as urine, blood samples and other samples from wounds, pus and other bodily fluids were used. However, there were no major advancements observed in the sensitivity of the later assay. Further, aforementioned methods involved amplification of products via PCR leading to longer detection time

and complicate the procedure. PCR is a sensitive and reliable technique with long procedure and requires preparation of target specific primers to carry out detection. Therefore, researcher have moved to other techniques to carry out rapid detection with similar or even better sensitivity.

Recently, a novel paper-based visual sensing platform was fabricated by Zourob and co-workers [127]. This was carried by using special magnetic bead complex for detection of proteolytic activity of MRSA proteases. A gold coating was put on top of the paper support which is not a robust platform and has to be handled very carefully. A self-assembled monolayer of a peptide probe was formed over the gold coating via gold-sulphur interactions. The sensing peptide probe was also conjugated to nanomagnetic bead by N-terminal interaction and the mechanism was based on a sandwich structure formed between nanobeads and a gold layer on the paper. On the back of the paper was placed an external magnet, which promotes breaking of peptide-magnetic nanobead complexes, detecting the MRSA bacterial strains. The paper-based method was an inexpensive technique with high sensitivity capable of visual detection of MRSA. The similar technique can be utilized by researchers to fabricate the sensor over a more robust surface such as plastic sheets.

Surface plasmon resonance (SPR) based on colorimetric sensing

This technique uses the incident light on a metallic material which provides resonant oscillation of the electrons present on the metal surface, which is responsible for the conduction at the interface present in the positive and negative permittivity of the material. This is the standard tool for adsorption measurement of the metallic nanoparticles. SPR is one of the fundamental principles used for the fabrication of biosensors and other lab-on-a-chip devices [128]. Tawil and coworkers utilized gold thin film to produce a recordable SPR signal for the detection of MRSA. They prepared novel phage self-assembled and immobilized on the gold surface to carry out highly specific detection of MRSA. The phage displayed good selectivity in presence of other bacterial strains and also inhibited any further growth of MRSA. Finally, the detection was carried out using SPR [129]. This method

provided low sensitivity which may be due to limited amount of phage immobilized on the gold surface or due to the improper immobilization. To improve the sensitivity of the SPR based detection, novel amplified detection probes using LAMP were employed. Nawattanapaiboon et al. used LAMP amplified products conjugated with AuNps were used as the detection probes for MRSA bacterial DNA. The detection was carried out using surface plasmon resonance of AuNps conjugates, before and after hybridization with the target DNA [130]. The AuNps provide a larger surface area and more number to bioreceptor sites as compared to gold thin films leading to better LOD.

Polymerase chain reaction (PCR) based sensing

Polymerase chain reaction (PCR) is used to amplify a single copy or a few copies of a segment of DNA across several orders of magnitude, generating thousands to millions of copies of a particular DNA sequence. In addition to its many applications in molecular biology, PCR plays a critical role in the identification of medically important sequences and can be applied for developing important diagnostic tools [131]. Weissleder and co-workers extracted bacterial RNA from the clinical specimen as a target for detection [132]. The 16S rRNA region was amplified using an asymmetric reverse transcription-PCR technique. For the detection of this target RNA sequence, Magneto-DNA assay, a sandwich hybridization technique, consisting of two sensing probes was employed. The first probe consisted of a single-stranded DNAs conjugated with polymeric (polystyrene beads) microspheres, while the second probe contained magnetic nanoparticles conjugated with the ssDNA as detection probes. Later these probes were incubated with the target genes, to form a sandwich complex and were confirmed by micro-NMR studies. Finally, the magneto-DNA assay was used for the detection of mRNA of *mecA* gene, as well as for PVL gene of MRSA strain. Rajamani et al. carried out detection of *mecA* gene using five clinical samples from different sites using PCR [133]. They employed the disc diffusion method for testing susceptibility using the methicillin strip to confirm the MRSA. After detecting MRSA, chia seed extract and silver

nanoparticles were used for treatment of MRSA and chia seeds displayed better medicinal activity as compared to silver nanoparticles.

Other techniques

Many different techniques were developed by researcher all around the world. One such technique reported by Hiremath et al. to detect MRSA cells. They synthesized a custom-made lytic phage as bioreceptor element of a biosensor for the detection by magneto-elastic (ME) strip [134], which removes the need of any amplification and detects the whole MRSA cell. A ME strip was coated with chromium, followed by a consecutive layer of gold, which was responsible for preventing corrosion and better immobilization of phages on the surface. The immobilization of phages on ME strip was an issue which can be overcome by modification of the capsid head of phage by specific functional group that will go and bind to ME platform. After immobilization of phages, incubation with bovine serum albumin (BSA) was carried out to block all unwanted binding sites. Finally, the prepared ME strip was tested for MRSA detection and the LOD was observed at $3 \log \text{CFU} \cdot \text{mL}^{-1}$.

Optical fibre-based biosensor was fabricated for highly selective detection of PBP2a protein detection. The signal produced by these sensors is proportional to concentration of the chemical or biological element that interacts with the bioreceptor inside the fibres. The signals observed are in the form of variations produced in refractive index. Utilizing this technique, Inzana and co-workers fabricated a nano-scaled self-assembled film of antibodies complementary to protein2a (PBP2a), inside an optical fibre made of the long-period grating (LPG) [135]. LPG was coated with a film poly-allylamine hydrochloride and in poly-1-[p-(3'-carboxy-4'-hydroxyphenylazo) benzene sulfonamido-1,2-ethandiyl (PCBS) with free carboxyl groups at the end. Ionic self-assembled multilayer (ISAM) of monoclonal antibodies (MAb) specific to PBP2a were deposited on the LPG. The detection was carried out by recording attenuation of light transmitted through the optic fibre after exposure to

MRSA. In this system, MRSA attenuated from 11.7-73.5% light transmitted through LPG tube, whereas any attenuation below 6.3% was recognized as the minimum cut-off value for the sensor. The problems of proposed optical fibre was hour long detection time, prone to interference producing small unwanted signals and ISAM layers are not reusable and require to be coated after single use.

A novel technique for amplification of target gene sequence LAMP has been utilized. These LAMP products act as a good bioreceptor, leading to increase in the sensitivity of sensor. Utilizing LAMP products Kong and coworkers carried out the detection of Panton-Valentine Leukocidin (PVL) gene using resistive pulse sensing (RPS) technique [136]. The amplified products were called lamplicons which were incubated with two gold nanoparticle probes and coupled via biotin-avidin coupling. These coupled particles were put in the RPS setup with a tunable pore membrane which produced a measurable resistive pulse when the nano-assembly passed through the pore. This process achieved a detection limit of as low as 530 copies of the DNA and the process is quantitative, was completed in 2 hours. Lee and co-workers made a microfluidics based diagnostic assay with sensing probes attached to magnetic beads in the microfluidic channel for the detection of target DNA from MRSA bacterial strains [137]. The microfluidic system had an inbuilt system for hybridization and amplifications of the final product. The hybridization of target DNA from clinical samples takes place with the sensing probe, which is separated and transferred for the amplification of product using LAMP technique. The final obtained LAMP products are quantitatively detected using spectroscopy. This method achieved LOD at $10 \text{ fg}\cdot\text{mL}^{-1}$, which was 1000 times higher than the conventional PCR.

The table (5) enlists LOD, detection time, technique used and nano-material used in the novel systems developed for improving the output response. The systems using LAMP amplified products or other oligonucleotide-based detection can be made compatible for the detection of whole bacterial cells. This can be done by employing the appropriate biorecognition such as bacteriophage or other cell specific aptamers, which would reduce the work required to be carried out for amplification and

isolation of genes. Therefore, leading to direct detection of MRSA bacterial cells from the swabs taken from patients to perform on spot detection.

Table 5 Novel techniques and methods developed for detection of MRSA using nanomaterials

Magneto-elastic	Phage	3 log CFU·mL ⁻¹	MRSA culture	30 mins (immobilization time)	[134]
Optical fibre	ISAM ¹	10 ² CFU·mL ⁻¹	Protein 2a (PBP2a)	50 mins	[135]
RPS ²	Gold	530 copies of DNA	DNA	2 hours	[136]
Micro fluidic system	Magnetic beads	10 fg·mL ⁻¹	DNA	-	[137]
LFI- strip ³	Nano-collidal gold-based assay	2 CFU per 100g pork product	mecA	3 mins	[139]
LFB ⁴	Streptavidin-coated polymer nanoparticles	100 fg DNA per reaction	mecA	85 mins	[140]
ClearRead ⁵	Gold and Silver	500 ng or 10 ⁸ DNA molecules	mecA gene	30 mins	[141]

Point-of-care devices as an alternative to laboratory tests have been providing enticing results in theory and as a proof of concept at academic level [138]. One such paper-based devices that have caught interest of the researchers is the lateral flow immunoassay technology. A novel nano-colloidal

¹ ISAM- Ionic Self-assembled Multilayer

² RPS- Resistive Pulse Sensing

³ LFI- Lateral Flow Immunoassay

⁴ LFB- Lateral Flow Biosensor

⁵ ClearRead- a point-of-care diagnostic system used to carry out genomic detection at clinical level.

gold-based lateral flow immunoassay (LFI) strip was developed by Lu and co-workers to carry out detection of *mecA* gene [139]. Firstly, PCR amplification of the *mecA* gene was carried out with help of a pair of chemically labelled primers with fluorescein isothiocyanate (FITC). The conjugated colloidal-AuNPs labelled with anti-FITC polyclonal antibody was sprayed onto (Lateral flow immunoassay) LFI strip. Further, the amplified genes were used in a nano-colloidal gold-based assay in the LFI strip for detecting the extracted DNA. The detection has to be carried out very precisely to counter the issue of high precision which causes variations in the sensitivity even if a minor change occurs in the volume of the sample introduced to the strip. These challenges were addressed by Wang et al. and fabricated a reusable strip-based biosensor that could be used up to three times. The disposable lateral flow biosensor (LFB) was employed by to carry out the detection of MRSA (*mecA*) and *S. aureus* (*nuc*) bacterial strains [140]. They used multiple cross displacement amplification (MCDA) to amplify the gene specific sensor probes which help to carryout highly specific and selective detection. The LFB platform was modified with streptavidin-coated polymer nanoparticles (SA-DNPs) as the dye indicator responsible for the crimson color. The crimson colored line on LFB platform was observed when formation of complex between MCDA probes, SA-DNPs and the gene indicating detection of desired gene. The method could not only detect but also differentiate between the MRSA and *S. aureus* bacterial strains. The contamination from the previous results could be removed using AUDG enzyme and dUTP. It took 85 minutes to obtain results and provided detection limit of 100 fg DNA per reaction (in culture).

To compete with the emerging market of the next-gen diagnostics, LFI strips need to be reproduceable, sensitive, ease of operation and should provide results at par with the clinical systems. Further, efficiency the system can be improved by the addition of tailored nanomaterials such as quantum dots and UCNs into strips leading to better fluorescent signals and increased sensitivity.

Another novel point of care device was fabricated by Ramakrishnan et al. for the detection of *mecA* gene in clinical samples [141]. The procedure was called ClearRead (Figure 6), a customized colorimetric assay for detection of DNA molecules without any amplification. In this method, oligonucleotides are bound to a solid matrix as well as conjugated with AuNPs. The AuNPs were catalytically coated with silver resulting in a six-fold increase in the output signal while requiring only about ~500ng or 10^8 DNA molecules to detect target molecules such as *mecA* gene. This method was developed for detection of specific genomic sequences in clinical samples utilizing oligonucleotides and utilized light emitting diodes (LEDs) along with semiconductor sensor for carrying out the detection. Detection of various genomic sequences could be carried out using ClearRead at the clinical level.

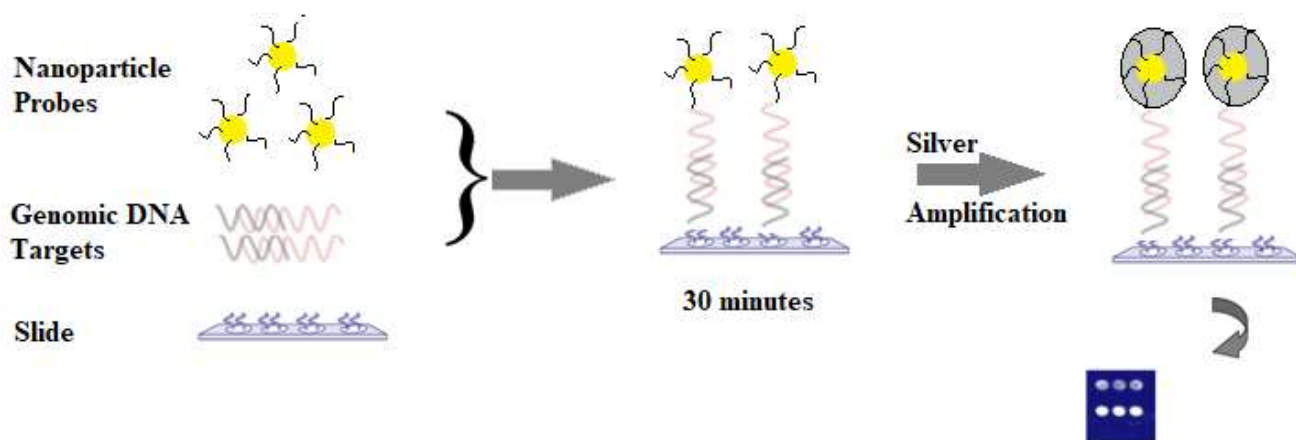


Fig 6. Schematic presentation of ClearRead procedure.

Conclusions and outlook

In the last two decades, methicillin-resistant *Staphylococcus aureus* has increased the burden on the healthcare system globally, with a mortality ratio of 64% [142]. With the ever-increasing number of MRSA (HA-MRSA and CA-MRSA) patients reported, the economic burden associated with the management of antibiotic-resistant infections be becoming a challenging task. The management and

treatment of HA-MRSA and CA-MRSA require skilled healthcare professionals and technicians to perform microbiological assays and handling of sophisticated instruments, indirectly increasing the cost. It has been estimated that the detection of MRSA cost around \$34,000 million in the United States and around €1500 million in Europe [143].

Despite the cost, automation and other advancements in conventional methods for detection of MRSA are still time-consuming and labour intensive. The use of nanomaterials in conventional colorimetric assays and as markers in PCR, help to enhance the sensitivity, specificity and selectivity. However, even after subsequent improvements, response time remains an issue. Therefore, rapid and accurate identification of MRSA is a prime concern for researchers. MRSA is no longer a medical issue of any particular country instead, it has become a global challenge and If not detected precisely on time is life-threatening with limited therapeutic choices.

To overcome this issue and for miniaturization of the sensing device, nanomaterial-based detection techniques are fast emerging. These techniques provide promising response time and even better selectivity and sensitivity towards MRSA biomarkers. Nanomaterials with promising optical, electrochemical and mechanical properties have been used for the fabrication of biosensor devices. Various electrochemical, fluorescence and mechanical based sensors have been fabricated for detection of various MRSA biomarkers. Many of these techniques developed have also been employed to detect MRSA in a clinical sample, presenting outstanding results. The colorimetric nanomaterial-based MRSA sensors have also shown outstanding results and results can be observed by unassisted eye, without the involvement of any complex instrumentation. Despite rapid advance in nanomaterial-based biosensors technology, yet there is no commercial sensor available for MRSA detection, due to few challenges still left to tackle. One such challenge faced is that many of the biosensors developed still require amplification of genes or DNA, prior to their detection. The reduction in time, selectivity and sensitivity are important characteristics that nanomaterial-based

biosensors should possess. However, current nanomaterial-based sensors fail at pre-clinical and clinical level due to inconsistent results. This can be accounted for the toxic effects that nanoparticles or nanomaterial may have on the human skin or body in general.

In this review, we try to provide insight into the recent advances in detection techniques for MRSA bacterial strains. Meanwhile, new biofunctionalized and biocompatible nanomaterials are emerging which help in reducing the toxicity towards the human body. This provides a wide scope and possibility for the application of nanomaterials for direct and on-spot detection of MRSA infection with desirable accuracy and speed. These functionalized nanomaterials would also open up a promising path for lab-on-a-chip and point-of-care devices and will aid in lowering secondary infections, mortality rate and economic burden.

References

1. Akhtar N (2010) Hospital acquired infections in a medical intensive care unit. *J. College Physic. Surgeons-Pakistan* 20 (6): 386–90.
2. Yang Y, Hu Z, Shang W, Hu Q, Zhu J, Yang J, Peng H, Zhang X, Liu H, Cong Y, Li S, Hu X, Zhou R, Rao X (2017) Molecular and phenotypic characterization revealed high prevalence of multidrug-resistant methicillin-susceptible *Staphylococcus aureus* in Chongqing, Southwestern China. *Microb Drug Resist* 23: 241-246.
3. Campoccia D, Montanaro L, Arciola CR (2006) The significance of infection related to orthopedic devices and issues of antibiotic resistance. *Biomaterials* 27:2331–2339.
4. Parmar A, Lakshminarayanan R, Iyer A, Mayandi V, Goh ETL, Lloyd DG, Maddar A (2018) Design and Syntheses of Highly Potent Teixobactin Analogues against *Staphylococcus aureus*, Methicillin-Resistant *Staphylococcus aureus* (MRSA), and Vancomycin-Resistant Enterococci (VRE) in Vitro and in Vivo. *J Med Chem* 61(5): 2009–2017. <https://doi.org/10.1021/acs.jmedchem.7b01634>
5. Kanafani ZA, Fowler VG (2009) Evans' Infections of Humans: Staphylococcal Infections. In: Brachman P., Abrutyn E. (eds) *Bacterial Infections of Humans*. Springer, Boston, MA.
6. Furukawa S, Kuchma S L, O'Toole GA (2006) Keeping Their Options Open: Acute versus Persistent Infections. *Journal of Bacteriology* 188(4): 1211–1217. <http://doi.org/10.1128/JB.188.4.1211-1217.2006>
7. Levy SB, Marshall B (2004) Antibacterial resistance worldwide: causes, challenges and responses. *Nature Medicine* volume10: S122–S129.

8. Klevens, R. Monina, Melissa A. Morrison, Joelle Nadle, Susan Petit, Ken Gershman, Susan Ray, Lee H. Harrison (2007) Invasive methicillin-resistant *Staphylococcus aureus* infections in the United States. *Jama* 298 (15): 1763-1771.
9. Herber OR, Schnepf W, Rieger MA (2007) A systematic review on the impact of leg ulceration on patients' quality of life. *Health and Quality of Life Outcomes* 5(1): 44.
10. Kuehnert MJ, Hill HA, Kupronis BA, Tokars JJ, Solomon SL, Jernigan DB (2005) Methicillin-resistant-*Staphylococcus aureus* hospitalizations. United States. *Emerg Infect Dis* 11: 868–872.
11. Yoshikawa TT, Bradley SF (2002) *Staphylococcus aureus* infections and antibiotic resistance in older adults. *Clinical infectious diseases* 34(2): 211-216.
12. Jones ME, Draghi DC, Thornsberry C, Karlowsky JA, Sahm DF, Wenzel RP (2004) Emerging resistance among bacterial pathogens in the intensive care unit—a European and North American Surveillance study (2000–2002). *Ann. Clin Microbiol Antimicrob* 29: 3–14.
13. Guidelines for UK practice for the diagnosis and management of methicillin-resistant *Staphylococcus aureus* MRSA infections presenting in the community (2008) *Journal of Antimicrobial Chemotherapy*
14. Palavecino E (2004) Community-acquired methicillin-resistant *Staphylococcus aureus* infections. *Clin Lab Med* 24: 403–418.
15. Okuma K, Iwakawa K, Turnidge JD et al (2002) Dissemination of new methicillin-resistant *Staphylococcus aureus* clones in the community. *J Clin Microbiol* 40:4289–4294.
16. Strimbu K, Tavel JA (2010) What are Biomarkers? *Curr Opin HIV AIDS*. 5(6): 463–466.

17. International Working Group on the Classification of Staphylococcal Cassette Chromosome Elements (IWG-SCC) (2009) Classification of Staphylococcal Cassette Chromosome mec (SCCmec): Guidelines for Reporting Novel SCCmec Elements. *antimicrobial agents and chemotherapy* 53: 4961–4967. doi:10.1128/AAC.00579-09
18. Munita JM, Arias CA (2016) Mechanisms of Antibiotic Resistance. *Microbiol Spectr.* 4(2) doi: 10.1128/microbiolspec.VMBF-0016-2015
19. Szmiegielski S, Prevost G, Monteil H (1999) Leukocidal toxins of staphylococci". *Zentralbl Bakteriol* 289 (2): 185–201. doi:10.1016/S0934-8840(99)80105-4.
20. Kaneko J, Kamio Y (2004) Bacterial two-component and hetero-heptameric pore-forming cytolytic toxins: structures, pore-forming mechanism, and organization of the genes. *Biosci Biotechnol Biochem* 68 (5): 981–1003. doi:10.1271/bbb.68.981.
21. Goering RV, McDougal LK, Fosheim GE, Bonnstetter KK, Wolter DJ, Tenover FC (2007) Epidemiologic distribution of the arginine catabolic mobile element among selected methicillin-resistant and methicillin-susceptible *Staphylococcus aureus* isolates. *J Clin Microbiol* 45 (6):1981-4. doi:10.1128/JCM.00273-07.
22. Takadama S, Nakaminami H, Sato A, Shoshi M, Fujii T, Noguchi N (2018) Dissemination of Pantone-Valentine leukocidin-positive methicillin-resistant *Staphylococcus aureus* USA300 clone in multiple hospitals in Tokyo, Japan. *Clin Microbiol Infect.* doi: 10.1016/j.cmi.2018.02.012
23. Ellington MJ, Yearwood L, Ganner M, East C, Kearns AM (2008) Distribution of the ACME-arcA gene among methicillin-resistant *Staphylococcus aureus* from England and Wales. *J Antimicrob Chemother* 61:73–77. doi:10.1093/jac/dkm422

24. Paul SK, Ghosh S, Kawaguchiya M, Urushibara N, Hossain MA, Ahmed S, Mahmud C, Jilani MSA, Haq JA, Ahmed AA, Kobayashi N (2014) Detection and Genetic Characterization of PVL-Positive ST8-MRSA-IVa and Exfoliative Toxin D-Positive European CA-MRSA-Like ST1931 (CC80) MRSA-Iva Strains in Bangladesh. *Microb Drug Resist* 20(4):325-36. doi: 10.1089/mdr.2013.0153.
25. Chadwick SG, Prasad A, Smith WL, Mordechai E, Adelson ME, Gyax SE (2013) Detection of Epidemic USA300 Community-Associated Methicillin-Resistant *Staphylococcus aureus* Strains by Use of a Single Allele-Specific PCR Assay Targeting a Novel Polymorphism of *Staphylococcus aureus* pbp3. *J Clin Microbiol* 51(8):2541-50. doi:10.1128/JCM.00417-13.
26. Cho IH, Irudayaraj J (2013) In-Situ Immuno-Gold Nanoparticle Network ELISA Biosensors for Pathogen Detection. *Int J Food Microbiol* 164(1):70-75.
27. Yu H, Zhao G, Dou W (2015) Simultaneous Detection of Pathogenic Bacteria using Agglutination Test based on Colored Silica Nanoparticles. *Curr Pharm Biotechnol* 16 (8): 716-723.
28. Onori M, Coltella L, Mancinelli L, Argentieri M, Menichella D, Villani A, Grandin A, Valentini D, Raponi M, Russo C (2014) Evaluation of a Multiplex PCR Assay for Simultaneous Detection of Bacterial and Viral Enteropathogens in Stool Samples of Paediatric Patients. *Diagn Microbiol Infect Dis* 79 (2): 149-154.
29. Sheu DS, Wang YT, Lee CY (2000) Rapid Detection of Poly hydroxy alkanoate-Accumulating Bacteria Isolated from the Environment by Colony PCR. *Microbiology* 146 (8): 2019-2025.
30. Oblath EA, Henley WH, Alarie JP, Ramsey JM (2013) A Microfluidic Chip Integrating DNA Extraction and Real-Time PCR for the Detection of Bacteria in Saliva. *Lab Chip* 13 (7): 1325-1332.

31. Yuen JWM, Chung TWK, Loke AY (2015) Methicillin-Resistant *Staphylococcus aureus* (MRSA) Contamination in Bedside Surfaces of a Hospital Ward and the Potential Effectiveness of Enhanced Disinfection with an Antimicrobial Polymer Surfactant. *Int J Environ Res Publ Health* 12: 3026-3041.
32. Silbert S, Kubasek C, Uy D, Widen R (2014) Comparison of ESwab with Traditional Swabs for Detection of Methicillin-Resistant *Staphylococcus aureus* Using Two Different Walk-Away Commercial Real-Time PCR Methods. *J Clin Microbiol* 52: 2641-2643.
33. Hombach H, Maurer FP, Pfiffner T, Böttger EC, Furrer R (2015) Standardization of Operator-Dependent Variables Affecting Precision and Accuracy of the Disk Diffusion Method for Antibiotic Susceptibility Test. *J Clin Microbiol* 53: 3864-3869.
34. Shin JH, Kim EC, Kim S, Koh EH, Lee DH, Koo SH, Cho JH, Kim JS, Ryoo NH (2013) A multicentre study about pattern and organisms isolated in follow-up blood cultures. *Annals of Clinical Microbiology* 16(1): 8-12.
35. Robotham JV, Graves N, Cookson BD, Barnett AG, Wilson JA, Edgeworth JD, Batra R, Cuthbertson BH, Cooper BS (2011) Screening, isolation, and decolonisation strategies in the control of methicillin resistant *Staphylococcus aureus* in intensive care units: cost effectiveness evaluation. *Bmj* 343: p.d5694.
36. Stürenburg E, (2009) Rapid detection of methicillin-resistant *Staphylococcus aureus* directly from clinical samples: methods, effectiveness and cost considerations. *GMS German Medical Science* 7.
37. Matsui H et al (2011) Development of an Immunochromatographic Strip for Simple Detection of Penicillin-Binding Protein 2a. *Clin Vaccine Immunol* 18:248-253
38. Liu Y et al (2014) Development of an immunoaffinity solid phase microextraction method for the identification of penicillin binding protein 2a. *J Chromatogr A* 1364:64-73 (2014).

39. Kumar SM et al. (2008) Current Trends in Rapid Diagnostics for Methicillin-Resistant *Staphylococcus aureus* and Glycopeptide-Resistant *Enterococcus* Species. *J Clin Microbiol* 46:1577-1587.
40. Coia JE, Duckworth GJ, Edwards DI, Farrington M, Fry C, Humphreys H et al (2006) Guidelines for the control and prevention of methicillin-resistant *Staphylococcus aureus* (MRSA) in healthcare facilities. *J Hosp Infect* 63 suppl 1:S1-44
41. Ellem JA, Olma T, O'Sullivan MVN (2015) Rapid Detection of Methicillin-Resistant *Staphylococcus aureus* and Methicillin-Susceptible *S. aureus* Directly from Positive Blood Cultures by Use of the BD Max Staph SR Assay. *J Clin Microbiol* 53:3900-3904.
42. Warnke P, Frickmann H, Ottl P, Podbielski, A. (2014) Nasal Screening for MRSA: Different Swabs – Different Results. *PLoS One* 9:e111627.
43. Holtfreter S, Grumann D, Balau V, Barwich A, Kolata J, Goehler A, Weiss S, Holtfreter B, Bauerfeind SS, Döring P, Friebe E, Haasler N, Henselin K, Kühn K, Nowotny S, Radke D, Schulz K, Schulz SR, Trübe P, Vu CH, Walther B, Westphal S, Cuny C, Witte W, Völzke H, Grabe HJ, Kocher T, Steinmetz I, Bröker BM(2016) Molecular epidemiology of *Staphylococcus aureus* in the general population in Northeast Germany-results of the Study of Health in Pomerania (SHIP-TREND-0). *J. Clin. Microbiol* 54(11): 2774–2785., doi: 10.1128/JCM.00312-16.
44. Faron ML, Buchan BW, Vismara C, Lacchini C, Bielli A, Gesu G, Liebrechts T, van Bree A, Jansz A, Soucy G, Korver J, Ledeboer NA (2016) Automated Scoring of Chromogenic Media for the Detection of MRSA Using the WASPLab Image Analysis Software. *J Clin Microbiol* 54: 620-624.
45. Rajendran R, Rayman G (2014) Point-of-Care Blood Glucose Testing for Diabetes Care in Hospitalized Patients: An Evidence-Based Review. *J Diabetes Sci Technol* 8(6):1081-1090.

46. Warnke P, Annette Devide, Mirjam Weise, Hagen Frickmann, Norbert Georg Schwarz, Holger Schäffler, Peter Ottl, Andreas Podbielski (2016) Utilizing Moist or Dry Swabs for the Sampling of Nasal MRSA Carriers? An In Vivo and In Vitro Study. PLoS One 11(9):e0163073
47. Pinchuk IV, Beswick EJ, Reyes VE (2010) Staphylococcus enterotoxins. Toxins (Basel) 2(8):2177–2197.
48. Wu S, Duan N, Gu H, Hao L, Ye H, Gong W, Wang Z (2016) A review of the methods for detection of staphylococcus aureus enterotoxins. Toxins (Basel) 8(7): pii: E176. doi:10.3390/toxins8070176.
49. Poil MA, Rivera VR, Neal D (2002) Sensitive and specific colorimetric ELISAS for Staphylococcus aureus enterotoxins A and B in urine buffer. Toxicon 40(12):1723-6.
50. Templeman LA, King KD, Anderson GP, Ligler FS (1996) Quantitating staphylococcal enterotoxin B in diverse media using a portable fiber-optic biosensor. Anal Biochem 233:50-57.
51. Goldman ER, Anderson GP, Tran PT, Mattoussi H, Charles PT, Mauro JM (2002) Conjugation of luminescent quantum dots with antibodies using an engineered adaptor protein to provide new reagents for fluorimmunoassays. Anal Chem 74(4):841-7.
52. Poojary NS, Ramlal S, Urs RM, Sripathy MH, Batra HV (2014) Application of monoclonal antibodies generated against Pantone-Valentine Leukocidin (PVL-S) toxin for specific identification of community acquired methicillin resistance Staphylococcus aureus. Microbiol Res 169(12):924-30. doi: 10.1016/j.micres.2014.05.002.
53. Prevost G, Cribier B, Couppez P, Petiau P, Supersac G, Finck-Barbançon V, Monteil H, Piemont Y (1995) Pantone-Valentine leucocidin and gamma-hemolysin from Staphylococcus aureus ATCC

49775 are encoded by distinct genetic loci and have different biological activities. *Infect Immun* 63(10):4121-9.

54. Poojary NS, Ramlal S, Urs RM, Sripathy MH, Batra HV (2014) Application of monoclonal antibodies generated against Panton-Valentine Leukocidin (PVL-S) toxin for specific identification of community acquired methicillin resistance *Staphylococcus aureus*. *Microbiol Res* 169(12):924-30.

55. Malhotra-Kumar S, Haccuria K, Michiels M, Ieven M, Poyart C, Hryniewicz W, Goossens H; MOSAR WP2 Study Team (2008) Current trends in rapid diagnostics for methicillin-resistant *Staphylococcus aureus* and glycopeptide-resistant enterococcus species. *J Clin Microbiol* 46(5):1577-87a

56. Nijhuis RH, van Maarseveen NM, van Hanne EJ, van Zwet AA, Mascini EM (2014) A rapid and high-throughput screening approach for methicillin-resistant *Staphylococcus aureus* based on the combination of two different real-time PCR assays. *J Clin Microbiol* 52(8):2861-7.

57. Liu Y, Zhang J, Ji Y (2016) PCR-based Approaches for the Detection of Clinical Methicillin-resistant *Staphylococcus aureus*. *Open Microbiol J* 10: 45-56.

58. Toleman MS, Reuter S, Coll F, Harrison EM, Blane B, Brown NM, Török ME, Parkhill J, Peacock SJ (2016) Systematic Surveillance Detects Multiple Silent Introductions and Household Transmission of Methicillin-Resistant *Staphylococcus aureus* USA300 in the East of England. *J Infect Dis* 214(3):447-53.

59. Shen F, Davydova EK, Du W, Kreutz JE, Piepenburg O, Ismagilov RF (2011) Digital isothermal quantification of nucleic acids via simultaneous chemical initiation of recombinase polymerase amplification reactions on SlipChip. *Anal Chem* 83(9):3533-40

60. Michael S. Calderwood (2015) Editorial Commentary: Duration of Colonization with Methicillin-Resistant *Staphylococcus aureus*: A Question with Many Answers. *Clin Infect Dis* 60(10):1497–1499.
61. Xu J, Wang Y, Hu S. (2017) Nanocomposites of graphene and graphene oxides: Synthesis, molecular functionalization and application in electrochemical sensors and biosensors. A review. *Microchim Acta* 184:1. <https://doi.org/10.1007/s00604-016-2007-0>
62. Liu Y, Yu J (2016) Oriented immobilization of proteins on solid supports for use in biosensors and biochips: a review. *Microchim Acta* 183:1. <https://doi.org/10.1007/s00604-015-1623-4>
63. Xu S (2012) Electromechanical biosensors for pathogen detection. *Microchim Acta* 178:245. <https://doi.org/10.1007/s00604-012-0831-4>
64. Zhong Z, Gao X, Gao R et al (2018) Selective capture and sensitive fluorometric determination of *Pseudomonas aeruginosa* by using aptamer modified magnetic nanoparticles. *Microchim Acta* 185:377. <https://doi.org/10.1007/s00604-018-2914-3>.
65. Shoaie N, Forouzandeh M, Omidfar K (2018) Voltammetric determination of the *Escherichia coli* DNA using a screen-printed carbon electrode modified with polyaniline and gold nanoparticles. *Microchim Acta*. 185: 217. <https://doi.org/10.1007/s00604-018-2749-y>
66. Liu AZZ, Bodapati S, Teed R, Vaithilingam S, Khuri-Yakub BT, Chen X, Dai H, Gambhir SS (2010) Ultrahigh sensitivity carbon nanotube agents for photoacoustic molecular imaging in living mice. *Nano. Lett.* 10 2168–2172.
67. Strayer AL, Ochoy I, Tan W, Jones J, Paret M (2016) Low concentrations of a silver-based nanocomposite to manage bacterial spot of tomato in the greenhouse. *Plant Disease* 7 1460–1465.

68. Colvin VL (2004) The potential environmental impact of engineered nanomaterials, *Nat Biotechnol* 22(6):760.
69. Huang PJJ, Liu J (2013) Separation of short single- and double-stranded DNA based on their adsorption kinetics difference on graphene oxide. *Nanomaterials (Basel)* 3(2):221-228
70. Antuña-Jiménez D, Díaz-Díaz G, Blanco-López MC, M. Lobo-Castañón J, Miranda-Ordieres AJ, Tuñón-Blanco P (2012) Chapter 1 - Molecularly Imprinted Electrochemical Sensors: Past, Present, and Future. *Molecularly Imprinted Sensors*, Pages 1-34.
71. Faulkner LR, Bard AJ (2001) *Electrochemical Methods: Fundamentals and Applications*, John Wiley, New York. 2: 482
72. Mandal SS, Navratna V, Sharma P, Gopal B, Bhattacharyya AJ (2014) Titania nanotube-modified screen-printed carbon electrodes enhance the sensitivity in the electrochemical detection of proteins. *Bioelectrochemistry* 98:46–52.
73. Xia F, White RJ, Zuo X, Patterson A, Xiao Y, Kang D, Gong X, Plaxco KW, Heeger AJ (2010) An Electrochemical Super Sandwich Assay for Sensitive and Selective DNA Detection in Complex Matrices. *J. AM. CHEM. SOC.* 132, 14346–14348
74. Watanabe K, Kuwata N, Sakamoto H, Amano Y, Satomura T, Suye S-I (2015) A smart DNA sensing system for detecting methicillin-resistant *Staphylococcus aureus* using modified nanoparticle probes. *Biosens Bioelectron* 67:419-23
75. Xu L, Liang W, Wen Y, Wang L, Yang X, Ren S, Jia N, Zuo X, Liu G (2017) An ultrasensitive electrochemical biosensor for the detection of *mecA* gene in methicillin-resistant *Staphylococcus aureus*. *Biosens Bioelectron* 99:424-430

76. Louis R., Krause MS (2002) Theory of square wave voltammetry. *Analytical Chemistry* 41(11):1362–1365. doi:10.1021/ac60280a005.
77. Chen A, Shah B (2013) Electrochemical sensing and biosensing based on square wave voltammetry. *Analytical Methods* 5(9): 2158-2173.
78. Osteryoung JG, Osteryoung RA (1985) Instrumentation. *Anal. Chem.* 57 (1): 101–110.
79. Cihalova K, Hegerova D, Dostalova S, Jelinkova P, Krejcova L, Milosavljevic V, Krizkova S, Kopelab P, Adam V (2016) Particle-based immunochemical separation of methicillin resistant *Staphylococcus aureus* with indirect electrochemical detection of labelling oligonucleotides. *Anal Methods* 8:5123.
80. Macdonald JR (1992) Impedance spectroscopy. *Ann Biomed Eng* 20(3):289–305.
81. Al-syadi AM, Yousef ES, El-Desoky MM, Al-Assiri MS (2013) Impedance spectroscopy of V₂O₅–Bi₂O₃–BaTiO₃ glass–ceramics. *Solid State Sci* 26:72–82. doi: 10.1016/j.solidstatesciences.2013.10.002
82. Hernández S, Tortello M, Sacco A, Quaglio M, Meyer T, Bianco S (2014) New transparent laser-drilled fluorine-doped tin oxide covered quartz electrodes for photo-electrochemical water splitting. *Electrochim Acta* 131:184–94.
83. Lanfredi S, Saia PS, Lebullenger R, Hernandez AC (2002) Electric conductivity and relaxation in fluoride, fluorophosphate and phosphate glasses: analysis by impedance spectroscopy. *Solid State Ion* 146:329–39.
84. Robinson JF, Kayinamura YP (2009) Charge transport in conducting polymers: insights from impedance spectroscopy. *Chem Soc Rev* 38:3339–47.

85. Stassi S, Sacco A, Canavese G (2014) Impedance spectroscopy analysis of the tunneling conduction mechanism in piezoresistive composites. *J Phys D: Appl Phys* A 47:345306.
86. Scrosati B, Croce F, Persi L (2000) Impedance spectroscopy study of PEO-based nanocomposite polymer electrolytes. *J Electrochem Soc* 147:1718–21.
87. Pollard R, Comte T (1989) Determination of transport properties for solid electrolytes from the impedance of thin layer cells. *J Electrochem Soc* 136:3734–48.
88. Robertson B, Tribollet B, Deslouis C (1988) Measurement of Diffusion Coefficients by DC and EHD Electrochemical Methods. *J Electrochem Soc* 135:2279–84.
89. Bousse L, Bergveld P (1983) On the impedance of the silicon dioxide/electrolyte interface. *J Electroanal Chem Interfacial Electrochem* 152:25–39.
90. Roy SK, Orazem ME (2007) Error Analysis of the Impedance Response of PEM Fuel Cells. *J Electrochem Soc* 154: B883–B891.
91. Costamagna P, Costa P, Antonucci V (1998) Micro-modelling of solid oxide fuel cell electrodes. *Electrochim Acta* 43:375–94.
92. Hidalgo D, Sacco A, Hernández S, Tommasi T (2015) Electrochemical and impedance characterization of Microbial Fuel Cells based on 2D and 3D anodic electrodes working with seawater microorganisms under continuous operation. *Bioresour Technol* 195:139–46.
93. Kumar S, Singh PK, Chilana GS (2009) Study of silicon solar cell at different intensities of illumination and wavelengths using impedance spectroscopy. *Sol Energy Mater Sol Cells* 93:1881–4.

94. Halme J, Vahermaa P, Miettunen K, Lund P (2010) Device physics of dye solar cells. *Adv Mater* 22:E210–E234.
95. Cui N, Luo JL. (2000) An AC impedance study of self-discharge mechanism of nickel–metal hydride (Ni–MH) battery using Mg₂Ni-type hydrogen storage alloy anode. *Electrochim Acta* 45:3973–81.
96. Sun Y-K, Kim D-W, Choi Y-M (1999) Synthesis and characterization of spinel LiMn₂–xNi_xO₄ for lithium/polymer battery applications. *J Power Sources* 79:231–7.
97. Lamberti A, Garino N, Sacco A, Bianco S, Chiodoni A, Gerbaldi C (2015) As-grown vertically aligned amorphous TiO₂ nanotube arrays as high-rate Li-based microbattery anodes with improved long-term performance. *Electrochim Acta* 151:222–9.
98. Wang Z, Zhang J, Chen P, Zhou X, Yang Y, Wu S, Niu L, Han Y, Wang L, Chen P, Boey F, Zhang Q, Liedberg B, Zhang H (2011) Label-free, electrochemical detection of methicillin-resistant staphylococcus aureus DNA with reduced graphene oxide-modified electrodes. *Biosens Bioelectron* 26: 3881–3886.
99. Yang Z, Wang Y, Zhang D (2017) A novel multifunctional electrochemical platform for simultaneous detection, elimination, and inactivation of pathogenic bacteria based on the Vancomycin-functionalised AgNPs/3D-ZnO nanorod arrays. *Biosens Bioelectron* 98:248-253. <http://dx.doi.org/10.1016/j.bios.2017.06.058>
100. Templier V, Roupioz Y (2017) On the challenges of detecting whole Staphylococcus aureus cells with biosensors. *J Appl Microbiol.* 123(5):1056-1067. doi: 10.1111/jam.13510.
101. Scholz F (2013) *Electroanalytical Methods: Guide to Experiments and Applications*. Springer pp. 109.

102. Eduardo L, Joaquín G, Ángela M (2014) Recent advances on the theory of pulse techniques: A mini review. *Electrochemistry Communications* 43: 25–30. doi:10.1016/j.elecom.2014.03.004.
103. Armada PG, Losada J, Vicente-Pérez, Sd (1996). Cation Analysis Scheme by Differential Pulse Polarography. *Journal of Chemical Education* 73 (6):544. doi:10.1021/ed073p544
104. Liu M, Xiang H, Hua E, Wang L, Jing X, Cao X, Sheng S, Xie G (2014) Ultrasensitive Electrochemical Biosensor for the Detection of the *mecA* Gene Sequence in Methicillin Resistant Strains of *Staphylococcus aureus* Employing Gold Nanoparticles, *Analytical Letters* 47(4): 579-591.
105. Wolfbeis O.S. (2002) Fiber-Optic Chemical Sensors. *Anal Chem* 74 (12): 2663– 2678.
106. Cámara C, Moreno MC, Orellana G (1991) Chemical Sensing with Fiberoptic Devices. *Biosensors with Fiberoptics* pp. 29–84.
107. Lübbbers DW (1992) Fluorescence Based Chemical Sensors, in: *Advances in Biosensors*, Vol. 2, JAI Press, New York pp. 215–260.
108. Strohsahl CM, Miller BL, Krauss TD (2009) Detection of methicillin-resistant *Staphylococcus aureus* (MRSA) using the NanoLantern™ Biosensor. *Proceedings Volume 7167, Frontiers in Pathogen Detection: From Nanosensors to Systems; 71670S*. doi: 10.1117/12.808872
109. Cihalova K, Hegerova D, Jimenez AM, Milosavljevic V, Kudr J, Skalickova S, Hynek D, Kopel P, Vaculovicova M, Adam V (2016) Antibody-free detection of infectious bacteria using quantum dots-based barcode assay. *J Pharm Biomed Anal* 134:325-332. <http://dx.doi.org/10.1016/j.jpba.2016.10.025>

110. Chan PH, Chen YC (2012) Human Serum Albumin Stabilized Gold Nanoclusters as Selective Luminescent Probes for *Staphylococcus aureus* and Methicillin-Resistant *Staphylococcus aureus*. *Anal Chem* 84 (21): 8952–8956.
111. Zhao Z, Yan R, Yi X, Li J, Rao J, Guo Z, Yang Y, Li W, Li YQ, Chen C. (2017) Bacteria-Activated Theranostic Nanoprobes against Methicillin-Resistant *Staphylococcus aureus* Infection. *ACS Nano* 11(5):4428-4438.
112. Brédas JL, Norton JE, Cornil J, Coropceanu V (2009) Molecular understanding of organic solar cells: the challenges. *Acc Chem Res* 42(11):1691-9. doi: 10.1021/ar900099h.
113. Liu J, Cheng J, Zhang Y (2013) Upconversion nanoparticle based LRET system for sensitive detection of MRSA DNA sequence. *Biosens Bioelectron* 43:252-6.
114. Zhang CY, Johnson LW (2006) Quantum Dot-Based Fluorescence Resonance Energy Transfer with Improved FRET Efficiency in Capillary Flows. *Anal. Chem.*, 78, 5532-5537.
115. Ning Y, Gao Q, Zhang X, Wei K, Chen L (2016) A Graphene Oxide–Based Sensing Platform for the Determination of Methicillin-Resistant *Staphylococcus aureus* Based on Strand-Displacement Polymerization Recycling and Synchronous Fluorescent Signal Amplification. *J Biomol Screen* 21(8):851-7.
116. Ning Y, Zou L, Gao Q, Hu J, Lu F (2018) Graphene oxide-based fluorometric determination of methicillin-resistant *Staphylococcus aureus* by using target-triggered chain reaction and deoxyribonuclease-assisted recycling. *Mikrochim Acta*. 185(3):183. doi: 10.1007/s00604-018-2702-0.

117. Xu X, Li H, Hasan D, Ruoff RS, Wang AX, Fan DL (2013) Near-Field Enhanced Plasmonic-Magnetic Bifunctional Nanotubes for Single Cell Bioanalysis. *Adv Funct Mater* 23(35): 4332-8. doi:10.1002/adfm.201203822
118. Blackie EJ, Le Ru EC, Etchegoin PG (2009) Single-Molecule Surface-Enhanced Raman Spectroscopy of Nonresonant Molecules. *J Am Chem Soc* 131(40): 14466–14472. doi:10.1021/ja905319w
119. Nie S, Emory SR (1997) Probing Single Molecules and Single Nanoparticles by Surface-Enhanced Raman Scattering. *Science* 275 (5303): 1102–6. doi:10.1126/science.275.5303.1102
120. Fan Z, Kanchanapally R, Ray PC (2013) Hybrid Graphene Oxide Based Ultrasensitive SERS Probe for Label-Free Biosensing. *J Phys Chem Lett* 4 (21): 3813–3818.
121. Huh YS, Chung AJ, Erickson D (2009) Surface enhanced Raman spectroscopy and its application to molecular and cellular analysis. *Microfluid Nanofluid.* 6:285–297.
122. Germain ME, Knapp MJ (2009) Optical explosives detection: from color changes to fluorescence turn-on. *Chemical Society Reviews* 38(9): 2543-2555.
123. Storhoff JJ, Lucas AD, Garimella V, Bao YP, Müller UR (2004) Homogeneous detection of unamplified genomic DNA sequences based on colorimetric scatter of gold nanoparticle probes. *Nat Biotechnol* 22(7):883-7.
124. Ocsoy I, Yusufbeyoglu S, Yılmaz V, McLamore ES, Ildız N, Ulgen A (2017) DNA Aptamer Functionalized Gold Nanostructures for Molecular Recognition and Photothermal Inactivation of Methicillin-Resistant *Staphylococcus aureus*. *Colloids Surf B Biointerfaces*. Nov 1;159:16-22. doi: 10.1016/j.colsurfb.2017.07.056

125. Abd-El-Hady H, El-Said W, El-Enbaawy M, Salah Eldin TA (2014) Preparation of mecA Biosensor Based on Gold Nanoparticles to Determine Methicillin Resistant Staphylococcus Aureus (MRSA) Strains from Human and Animals. Journal of Agriculture and Veterinary Science. 7(8) Ver. I: 64-71.
126. Chan WS, Tang BS, Boost MV, Chow C, Leung PH (2014) Detection of methicillin-resistant Staphylococcus aureus using a gold nanoparticle-based colorimetric polymerase chain reaction assay. Biosens Bioelectron 53:105-11. doi: 10.1016/j.bios.2013.09.027
127. Suaifan GARY, Alhogail S, Zourob M (2017) Rapid and low-cost biosensor for the detection of Staphylococcus aureus. Biosens Bioelectron 90:230-237. <http://dx.doi.org/10.1016/j.bios.2016.11.047>
- 128 Ghosh SK, Pal T (2007) Interparticle coupling effect on the surface plasmon resonance of gold nanoparticles: from theory to applications. Chemical reviews, 107(11), 4797-4862.
129. Tawil N, Sacher E, Mandeville R, Meunier M (2012) Surface plasmon resonance detection of E. coli and methicillin-resistant S. aureus using bacteriophages. Biosens Bioelectron 37(1):24-9.
130. Nawattanapaiboon K, Kiatpathomchai W, Santanirand P, Vongsakulyanon A, Amarit R, Somboonkaew A, Sutapun B, Sriksirin T (2015) SPR-DNA array for detection of methicillin-resistant Staphylococcus aureus (MRSA) in combination with loop-mediated isothermal amplification. Biosens Bioelectron 74:335-40.
131. Erlich HA (1989) Polymerase chain reaction. Journal of clinical immunology. 9(6): 437-447.
132. Chung HJ, Castro CM, Im H, Lee H, Weissleder R. (2013) A magneto-DNA nanoparticle system for rapid detection and phenotyping of bacteria. Nat Biotechnol 8(5):369-75. doi: 10.1038/nnano.2013.70

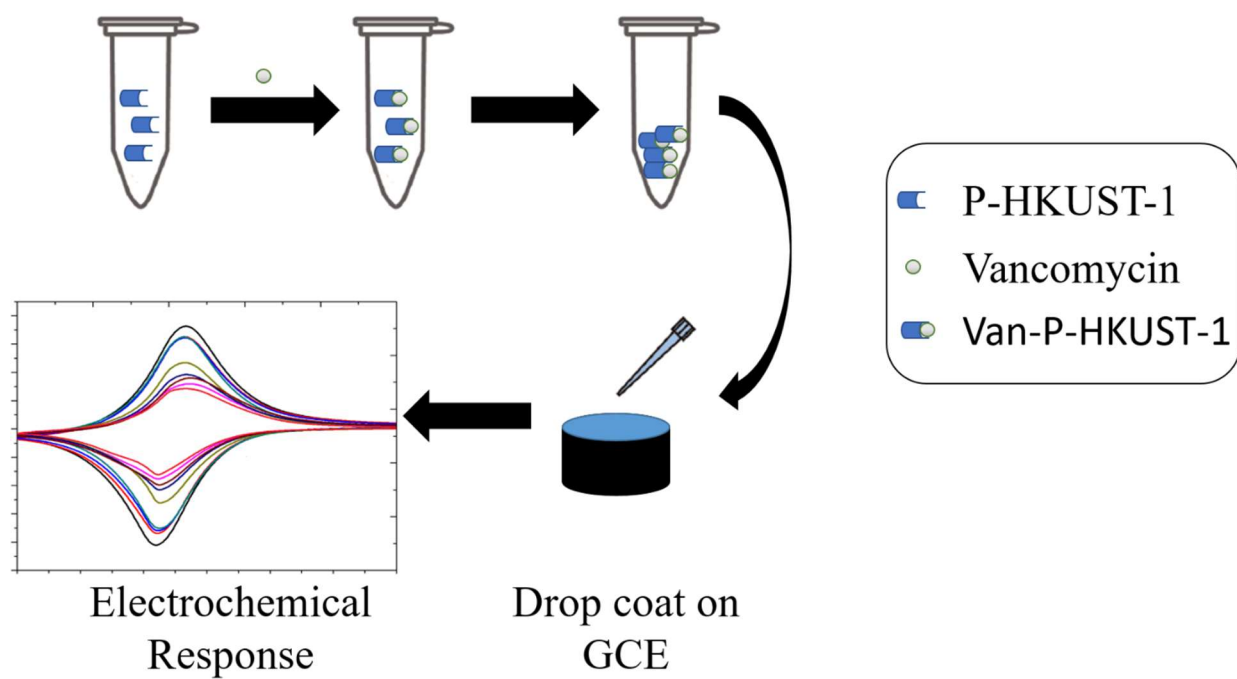
133. Rajamani M, Johnney J, Ragunathan R (2017) Detection of *mecA* Gene Associated with Methicillin Resistant *Staphylococcus aureus* and its Alternatives using Nanoparticles and Chia Seeds. *Int J Med Res Health Sci.* 6(11): 67-75
134. Hiremath N, Guntupalli R, Vodyanoy V, Chin BA, Park MK (2015) Detection of methicillin-resistant *Staphylococcus aureus* using novel lytic phage-based magnetoelastic biosensors. *Sensors and Actuators B: Chemical* 210: 129-136. <https://doi.org/10.1016/j.snb.2014.12.083>
135. Bandara AB, Zuo Z, Ramachandran S, Ritter A, Heflin JR, Inzana TJ (2015) Detection of methicillin-resistant staphylococci by biosensor assay consisting of nanoscale films on optical fiber long-period gratings. *Biosens Bioelectron* 70:433-40. doi: 10.1016/j.bios.2015.03.041
136. Yang AK, Lu H, Wu SY, Kwok HC, Ho HP, Yu S, Cheung AK, Kong SK (2013) Detection of Pantone-Valentine Leukocidin DNA from methicillin-resistant *Staphylococcus aureus* by resistive pulse sensing and loop-mediated isothermal amplification with gold nanoparticles. *Anal Chim Acta* 782:46-53. doi: 10.1016/j.aca.2013.04.004
137. Wang CH, Lien KY, Wu JJ, Lee GB. (2011) A magnetic bead-based assay for the rapid detection of methicillin-resistant *Staphylococcus aureus* by using a microfluidic system with integrated loop-mediated isothermal amplification. *Lab Chip.* Apr 21;11(8):1521-31. doi: 10.1039/c0lc00430h.
138. Chin CD, Linder V, Sia SK (2012) Commercialization of microfluidic point-of-care diagnostic devices. *Lab Chip.* 12: 2118–2134. doi: 10.1039/c2lc21204h
139. Zhang H, Ma L, Hua MZ, Wang S, Lu X (2016) Rapid detection of methicillin-resistant *Staphylococcus aureus* in pork using a nucleic acid-based lateral flow immunoassay. *International Journal of Food Microbiology* 243. doi: 10.1016/j.ijfoodmicro.2016.12.003

140. Wang Y, Yan W, Fu S, Hu S, Wang Y, Xu J, Ye C (2018) Multiple Cross Displacement Amplification Coupled with Nanoparticles-Based Lateral Flow Biosensor for Detection of *Staphylococcus aureus* and Identification of Methicillin-Resistant *S. aureus*. *Front Microbiol.* 9: 907. doi: 10.3389/fmicb.2018.00907.
141. Ramakrishnan R, Buckingham W, Domanus M, Gieser L, Klein K, Kunkel G, Prokhorova A, Riccelli PV (2004) Sensitive Assay for Identification of Methicillin-Resistant *Staphylococcus aureus*, Based on Direct Detection of Genomic DNA by Use of Gold Nanoparticle Probes, (Nanosphere, Inc., Northbrook, IL 60062; * author for correspondence). Abstracts of Oak Ridge Posters. *Clin Chem* 50(10):1949-52.
142. WHO. Antimicrobial resistance - fact sheet No 194, updated on April 2015. Available from: <http://www.who.int/mediacentre/factsheets/fs194/en/>.
143. Roca I, Akova M, Baquero F, Carlet J, Cavaleri M, Coenen S, et al (2015) The global threat of antimicrobial resistance: science for intervention. *New Microbes and New Infections*.

CHAPTER THREE

A poly(acrylic acid)-modified copper-organic framework for electrochemical determination of vancomycin

Graphical Abstract



A poly(acrylic acid)-modified copper-organic framework for electrochemical determination of vancomycin

Atal A. S. Gill, Sima Singh, Nikhil Agrawal, Zondi Nate, Tirivashe E. Chiwunze, Neeta Bachheti Thapliyal, Ruchika Chauhan & Rajshekhar Karpoomath 

Microchimica Acta **187**, Article number: 79 (2020) | [Cite this article](#)

198 Accesses | **1** Citations | **0** Altmetric | [Metrics](#)

Abstract

A copper(II) benzene-1,3,5-tricarboxylate (BTC) metal-organic framework (MOF) was modified with poly(acrylic acid) (PAA) and then used in an electrochemical sensor for vancomycin. The MOF, synthesized via a single-pot method, has enhanced solubility and dispersibility in water as compared to HKUST-1 but without compromising its crystallinity and porosity. The MOF was placed on a glassy carbon electrode (GCE) where it shows enhanced electrocatalytic properties. This is assumed to be due to the presence of the poly(acrylic acid) that forms a network between various HKUST-1 crystals through dimer formation between the carboxy groups of BTC and PAA. This also led to better dispersion of the MOF and to improved interaction between MOF and vancomycin. The structural, spectral and electrochemical properties of the MOFs and their vancomycin complexes was characterized. The modified GCE is shown to be a viable tool for electrochemical determination (best at a working potential of 784 mV vs. Ag/AgCl) of the antibiotic vancomycin in spiked urine and serum samples. Response is linear in the 1–500 nM vancomycin concentration range, and the detection limit is 1 nM, with a relative standard deviation of $\pm 4.3\%$.

Abstract

A copper(II) benzene-1,3,5-tricarboxylate (BTC) metal-organic framework (MOF) was modified with poly(acrylic acid) (PAA) and then used in an electrochemical sensor for vancomycin. The MOF, synthesized via a single-pot method, has enhanced solubility and dispersibility in water as compared to HKUST-1 but without compromising its crystallinity and porosity. The MOF was placed on a glassy carbon electrode (GCE) where it shows enhanced electrocatalytic properties. This is assumed to be due to the presence of the poly(acrylic acid) that forms a network between various HKUST-1 crystals through dimer formation between the carboxy groups of BTC and PAA. This also led to better dispersion of the MOF and to improved interaction between MOF and vancomycin. The structural, spectral and electrochemical properties of the MOFs and their vancomycin complexes was characterized. The modified GCE is shown to be a viable tool for electrochemical determination (best at a working potential of 784 mV vs. Ag/AgCl) of the antibiotic vancomycin in spiked urine and serum samples. Response is linear in the 1 - 500 nM vancomycin concentration range, and the detection limit is 1 nM, with a relative standard deviation of $\pm 4.3\%$.

Keywords: cyclic voltammetry; electrical impedance spectroscopy; differential pulse voltammetry; Methicillin resistant *Staphylococcus aureus*; drug delivery; redox active MOF.

1. Introduction

Bacterial resistance to the largely accessible anti-microbial drugs poses one of the most significant risk to human health and can cause tremendous healthcare and economic burden. Medications such as penicillin and methicillin are commonly prescribed for anti-microbial therapy. However, after certain period of administration, it was reported to result in an anti-microbial drugs resistance which promoted the increased use of vancomycin [1]. Vancomycin is a glycopeptide antibiotic commonly administered for the treatment of various gram-positive severe bacterial infections, especially *Staphylococcus aureus*, *Clostridium difficile* and *Staphylococcal enterocolitis*. Vancomycin works by inhibiting cell wall formation by combining with D-alanyl-D-alanine sequence of the bacterial cell wall [2]. Vancomycin is traditionally viewed as a drug of “last resort”, prescribed only when other antibiotics fail. However, high vancomycin dose has revealed to cause several side-effects such as common phlebitis, epidermal necrosis, nephrotoxicity, and neutropenia pathology related to histamine release known as the red man syndrome, ototoxicity and thrombocytopenia [3]. Further, lower exposure put patients at danger of therapy inability. Therefore, proper control of vancomycin levels in a narrow range can minimize the side effects and increase the pharmacological response. Therefore, screening and detection of vancomycin, both quantitatively and qualitatively, is essential.

Several conventional methods such as spectroscopy, spectrophotometry, chromatography, immunoassay and capillary electrophoresis have been used to detect vancomycin in different matrices [4]. However, earlier reported methodologies for the determination of vancomycin have a few constraints. These techniques require large capital requirement for installation and instrumentation, trained professionals and are time consuming. Therefore, to avoid such a financial burden and carry out the rapid detection of vancomycin, nanomaterial-based detection techniques have been developed. Nanomaterials such as graphene, CNT's and carbon black [5] were used as electrode modifiers to carry out vancomycin detection through electrochemical route and molecularly imprinted polymers

were employed for detection via optical fibers [6]. These nanomaterials exhibited certain drawbacks like lower selectivity in case of electrochemical route and complex preparation procedure in case of the optical fiber. Therefore, it is important to develop a specific, easy and accessible method for detection of vancomycin.

It is well known that electrochemical analytical approach has attracted interest due to its high sensitivity, specificity and simplicity at an economical cost. Nowadays, with the rapid development of sensing methods, great attention has been focused on the use of nanomaterials and electrochemical methods [7-12]. In the present work, we focus on a novel class of materials, known as metal organic frameworks (MOFs), which are nano-porous in nature. Many electrochemically active MOFs such as Cu-MOF, Ni-MOF and Co-MOF have been used as electroactive signal probes, redox-active species and electrocatalyst for detection of various analytes [13], but the limited solubility/dispersibility of MOFs in water is still a hindrance. Hence, there is a requirement to overcome the dispersibility of MOFs and further increase its electrical conductivity. Polyacrylic acid (PAA) is a polymer which is generally employed to improve water solubility of materials and has also shown affinity towards vancomycin [14]. Therefore, it is anticipated that addition of PAA to MOFs structure would result in enhanced water dispersibility, conductivity and affinity towards vancomycin.

In this study, we synthesize a novel water dispersible MOF through hydrothermal route via a single pot reaction. The synthesized MOF (P-HKUST-1) is modified from its parent MOF (HKUST-1) by adding PAA into its structure. PAA was introduced in the reaction mixture during the synthesis of HKUST-1. This leads to the formation of novel water soluble MOF, indicated as P-HKUST-1. Finally, P-HKUST-1 based electrode was employed to carry out the detection of vancomycin and the change in the redox peaks on addition of vancomycin was recorded. The practical applicability of the method was investigated by detecting vancomycin in spiked urine and animal serum sample.

2. Method

2.1 Chemicals, reagents and instrumentation

Copper nitrate trihydrate, 1,3,5- benzene tricarboxylic acid (BTC) and potassium chloride were purchased from Merck, South Africa. Vancomycin hydrochloride (Vancocin HCl), polyacrylic acid (PAA), dimethylformamide (DMF), potassium ferrocyanide and ethanol (95%) were purchased from Sigma-Aldrich, South Africa (<https://www.sigmaaldrich.com/south-africa.html>). Potassium ferricyanide was purchased from Saarchem (<https://www.merckgroup.com/en/locations.html?businessUnit-ALL,regions-regions:africa,countries-ALL,page-0,filter-locations>). Sodium dihydrogen orthophosphate dehydrate (Merck, South Africa, <https://www.sigmaaldrich.com/south-africa.html>) and sodium phosphate dibasic dehydrate (Sigma-Aldrich, Germany) were used to prepare 0.1 M phosphate buffer of different pH to carry out pH study. Double distilled (DD) water was used throughout the experiment. Field emission - scanning electron microscope (FE-SEM; ZEISS Ultra Plus, Germany), high resolution-transmission electron microscopy (HR-TEM; JEOL 2100 HRTEM, Korea), X-ray diffraction (XRD; PanAlytical Empyrean, Germany), Brunauer–Emmett–Teller (BET; Micromeritics Tristar II 3020 2.00, USA), UV spectrophotometer (UV-1800, Shimadzu, South Africa), Fourier transform infrared spectroscopy (Bruker® Alpha-P ATR–FT-IR, Germany) and electrochemical setup (CHI 660E, USA) consisting of a working electrode (glassy carbon electrode- 3 mm diameter, part number: CHI104), a reference electrode (Ag/AgCl, part number: CHI111) and a counter electrode (platinum wire, part number:115) were used in the study.

2.2 Synthesis of HKUST-1 and P-HKUST-1

HKUST-1 was synthesized according to the reported method without any modifications [15]. P-HKUST-1 was synthesized in a single step method using copper nitrate, BTC and PAA. 1 g of copper

nitrate was dissolved in 50 mL of ethanol. 0.35 g of BTC was dissolved in 25 mL DMF and 0.20 g of PAA in 25 mL DD water. All the three prepared solutions were transferred to hydrothermal autoclave (200 mL) and kept at 85 °C for 24 hours. The product was washed with DD water and then with ethanol three times, was finally centrifuged at 3000 rpm and dried in oven at 70 °C for 24 hrs. The final product (P-HKUST-1) was collected.

2.3 Preparation of complexes with vancomycin

Vancomycin (1 mg) and HKUST-1 (1 mg) were added to 1 mL of water and sonicated for 5 mins. The complex obtained was filtered and washed subsequently with DD water and ethanol. It was kept for drying in oven at 70 °C for 24 hrs. A similar procedure was followed to obtain P-HKUST-1 and vancomycin complex. The complexes are represented as Van-HKUST-1 and Van-P-HKUST-1, respectively. The formation of the complexes was confirmed by FTIR, XRD, and UV-spectroscopy (details in supplementary information).

2.4 Preparation of electrode

To obtain a mirror-like finish on the glassy carbon electrode (GCE) surface, it was polished with alumina powder (0.3 and 0.05 μm). Further, GCE was rinsed with water and dried under infrared (IR) lamp. 1 mg.mL^{-1} aliquots of HKUST-1, P-HKUST-1, Van-HKUST-1 and Van-P-HKUST-1 in DD water were prepared. These aliquots were used to modify the electrode to carry out subsequent electrochemical studies. The electrode was prepared by drop casting 5 μL from the respective aliquots of the samples onto the clean and dry GCE surface. The electrochemical studies were carried out in 2.5 mM potassium ferricyanide/ potassium ferrocyanide ($\text{Fe}(\text{CN})_6^{3-/4-}$) as redox couple in 1 M KCl. The potential window for recording the voltammograms was from 0.4 V to 1.0 V. Due to the presence of free polymer chains in P-HKUST-1, multiple cycles were carried out until a constant current was

obtained as shown in Fig. S1. Every reading was carried out in triplets and the average of each reading was plotted in the voltammograms with their respective calibration plots.

2.5 Preparation of urine and serum samples

To check the feasibility of the diagnostic assay, the detection and determination of vancomycin was carried out in an unknown human urine sample (obtained from a healthy lab personnel) followed by serum sample. The unknown urine samples were diluted up to 10 times to reduce matrix effects. It was further used for the detection of vancomycin using P-HKUST-1 modified electrode. The diluted urine samples were spiked with 0 nM, 1 nM, 100 nM, 250 nM, and 500 nM vancomycin, which was detected by addition of 1 mg P-HKUST-1 to each of the real sample. We are thankful to Dr. Thirumula Govenders lab at University of KwaZulu-Natal, Westville, South Africa for the sheep blood serum sample, which was used to carry out further studies. The sample was diluted 10 times to reduce the matrix effects and the identical procedure as of the urine sample was followed to carry out detection of vancomycin in the serum sample of different dilutions.

3. Results and discussion

3.1 Choice of material

The synthesis of water dispersible copper benzene tricarboxylic acid modified with polyacrylic acid was carried out through hydrothermal route via a single pot reaction. The post synthetic modification of HKUST-1 with PAA was not a feasible reaction and therefore, PAA was introduced in the reaction mixture during the synthesis of HKUST-1 which leads to the formation of novel water soluble MOF, indicated as P-HKUST-1. This was achieved by carboxylic acid dimer formation between BTC and PAA. Additionally there were no changes in the crystalline structure of P-HKUST-1 from that of HKUST-1. This shows that the intrinsic properties of HKUST-1 were preserved. Finally, the parent and modified MOF were tested to detect vancomycin.

In the preliminary computational studies carried out, it was seen that vancomycin readily forms complex with HKUST-1. This can be due to the cationic groups present in vancomycin structure which go and bind with the anionic groups of the MOF. The carboxylic acid groups in the linker molecules in the MOF structure act as a promising site for vancomycin to form a complex. However, in case of P-HKUST-1 it was anticipated that vancomycin would more readily form complex with P-HKUST-1 and cause disruption in the electrochemical conductivity. This is because, of the incorporation of PAA in addition to the linker groups. PAA is an anionic polymer which is generally employed to improve water solubility of materials and has also shown affinity towards vancomycin [16]. Further, the introduction of polyacrylic acid to HKUST-1 can also lead to chelation of PAA with copper ions. The PAA acts as an electron donating ligand which helps in faster electron transfer by aiding in reduction of copper ion cores and increase in conductivity and also prevents any possible repulsions between the positively charged copper ions and vancomycin. Therefore, these can result in the increase in the binding affinity of vancomycin to the P-HKUST-1, which further would lead to better output response as compared to HKUST-1 for carrying out the detection of vancomycin.

Additionally, the synthesized P-HKUST-1 MOF offers more potential applications. Copper ions have been reported to instantly kill the MRSA bacterial strains and because MOF acts as a reservoir of copper ions it may be used to treat MRSA skin infections [17, 18]. PAA is FDA approved polymer which helps reducing the toxicity levels of HKUST-1. Therefore, the modified MOF can be used for treatment of MRSA bacterial skin infections. Additionally, the solubility also increases the ease of conjugation of P-HKUST-1 biological entities, making it suitable for bio sensing application.

3.2 Detection mechanism

P-HKUST-1 was employed as a single shot assay which forms a complex with vancomycin and provides an observable output response. The output was in the form of a decrease in the peak current

where $[\text{Fe}(\text{CN})_6]^{3-/4-}$ was employed as the redox couple. Here, we take a 1 mg.mL^{-1} aliquot of P-HKUST-1 as the base (0 M vancomycin) or stock solution. To the above aliquot we add a known concentration of vancomycin to the solution, after which the complex was centrifuged and collected. This complex was then dispersed in 1 mL of DI water from which 5 μL was drop coated onto the GCE. Finally, voltammograms for each complex formed were recorded for varying concentrations of vancomycin. Further, the assay was also tested in different matrices and in presence of various interfering agents. The aliquots were prepared in presence of different interferents in 1 mL DI water and using 1 mL of biological matrices.

3.3 Electrochemical response of MOFs

The redox activity of HKUST-1 and P-HKUST-1 was carried out and compared at varying pH buffers (4.0, 7.0, and 8.5) (at a scan rate of 0.1 V.s^{-1}). The electrochemical responses of the modified electrodes and GCE were recorded and shown in Fig 1. The potential window from -0.8 V to 0.8 V was used to carry out to check the redox activity of the MOFs. It can be seen that HKUST-1 had almost no current capacitive current and had almost the equal current as the GCE. However, P-HKUST-1 displayed capacitive currents as we moved towards the positive potentials. Further, it was observed that P-HKUST-1 displayed higher peak currents as compared to HKUST-1 at all pH values as shown in Figure 1 b, c, and d. The peaks O1 and O2 as shown in Fig. 1a represent the oxidation of copper ion core from Cu(II) to Cu(I) and finally to Cu. During the reverse scan a hump and peak was observed (R1 and R2) showing the reduction of Cu to Cu(I) and then to Cu(II). Additionally, it was observed that highest peak currents were obtained at 4.0 pH and current keeps decreasing as the pH was increased from 7.0 to 8.5. This can be attributed to the higher presence of anionic charge on the electrode material. This leads to rapid electron flow due to faster diffusion of acidic ions towards the electrode surface, resulting in higher peak currents.

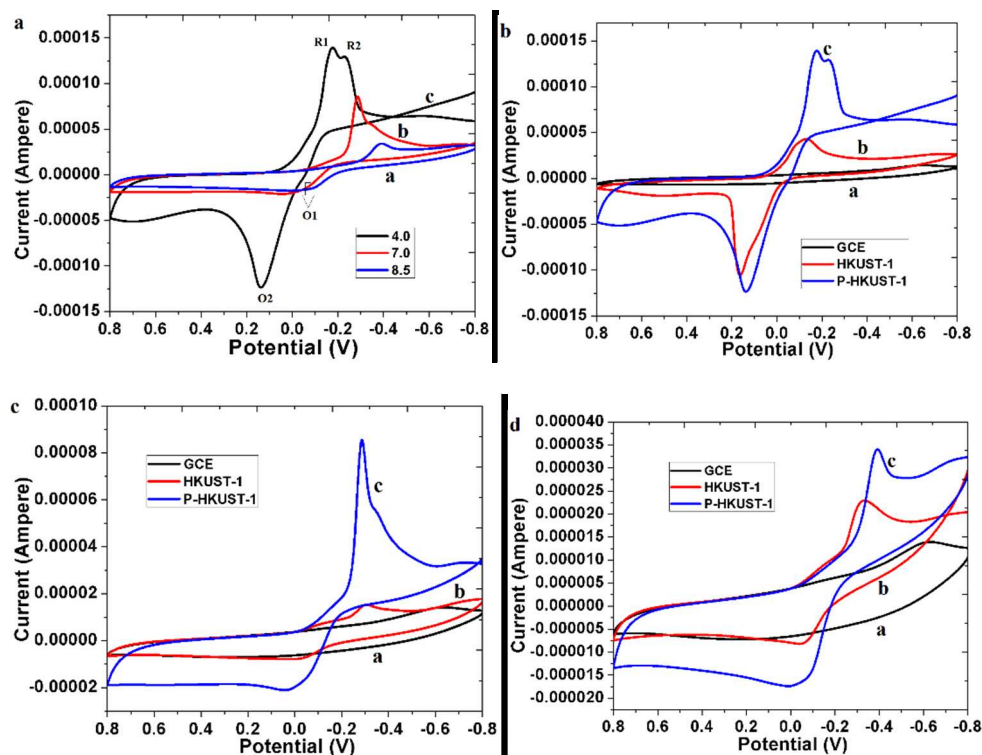


Fig. 1 (a) CV of P-HKUST-1 at different pH [4.0 (a), 7.0(b), 8.5(b)]. R1, R2 are the reduction peaks and O1, O2 are the oxidation peaks of copper ion core of P-HKUST-1. (b) CV in 0.1 M phosphate buffers at pH 4 of GCE (a), HKUST-1 (b) and P-HKUST-1 (c) (c) CV in 0.1 M phosphate buffers at pH 7 of GCE (a), HKUST-1 (b) and P-HKUST-1 (c) (d) CV in 0.1 M phosphate buffers at pH 8.5 of GCE (a), HKUST-1 (b) and P-HKUST-1 (c).

3.4 Performance of diagnostic assay

To carry out the detection of vancomycin, cyclic voltammograms of P-HKUST-1 and vancomycin spiked P-HKUST-1 (Van-P-HKUST-1) were recorded. The cyclic voltammetry was carried out in 2.5 mM $[\text{Fe}(\text{CN})_6]^{3-/4-}$ in 1 M KCl and phosphate buffer in the ratio 1:1 as the redox couple and at a scan rate of 0.1 Vs^{-1} . As seen in Fig. 2a, there was a significant decrease in the redox peak obtained at Van-P-HKUST-1/GCE in comparison to P-HKUST-1/GCE. The decrease in the peak currents was observed at $E_{\text{pa}} = 0.784 \text{ V}$ and $E_{\text{pc}} = 0.724 \text{ V}$, which is the working potential of the electrode. This can be attributed to vancomycin's interaction with PAA and HKUST-1 crystals in P-HKUST-1's

structure, disrupting the electron flow and resulting in hindrance to the flow of electrons thus resulting in lower redox peak currents. Further, optimization of the pH conditions was carried out using 2.5 mM $[\text{Fe}(\text{CN})_6]^{3-/4-}$ in 1 M KCl and phosphate buffer in the ratio 1:1 as the redox couple. The pH range was varied from 5.0 to 8.5 and it was found that maximum current was obtained at 7.0 pH, as shown in Fig. 2b. Hence, all further electrochemical studies were carried out at pH 7.0.

Further, Control studies were carried out to check if any interference caused by the active copper site of P-HKUST-1. The studies were carried out in blank buffer solution of pH 7. There were no peaks observed in the potential window 0.4 to 1.0 V (at scan rate, 0.1 V.s^{-1}) which confirmed that no interference in the redox reaction of $[\text{Fe}(\text{CN})_6]^{3-/4-}$ redox couple occurred as shown in the Fig. 2c.

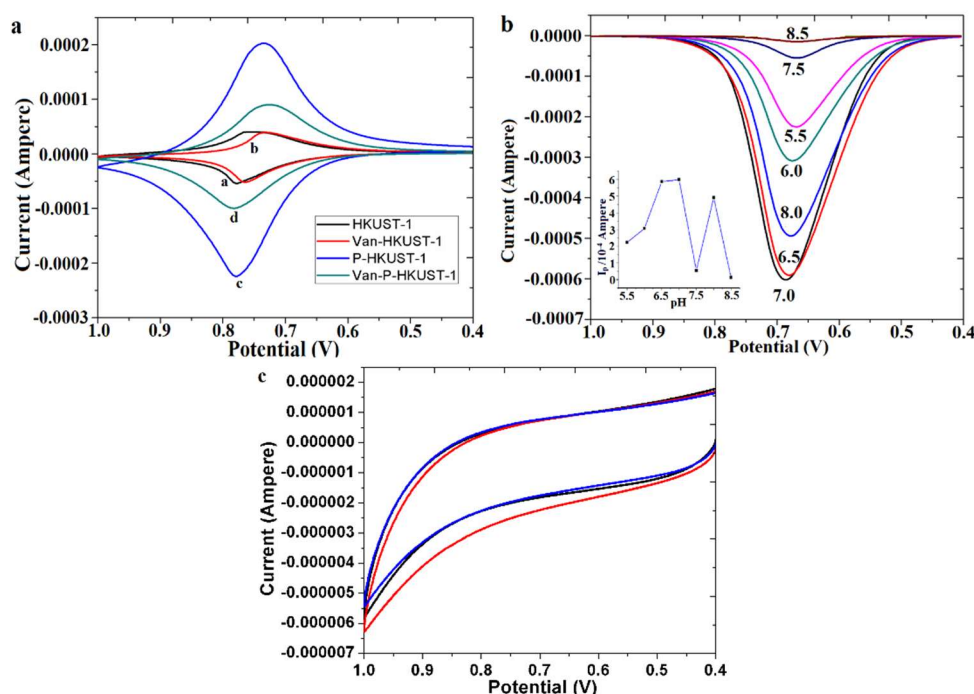


Fig. 2 (a) Cyclic voltammograms in 2.5 mM $[\text{Fe}(\text{CN})_6]^{3-/4-}$ in 1 M KCl at different modified electrodes (i.e. (a) HKUST-1/GCE, (b) Van-HKUST-1/GCE, (c) P-HKUST-1/GCE, (d) Van-P-HKUST-1/GCE) (b) pH plot for P-HKUST-1/GCE in 2.5 mM $[\text{Fe}(\text{CN})_6]^{3-/4-}$ in 1 M KCl and phosphate buffer in (1:1), with varying pH from 5.5 to 8.5 at a scan rate of 0.1 Vs^{-1} . [Inset- pH vs current (I_p) plot] (c)

Control studies carried out for P-HKUST-1/GCE in pH 7 phosphate buffer at a scan rate of 0.1 V.s^{-1} with three consecutive voltammograms.

To electrochemically determine the concentration of vancomycin, the assay was tested using 1 mg.mL^{-1} of P-HKUST-1 in water. To the P-HKUST-1 solution, a known concentration of vancomycin was added with stirring and subsequently electrochemical measurements were recorded. The concentration of the drug was varied from 0.1 nM - 1000 nM and cyclic voltammograms were recorded in phosphate buffer (pH 7.0) containing $2.5 \text{ mM } [\text{Fe}(\text{CN})_6]^{3-/4-}$ and 1 M KCl at a scan rate of 0.1 V.s^{-1} , as shown in Fig. 3a. As expected, on increasing the concentration of vancomycin there was a decrease in the redox peaks. A linear response was obtained in the concentration range 1 nM - 500 nM . The calibration plot was plotted for the change in redox peaks with varying concentrations (Fig. 3b). The linear regression equation can be expressed as:

$$I_p (10^{-4} \text{ A}) = -0.02762 + 1.87551 [\text{Van}] (\text{nM}); R = 0.98349$$

The minimum limit of detectable concentration of vancomycin came out to be 1 nM with a relative standard deviation of $\pm 4.27\%$ and sensitivity equal to $496.429 \mu\text{A} \cdot \mu\text{M}^{-1} \cdot \text{cm}^{-2}$. The technique displayed better response than other pre-existing work as shown in Table 1. The higher concentrations were not detected because of the limited amount of binding or interaction sites available for vancomycin.

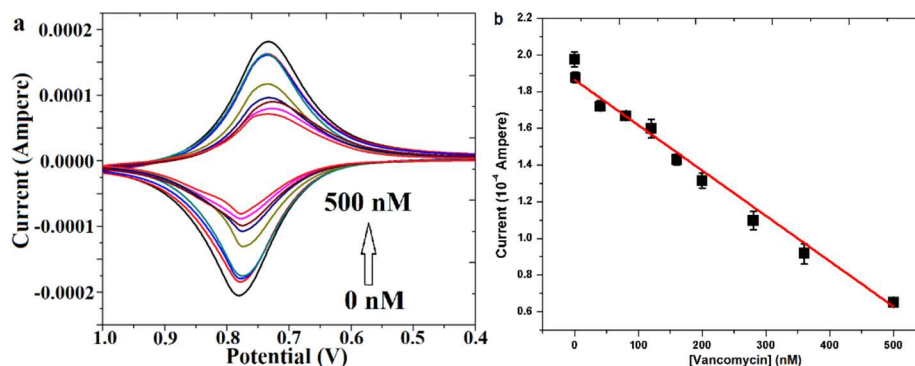


Fig. 3 (a) Cyclic voltammograms of 2.5 mM $[\text{Fe}(\text{CN})_6]^{3-/4-}$ in 1 M KCl and phosphate buffer (0.1 M) at pH of 7.0 using Van-P-HKUST-1/GCE (scan rate 0.1 V.s⁻¹) with varying concentration of vancomycin from 0 nM to 500 nM, **(b)** calibration plot of [vancomycin] vs I_p . The readings were carried out in triplicates and the standard deviation was calculated and the calibration plot was plotted as the average the three readings.

Table 1 Comparison of other techniques with the proposed sensor for vancomycin determination

Method	Technique	LOD	Matrices	Reference
Electrochemical	Square wave voltammetry	0.20 mM	Human serum	5
Optical Fibre	Long period grating (LPG)	10 nM	Urine	6
Spectrophotometric	UV spectroscopy	11 nM	Pharmaceutical forms	21
Cantilever	differential deflection	0.2 μM	Serum	22
Fluorescence quenching	Fluorescence	0.15 nM	Water and serum	23
Fluorescence quenching	Fluorescence	7.0 nM, 96.6 nM	Aqueous and serum	24
Nano-Molecularly imprinted polymer	Surface plasmon resonance	1.3 nM	Milk	25
Electrochemical	Cyclic voltammetry	1 nM (lowest detected concentration)	Urine and Serum	This work

3.5 Selectivity studies

In order to test the selectivity of the novel MOF as an assay for vancomycin detection, interference studies were carried out using 0.1 mM analogous drugs (ciprofloxacin and gentamicin) and 0.1 mM

of ions (Na, Mg, K, SO₄, Cl, HCO₃). These were incubated with an aliquot of Van-P-HKUST-1 (1 mg.mL⁻¹) for 5 mins and were tested using cyclic voltammetry. In case of analogous drugs a significant decrease in the current output was observed, which can be attributed to a few van-der-walls interactions that occur with P-HKUST-1 and the drugs. The lowering of peak current was observed from the initial value as compared to vancomycin in buffer. However, on introducing vancomycin to the aliquot, further decrease in the peak current was observed and only 2.3% variation from the original value at 500 nM was recorded. This signifies that the diagnostic assay was responsive towards vancomycin even after the introduction of interferents. In addition no change in the linear range and lowest detection concentration was observed.

In the presence of metal ions, it was observed that initial peak currents were not changed significantly. However, as the vancomycin concentration was increased, the decrease in peak current was not as prominent as the observed in buffer. This may be due to the presence of magnesium ions present which decrease the binding affinity of vancomycin [19]. Due to the decrease in binding affinity, P-HKUST-1s electron flow was higher, hence, resulting in higher peak currents (71.42% higher) at 500 nM concentration of vancomycin. The results of Van-P-HKUST-1/GCE in presence of the interferents are shown in Fig. 4 a, b. Their corresponding calibration plots were plotted which are available in the supplementary information (Fig. S12) and the lowest detectable concentration and linear range for vancomycin was unchanged in the presence of the above mentioned interfering agents (details in Table S2). Additionally, material was also checked as a potential sensor in the same working window for various important biological entities and pollutants such as cystamine, paracetamol, catechol, folic acid, glutamic acid and mercury. The modified electrode was tested via cyclic voltammetry in presence of various other interfering agents individually. The electrolyte was prepared in pH 7 buffer and 0.1 mM solution (ratio 9:1) of each interfering agent mentioned above as shown in Fig. S13. The life time of P-HKUST-1 and Van-P-HKUST-1 was checked over a period of

5 weeks. The modified electrode retained 97.2% of their original current peaks as shown in Fig. 4 c and a relative standard deviation of 3.4% was achieved. However, the analytic response for both electrodes started degrading after 6 weeks and did not provide similar redox peaks.

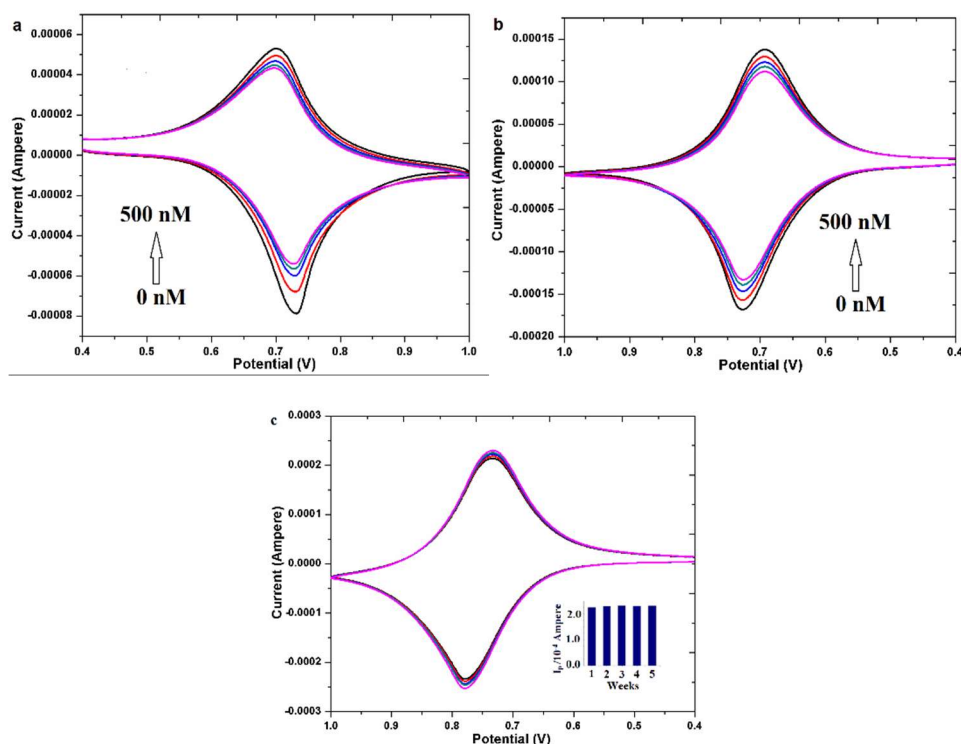


Fig. 4 Cyclic voltammograms in 2.5 mM $[\text{Fe}(\text{CN})_6]^{3-/4-}$ (1 M KCl, at 0.1 V.s⁻¹) of Van-P-HKUST-1 modified electrode in presence of (a) other drugs (ciprofloxacin and gentamicin). (b) Metal ions such as (Na, Mg, K), with varying concentrations of vancomycin (0 nM, 1 nM, 100 nM, 250 nM, 500 nM) (c) Stability test for P-HKUST-1/GCE over the period of 5 weeks was also carried out.

3.6 Real Sample analysis

Therapeutic drug monitoring of vancomycin is essential to determine the dosage modification for patients in hospitals. Patients are usually already weak; hence, urine is convenient to obtain, rather than the invasive procedure of blood sampling. In addition, 75-80% vancomycin is excreted in its pristine form after the first day of consumption in urine [20]. Therefore, urine can be used as a good source to monitor the drug levels still present in the patient's body. To carry out detection, urine sample was diluted 10 times to reduce matrix effects, if any. The aliquots of 1 mg.mL⁻¹ of P-HKUST-

1 were prepared in the human urine sample. These aliquots were spiked with known concentrations of vancomycin and the current decreases with the increase in the concentration of vancomycin spiked. The voltammograms of urine sample are shown (in Fig. 5 a) with concentration varying from 0 nM to 500 nM. The corresponding calibration curve was plotted which is available in the supplementary information (fig. S14) and the linear range of the method was unaltered in the urine sample with less than 5% variations from the original buffer.

Similarly, the blood serum sample was diluted 10 times to reduce matrix effects. Aliquots of 1 mg/ml of P-HKUST-1 in the serum samples were prepared. These aliquots were spiked with known concentrations of vancomycin and the current decreases with the increase in the concentration of vancomycin spiked. The decrease in the peak current values can be due to complex matrix of serum which combines with the P-HKUST-1 structure reducing the electrocatalytic activity towards the redox couple. This was seen as the initial peak currents at 0 M vancomycin concentration a much lower as compared to buffer. The voltammograms for serum sample are shown (in Fig. 5 b) below with concentration varying from 0 nM to 500 nM. Their corresponding calibration plots were plotted which are available in the supplementary information and the linear range proposed method. The data in Table S2 shows the values of lowest detected concentration, sensitivity, range and linear equations for interfering agents and in biological matrices.

Finally, the proposed sensing technique has its limitations. The method uses P-HKUST-1 as a single shot assay which can only be used once to carry out the detection of vancomycin. Thus, method possesses no reversibility and the material cannot be regenerated. In the presence of biological matrices and interfering agents, alterations in the output current values may occur. However, these changes did not affect the detection of vancomycin and the lowest detectable concentration and linear range remained the same.

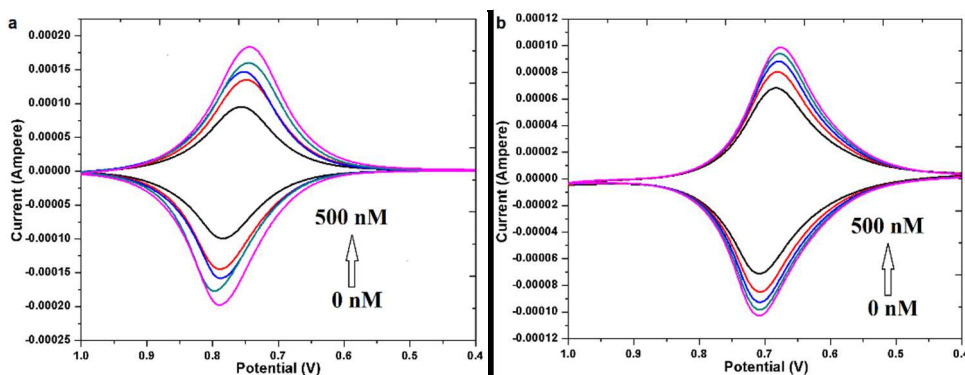


Fig. 5 (a) CV curves of P-HKUST-1 in 2.5 mM $[\text{Fe}(\text{CN})_6]^{3-/4-}$ in 1 M KCl as the redox couple and electrolyte (scan rate of 0.1 V.s^{-1}) at different concentration spikes of vancomycin in human urine sample (0 nM, 1 nM, 100 nM, 250 nM, 500 nM) **(b)** CV curves in animal serum sample (Vancomycin concentration: 0 nM, 1 nM, 100 nM, 250 nM, 500 nM).

4. Conclusions and Perspectives

In summary, we synthesize a polyacrylic acid modified HKUST-1 MOF as a diagnostic assay for the electrochemical detection of vancomycin by cyclic voltammetry. The lowest detectable concentration limit came out to 1 nM. The method had a few limitations which arise due to limitations in selectivity and reversibility of the material. However, the MOF material still detected vancomycin in presence of variety interfering agents without any change in the lowest detection concentration and linear range. Finally, the modified MOF (P-HKUST-1) can have various applications. It can be used for drug delivery of vancomycin which is shown to form complex with the drug. The inclusion of polyacrylic acid lowers the toxicity of the parent MOF (HKUST-1) and also makes it water soluble and easily dispersible. These parameters lead to further possibilities for the applicability of P-HKUST-1 for bioconjugation and using it as a biosensor. Further, P-HKUST-1 can also be used for the treatment of MRSA infections on skin. This is because of the vancomycin delivery and also because P-HKUST-1 can act as a reservoir of copper metal ions which aid in ablation of MRSA bacteria.

References

- [1] Gill A, Singh S, Thapliyal N, Karpoormath R (2019) Nanomaterial-based optical and electrochemical techniques for detection of methicillin-resistant *Staphylococcus aureus*: a review. *Microchim Acta* 186: 114. <https://doi.org/10.1007/s00604-018-3186-7>
- [2] Reynolds PE (1989) Structure, biochemistry and mechanism of action of glycopeptide antibiotics. *Eur J Clin Microbiol Infect Dis* 8(11):943–950
- [3] Lestner JM, Hill LF, Heath PT, Sharland M (2016) Vancomycin toxicity in neonates: a review of the evidence. *Curr Opin Infect Dis* 29:237–247. <https://doi.org/10.1097/QCO.0000000000000263>
- [4] Vila MMDC, de Oliveira RM, Gonçalves MM (2007) Analytical methods for vancomycin determination in biological fluids and in pharmaceuticals. *Quim. Nova* 30(2): 395-399
- [5] Hadi M, Mollaei T (2018) Electroanalytical Determination of Vancomycin at a Graphene-modified Electrode: Comparison of Electrochemical Property between Graphene, Carbon Nanotube, and Carbon Black. *Electroanalysis* 30: 1–6
- [6] Korposh S, Chianella I, Guerreiro A, Caygill S, Piletsky S, James SW, Tatam RP (2014) Selective vancomycin detection using optical fibre long period gratings functionalised with molecularly imprinted polymer nanoparticles. *Analyst*. 139(9): 2229–2236. doi:10.1039/c3an02126b.
- [7] Gupta VK, Atar N, Yola ML, Üstündağ Z, Uzune L (2014) A novel magnetic Fe@Au core-shell nanoparticles anchored graphene oxide recyclable nanocatalyst for the reduction of nitrophenol compounds. *Water Research*. Volume 48, 210-217.
- [8] Srivastava, S. K., Gupta, V. K., & Jain, S. (1996). PVC-based 2, 2, 2-cryptand sensor for zinc ions. *Analytical chemistry*, 68(7), 1272-1275.

- [9] Yola, M. L., Gupta, V. K., Eren, T., Şen, A. E., & Atar, N. (2014). A novel electro analytical nanosensor based on graphene oxide/silver nanoparticles for simultaneous determination of quercetin and morin. *Electrochimica Acta*, 120, 204-211.
- [10] Gupta, V.K., Karimi-Maleh, H. and Sadegh, R., 2015. Simultaneous determination of hydroxylamine, phenol and sulfite in water and waste water samples using a voltammetric nanosensor. *Int. J. Electrochem. Sci*, 10, pp.303-316.
- [11] Karimi-Maleh, H., Tahernejad-Javazmi, F., Atar, N., Yola, M.L., Gupta, V.K. and Ensafi, A.A., 2015. A novel DNA biosensor based on a pencil graphite electrode modified with polypyrrole/functionalized multiwalled carbon nanotubes for determination of 6-mercaptopurine anticancer drug. *Industrial & Engineering Chemistry Research*, 54(14), pp.3634-3639.
- [12] Gupta, V.K., Kumar, S., Singh, R., Singh, L.P., Shoor, S.K. and Sethi, B., 2014. Cadmium (II) ion sensing through p-tert-butyl calix [6] arene based potentiometric sensor. *Journal of Molecular Liquids*, 195, pp.65-68.
- [13] Anik, Ü., Timur, S., & Dursun, Z. (2019). Metal organic frameworks in electrochemical and optical sensing platforms: a review. *Microchimica Acta*, 186(3): 196. DOI:10.1007/s00604-019-3321-0.
- [14] Sofi FA, Bhat MA, Majid K (2019) Cu²⁺-BTC based metal–organic framework: a redox accessible and redox stable MOF for selective and sensitive electrochemical sensing of acetaminophen and dopamine. *New J. Chem.* 43: 3119-3127. <http://dx.doi.org/10.1039/C8NJ06224B>
- [15] Jeong NC, Samanta B, Lee CY, Farha OK, Hupp JT (2012) Coordination-Chemistry Control of Proton Conductivity in the Iconic Metal–Organic Framework Material HKUST-1. *J. Am. Chem.Soc.* 134, 51–54. dx.doi.org/10.1021/ja2110152 |

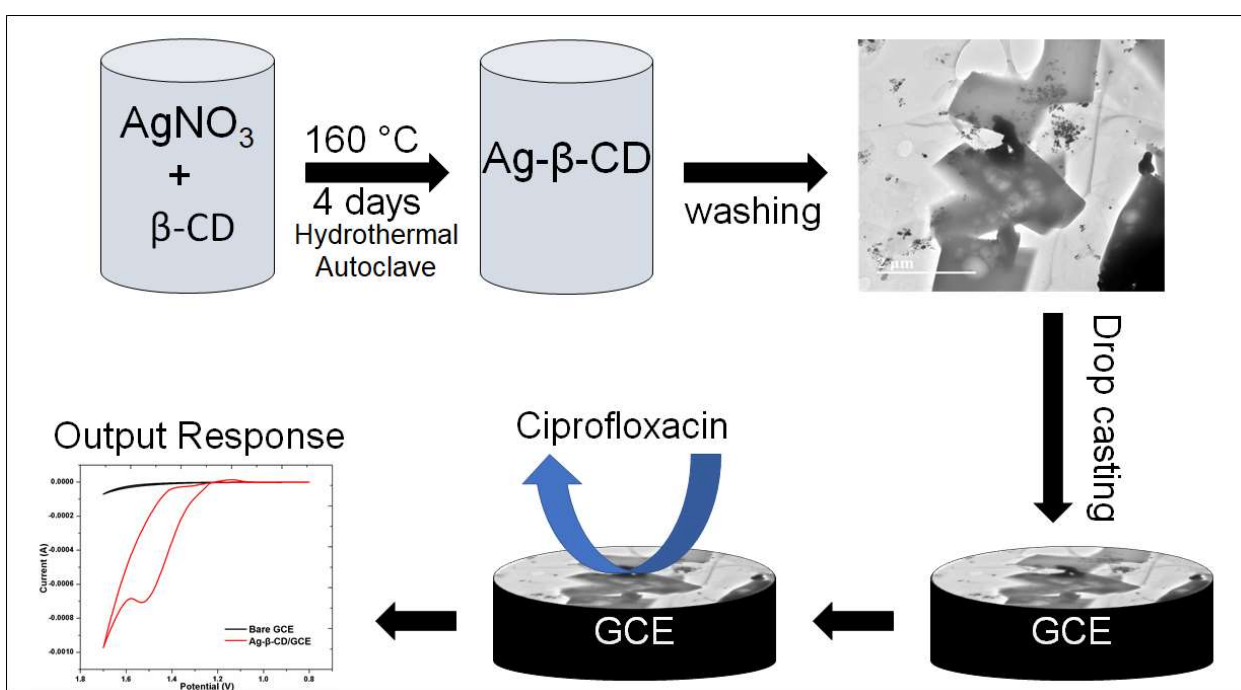
- [16] Sikwal DR, Kalhapure RS, Rambharose S, Vepuri S, Soliman M, Mocktar C, Govender T. (2016) Polyelectrolyte complex of vancomycin as a nanoantibiotic: Preparation, in vitro and in silico studies. *Materials Science and Engineering C* 63: 489–498. <http://dx.doi.org/10.1016/j.msec.2016.03.019>
- [17] Warnes SL, Keevil CW (2016) Lack of involvement of Fenton chemistry in death of methicillin-resistant and methicillin-sensitive strains of *Staphylococcus aureus* and destruction of their genomes on wet or dry copper alloy surfaces. *Appl Environ Microbiol* 82:2132–2136. doi:10.1128/AEM.03861-15.
- [18] Xiao J, Zhu Y, Huddleston S, Li, Xiao B, Farha OK, Ameer GA. (2018) Copper Metal-Organic Framework Nanoparticles Stabilized with Folic Acid Improve Wound Healing in Diabetes. *ACS Nano*. 27;12(2):1023-1032. doi: 10.1021/acsnano.7b01850.
- [19] Irving CS, Lapidot (1978) A Effects of Binding and Bactericidal Action of Vancomycin on *Bacillus licheniformis* Cell Wall Organization as Probed by ^{15}N Nuclear Magnetic Resonance Spectroscopy. *ANTIMICROBIAL AGENTS AND CHEMOTHERAPY*. p. 695-703, 0066-4804/78/0014-0695\$02.00/0
- [20] Matzke GR, Zhanel GG, Guay DR (1986) Clinical pharmacokinetics of vancomycin. *Clin Pharmacokinet*. 11(4):257-82. doi: 10.2165/00003088-198611040-00001.
- [21] Sastry C, Rao T, Rao P (2002) *Microchim Acta* 140: 109. <https://doi.org/10.1007/s00604-002-0900-1>
- [22] Bai X, Lu B, Chen X, Zhang B, Tang J (2014) Reversible detection of vancomycin using peptide-functionalized cantilever array sensor. Volume 62, Pages 145-150

- [23] Liang W, Liu S, Liu Z, Li D, Wang L, Hao C, He Y (2015) Electron transfer and fluorescence “turn-off” based CdTe quantum dots for vancomycin detection at nanogram level in aqueous serum media. *New J. Chem.*, 39, 4774-4782.
- [24] Ng SM, Wu X, Khyasudeen MF, Nowakowski PJ, Tan H-S, Xing B, Yeow EKL. (2018) Vancomycin Determination by Disrupting Electron-Transfer in a Fluorescence Turn-On Squaraine–Anthraquinone Triad. *ACS Sens.* 361156-1163. <https://doi.org/10.1021/acssensors.8b00188>.
- [25] Altintas Z (2018) Surface plasmon resonance based sensor for the detection of glycopeptide antibiotics in milk using rationally designed nanoMIPs. *Scientific Reports*. volume 8, 11222.

CHAPTER FOUR

One pot synthesis of β -cyclodextrin modified silver nanoparticles for highly sensitive detection of ciprofloxacin

Graphical Abstract



Abstract

This study emphasizes on electrochemical detection of ciprofloxacin in animal serum and runoff water using silver nanoparticle modified β -cyclodextrin (Ag- β -CD) composite. The Ag- β -CD composite was synthesized via hydrothermal route, which resulted in a high product yield. Morphological and spectral characterizations of the Ag- β -CD composite was carried out. The Ag- β -CD composite was used to detect ciprofloxacin by employing differential pulse voltammetry (DPV) and cyclic voltammetry (CV). Ag- β -CD modified electrode displayed good specificity towards electro-oxidation of ciprofloxacin. Further, the sensor gave the best response towards electro-oxidation of ciprofloxacin near the human physiological pH of 7.5. A linear response was obtained between the concentration range of 0.1 nM to 50 nM and limit of detection (LOD) at 0.028 nM. The result of the LOD showed a high sensitivity of $26,697.312 \mu\text{A mM}^{-1} \text{cm}^{-2}$ towards ciprofloxacin. The current work has a rationally synthesized and characterized nanocomposite with very high potential of rapid and sensitive detection of ciprofloxacin in spiked animal blood serum and domestic run off water samples. High sensitivity and low LOD results illustrate good practicability for detection of ciprofloxacin in the near future.

Keywords: silver nanoparticles; β -cyclodextrin; ciprofloxacin; cyclic voltammetry; differential pulse voltammetry; electrochemical detection.

1. Introduction

Ciprofloxacin is a third generation quinolone, which is widely used in clinical management against of bacterial infections and works by terminating the growth of bacteria. It has a wide range of applicability for the treatment of bacterial infections in humans, poultry breed and livestock [1-4]. It is prescribed more frequently for bacterial treatment in both humans and animals; as a result, it develops resistance against therapy. The frequent use of ciprofloxacin in humans or animals, result in excess amount of ciprofloxacin in environment (water) in an excreted form. As a result, it disturbs the ecological environmental system and human health. This can also cause various side-effects to patients on ciprofloxacin therapy or even healthy people due to improper monitoring. To avoid the toxicities in both human and animals, there is a need to determine the quantitative analysis of ciprofloxacin for regular monitoring.

Various conventional and non-conventional methods have been used to detect ciprofloxacin in different matrices, which include spectroscopy, capillary electrophoresis, liquid chromatography-mass spectroscopy, immunoassay, spectrofluorimetry, high performance liquid chromatography and electrochemical methods [5-12]. Electrochemical techniques such as impedance spectroscopy and voltammetry provide rapid results with high sensitivity and low operational machinery cost. For the detection of ciprofloxacin via electrochemical route, many nanomaterials and other composite materials have been used such as CNT's, porous nafion, polyaniline, metal oxide nanoparticles, graphene and β -cyclodextrin [13-17]. The use of nanomaterial and nanocomposite material provides higher surface area for the electrons to transfer and the analyte to undergo oxidation or reduction more effectively.

In the present study, we use β -cyclodextrin modified with silver nanoparticles to carry out the detection of ciprofloxacin. β -cyclodextrin is a cyclic oligosaccharides with 7 β (1-4)-glucopyranose

units. These have been extensively used for sensing and drug delivery purposes because of their ability to encapsulate and attract the hydrophobic molecules into its cavity, providing effective interaction sites for the analyte molecules. In previous studies, β -cyclodextrin has been modified with nanomaterials (such as silver nanoparticles and graphene) to carry out optical, fluorescence and electrochemical detection of various analytes [18, 19]. Here, we present a new method for the preparation of silver modified β -cyclodextrin (Ag- β -CD) composite using hydrothermal synthesis route. This method helps to avoid the complicated chemical modifications, which required to conjugating the nanoparticles in β -cyclodextrin and also providing a very high yield. This Ag- β -CD complex was used to carry out the detection of ciprofloxacin. β -cyclodextrin provides a cavity for the drug molecule to come and selectively get trapped and finally undergo the redox reaction. Further, silver nanoparticles help in increasing conductivity of the composite and in turn increasing the sensitivity of the sensing platform. Finally, to check the practical applicability of Ag- β -CD composite modified electrode, ciprofloxacin was detected in spiked domestic run off waste water and animal (sheep) serum sample.

2. Method

2.1 Chemicals, reagents and instrumentation

Sodium dihydrogen orthophosphate dehydrate and silver nitrate were ordered from Merck, South Africa. β -cyclodextrin, Ibuprofen, ciprofloxacin, potassium ferrocyanide, norfloxacin and methanol were obtained from Sigma-Aldrich, South Africa. De-ionized (DI) water was used for making all solutions and washing purposes. Sodium phosphate dibasic dehydrate was bought from Sigma-Aldrich (Germany) and potassium ferricyanide was obtained from Saarchem (Merck, South Africa). Field emission - scanning electron microscope (FE-SEM; ZEISS Ultra Plus, Germany), high resolution-transmission electron microscopy (HR-TEM; JEOL 2100 HRTEM, Korea), Brunauer–

Emmett–Teller (BET; Micromeritics Tristar II 3020 2.00, USA). The X-ray diffraction patterns (XRD) were recorded by a Bruker D2 diffractometer at 40 kV and 50 mA with measurement angle 2θ varying from 5° – 90° with a scan speed of $0.01^{\circ} 2\theta \text{ s}^{-1}$. Additionally, Co K alpha radiation ($\lambda = 1.7902 \text{ \AA}$) was used as secondary graphite monochromated radiation. ^1H NMR spectra were recorded in DMSO-d_6 (^1H : 2.50 ppm) as solvent using Bruker AV 400 MHz spectrometers. Parameters such as chemical shift and coupling constants were recorded in ppm and Hz respectively, UV spectrophotometer (UV-1800, Shimadzu, South Africa), Fourier transform infrared spectroscopy (Bruker® Alpha-P ATR–FT-IR, Germany) and electrochemical setup (CHI 660E, USA) consisting of a working electrode (glassy carbon electrode- 3 mm diameter), a reference electrode (Ag/AgCl) and a counter electrode (platinum wire) were used in the study

2.2 Synthesis of β -cyclodextrin modified silver nanoparticle composite

A very simple route was employed to synthesize β -cyclodextrin modified silver nanoparticle composite. 0.3 g of silver nitrate, 1.1 g of β -cyclodextrin was dispersed and 0.1 g of ibuprofen was dissolved in 10 mL methanol and transferred to a 200 mL autoclave. The autoclave was then put in the oven for four days at 160°C . Finally the autoclave was taken out of oven and cooled to room temperature. Then, the material was centrifuged at 3000 rpm and washed with water and methanol, after that dried at 70°C for 24 hours, prepared composite (Ag- β -CD) was collected and stored. In addition, this reaction was also carried out sequentially in water (w) and methanol: water (mw) (1:1) solvents, at the same experimental condition. Finally, the products obtained were washed and dried at 70°C for 24 hours. These products were labeled as Ag- β -CD (w) and Ag- β -CD (mw) in accordance with their solvents.

2.3 Preparation of electrode

To prepare the electrode for electrochemical measurements, initially the glassy carbon electrode (GCE) was cleaned on the cleaning pad with alumina powder (0.3 and 0.05 μm). After cleaning, GCE was rinsed with water and till a mirror like shine was obtained on the surface. 1 mg mL⁻¹ aliquots of Ag- β -CD composite in DI water were prepared. The GCE was drop-coated with 5 μL of Ag- β -CD composite and kept under the IR lamp for drying for 20 mins. The modified electrode was labelled as Ag- β -CD/GCE and was used to carry out further electrochemical studies.

2.4 Preparation of serum sample and waste water sample

We are thankful to Dr. Thirumula Govenders lab at University of KwaZulu-Natal, Westville, South Africa for the sheep blood serum sample, which was used to carry out further studies. To check the feasibility of the modified electrode, detection and quantitative determination of ciprofloxacin was carried out in an unknown serum sample. The unknown serum samples were diluted up to 10 times to reduce matrix effects and was then used for the detection of ciprofloxacin using Ag- β -CD composite modified electrode. The diluted serum samples were spiked with 0 nM, 0.1 nM, 20 nM, 40 nM, and 50 nM ciprofloxacin and differential pulse voltammetry (DPV) was carried out. Further, detection of ciprofloxacin was also carried out in domestic run-off water from a local home. The water samples were collected and spiked with 0 nM, 0.1 nM, 20 nM, 40 nM, and 50 nM ciprofloxacin and cyclic voltammetry (CV) was carried out. Interfering studies to check the specificity of electrode towards ciprofloxacin were also carried out in presence of various metal ions and organic impurities to check the feasibility of the proposed sensors in presence of other interferents.

3. Results and Discussion

3.1 Choice of material

In this study, we use the hydrothermal route to prepare the Ag- β -CD nanocomposite. Previously, Ag- β -CD composite had been synthesized via chemical modification using thiol bonds [18]. This route

was employed because of the various advantages it provides such as facile technique, easy handling, higher yield (~80.42%), single pot synthesis and better temperature control. The synthesis was carried out in methanol and water as the solvents and a template molecule (IBF) to check its effect on the morphology of the composite. The presence of template molecule did not have any effect on the morphologies of any composites prepared. However, on changing the solvents it was observed that there was a change in the morphologies of the composites. In case of Ag- β -CD, it was observed that silver nanoparticles were incorporated into the β -cyclodextrin sheets and furthermore, decorated with silver nanoparticles were obtained. This composite illustrated good electro-conductivity and similar morphological characteristics of silver nanoparticles to the previously reported methods. However, on introduction of water into the solvent system it was seen that low electro-conductive composites (Ag- β -CD (w), Ag- β -CD (mw)) were obtained. This can be a result of coating of β -cyclodextrin over the silver nanoparticles, leading to poor conductivity. Therefore, Ag- β -CD was employed to study the electrochemical detection of ciprofloxacin.

β -cyclodextrin was chosen for detection of ciprofloxacin because of its inherent quality to form complexes with various guest molecules which is attributed to the hydrophobic internal cavity along with the hydrophilic exterior [20]. Therefore, β -cyclodextrin provides high specificity towards the detection of ciprofloxacin by providing a suitable site for the drug to rest and undergo oxidation. Incorporation of silver nanoparticles with β -cyclodextrin leads to increase in electrochemical conductivity and hence increasing the sensitivity of the composite sensing material. This composite also has a potential as a drug carrier for drug delivery purposes due to the low toxicity levels of cyclodextrin and silver nanoparticles. Additionally, the hydrophobic cavities provide a site where the drug can be stored and slow and controlled release can be achieved [21].

3.2 Characterization of β -cyclodextrin modified silver nanoparticle composite

The synthesis procedure lead to the modification of β -CD with silver nanoparticles via the modification of --OH bonds of cyclodextrin molecules. Silver nanoparticles act as metal precursor to initialize the assembly with β -cyclodextrin for the formation of the composite. ^1H NMR spectrum of β -cyclodextrin and Ag- β -CD was performed in DMSO-d_6 solvent. Overlapping image of those spectra (Fig. 1) shows that there were significant deviations in chemical shifts of hydroxyl protons only. These deviations in chemical shift value indicate the role of hydroxyl proton in the Ag- β -CD formation. Magnitude of change in chemical shifts occurs in ^1H NMR spectra is consequences of shielding or deshielding effect exert by Ag on O-H proton in Ag- β -CD composite. Shifting of primary hydroxyl proton (7-OH) 4.45 ppm to 4.43 ppm (9.8 Hz), similarly two secondary hydroxyl proton shifted 5.72 ppm to 5.70 ppm (6.2 Hz) and 5.67 ppm to 5.66 ppm (4.2 Hz). All these findings from ^1H NMR spectrum are in favor of formation of Ag- β -CD architecture. It was also observed that there were no traces of the template molecule found in final product obtained. However, there was no change in the morphology of final product observed when the template was added or not to the autoclave.

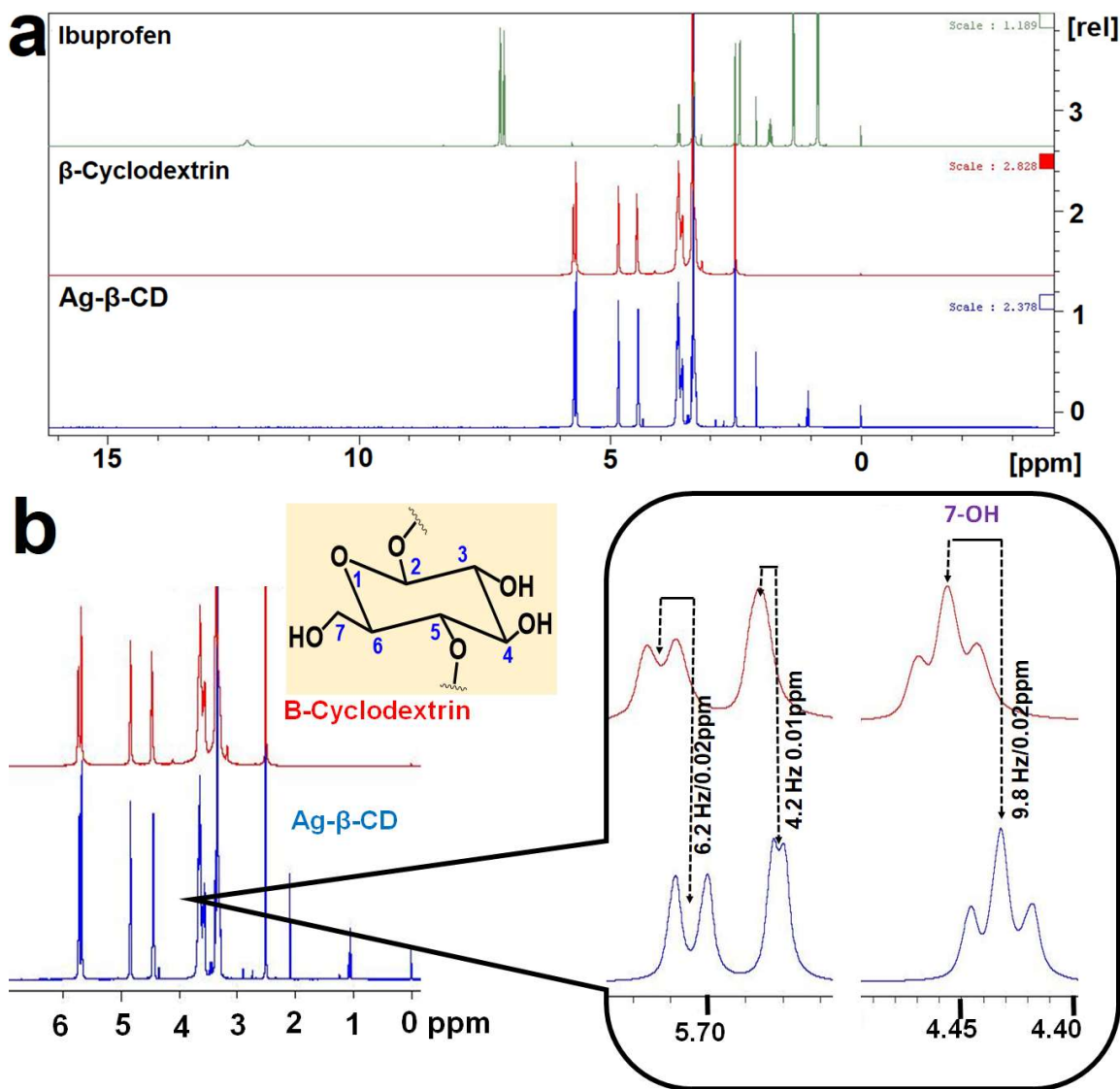
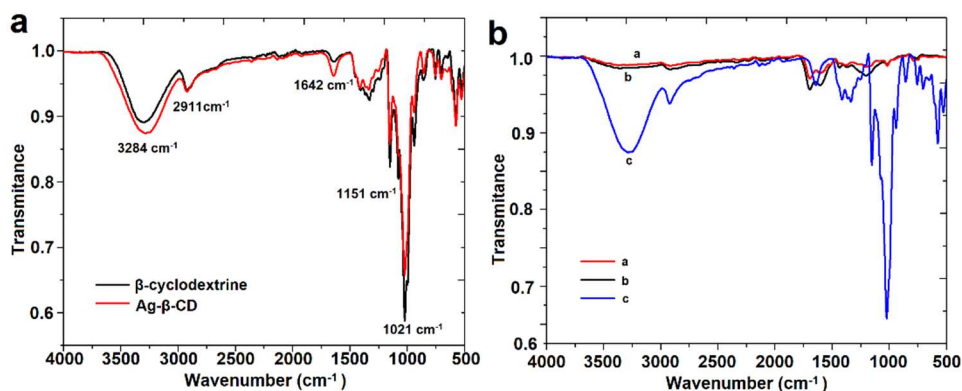


Fig. 1. (a) ^1H NMR spectra's of Ibuprofen, β -cyclodextrin and silver nanoparticles modified β -cyclodextrin (Ag- β -CD). (b) NMR showing the peak shifts that occur in the β -cyclodextrin structure at the $-\text{OH}$ functional groups.

To confirm the chemical composition, FTIR spectrum (Fig. 2a) was evaluated and changes were observed after the addition of silver nanoparticles to the β -cyclodextrin molecule. A wide peak at 3284 cm^{-1} is due to O-H stretch and a peak at 2922 cm^{-1} is observed due to C-H symmetric/asymmetric stretch. An additional peak at 1642 cm^{-1} is due to the deformation bands of water (H-O-H) present in

β -cyclodextrin molecule. Further, peaks at 1151 cm^{-1} , 1021 cm^{-1} indicate the overtone stretching of C-H bond and C-O stretching respectively [22]. Further, FTIR spectra (Fig. 2b) comparing the peaks of Ag- β -CD, Ag- β -CD (w) and Ag- β -CD (mw) shows the diminishing of peaks at 3284 cm^{-1} , 1151 cm^{-1} and 1021 cm^{-1} . This can be attributed to the coating of β -cyclodextrin on silver nanoparticles which blocks the -OH and C-O groups. No deformation band due to water molecules (H-O-H) are observed at 1642 cm^{-1} . This may be due to silver nanoparticles occupying the cavities of β -cyclodextrin.

UV-spectroscopy was carried out to check the optical properties of the prepared composites. As seen in Fig. 2c, Ag- β -CD shows characteristic peak at 421 nm , which confirms the presence of silver nanoparticles in the composite [23]. Further, Fig. 2d shows, Ag- β -CD (mw) has a band edge around 450 nm which is a characteristic peak for silver nanoparticles. However, in case of Ag- β -CD (w), no absorbance peak was observed. This is due to silver nanoparticles being completely coated with β -cyclodextrin molecules.



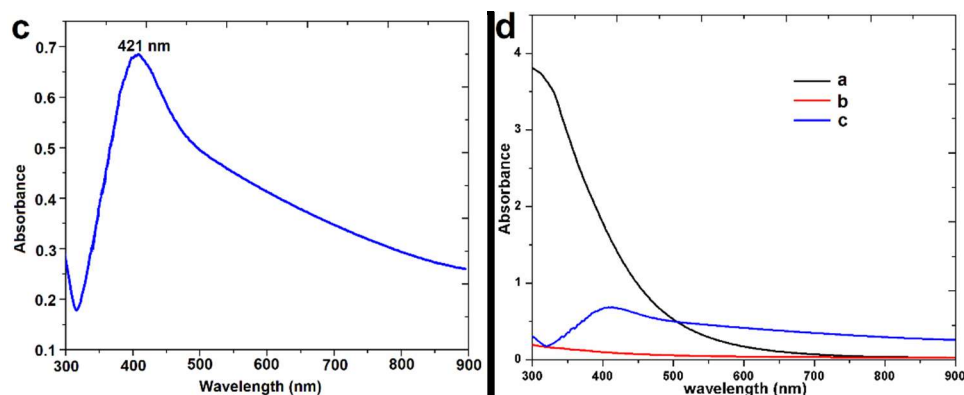


Fig. 2. (a) FTIR spectrum of β -cyclodextrin and Ag- β -CD. (b) FTIR of a) Ag- β -CD (w), b) Ag- β -CD (mw) and c) Ag- β -CD. (c) UV-absorbance curve of Ag- β -CD in water. (d) UV-absorbance curves of a) Ag- β -CD (w), b) Ag- β -CD (mw) and c) Ag- β -CD in water (1 mg.mL^{-1}).

Further, the morphological studies were carried out using FE-SEM and HR-TEM imaging. From the FE-SEM images for Ag- β -CD (Fig. 3a), it can be concluded that rectangular plates decorated with silver nanoparticles were formed. Elemental analysis from EDX depicted that only carbon (29.78%), silver (38.48%) and oxygen (31.74%) were present in the composite material as seen in Fig. 3b. The elemental mapping of the composite demonstrated that silver nanoparticles were also incorporated in the rectangular plates formed as seen in Fig. 3c. Further, HR-TEM images also displayed silver nanoparticles with rectangular plates (Fig. 3 d, e), which is similar to morphological characteristics as seen in FE-SEM.

BET analysis was carried out to find the pore size and surface area of the composites formed. The BET surface area came out be $3.2974 \text{ m}^2 \text{ g}^{-1}$ with an average pore size of 377.951 \AA and the isotherm obtained was similar to that of mesoporous materials as seen in Fig. 3f. Further, XRD analysis of the prepared composite confirm the presence of silver nanoparticles. Fig. 3g shows the peaks (2θ) at 37.94 , 44.04 , 64.2 and 77.14 with their corresponding planes as (111), (200), (220) and (311) respectively [23]. Further, a few small peaks from 10 to 35 degree can be attributed to the β -cyclodextrin present in the complex [24].

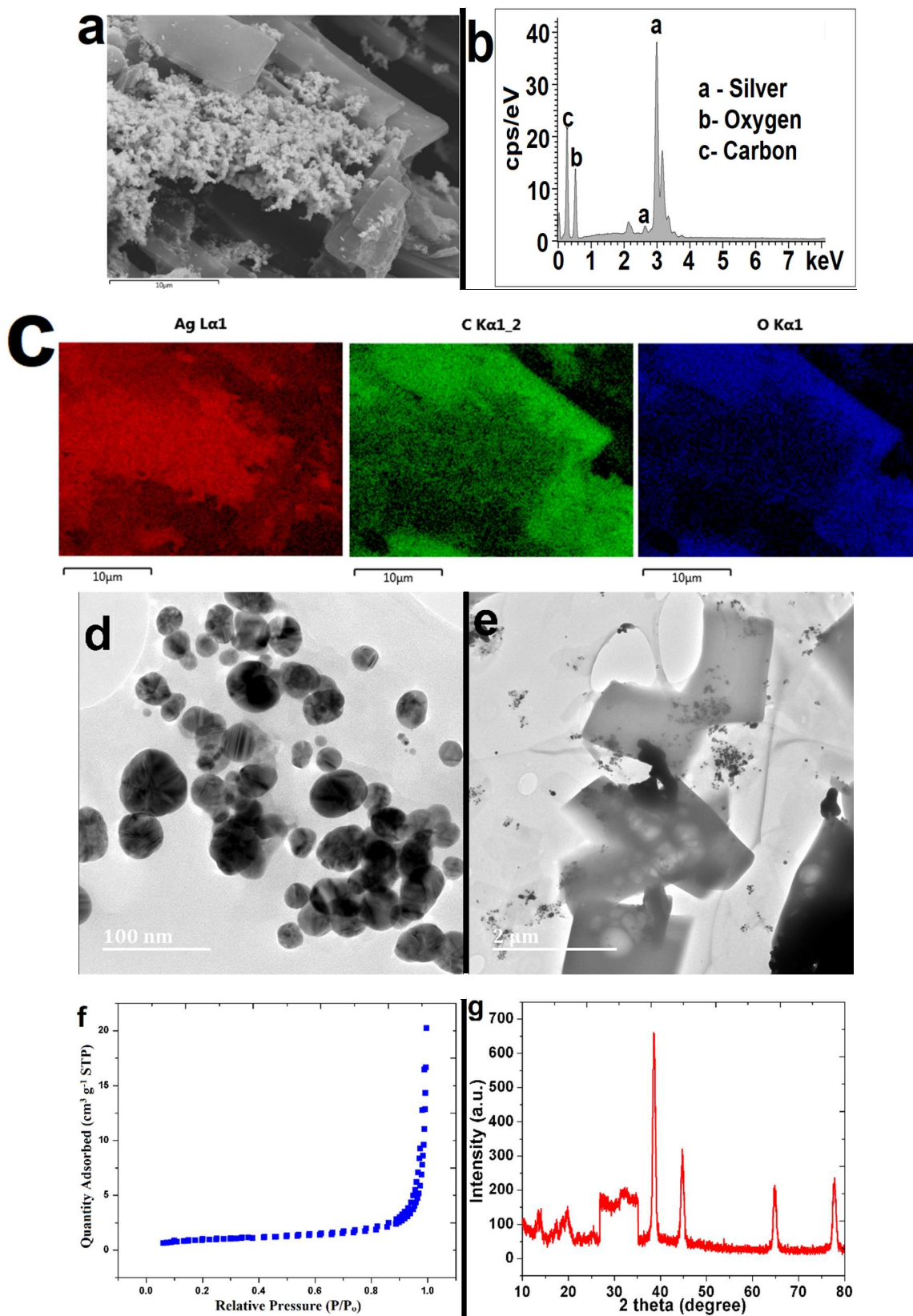


Fig. 3. (a) FE-SEM image of Ag- β -CD. (b) EDX analysis of Ag- β -CD. (c) Elemental mapping of Ag- β -CD composite showing equal distribution of silver nanoparticles on β -cyclodextrin sheets. (d) HR-TEM analysis of Ag- β -CD at 100 nm, with silver nanoparticles. (e) HR-TEM at 2 μ m showing the sheets and silver nanoparticles separately. (f) N₂ adsorption and desorption isotherms obtained from BET analysis of Ag- β -CD. (g) XRD of Ag- β -CD with characteristic peaks of silver nanoparticles and β -cyclodextrin.

3.3 Electrochemical characterization

The composite modified electrode was electrochemically characterized using cyclic voltammetry, which was carried out in 2.5 mM [Fe(CN)₆]^{3-/4-} in 1 M KCl as the electrolyte. The effective surface area of the modified electrode was calculated using Randles-Sevcik [25] equation:

$$I_p = 2 \cdot 69 \times 10^5 A \sqrt{D} (\sqrt{n})^3 \sqrt{v} C_0$$

where C_0 is the concentration in mol.cm⁻³, “ I_p ” is the peak current (Amp), “ A ” is the surface area of the electrode in cm², “ n ” is the number of electrons transferred (for K₃[Fe(CN)₆], $n=1$), “ D ” is the diffusion coefficient (7.60×10⁻⁶ cm².s⁻¹ for K₃[Fe(CN)₆]) and “ v ” is the scan rate (V.s⁻¹). The slope of plot I_{pa} vs $v^{1/2}$ in Fig. 4a [Inset] was used to calculate the effective surface area. The effective surface areas for GCE and Ag- β -CD /GCE were found to be 0.03808 cm² and 0.04787 cm², respectively. High effective surface area of Ag- β -CD composite is anticipated to be one of the cause for higher peak currents. Additionally, charge transfer kinetics of the modified electrode were studied using electrochemical impedance spectroscopic (EIS) as seen in Fig. 4b. The frequency range was selected between 1 to 10⁵ Hz and initial potential was set to 0.206 V. The obtained data is represented as Nyquist Plot in the form of Randles equivalent circuit. The values of the components of circuit are mentioned in Table 1 which are double layer capacitance (C_{dl}), charge transfer resistance (R_{ct}), warburg impedance (W) and the resistance of the solution (R_s). Lower R_{ct} value of composite depicts that better charge transfer takes place with the modified electrode as compared to the GCE.

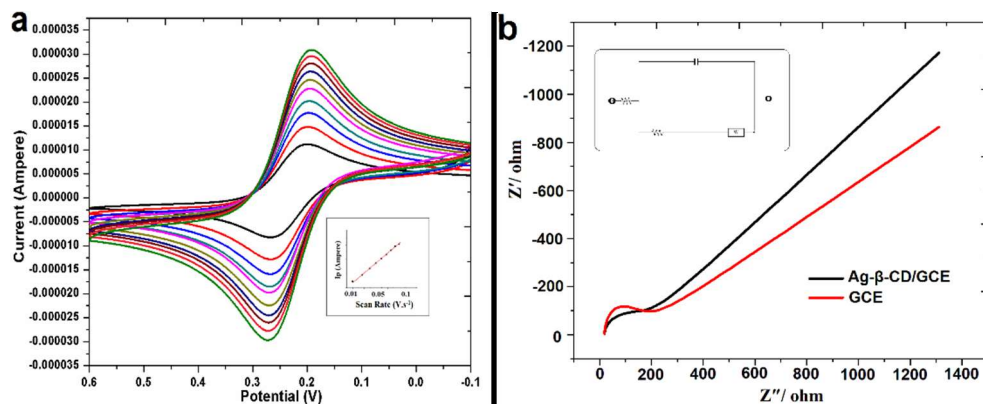


Fig. 4. (a) Scan rate studies of Ag-β-CD /GCE from (0.01 to 0.10 V s⁻¹) carried out in 2.5 mM [Fe(CN)₆]^{3-/4-} in 1 M KCl, Inset- calibration plot for anodic peak current vs root of scan rate. **(b)** EIS spectra in 2.5 mM [Fe(CN)₆]^{3-/4-} in 1 M KCl at GCE, Ag-β-CD/GCE. Inset- Randles equivalent circuit model.

Table 1 Components of Randles equivalent circuit for GCE and Ag-β-CD/GCE

Material	R _s (Ω)	R _{ct} (Ω)	C _{dl} (F g ⁻¹)	W (Ω s ^{-1/2})
GCE	23.1	240.9	4.788 e ⁻⁷	0.0002632
Ag-β-CD/GCE	21.2	131.3	5.659 e ⁻⁷	0.0002245

3.4 Electrochemical detection of ciprofloxacin

The detection of ciprofloxacin was carried out using cyclic voltammetry and differential pulse voltammetry using the composite modified electrode. Cyclic voltammetry measurements were carried out with 0.1 mM ciprofloxacin in 0.1 mM phosphate buffer (pH 7.0). The modified electrode provided substantial increase in the peak current due to high electro-catalytic activity towards electro-oxidation of ciprofloxacin as seen in Fig. 5a. This can be attributed to the faster electron transfer due to the silver nanoparticles and simultaneously hydrophobic sites of β-cyclodextrin are favorable for ciprofloxacin oxidation. The drug undergoes an irreversible reaction, which is seen in the voltammogram (Fig. 5a), as only anodic peak at the potential of 1.532 V is seen. In addition, Ag-β-CD/GCE show high sensitivity towards ciprofloxacin as compared to the GCE due to higher current

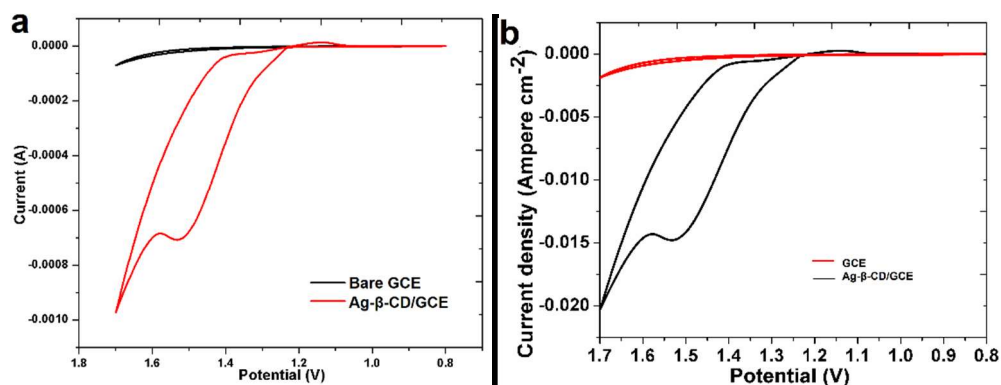
density obtained (Fig. 5b). Hence, making it a good candidate for carrying out electrochemical detection of ciprofloxacin.

Further, to study the reaction taking place at the electrode interface, scan rate studies were carried out. Cyclic voltammograms were recorded at varying scan rates from 0.01 to 0.1 V.s⁻¹ (Fig. 5c). The linear relation between scan rate and anodic peak currents was obtained (Fig. 5d), depicting that adsorption controlled reaction took place at the electrode interface.

The effect of pH on the anodic current was also studied to check the most appropriate pH for the sensor to work. The studies were carried out via differential pulse voltammetry in phosphate buffer (0.1 M) (ranging from 5.0 to 8.0) in 0.1 mM ciprofloxacin as seen in voltammograms in Fig. 5e. A linear relation between E_p vs pH (Fig. 5f) was obtained as

$$E_p = 1.265 - 0.054 \text{ pH}$$

The values of slope is close to the nernstian value of 0.059 V/pH at 25 °C, which depicts that equal number of electrons and protons are involved during the electro-oxidation of ciprofloxacin. A potential shift from positive (1.4 V) to negative (1.3 V) can be attributed to proton-coupled electron transfer taking place at the electrode interface. Finally, 7.5 pH was the optimum for the reaction and was used for further studies.



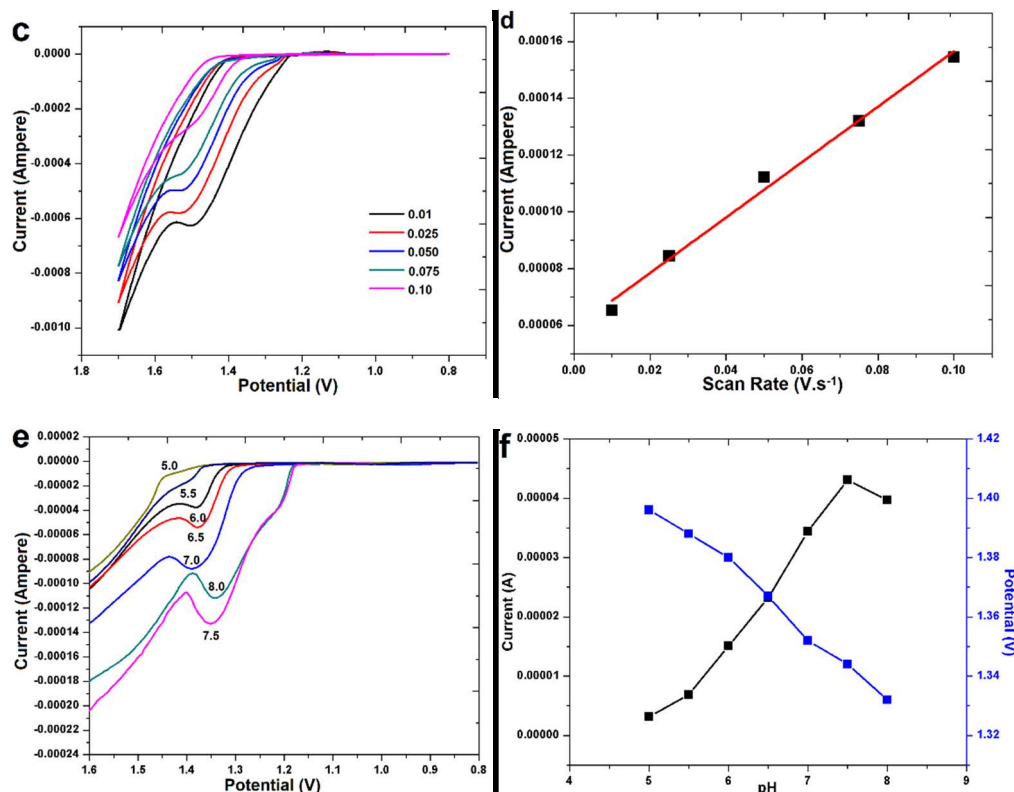


Fig. 5. (a) Cyclic voltammograms in 0.1 mM ciprofloxacin in 0.1 M phosphate buffer (pH 7.0) at different modified electrodes (i.e. GCE, Ag-β-CD/GCE) Scan rate = 0.1 V.s⁻¹. (b) Cyclic voltammograms between current density vs potential, showing the high sensitivity of electrode towards electrooxidation of ciprofloxacin. (c) Scan rate studies at Ag-β-CD/GCE in 0.1 mM ciprofloxacin+0.1 M phosphate buffer (pH 7.0) by varying scan rates from 0.01 V.s⁻¹ to 0.1 V.s⁻¹. (d) Calibration plot of scan rate vs current plotted for the scan rate studies in ciprofloxacin. (e) pH studies in 0.1 mM ciprofloxacin in 0.1 M phosphate buffer at Ag-β-CD/GCE with varying pH, at scan rate = 0.1 V.s⁻¹. (f) pH vs current vs potential plot for variations in potentials and peak currents in different pH buffers.

3.5 Analytical performance

DPV was used to check the analytical performance of the modified electrode for detection of ciprofloxacin. The oxidation peak for ciprofloxacin was obtained at the potential of 1.308 V. Composite modified electrode provided a linear relationship between concentrations of ciprofloxacin and peak current between the ranges of 0.1 nM to 50 nM as shown in Fig. 6a. The linear regression equation is expressed as:

$$I_p (10^{-5}A) = 1.44384e^{-7} + 1.27802e^{-6} [\text{ciprofloxacin}] (\text{nM}); R= 0.97863$$

The LOD for the fabricated sensing electrode was calculated using the calibration plot from Fig. 6b, which came out to be 0.028 nM (using the relations $3S/N = 0.028 \pm 0.0083$ nM) with high sensitivity of $26,697.312 \mu A \text{ mM}^{-1} \text{ cm}^{-2}$. The present work provided lower LOD as compared to previous sensing methods as listed in Table 2.

Table 2 Comparison of previous modified electrodes for detection of ciprofloxacin

Modified Electrode	Technique	LOD	Matrices	References
MWCNT	Chronoamperometry	6 μM	Urine and serum samples.	13
porous-Nafion-MWCNT/BDD	DPV	0.005 μM	Natural waters and wastewater effluents.	14
MgFe ₂ O ₄ Nanoparticles/MWCNTs	CV	0.01 μM	Human urine, Plasma, tablet.	15
β -cyclodextrin and l-arginine modified carbon paste electrode	DPV	0.01 μM	Pharmaceutical formulations and human serum samples.	16
Silver nanoparticle modified β -cyclodextrin/GCE	DPV	0.000028 μM	Animal Serum and Domestic run-off water.	This work.

Further, the capability of the sensor was tested in presence of various interfering agents. Interfering agents that were tested were cystamine, norfloxacin, L-glutamic acid, folic acid and metal ions (Na^+ , Mg^{2+} and K^+). Other possible interferences from compounds commonly occurring in our physiological systems such as ascorbic acid, lactose, uric acid and dopamine would have no effect.

This is because these compound do not oxidize in the chosen potential window. DPV was carried out to check the interference caused by respective interfering agents to the ciprofloxacin response. For this, 1 mM solution of each interfering agent was added to the ciprofloxacin (0.1 mM) solution in phosphate buffer (0.1 M). Fig. 6c shows less than 2.4% deviation was observed, this indicated the high specificity of Ag- β -CD/GCE towards ciprofloxacin. The stability of proposed electrode was tested at the interval of 24 hours using DPV with ciprofloxacin (0.1 mM) in phosphate buffer (0.1 M). The peak current response was stable for four days (Fig. 6d), however, on the fifth day a decrease in the output peak current was observed. This may be due to the adsorption based detection of ciprofloxacin which blocked the active sites for ciprofloxacin to oxidize.

For practical application of the sensor, Ag- β -CD/GCE was used to detect ciprofloxacin in domestic run off waste water and animal serum samples. Both the samples were diluted 10 times to reduce any matrix effects that may be caused during the detection of ciprofloxacin. Firstly, DPV was used to carry out the detection of ciprofloxacin in spiked serum sample. Voltammograms in Fig. 6e shows the increase in oxidation peak currents on increasing the concentration of ciprofloxacin in the animal serum sample. Further, cyclic voltammetry (scan rate = 0.1 V.s⁻¹) was used to carry out the detection of the drug in run-off water. On increasing ciprofloxacin concentration, an increase in the oxidation peak currents is observed as seen in Fig. 6g. Calibration plots for the real samples were plotted and a linear relation was obtained (Fig. 6f, h). Therefore, Ag- β -CD/GCE electrode has the potential of carrying out detection of ciprofloxacin in biological matrices as well as environmental samples.

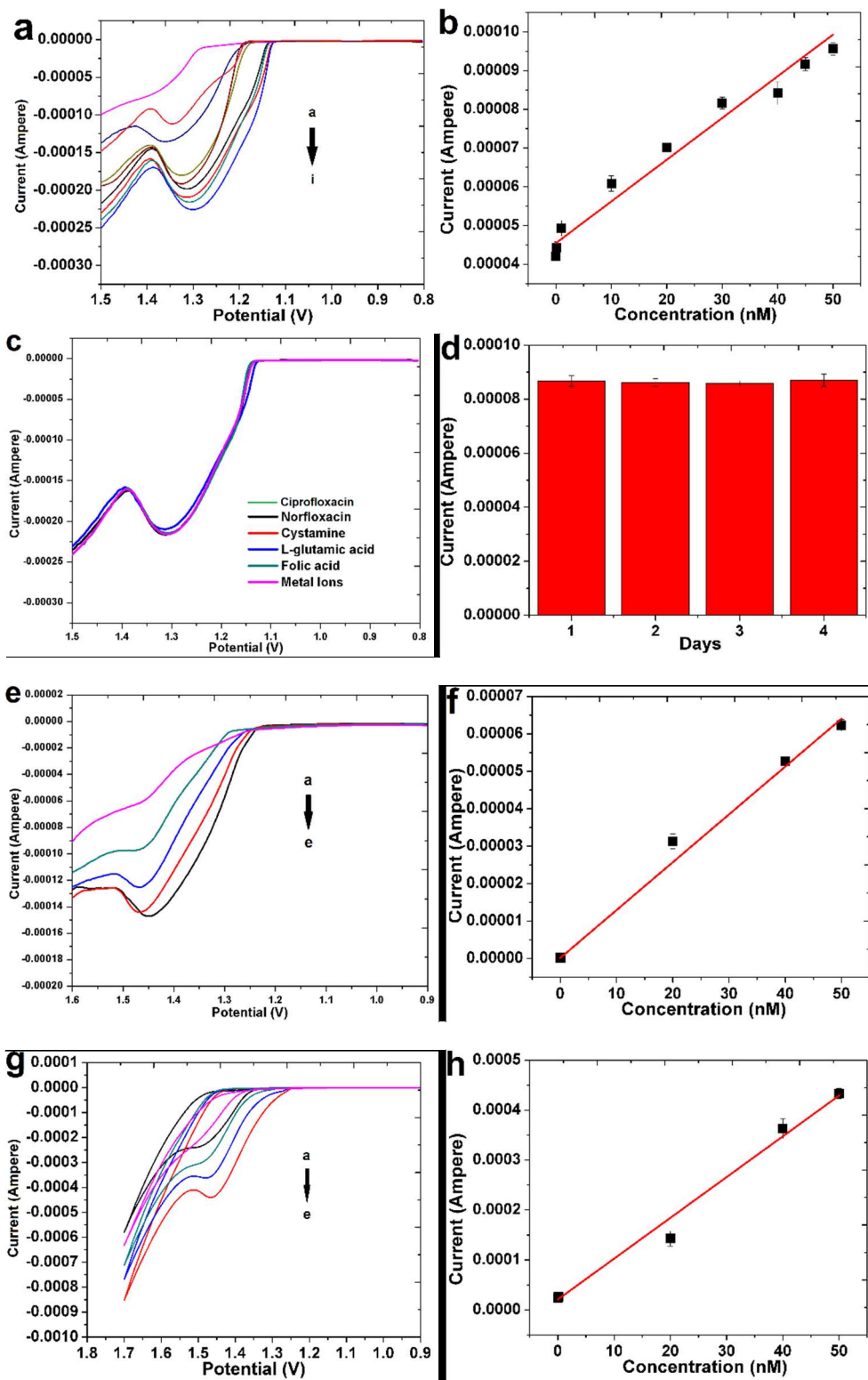


Fig. 6. (a) DPV in 0.1 M phosphate buffer (pH 7.5) at Ag- β -CD/GCE at varying concentration of ciprofloxacin from 0.1 nM [a] to 50 nM [i]. (b) Calibration plot of [ciprofloxacin] vs peak currents. (c) DPV at Ag- β -CD/GCE in 0.1 mM ciprofloxacin in 0.1 M phosphate buffer (pH 7.5), by adding (1 mL of 1 mM) each interfering agent separately and DPVs are recorded. (d) Stability of Ag- β -CD/GCE to 0.1 mM ciprofloxacin in 0.1 M phosphate buffer (pH 7.5) by DPV for four days. (e) DPV curve of Ag- β -CD/GCE in animal serum sample spiked with increasing concentrations of ciprofloxacin from a to e. (f) Calibration plot for [ciprofloxacin] vs peak currents in serum sample. (g) CV curve of run-off water sample spiked with increasing concentrations of ciprofloxacin from a to e. (h) Calibration plot for [ciprofloxacin] vs peak currents in run-off water sample.

4. Conclusion

In summary, novel method for the synthesis of Ag- β -CD with high yield (~80%) was developed. This synthesized composite was successfully applied to carry out highly sensitive detection of ciprofloxacin at a favorable pH for physiological samples. A lower LOD (0.028 nM) as compared to previous electrochemical methods was achieved with a linear response from 0.1 nM to 50 nM. Additionally, the composite also provided high sensitivity of $26,697.312 \mu\text{A mM}^{-1} \text{ cm}^{-2}$ and good specificity towards ciprofloxacin. The composite modified electrode was successful in detecting the drug in run-off water and animal serum sample. Further, changes in the solvent provided different colored Ag- β -CD composites, which can be applied for colorimetric detection or even for drug delivery purposes. Additionally, the synthesis technique can also be used to modify β -CD with various other metal nanoparticles to form novel nanocomposite for a variety of applications such as in electrochemistry, drug delivery and optical sensors.

References

- [1] X. Zhang, Y. Wei, Y. Ding, Electrocatalytic Oxidation and Voltammetric Determination of Ciprofloxacin Employing Poly (alizarin red)/Graphene Composite Film in the Presence of Ascorbic acid, Uric acid and Dopamine, *Anal. Chim. Acta.* 835 (2014) 29-36.
- [2] A.A. Ensafi, A.R. Allafchian, R. Mohammadzadeh, Characterization of MgFe_2O_4 Nanoparticles as a Novel Electrochemical Sensor: Application for the Voltammetric Determination of Ciprofloxacin, *Anal. Sci.* 28.7 (2012) 705-710.
- [3] N. Diab, I. Abu-Shqair, R. Salim, M. Al-Subu, The Behavior of Ciprofloxacin at a DNA Modified Glassy Carbon Electrodes, *Int. J. Electrochem. Sci.* 9 (2014) 1771-1783.
- [4] L. Fotouhi, M. Alahyari, Electrochemical Behavior and Analytical Application of Ciprofloxacin Using a Multi-walled Nanotube Composite Film-Glassy Carbon Electrode, *Colloids Surf. B.* 81.1 (2010) 110-114.
- [5] H.Y. Ji, D.W. Jeong, Y.H. Kim, H. Kim, D. Sohn, H.S. Lee, Hydrophilic Interaction Liquid Chromatography–Tandem Mass Spectrometry for the Determination of Levofloxacin in Human Plasma, *J. Pharm. Biomed. Anal.* 41.2 (2006) 622-627.
- [6] U. Neckel, C. Joukhadar, M. Frossard, W. Jäger, M. Müller, B.X. Mayer, Simultaneous Determination of Levofloxacin and Ciprofloxacin in Microdialysates and Plasma by High-Performance Liquid Chromatography, *Anal. Chim. Acta.*, 463.2 (2002) 199-206.
- [7] S. Mostafa, M. El-Sadek, E.A. Alla, Spectrophotometric Determination of Ciprofloxacin, Enrofloxacin and Pefloxacin through Charge Transfer Complex Formation, *J. Pharm. Biomed. Anal.* 27.1 (2002) 133-142.
- [8] C. Tong, G. Xiang, Sensitive Determination of Norfloxacin by the Fluorescence Probe of Terbium (III)-sodium Dodecylbenzene Sulfonate and its Luminescence Mechanism *J. Fluoresc.* 16.6 (2006) 831-837.

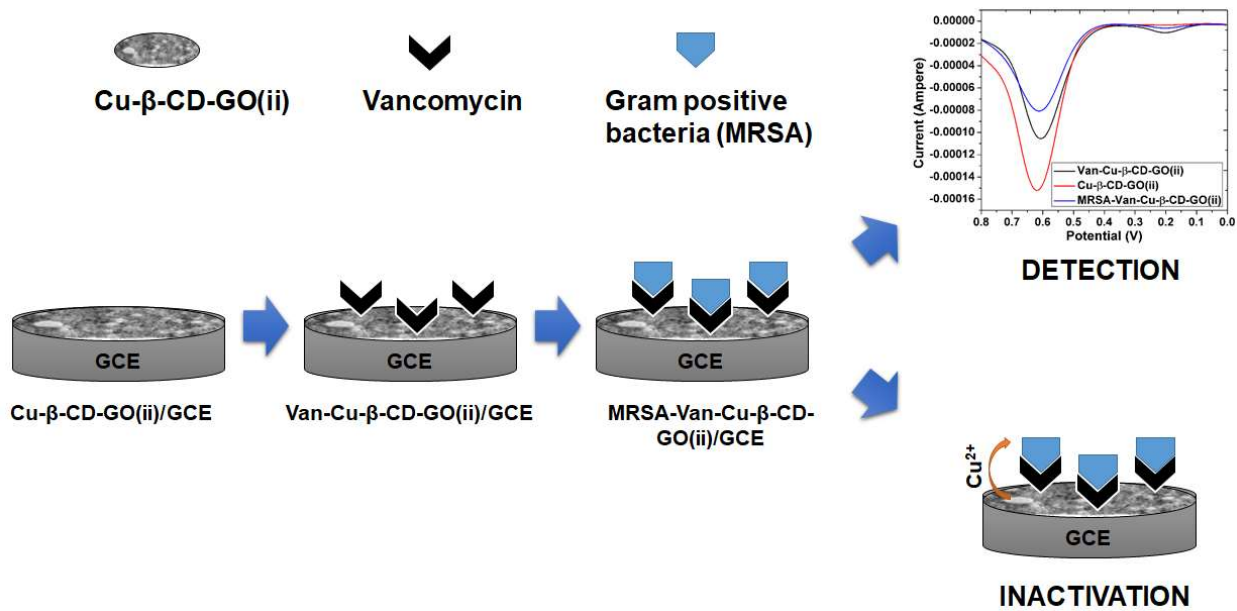
- [9] R.H.O. Montes, M.C. Marra, M.M. Rodrigues, E.M. Richter, R.A.A. Munoz, Fast Determination of Ciprofloxacin by Batch Injection Analysis with Amperometric Detection and Capillary Electrophoresis with Capacitively Coupled Contactless Conductivity Detection, *Electroanalysis*. 26.2 (2014) 432-438.
- [10] G.G. Snitkoff, D.W. Grabe, R. Holt, G.R. Bailie, Development of An Immunoassay for Monitoring the Levels of Ciprofloxacin Patient Samples, *J. Immunoassay Immunochem*. 19.4 (1998) 227-238.
- [11] H. Sun, L. Li, X. Chen, Flow-injection Enhanced Chemiluminescence Method for Determination of Ciprofloxacin in Pharmaceutical Preparations and Biological Fluids, *Anal. Bioanal. Chem*. 384.6 (2006) 1314-1319.
- [12] A. Radi, M.A. El Ries, S. Kandil, Electrochemical Study of the Interaction of Levofloxacin with DNA, *Anal. Chim. Acta*. 495.1 (2003) 61-67.
- [13] L. Fotouhi, M. Alahyari, Electrochemical behavior and analytical application of ciprofloxacin using a multi-walled nanotube composite film-glassy carbon electrode, *Colloids and Surfaces B: Biointerfaces*. 81.1 (2010) 110-114.
- [14] P. Gayen, B.P. Chaplin, Selective electrochemical detection of ciprofloxacin with a porous nafion/multiwalled carbon nanotube composite film electrode, *ACS applied materials & interfaces* 8.3 (2016) 1615-1626.
- [15] A.A. Ensafi, A.R. Allafchian, R. Mohammadzadeh, Characterization of MgFe₂O₄ nanoparticles as a novel electrochemical sensor: application for the voltammetric determination of ciprofloxacin, *Analytical Sciences*. 28.7 (2012) 705-710.
- [16] F. Zhang, S. Gu, Y. Ding, Z. Zhang, L. Li, A novel sensor based on electropolymerization of β -cyclodextrin and l-arginine on carbon paste electrode for determination of fluoroquinolones, *Analytica chimica acta*. 770 (2013) 53-61.

- [17] A.S. Lim, M.U. Ahmed, A Simple DNA-based Electrochemical Biosensor for Highly Sensitive Detection of Ciprofloxacin Using Disposable Graphene, *Analytical Sciences* 32.6 (2016) 687-693.
- [18] X. Chen, S.G. Parker, G. Zou, W. Su, Q. Zhang, β -Cyclodextrin-functionalized silver nanoparticles for the naked eye detection of aromatic isomers, *ACS nano*. 4(11) (2010) 6387-6394.
- [19] N. Agnihotri, A.D. Chowdhury, A. De, Non-enzymatic electrochemical detection of cholesterol using β -cyclodextrin functionalized graphene, *Biosensors and Bioelectronics*. 63 (2015) 212-217.
- [20] D. Valle, E.M. Martin, Cyclodextrins and their uses: a review, *Process biochemistry*. 39.9 (2004) 1033-1046.
- [21] B. Singh, A. Dhiman, A. Kumar, Slow release of ciprofloxacin from β -cyclodextrin containing drug delivery system through network formation and supramolecular interactions, *International journal of biological macromolecules*. 92 (2016) 390-400.
- [22] H. Rachmawati, C.A. Edityaningrum, R. Mauludin, Molecular Inclusion Complex of Curcumin– β -Cyclodextrin Nanoparticle to Enhance Curcumin Skin Permeability from Hydrophilic Matrix Gel, *AAPS PharmSciTech*. 14 (2013) 4. DOI: 10.1208/s12249-013-0023-5.
- [23] Y-F Li, W-P Gan, J. Zhou, Z-Q Lu, C. Yang, T-T Ge, Hydrothermal synthesis of silver nanoparticles in Arabic gum aqueous solutions, *Transactions of Nonferrous Metals Society of China*. 25 (6) (2015) 2081-2086.
- [24] N. Papadopoulos, H.S. Karayianni, P.E. Tsakiridis, M. Perraki, E. Hristoforou, Cyclodextrin inclusion complexes as novel MOCVD precursors for potential cobalt oxide deposition, *Applied Organometallic Chemistry*. 24(2) (2009) 112 – 121.
- [25] L.R. F, A.J. Bard, *Electrochemical Methods: Fundamentals and Applications*, John Wiley, New York, 2001.

CHAPTER FIVE

A novel porous nanocomposite of vancomycin@Cu- β -CD-GO for sensitive electrochemical detection and inactivation of Methicillin-resistant *Staphylococcus aureus*

Graphical Abstract





A novel copper-based 3D porous nanocomposite for electrochemical detection and inactivation of pathogenic bacteria

Atal A.S. Gill ^a, Sima Singh ^a, Zondi Nate ^a, Ruchika Chauhan ^a, Neeta B. Thapliyal ^{a, b}, Rajshekhar Karpoomath ^a , Shital M. Maru ^c, T.M. Reddy ^d

Show more ✓

<https://doi.org/10.1016/j.snb.2020.128449>

Get rights and content

Abstract

A novel porous nanocomposite was synthesized *via* hydrothermal route using copper salt, β -cyclodextrin, and graphene oxide (Cu- β -CD-GO) as its precursors. The novel porous nanocomposite possessed features like large Brunauer–Emmett–Teller (BET) surface area ($76.8309 \text{ m}^2 \text{ g}^{-1}$) and good electrochemical conductivity. Thus it could be used as an efficient electrode modifier for carrying out electrochemical studies. The composite was functionalized with vancomycin (Van) for detection of Methicillin-resistant *Staphylococcus aureus* (MRSA). Differential pulse voltammetry (DPV) was used to carry out the electrochemical detection of MRSA and achieved a very low limit of detection (LOD) 5 CFU mL^{-1} with good sensitivity. The Van conjugation with the composite not only acted as a capture probe for bacteria but also provided good antibacterial activity against MRSA. The Van conjugated composite (Van-Cu- β -CD-GO) provided low minimum inhibitory concentration (MIC) value of $1.93 \text{ } \mu\text{g mL}^{-1}$. Due to good sensitivity and low MIC value, this novel porous nanocomposite (Van-Cu- β -CD-GO) provides an excellent platform for theranostic approach for MRSA.

Keywords: copper nanoparticles; graphene oxide; β -cyclodextrin; electrochemical detection; methicillin-resistant *S. aureus* (MRSA); vancomycin; antibacterial.

1. Introduction

Over the past few years, infection of *Staphylococcus aureus* (*S. aureus*) has been one of the most prevalent communicable diseases in hospitals and health care facilities. It causes various diseases in humans, from mild skin infections to fatal sepsis that leads to organ failure in multiple cases.¹ More specifically, methicillin-resistant *S. aureus* (MRSA) is resistant to most of the available drugs of class penicillin and β -lactam.² These MRSA bacteria are clinically responsible for several cases of morbidity and mortality due to their environmental tolerance, antimicrobial resistance, and potential outbreak.³ The probability of MRSA pathogens can be significantly reduced if they can be diagnosed and treated at an early stage. Therefore, a new technique for the rapid and early diagnosis of MRSA is urgently needed to limit the spread of these infections and minimize the expenditure of public resources on unsuccessful therapies.

Several detection techniques have been previously employed to detect MRSA like fluorescence, culturing, electrochemical, polymerase chain reaction, and many others have been developed.⁴ Nevertheless, these procedures can be further improved and more effective detection methods and novel nanomaterials can be synthesized to improve the efficiency of the existing methods. Therefore, the development of novel materials and techniques has been a research interest for scientists. However, a method that can detect and simultaneously kill the bacteria have not been explored extensively. Theranostic approach based nanomaterials would tackle the limitations of both detection and treatment and consequently will also reduce the economic burden.

β -cyclodextrin (β -CD) has been explored in the field of drug delivery and electrochemical sensing due to low toxicity and its ability to form host-guest assembly with a variety of organic and inorganic materials.⁵⁻
⁷ However, β -CD being an organic molecule exhibits low electro-conductivity. Therefore it needs to be supported with some other conducting material to achieve good response. Therefore, various electrochemical sensors have been fabricated by modifying β -CD with graphene oxide, metal

nanoparticles, and metal oxide nanoparticles. Graphene oxide is a two-dimensional nanomaterial which shows high electro-conductivity. Further, graphene and graphene oxide based composite have shown good electro-catalytic performance and a good sensing platform.⁸

Vancomycin (Van) has been used as an antibiotic for the treatment of MRSA infection extensively. It works by forming five hydrogen bonds with D-alanyl-D-alanine sequence in the bacterial cell wall and prevents any further bacterial growth. Therefore, this has led to the use of Van as a capturing probe to carry out the detection of MRSA.^{9,10} Although this would lead to lack of specificity against other gram-positive bacterial strains, but it would also work as an anti-bacterial for agent for the treatment of the infection.

Additionally, copper and copper complexes based materials and films have shown antibacterial activity against MRSA and other bacterial infections.¹¹⁻¹³ Therefore, biofilms with copper complexes or nanoparticles can be made and coated for the treatment of bacterial infections. Additionally, copper nanoparticles and complexes have been employed for the synthesis of electrochemical sensors due to their high electroconductivity and good electro-catalytic activity. Therefore, copper can be used as a potential electrode modifier to carry out detection as well as treatment of bacterial infections.

The present study uses the hydrothermal route to synthesize copper- β -cyclodextrin (Cu- β -CD) and copper- β -cyclodextrin-graphene oxide (Cu- β -CD-GO) based nanocomposite. This route provides various advantages such as facile technique, better temperature control, and easy handling. Further, the prepared nanocomposite consists of copper (Cu(II)) ions and β -CD as its precursors. These were selected due to their specific properties that they would provide such as higher electrochemical conductivity and treating MRSA infections. Copper and copper ions have been reported to kill the MRSA and MSSA bacterial strains within a couple of hours of contact.¹⁴ Hence, incorporating copper nanoparticles to the nanocomposite would not only aid in enhancing the electro-catalytic properties but also would aid in the killing of the bacterial cells. Further, β -CD is the most studied of all other

cyclodextrin available, which is due to its low toxicity levels. It has been administered to animals through oral, intraperitoneal, intravenous, and subcutaneous routes. It shows kidney damage, renal damage, and even mortality signs after a recommended dose. However, at smaller concentrations it can be subjected to infected patients and, therefore, can be used to treat skin-related MRSA infections without subjecting to high level of risks to public health. Finally, GO was added to the above composite to further improve the electro-conductivity of the composite. GO has been previously used to increase the conductivity of various materials, which results in providing better charge transfer characteristics. Additionally, it also increases effective surface area of the working electrode, which would result in more quantity of vancomycin being immobilized on the composite modified electrode. This would, in turn, increase the number of binding sites and lead to better detection and inactivation of MRSA.

2. Materials and method

2.1 Chemicals, reagents, and instrumentation

Copper nitrate, cyclohexanol, sodium dihydrogen orthophosphate dehydrate, and triethylamine were purchased from Merck, South Africa. Phosphate buffer saline tablets, dimethylformamide (DMF), graphene oxide (GO), β -cyclodextrin, potassium ferrocyanide and ethanol (95%) were obtained from Sigma-Aldrich, South Africa. Sodium phosphate dibasic dehydrate, and potassium ferricyanide was purchased from Saarchem. (Merck, South Africa). De-ionized (DI) water was used throughout the experiment for washing and cleaning purposes. Field emission - scanning electron microscope (FE-SEM; ZEISS Ultra Plus, Germany), high resolution-transmission electron microscopy (HR-TEM; JEOL 2100 HRTEM, Korea), Brunauer–Emmett–Teller (BET; Micromeritics Tristar II 3020 2.00, USA). The X-ray diffraction patterns (XRD) (BRUKER AXS (Germany)), ^1H NMR spectra were recorded in DMSO-d_6 (^1H : 2.50 ppm) as solvent using Bruker AV 400 MHz spectrometers.

Parameters such as chemical shift and coupling constants were recorded in ppm and Hz respectively,, UV spectrophotometer (UV-1800, Shimadzu, South Africa), Fourier transform infrared spectroscopy (Bruker® Alpha-P ATR–FT-IR, Germany) and electrochemical setup (CHI 660E, USA) consisting of a working electrode (glassy carbon electrode- 3 mm diameter), a reference electrode (Ag/AgCl) and a counter electrode (platinum wire) were used in the study

2.2 Synthesis of β -cyclodextrin modified copper nanoparticle (Cu- β -CD) composite

To synthesize the composite, 0.45 g of copper nitrate was dissolved in 30 mL of ethanol and kept for stirring at room temperature. Further, 0.23 g of β -cyclodextrin was dissolved in 30 mL of DMF and added to the above solution. After stirring for 30 mins, triethylamine and cyclohexane (1:1) were added to the mixture, and the stirring was continued for additional 30 mins. Finally, the contents were transferred to hydrothermal autoclave (200 mL). The autoclave was then kept in an oven at 115 °C for 24 hours. The product obtained was centrifuged and washed with ethanol and water consecutively 3 times. Finally, the collected composite was dried at 70 °C for 24 hours.

2.3 Synthesis of Cu- β -CD-GO nanocomposite

A similar procedure as that of Cu- β -CD was followed to synthesize Cu- β -CD-GO nanocomposite. In addition to the previous precursors, graphene oxide (2.5 mg (i), 5 mg (ii)) was also added to the solution for stirring and finally transferred to the autoclave (200 mL). The product was kept at 115 °C for 24 hours in the oven, and the obtained product was then centrifuged and washed with water and ethanol consecutively. Finally, the composite was dried at 70 °C for 24 hours.

2.4 Preparation of electrode

Glassy carbon electrode (GCE) was modified with different nanocomposites synthesized to carry out all electrochemical measurements. Before the coating of GCE, it was cleaned using alumina slurry

(0.05 μm) on the polishing pad. After polishing, the GCE was rinsed with DI water. Finally, 1 mg mL^{-1} aliquots of Cu- β -CD, Cu- β -CD-GO(i), and Cu- β -CD-GO(ii) were prepared. From the aliquots, 5 μL was drop cast on the GCE and dried under the infrared lamp for 20 mins. The modified electrode was labelled as Cu- β -CD/GCE, Cu- β -CD-GO(i)/GCE, and Cu- β -CD-GO(ii)/GCE respectively. After preparation of Cu- β -CD-GO(ii)/GCE, the electrode was activated in 0.1 M EDC/NHS solution. Following activation, the electrode was incubated in 1.2 mM solution of vancomycin for 2 hours. This final electrode was labeled as Van-Cu- β -CD-GO(ii)/GCE and was used to carry out the detection. To carry out the detection, the Van-Cu- β -CD-GO(ii)/GCE was incubated in the bacterial solution for 30 mins, and DPV was recorded.

2.5 In vitro antibacterial activity

The minimum inhibitory level (MIC) of the drug-conjugated composite was measured using the 96 well plate technique recorded with minor alteration. MIC values were determined against methicillin-resistant *Staphylococcus aureus* Rosenbach ATCC ® BAA-1683 (MRSA) for Cu- β -CD, Cu- β -CD-GO, Van-Cu- β -CD-GO, and powdered Van. The cultures of bacteria (MRSA and E.coli) were grown for 18 hours in a shaking incubator set in 100 rpm in Nutrient Broth (Biolabs, South Africa) at 37 °C. The bacterial cultures were adjusted with sterile distilled water to achieve a concentration equivalent to 0.5 McFarland Standard using a DEN-1B McFarland densitometer (Latvia). To achieve a final concentration of 10^7 colony forming units (CFU) mL^{-1} , bacterial cultures were further diluted (1:150) with sterile distilled water. Stock solutions of Cu- β -CD, Cu- β -CD-GO, Van-Cu- β -CD-GO, and powdered Van were prepared by dissolving in PBS by sonication and sterilized through a 0.2 μm syringe filter. Using 96 well plates, a serial dilution of Cu- β -CD, Cu- β -CD-GO, Van-Cu- β -CD-GO, and powdered Van were prepared in Mueller-Hinton Broth 2 (MHB). These were then further incubated with the diluted cultures in a shaking incubator set at 100 rpm at 37 °C for 18 hrs. After completion of incubation, 10 μL of the Cu- β -CD, Cu- β -CD-GO, Van-Cu- β -CD-GO and powdered

Van both were spotted onto the MHA plates and incubated for a further 24 hrs at 37 °C. This procedure was repeated every day for three days, and all MIC studies were performed three times. Powder Van was utilized as positive control.

3. Results and Discussion

3.1 Electrochemical characterization

The modified electrode was characterized to calculate its effective surface area and charge transfer kinetics using CV and EIS, respectively. To calculate the effective surface area of the different modified electrodes, cyclic voltammograms were run in 1 mM $[\text{Fe}(\text{CN})_6]^{3-/4-}$ in 1 M KCl. The best working potential of the electrode came out to be 764 mV vs. Ag/AgCl as the reference electrode. Therefore, the potential window was chosen from 0.2 V to 1.0 V. The voltammograms for Cu- β -CD/GCE and Cu- β -CD-GO(ii)/GCE were recorded at varying scan rate from 0.01 V s⁻¹ to 0.15 V s⁻¹ (Figure 1a). The data obtained from the cyclic voltammograms were used to calculate the effective surface area of the electrode using Randles-Sevcik equation ¹⁵:

$$I_p = 2 \cdot 69 \times 10^5 A \sqrt{D} (\sqrt{n})^3 \sqrt{v} C_0$$

where I_p is the peak current (Amp), A is the surface area of the electrode in cm², n is the number of electrons transferred (for $\text{K}_3[\text{Fe}(\text{CN})_6]$, $n=1$), v is the scan rate (V.s⁻¹), D is the diffusion coefficient (7.60×10^{-6} cm².s⁻¹ for $\text{K}_3[\text{Fe}(\text{CN})_6]$), and C_0 is the concentration in mol.cm⁻³. The slope of the plot of I_{pa} vs $v^{1/2}$ (Figure 1a [inset]) was used to calculate the effective surface areas of modified electrodes. The effective surface areas for Cu- β -CD/GCE and Cu- β -CD-GO(ii)/GCE were found to be 0.10869 cm² and 0.202036 cm² respectively. Larger surface area will help in higher quantity of vancomycin to be immobilized on the working electrode, leading to better detection of bacteria.

Further, EIS was carried out, with the range of frequency set from 1 to 10^5 Hz (Figure 1b). Data obtained from the EIS is represented as Nyquist Plot and provided in the form of the Randles equivalent circuit as seen in Figure 1b [inset]. The components of circuit are double-layer capacitance (C_{dl}), Warburg impedance (W), the resistance of the solution (R_s), and charge transfer resistance (R_{ct}). The values of each component are provided in a tabular form in Table 1. Lower value of charge transfer resistance meant better charge transfer kinetics of Cu- β -CD-GO(ii)/GCE as compared to others. Hence, Cu- β -CD-GO(ii)/GCE was chosen to be the material of choice to carry out the detection and also the inactivation of MRSA bacteria.

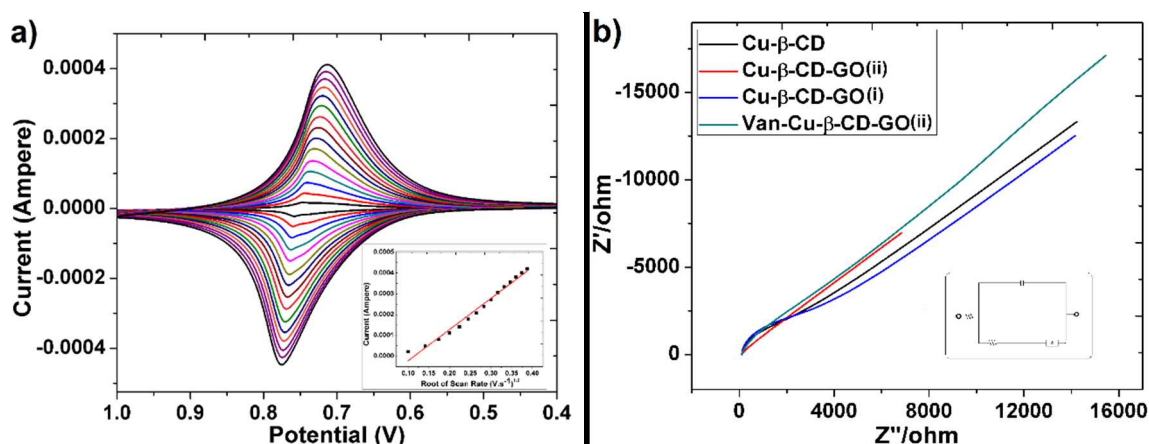


Figure 1. (a) Scan rate studies of Cu- β -CD-GO(ii)/GCE from (0.01 to 0.10 V s⁻¹) carried out in 1 mM [Fe(CN)₆]^{3-/4-} in 1 M KCl, Inset- calibration plot for anodic peak current vs root of scan rate. (b) EIS spectra in 1 mM [Fe(CN)₆]^{3-/4-} in 1 M KCl at GCE, Cu- β -CD-GO(i)/GCE, Cu- β -CD-GO(ii)/GCE, Van-Cu- β -CD-GO(ii)/GCE. Inset- Randles equivalent circuit model.

Table 1 Components of Randles equivalent circuit for GCE and Ag- β -CD/GCE

Material	R_s (Ω)	R_{ct} (Ω)	C_{dl} (F g ⁻¹)	W (Ω s ^{-1/2})
GCE	23.1	240.9	4.788×10^{-7}	0.0002632
Cu- β -CD/GCE	112.4	1698	3.426×10^{-7}	0.0000213

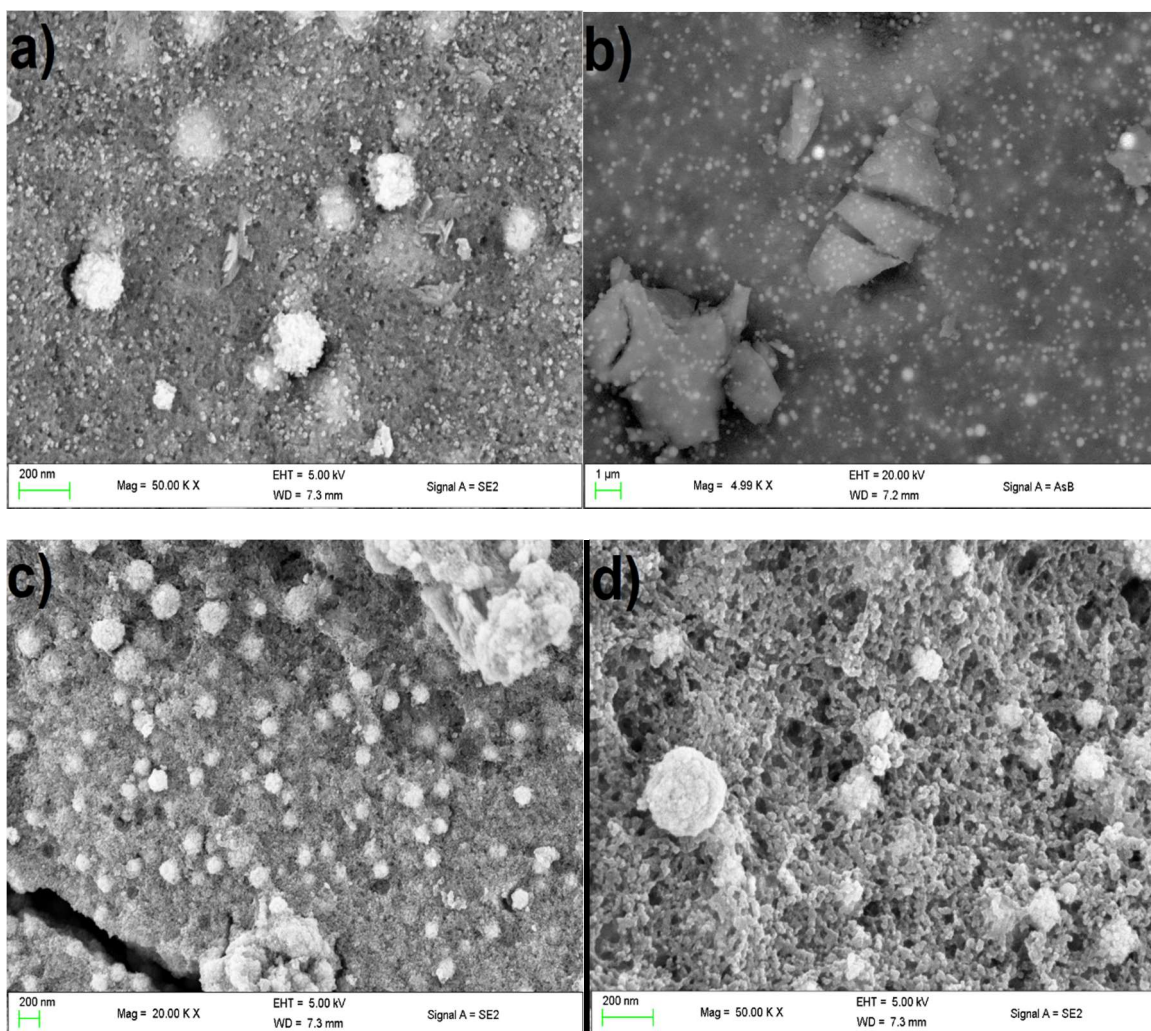
Cu- β -CD(i)/GCE	111.9	2382	3.278 e^{-7}	0.00002275
Cu- β -CD(ii)/GCE	111	0.001	3.946 e^{-7}	0.0000405
Van-Cu- β -CD(ii)/GCE	111.9	324.1	3.721 e^{-7}	0.00001732

3.2 Morphological characterization

The morphology of the prepared composites was examined using FE-SEM and HR-TEM. The FE-SEM image of Cu- β -CD (Figure 2a) shows that copper/copper oxide nanoparticles were uniformly distributed throughout the structure of the composite. It could be seen distinctly in the backscatter image (Figure 2b) of composite, which illustrates the bright spots as the copper/copper oxide nanoparticles present in the composite. Further, adding GO to the structure of the composite led to the formation of a porous structure and led to formation of smaller sized of copper/copper oxide nanoparticles, as seen in case of Cu- β -CD-GO(i) (Figure 2c). On further increasing the concentration of GO (Cu- β -CD-GO(ii)), it was observed that, porous network of β -CD and GO was formed with copper/copper oxide nanoparticles forming nodes within the porous structure (Figure 2d). The HR-TEM images show the copper/copper oxide nanoparticles covered with β -CD in the Cu- β -CD composite as seen in Figure 2e. However, a more condense structure beings to form Cu- β -CD-GO composite on addition of GO to the Cu- β -CD, as is seen (Figure 2f) due to π - π interaction and inter-hydrogen bonding between β -CD and GO.¹⁶ In case of Cu- β -CD-GO(ii), a condensed porous network, with copper/copper oxide nanoparticles uniformly distributed are obtained as seen in Figure 2g.

The high porosity of the Cu- β -CD-GO(ii) composite was confirmed using BET analysis. From the isotherms obtained, as shown in Figure 2h, Cu- β -CD displays type II isotherm with H4 hysteresis loop, depicting slit-like pores and particles with irregular pore shape. In case of Cu- β -CD-GO(ii), a type IV isotherm was obtained similar to that of mesoporous materials with H2 hysteresis loop, which

depicts narrow mouth pores with long channels like pore networks.¹⁷ The BET surface area for Cu- β -CD-GO(ii) came out to be 76.8309 m² g⁻¹ as compared to 6.4924 m² g⁻¹ of the Cu- β -CD composite, and their pore sizes came out to be as 347.485 Å and 682.315 Å respectively. These results were in accordance with the FE-SEM images of the composites. Therefore, Cu- β -CD-GO(ii) is predicted to be the better candidate for electrochemical measurements because of its higher surface area which would aid in more quantity of vancomycin to be immobilized over it. This would further result in better detection of the bacterial strains.



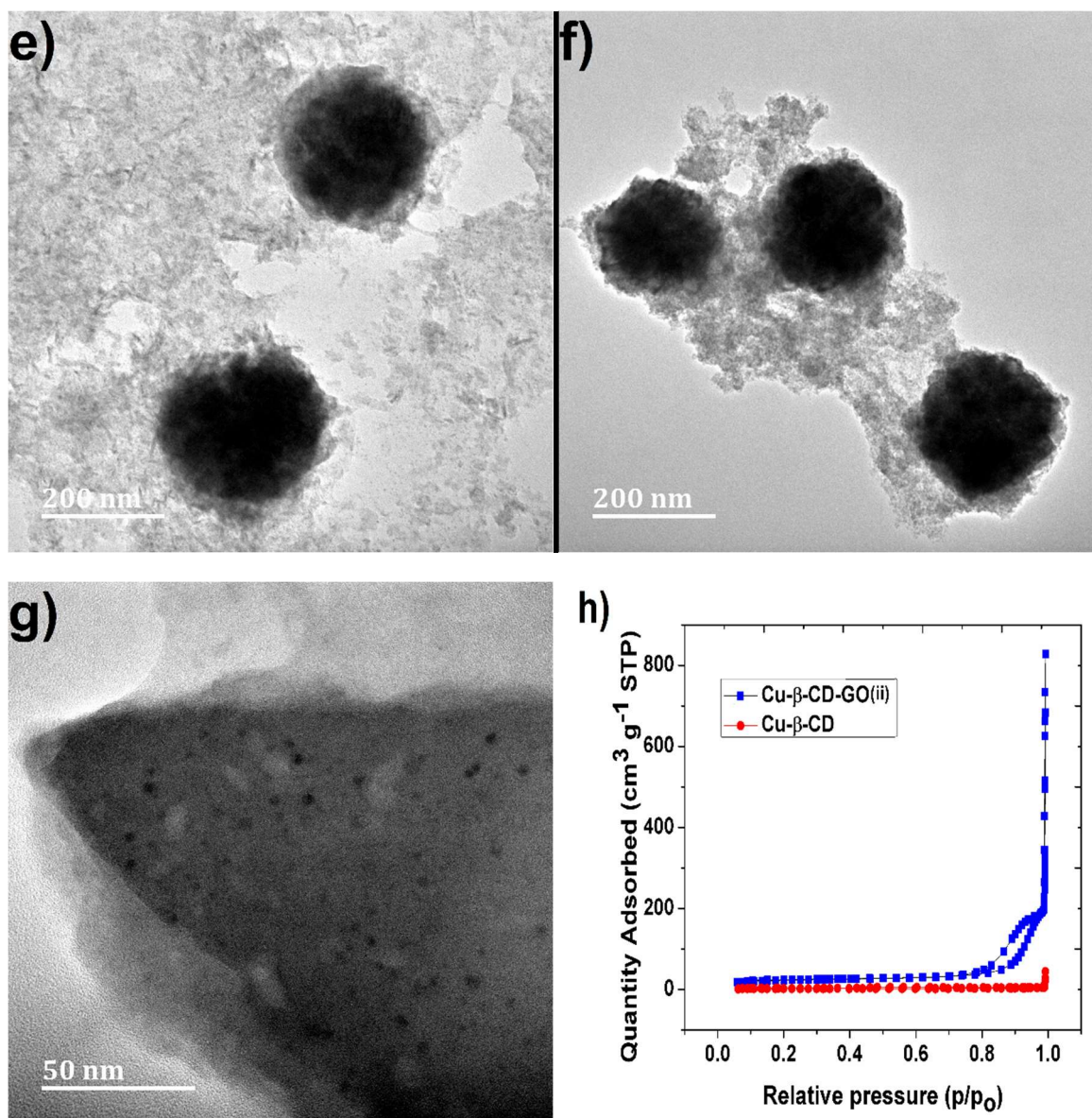


Figure 2. (a) FE-SEM image of Cu- β -CD (b) Backscatter (FE-SEM) image of Cu- β -CD (c) FE-SEM image of Cu- β -CD-GO(i) (d) FE-SEM image of Cu- β -CD-GO(ii) (e) HR-TEM image of Cu- β -CD showing distinct nanoparticles in β -CD sheets. (f) HR-TEM image of Cu- β -CD-GO(i) showing distinct nanoparticles in clustered β -CD and GO composite (g) HR-TEM image of Cu- β -CD-GO(ii) showing distinct smaller and distinct nanoparticles in a condense β -CD and GO composite. (h) N₂ adsorption and desorption isotherms obtained from BET analysis of Cu- β -CD and Cu- β -CD-GO(ii).

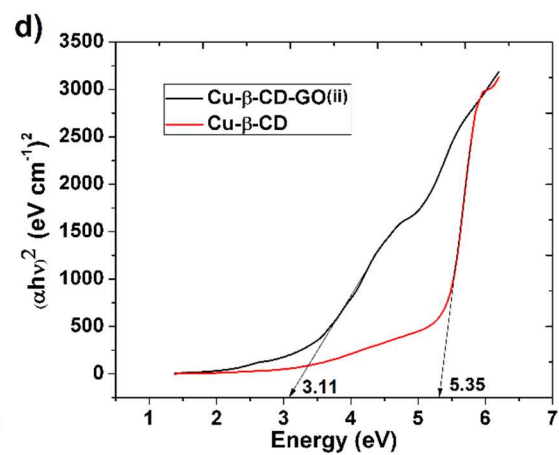
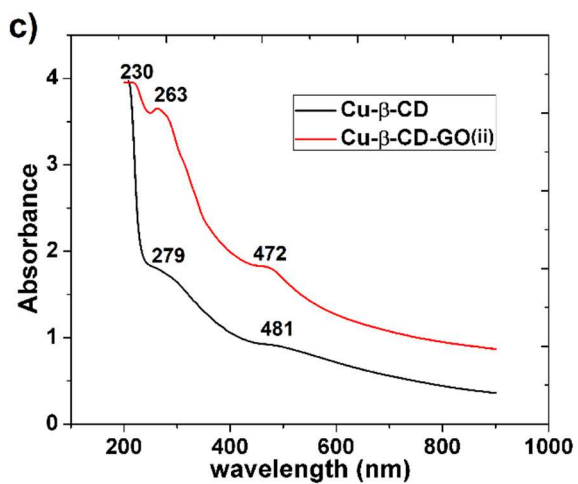
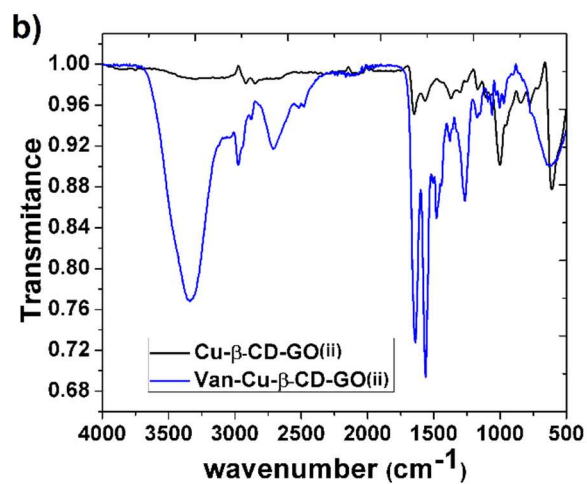
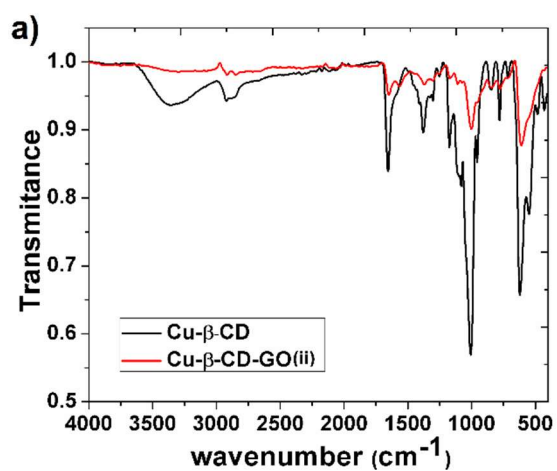
3.3 Spectral characterization

The chemical analysis of the synthesized composites was carried out using FTIR, as shown in Figure 3a. The wide peak at 3373 cm^{-1} is observed due to --OH stretching of alcohol of $\beta\text{-CD}$ molecule. Peak at 2921 cm^{-1} is due to the C-H stretch of the $\beta\text{-CD}$ molecule. Further, the peaks from 400 cm^{-1} to 650 cm^{-1} can be summed up as the ring breathing and C-C bonds of the $\beta\text{-CD}$ molecule. The peaks around 700 cm^{-1} can be attributed to the Cu-O bonds, which confirm the incorporation of copper oxide nanoparticles into the composite formed. Further, in case of $\text{Cu-}\beta\text{-CD-GO(ii)}$ after the incorporation of GO it was observed that the intensity of peaks at 3373 cm^{-1} and 2921 cm^{-1} reduced, which can be due to the combining of GO with the --OH groups of $\beta\text{-CD}$. Additionally, the peaks from 400 cm^{-1} to 650 cm^{-1} disappeared, which can be due to more compact and crystalline structure was formed on addition of GO, which is also confirm from HR-TEM, which prevents the ring from breathing to occur. Finally, the immobilization of vancomycin on $\text{Cu-}\beta\text{-CD-GO(ii)/GCE}$ was confirmed by the sharp rise in the peak near 3300 cm^{-1} , which can be attributed to the --NH_2 and --OH functional groups present in the complex vancomycin structure (Figure 3b).

UV spectroscopy was carried out to check the absorbance properties of the composites, dissolved in DI water. Figure 3c shows, absorbance peak at 481 nm and 279 nm for $\text{Cu-}\beta\text{-CD}$. The peak at 481 nm is a characteristic peak for copper nanoparticles, and the peak at 279 nm can be attributed to the copper nanoparticles and --OH interactions. Further, absorbance peaks for $\text{Cu-}\beta\text{-CD-GO(ii)}$ were obtained at 472 nm , 263 nm , and 230 nm . A blue shift in the peaks was observed on addition of GO, which can be attributed to formation of a condensed structure. This leads to increase in the electron density, hence causing the blue shift to occur.¹⁸ Further, the peak at 230 nm is due to the addition of GO to the composite structure. Besides, the higher absorbance is due to the increase in the number of C=C bonds present in $\text{Cu-}\beta\text{-CD-GO(ii)}$, due to the addition of GO. Further, the bandgap for the composite was calculated using the tauc plot (Figure 3d), which came out to be 5.35 eV and 3.11 eV for $\text{Cu-}\beta\text{-CD}$ and $\text{Cu-}\beta\text{-CD-GO(ii)}$ respectively. This reduction in the bandgap can be attributed to

the addition of GO, GO leads to strong hydrogen bonds formed between oxygen-containing groups in GO and β -CD.¹⁹⁻²³ This reduction in the number of free oxygen groups leads to reduction in the bandgap of the composite.¹⁸ Therefore, the addition of GO lowers the extended light absorption edge towards visible region for the GO modified Cu- β -CD.

XRD measurements are performed using a multipurpose X-ray diffractometer D8-Advance from Bruker operated in a continuous θ - θ scan in locked coupled mode with Cu-K $_{\alpha}$ radiation. The sample is mounted in the center of the sample holder on a glass slide and leveled up to the correct height. The measurements run within a range in 2θ defined by the user with a typical step size of 0.034° in 2θ . A position-sensitive detector, Lyn-Eye, is used to record diffraction data at a typical speed of 0.5 sec/step, which is equivalent to an effective time of 92 sec/step for a scintillation counter. Further, the X-ray diffraction pattern was recorded confirmed the presence of Cu₂O and Cu nanoparticles in the composites formed (Figure 3e). The peaks at 36.305° , 38.635° , 42.35° , 61.39° , and 73.46° are seen in case of Cu- β -CD, which correspond to (111), (111), (200), (220) miller indices which represent the characteristic peaks for Cu₂O nanoparticles. Additionally, peaks at 42.35° , 73.46° correspond to the characteristic peaks for Cu nanoparticles with miller indices (111) and (220). This confirms that the copper nanoparticles present in the composite were in two phases. Further, the peaks for Cu- β -CD-GO(ii) were the same excluding the peak 38.635° which corresponds to Cu₂O. However, presence of other peaks confirms that both the phases are also present in Cu- β -CD-GO(ii).



e)

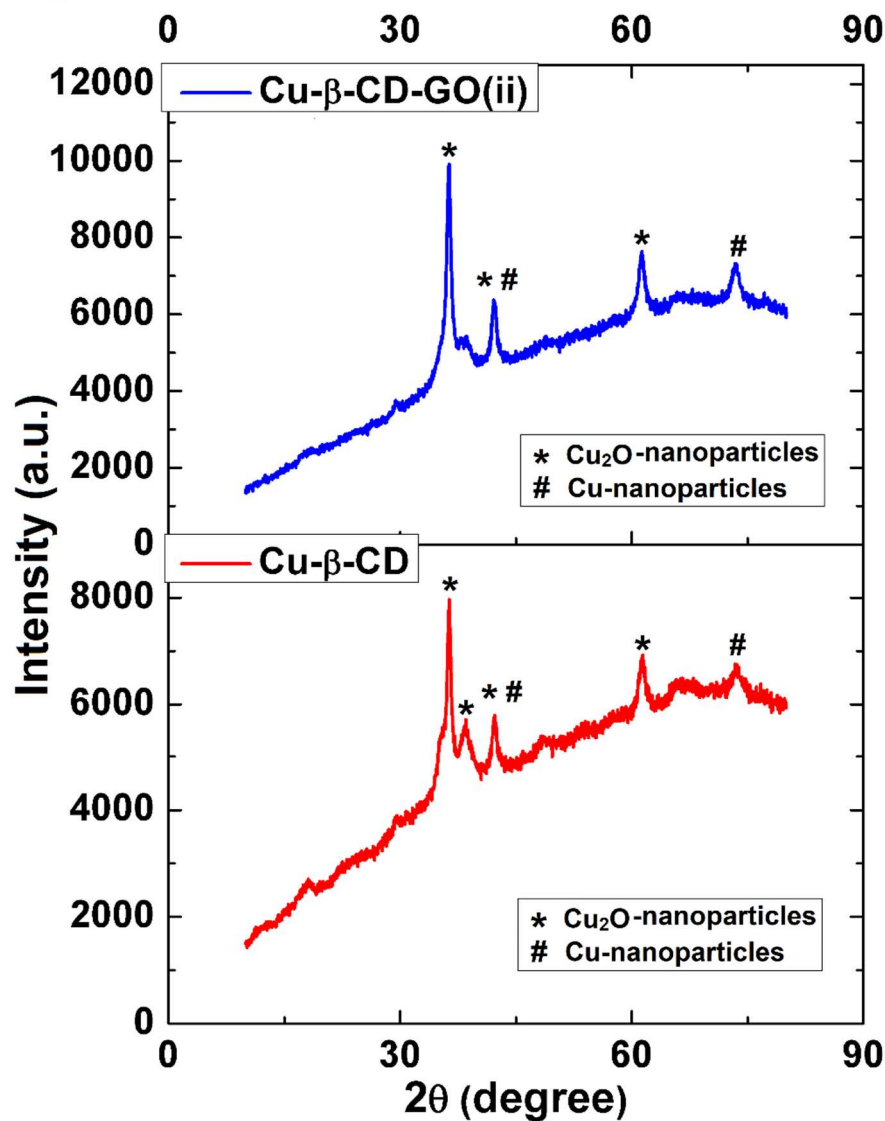


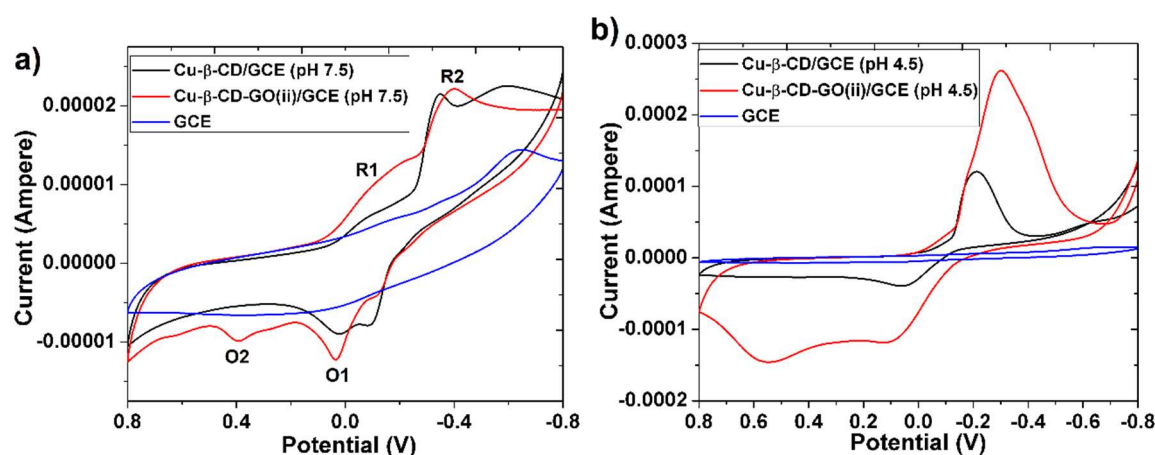
Figure 3. (a) FTIR spectrum of Cu-β-CD and Cu-β-CD-GO(ii). (b) FTIR spectrum of Cu-β-CD-GO(ii) and Van-Cu-β-CD-GO(ii). (c) UV-absorbance curve for Cu-β-CD and Cu-β-CD-GO(ii). (d) Tauc plot for Cu-β-CD and Cu-β-CD-GO(ii) which provides the band gap for each composite. (e) XRD analysis for Cu-β-CD and Cu-β-CD-GO(ii), which confirm the presence of both Cu₂O and Cu nanoparticles in the composite.

3.4 Electrochemical properties of composites

To study the redox activity of the composites, cyclic voltammetry was carried out. The potential window was selected from -0.8 V to +0.8 V at a scan rate of 0.1 V s⁻¹ in phosphate buffer (pH = 7.5).

As seen in the voltammograms (Figure 4a) both Cu- β -CD and Cu- β -CD-GO(ii) show four peaks, which represent reduction and oxidation of the copper present in the composite material. Peaks labeled as R1 and R2 represent the reduction of copper from Cu to Cu(I) and then to Cu(II). Additionally, the oxidation peaks representing Cu(II) to Cu(I) and Cu(I) to Cu are represented as O1 and O2.²⁵⁻²⁸ Further, it was observed that there is almost no capacitive current in case of both the composites as the current is almost same as the GCE.

Further, the redox activity of Cu- β -CD and Cu- β -CD-GO(ii) were studied in acidic (pH 4.5) and basic (pH 7.5) phosphate buffer solutions (Figure 4 b,c,d). It shows that copper ions undergo redox reactions are more readily in acidic buffer. This can be attributed to more electrons present for Cu(II) to undergo reduction itself and in turn providing a high oxidation peak current. Two oxidation peaks observed represent the two-step transition from Cu(II) to Cu. Similarly, higher reduction peak currents are obtained due to oxidation reaction, leading to Cu to go back to Cu(II) oxidation state. This pattern was observed for both the composite materials (with and without GO). Additionally, it is observed that in acidic pH the Cu- β -CD-GO(ii) composite shows high capacitive currents towards the positive potential as compared to Cu- β -CD, as seen in Figure 4b.



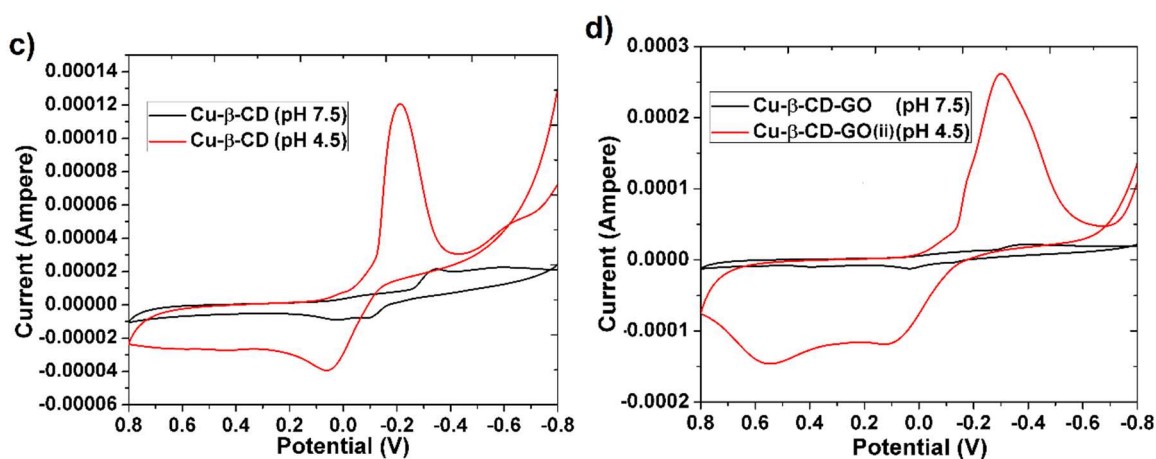


Figure 4. CV of Cu-β-CD and Cu-β-CD-GO(ii) at pH 7.5 phosphate buffer (0.1 M), R1, R2 are the reduction peaks and O1, O2 are the oxidation peaks of copper nanoparticles in the composite. **(b)** CV in 0.1 M phosphate buffers at pH 4.5 of Cu-β-CD and Cu-β-CD-GO(ii). **(c)** CV in 0.1 M phosphate buffers at pH 4.5, 7.5 of Cu-β-CD. **(d)** CV in 0.1 M phosphate buffers at pH 7.5 of Cu-β-CD-GO(ii).

3.5 Electrochemical response and optimization of conditions

DPV was used to check the detection capability of the electrochemical biosensor. The DPV measurements were carried out in 1 mM $[\text{Fe}(\text{CN})_6]^{3-/4-}$ in 0.01 M PBS as the redox couple. As seen in Figure 5a, the voltammograms of Cu-β-CD-GO(ii)/GCE, Van-Cu-β-CD-GO(ii)/GCE, and MRSA-Van-Cu-β-CD-GO(ii)/GCE, the output current decreases as vancomycin and bacteria attaches to the electrode. This is due to the non-conducting nature of the drug and MRSA bacteria. To further improve the conditions for the sensor, optimization of concentration of vancomycin required for immobilization and incubation time of bacteria were optimized using EIS and DPV respectively.

The Cu-β-CD-GO(ii)/GCE electrode after being incubated with EDC/NHS, it was immersed in varying concentration solution of vancomycin. It was observed that the R_{ct} value of the working electrode increased as the concentration of vancomycin was increased. At 1.2 mM a saturation in the R_{ct} value was attained which depicted maximum amount of vancomycin was immobilized on the modified electrode. Therefore, 1.2 mM was chosen as the optimum concentration of vancomycin for most efficient immobilization of the drug. Further, DPV measurements were conducted to optimize

the bacteria incubation time of the electrode. It was found that after 30 mins, a constant signal was obtained as seen in voltammograms in Figure 5c. This depicted that after 30 mins the working electrode was saturated with bacteria and hence this was selected as the optimal incubation time to carry out the studies.

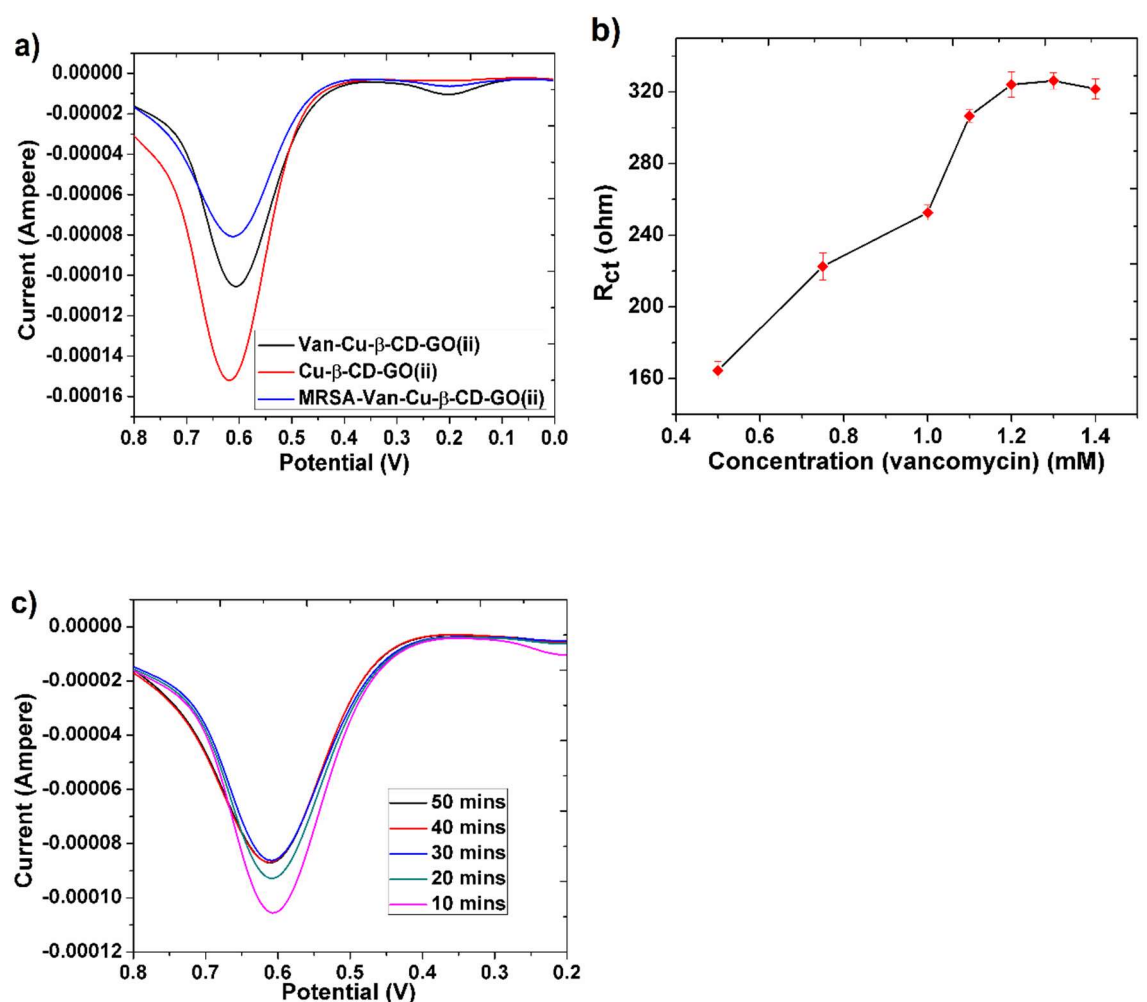


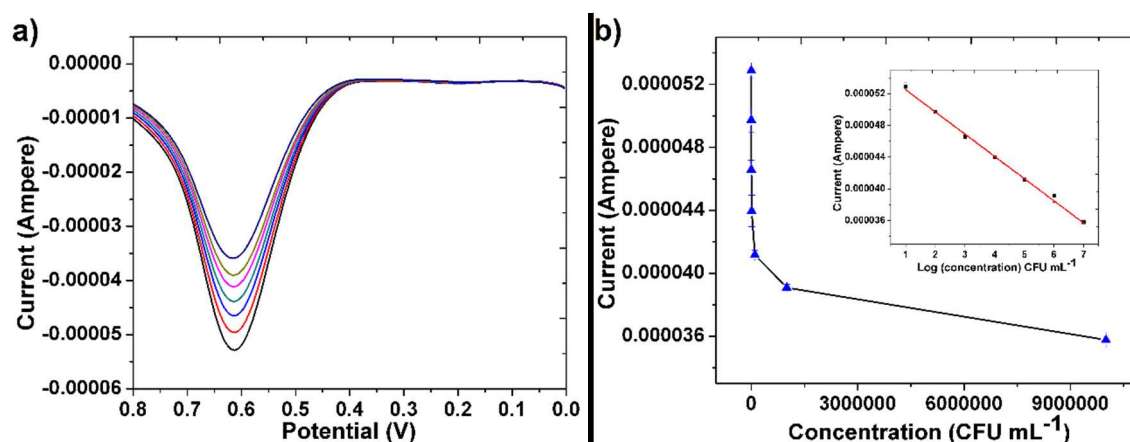
Figure 5. (a) DPV in 1 mM $[\text{Fe}(\text{CN})_6]^{3-/4-}$ in 0.01 M phosphate buffer saline (pH 7.4) at different modified electrodes to confirm the detection of MRSA. (b) calibration curve for the optimal concentration of vancomycin that can be immobilized over the modified electrode. (c) DPV of electrode for varying incubation time in bacteria.

3.6 Analytical performance for bacterial detection

After optimization of conditions, DPV was performed in 1 mM $[\text{Fe}(\text{CN})_6]^{3-/4-}$ in 0.01 M PBS as the redox couple, to carry out the detection of MRSA. The modified working electrode was incubated with varying concentrations of MRSA bacteria from 10 to 10^7 CFU mL^{-1} . As the concentration of MRSA was increased, a clear decrease in the current was observed, as seen in Figure 6a. This can be attributed to the non-conducting nature of bacteria, which leads to reduction in the currents obtained. The calibration plot was plotted with peak currents and bacterial concentration (Figure 6b). The linear regression for the plot came out to be:

$$I_p (10^{-5}\text{A}) = 5.5315e^{-7} + 2.8076e^{-6} \log [\text{MRSA}] (\text{CFU mL}^{-1}); R = 0.99724$$

The LOD for the fabricated electrode was calculated from the calibration plot (Figure 6b [Inset]), which came out to be 5 CFU mL^{-1} (using relation $S/N=3$). The present work provided better LOD than the previously mentioned techniques as mentioned in Table 2. Further, the reproducibility of the modified electrode was tested using five freshly prepared electrodes, and the response was recorded as seen in Figure 6c. Finally, the specificity study was carried out using *E.coli* as the control. After incubation with *E.coli*, no significant decrease in the peak current was observed from the initial van modified electrode, which shows its good specificity towards, as seen in Figure 6d.



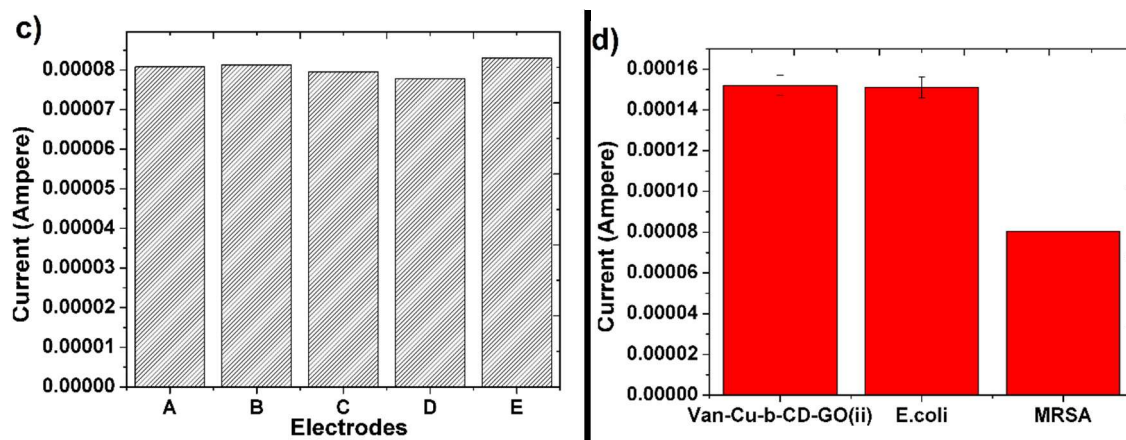


Figure 6. DPV 1 mM $[\text{Fe}(\text{CN})_6]^{3-/4-}$ in 0.01 M phosphate buffer saline (pH 7.4) at Van-Cu- β -CD-GO(ii) at varying concentration of MRSA from 10 to 10^7 CFU mL^{-1} . (b) Calibration plot for peak currents vs concentration of MRSA [inset- peak currents vs $\log[\text{concentration}]$]. (c) Repeatability checked by recording the current response at different modified electrodes. (d) Specificity carried out using *E.coli*, shows that there is no change in the peak current of the Van-Cu- β -CD-GO(ii)/GCE after incubation with *E.coli*.

Table 2 Comparison of previous methods for detection of MRSA

Material	Capture probe	LOD	Target detected	Technique	References
ZnO and Ag nanoparticles	Vancomycin	330 CFU mL^{-1}	MRSA Culture	EIS	9
Silica nanoparticles	Vancomycin	$10^7 \text{ CFU} \cdot \text{mL}^{-1}$	MRSA bacteria	Fluorescence	10
Gold and magnetic nanoparticles	IgG	$2 \times 10^7 \text{ CFU} \cdot \text{mL}^{-1}$	MRSA Culture	SWV	29
Gold nanopopcorn and GO	-	10 CFU mL^{-1}	MRSA bacterial strains	SERS	30
Van-Cu- β -CD(ii)	Vancomycin	5 CFU mL^{-1}	MRSA culture	DPV	This work.

3.7 In vitro antibacterial activity

To determine the minimum inhibitory concentration (MIC) of Cu- β -CD, Cu- β -CD-GO, Van-Cu- β -CD-GO, and powdered Van by 96 well-broth dilution technology was utilized to determine. It confirms and compares the potency and improvement of Van when it makes conjugate with Cu- β -CD-GO against MRSA as given in Table 3. After completion of 12 hours of study, MIC values were calculated to be 8.8 μ g/mL and 1.93 μ g/mL for powder Van and Van-Cu- β -CD-GO against MRSA at physiological pH 7.4. Which is much better than powder Van. The results of MIC value indicate that newly modified polymers with Van showed best activity as compared to powder Van. Overall results from our antimicrobial activity study suggest that Van-Cu- β -CD-GO can open a new door to research, therapy, and management of MRSA.

Table 3. Comparative in vitro antibacterial activity of Cu- β -CD, Cu- β -CD-GO, Van-Cu- β -CD-GO, and powdered Van against MRSA bacteria

Compound	MIC (μ g/mL)	
	12 hrs	24 hrs
Powder Van	8.8	8.8
Cu- β -CD	2.90	2.90
Cu- β -CD-GO	2.03	2.03
Van-Cu- β -CD-GO	1.93	1.93

4. Conclusion

In summary, a novel porous copper-based nanocomposite was successfully synthesized using a hydrothermal route. This material was conjugated with Van and used as a multipurpose electrode modifier for detection and treatment of MRSA. The material was successful in detecting MRSA bacterial strains and achieved a detection limit of 5 CFU mL⁻¹. Additionally, Van and copper provided a synergetic anti-bacterial effect towards MRSA. The lowering of MIC value from 8.8 µg/mL of Van to 1.93 µg/mL was observed due to the presence of copper nanocomposite. Finally, this work provides a novel nanocomposite that can have potential future applications in the field of electrochemistry due to its electro-active nature, electrocatalytic properties, and storage devices such as capacitors and batteries.

References

1. Ondusko, Devlynne S., and Dawn Nolt. "Staphylococcus aureus." *Pediatrics in review* 39, no. 6 (2018): 287-298.
2. Lewis, N., Parmar, N., Hussain, Z., Baker, G., Green, I., Howlett, J., Kearns, A., Cookson, B., McDonald, A., Wilson, M. and Ready, D., 2015. Colonisation of dentures by *Staphylococcus aureus* and MRSA in out-patient and in-patient populations. *European Journal of Clinical Microbiology & Infectious Diseases*, 34(9), pp.1823-1826.
3. Chambers, H. F., and F. R. Deleo. "Resistance of *Staphylococcus aureus* to penicillin and methicillin." *Nat. Rev. Microbiol* 7 (2009): 629-641.
- 4 Atal A. S. Gill, Sima Singh, Neeta Thapliyal, Rajshekhar Karpoomath. Nanomaterial-based optical and electrochemical techniques for detection of methicillin-resistant *Staphylococcus aureus*: a review. *Microchimica Acta* 4 16:81. <https://doi.org/10.1007/s00604-018-3186-7>.

5. Nidhi Agnihotri, Ankan Dutta Chowdhury, Amitabha De. Non-enzymatic electrochemical detection of cholesterol using β -cyclodextrin functionalized graphene. *Biosensors and Bioelectronics* 63 (2015) 212–217.
6. Xin Chen, Stephen G. Parker, Gang Zou, Wei Su, Qijin Zhang. β -Cyclodextrin-Functionalized Silver Nanoparticles for the Naked Eye Detection of Aromatic Isomers. *ACS Nano*. VOL. 4 ▪ NO. 11 ▪ 6387–6394 ▪ 2010.
7. Baljit Singh, Abhishek Dhiman, Rajneesh Kumar, Ajay Kumar, Slow release of ciprofloxacin from β -cyclodextrin containing drug delivery system through network formation and supramolecular interactions, *BIOMAC* 6334. *International Journal of Biological Macromolecules*. <http://dx.doi.org/10.1016/j.ijbiomac.2016.07.060>
8. Yujing Guo, Shaojun Guo, Jiangtao Ren, Yueming Zhai, Shaojun Dong, Erkang Wang. Cyclodextrin Functionalized Graphene Nanosheets with High Supramolecular Recognition Capability: Synthesis and Host-Guest Inclusion for Enhanced Electrochemical Performance. (2010) *ACS Nano*. Vol. 4, No. 7. <https://doi.org/10.1021/nn100939n>.
9. Zhiqing Yang, Yi Wang and Dun Zhang, A novel multifunctional electrochemical platform for simultaneous detection, elimination, and inactivation of pathogenic bacteria based on the Vancomycin-functionalised AgNPs/3D-ZnO nanorod arrays, (2017) *Biosensors and Bioelectronics*, <http://dx.doi.org/10.1016/j.bios.2017.06.058>.
10. Zhao, Zhiwei, Rong Yan, Xuan Yi, Jingling Li, Jiaming Rao, Zhengqing Guo, Yanmei Yang, Weifeng Li, Yong-Qiang Li, and Chunying Chen. Bacteria-activated theranostic nanoprobe against methicillin-resistant *Staphylococcus aureus* infection. *ACS nano* 11, no. 5 (2017): 4428-4438.

11. Bhardwaj, Abhishek K., Vinay Kumar, Vivek Pandey, Ram Naraian, and Ram Gopal. "Bacterial killing efficacy of synthesized rod shaped cuprous oxide nanoparticles using laser ablation technique." *SN Applied Sciences* 1, no. 11 (2019): 1426.
12. Holubnycha, V., Pogorielov, M., Korniienko, V., Kalinkevych, O., Ivashchenko, O., Peplinska, B. and Jarek, M., 2017, September. Antibacterial activity of the new copper nanoparticles and Cu NPs/chitosan solution. In *2017 IEEE 7th International Conference Nanomaterials: Application & Properties (NAP)* (pp. 04NB10-1). IEEE.
13. Beeton, Michael L., Janice R. Aldrich-Wright, and Albert Bolhuis. "The antimicrobial and antibiofilm activities of copper (II) complexes." *Journal of inorganic biochemistry* 140 (2014): 167-172.
14. Warnes, Sarah L., and C. William Keevil. "Lack of involvement of Fenton chemistry in death of methicillin-resistant and methicillin-sensitive strains of *Staphylococcus aureus* and destruction of their genomes on wet or dry copper alloy surfaces." *Appl. Environ. Microbiol.* 82, no. 7 (2016): 2132-2136.
15. L.R. F, A.J. Bard, *Electrochemical Methods: Fundamentals and Applications*, John Wiley, New York, 2001.
16. Guo, Y., Guo, S., Ren, J., Zhai, Y., Dong, S. and Wang, E., Cyclodextrin functionalized graphene nanosheets with high supramolecular recognition capability: synthesis and host– guest inclusion for enhanced electrochemical performance. *ACS nano*, 4(7) (2010) 4001-4010.
17. Kruk, Michal, and Mietek Jaroniec., Gas adsorption characterization of ordered organic–inorganic nanocomposite materials. *Chemistry of materials*, 13 (10) (2001) 3169-3183.

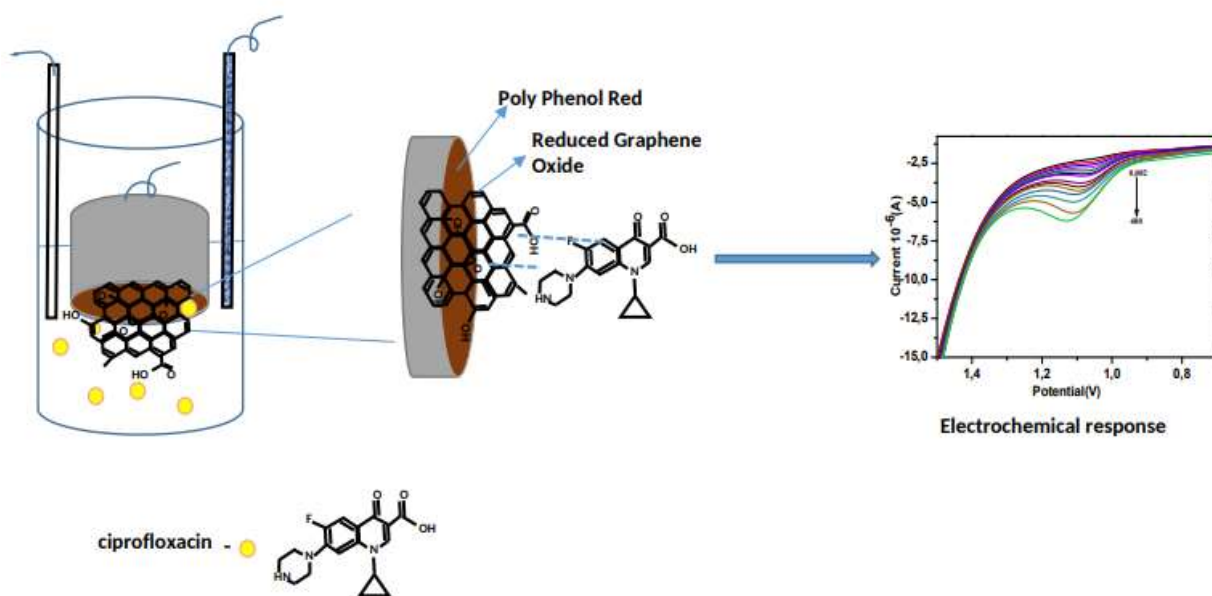
18. Acik, M. and Chabal, Y.J., 2013. A review on thermal exfoliation of graphene oxide. *Journal of Materials Science Research*, 2(1), p.101.
19. Scatena, L. F.; Brown, M. G.; Richmond, G. L. Water at Hydrophobic Surfaces: Weak Hydrogen Bonding and Strong Orientation Effects. *Science* 2001, 292, 908–912.
20. Stockton, W. B.; Rubner, M. F. Molecular-Level Processing of Conjugated Polymers. 4. Layer-by-Layer Manipulation of Polyaniline via Hydrogen-Bonding Interactions. *Macromolecules* 1997, 30, 2717–2725.
21. Wang, L. Y.; Wang, Z. Q.; Zhang, X.; Shen, J. C.; Chi, L. F.; Fuchs, H. A new approach for the fabrication of an alternating multilayer film of poly(4-vinylpyridine) and poly(acrylic acid) based on hydrogen bonding. *Macromol. Rapid Commun.* 1997, 18, 509–514.
22. Wang, L. Y.; Cui, S. X.; Wang, Z. Q.; Zhang, X.; Jiang, M.; Chi, L. F.; Fuchs, H. Multilayer Assemblies of Copolymer PSOH and PVP on the Basis of Hydrogen Bonding. *Langmuir* 2000, 16, 10490–10494.
23. Zhang, H. Y.; Fu, Y.; Wang, D.; Wang, L. Y.; Wang, Z. Q.; Zhang, X. Hydrogen-Bonding-Directed Layer-by-Layer Assembly of Dendrimer and Poly(4-vinylpyridine) and Micropore Formation by Post-Base Treatment. *Langmuir* 2003, 19, 8497–8502.
24. Salavati-Niasari, M. and Davar, F., 2009. Synthesis of copper and copper (I) oxide nanoparticles by thermal decomposition of a new precursor. *Materials Letters*, 63(3-4), pp.441-443.
25. Annamalai, S. K., Palani, B., & Pillai, K. C. (2012). Highly stable and redox active nano copper species stabilized functionalized-multiwalled carbon nanotube/chitosan modified electrode for efficient hydrogen peroxide detection. *Colloids and Surfaces A: Physicochemical and Engineering Aspects*, 395, 207-216.

26. Somasundrum, M., K. Kirtikara, and M. Tanticharoen. "Amperometric determination of hydrogen peroxide by direct and catalytic reduction at a copper electrode." *Analytica chimica acta* 319, no. 1-2 (1996): 59-70.
27. Zen, Jyh-Myng, Hsieh-Hsun Chung, and Annamalai Senthil Kumar. "Flow injection analysis of hydrogen peroxide on copper-plated screen-printed carbon electrodes." *Analyst* 125, no. 9 (2000): 1633-1637.
28. Kumar, A.S. and Zen, J.M., 2002. Electrochemical investigation of glucose sensor fabricated at copper-plated screen-printed carbon electrodes. *Electroanalysis: An International Journal Devoted to Fundamental and Practical Aspects of Electroanalysis*, 14(10), pp.671-678.
29. Cihalova K, Hegerova D, Dostalova S, Jelinkova P, Krejcova L, Milosavljevic V, Krizkova S, Kopelab P, Adam V (2016) Particle based immunochemical separation of methicillin resistant *Staphylococcus aureus* with indirect electrochemical detection of labelling oligonucleotides. *Anal Methods* 8:5123–5128.
30. Fan Z, Kanchanapally R, Ray PC (2013) Hybrid graphene oxide based ultrasensitive SERS probe for label-free biosensing. *J Phys Chem Lett* 4(21):3813–3818.

CHAPTER SIX

Highly selective electrochemical detection of ciprofloxacin using reduced graphene oxide/poly(phenol red) modified glassy carbon electrode

Graphical Abstract





Highly selective electrochemical detection of ciprofloxacin using reduced graphene oxide/poly(phenol red) modified glassy carbon electrode

Ruchika Chauhan, Atal A.S. Gill, Zondi Nate, Rajshekhar Karpoormath

Show more

<https://doi.org/10.1016/j.jelechem.2020.114254>

[Get rights and content](#)

Abstract

In this study, a novel sensor for highly selective and rapid detection of ciprofloxacin is fabricated. A facile strategy was employed to fabricate the modified electrode by electro-polymerization of phenol red [poly (phenol red)] (PPR) followed by drop casting of reduced graphene oxide (rGO). The rGO/PPR/GCE electrode enhanced sensitivity ($516.41 \mu\text{A} \mu\text{M}^{-1} \text{cm}^{-2}$) and low detection limit (LOD) (2nM) of ciprofloxacin due to selective adsorption, which was accomplished by a combination of electrostatic attraction at $-\text{SO}_3^-$ sites in the PPR film, and the formation of charge assisted hydrogen bonding between ciprofloxacin and rGO surface functional groups. The spectral and morphological studies of the novel nanocomposite were carried out using Fourier transform infrared spectroscopy (FTIR) and field emission scanning electron microscopy (FE-SEM). The electrochemical characteristics of modified material were studied by cyclic voltammetry (CV) and electrical impedance spectroscopy (EIS). Differential pulse voltammetry (DPV) was performed to study the response of ciprofloxacin towards the modified electrode. The composite modified electrode displayed good electro-catalytic activity towards the oxidation of ciprofloxacin at pH 5.5 and exhibited high sensitivity (detection limit 2nM) and specificity towards ciprofloxacin. The practical applicability was also tested by quantitative analysis of ciprofloxacin in the spiked animal serum sample. Recovery of analytes in spiked samples was $97 \pm 6\%$ over the range $0.002\text{--}400 \mu\text{M}$. It shows the developed electrode is a potential tool for a rapid, simple and sensitive detection of ciprofloxacin in serum sample.

Keywords: Phenol red; Reduced graphene oxide; ciprofloxacin; Electrochemical determination.

1. Introduction

Antibiotics have extensive applications in the prevention and treatment of numerous diseases as well as in the growth promotion of animals. Ciprofloxacin is one such antibiotic drug that is applied to cure several infectious diseases including but not limited to urinary tract infections, gastrointestinal infections, along with skin and soft tissue infections in humans and livestock[1]. Ciprofloxacin (Cfx) is a second-generation fluoroquinolone, which is not fully metabolized; because of this, it may persist in edible tissues or foodstuffs, such as milk or eggs. The European Union has set maximum residue limits for antibiotics in foodstuffs originated from animals (2377/90/EEC)[2]. Additionally, it is essential to reach the least number of identification points established in the 2002/657/EC European decision, to attain explicit identification of the antibiotic residues[3]. Therefore, highly selective and sensitive methods that provide reliable detection of antibiotics in foodstuff of animal origin are needed. Over the years, various techniques including high-performance liquid chromatography (HPLC) [4, 5], spectrophotometry[6, 7], fluorimetry[8, 9] have been proposed for the determination of Cfx in pharmaceutical preparations or biological samples. Most of the conventional methods used for Cfx detection are time-consuming with high instrumentation costs. Minimal studies concerning the electrochemical determination of Cfx have been reported [10-14]. Electrochemical sensors are suitable tool for rapid and sensitive analysis with wide application (medical, food and environmental) [15, 16].

For two decades, modified electrodes have been used as sensors for the electrochemical detection of various electroactive molecules like cysteamine, creatinine, dopamine, pyruvic acid, and folic acid [17-21]. Modification of electrodes to attain high sensitivity, selectivity, and compatibility necessitates extensive study. The excellent performance of modified electrodes depends upon various modifiers such as carbon materials, conducting polymers, and metal nanoparticles. Current research for emerging new electrode materials is now focused on conducting polymers and nano-metal colloids [22-25].

Poly (phenol red) (PPR) is a conducting polymer with an active quinone group in the polymeric chain which provides two electrons to redox reaction, as shown in Fig. 1 [26]. It contains OH and SO₃H functional groups which make it a good electron donor for transfer of charge between electrode and analytes; therefore, PPR thin film provides a highly favorable site for Cfx to undergo oxidation[27]. This leads to better interaction between the Cfx and PPR, leading to higher peak currents and also provides very good selectivity. Though conducting polymers exhibit poor electrochemical conductivity, and the derivatization of polymers with redox ions is a challenging task [28].

Consequently, the addition of a good electrochemical conductor is the proposed alternative. On the basis of π - π interactions between aromatic adsorbates and graphene, reduced graphene oxide (rGO) are excellent electrocatalytic and conducting material, and widely used as a rGO-polymer composite to enhance the sensitivity of the nanocomposite material because reduced graphene oxide (rGO) contains stronger π - π interaction rather than graphene oxide[29, 30]. These nanocomposites have been used for the detection of various biomarkers using different techniques such as electrochemical, optical, and fluorescence [31-33].

In the present study, for the first time, we proposed an electrochemically polymerized polyphenol red thin film on a glassy carbon electrode, which is further modified with rGO for highly selective detection of Cfx. The combination of PPR-rGO on GCE electrode provides a broad detection range and high selectivity towards the Cfx because of the electrostatic attraction of Cfx at $-\text{SO}_3^-$ sites in the PPR film, simultaneously the presence of rGO stimulates the sensitivity. Therefore, the electro-polymerized PPR thin film was developed on the glassy carbon electrode, which provided high catalytic activity towards the oxidation of Cfx. Further, the drop coating of reduced graphene oxide led to better charge transfer kinetics of the modified electrode by increasing its sensitivity. The final electrode having reduced graphene oxide/poly (phenol red)/glassy carbon electrode was denoted as (rGO/PPR/GCE). The modified electrode was further applied for the determination of Cfx in a sheep blood sample for its practical applicability.

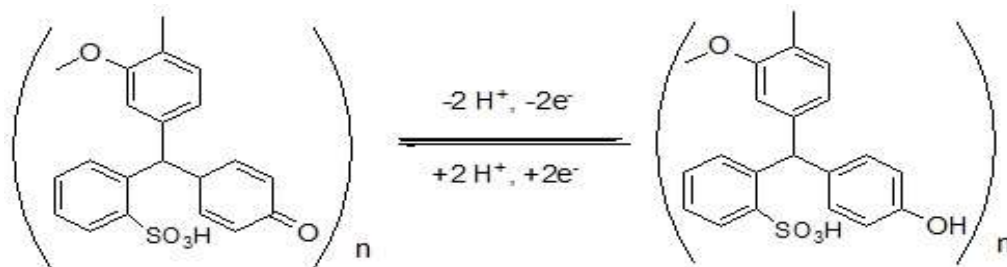


Figure. 1 Proposed structure and redox reaction of PPR.

2. Experimental Procedures

2.1. Materials

Ciprofloxacin (Sigma-Aldrich), phenol red (BDH Chemical Limited), graphene oxide powder (Sigma-Aldrich), potassium ferricyanide (Saarchem), potassium ferrocyanide (Sigma-Aldrich), hydrazine hydrate (Sigma-Aldrich), potassium chloride (Merck), L-ascorbic acid (Sigma-Aldrich),

glucose (ACE), deionised (DI) water (Millipore®). All used chemicals were of analytical grade. 0.1 M phosphate buffer (PB) of various pH were prepared by mixing different volumes of sodium dihydrogen orthophosphate dihydrate (Merck) and sodium phosphate dibasic dihydrate (Sigma-Aldrich).

2.2. Apparatus

All electrochemical studies related to present work were performed using the electrochemical workstation, CHI 660E (USA). The measurements were carried out in a three-electrode setup; Ag/AgCl electrode (reference electrode), GCE (working electrode, diameter 3 mm), and platinum wire (counter electrode). The pH measurements were carried out using pH meter (HANNA instruments, Woonsocket RI USA) with a glass electrode, field emission - scanning electron microscope (FE-SEM, ZEISS®, Germany), Fourier transform infrared (FTIR) spectroscopy (Bruker® Alpha-P ATR-FT-IR, Germany). All measurements were carried out at room temperature ($25 \pm 1^\circ\text{C}$).

2.3. Preparation of PPR

Before surface modification, the working electrode (GCE) was polished using 0.3 μm and 0.5 μm γ -alumina slurry on smoothing pads to get a mirror-like finish. Deionized (DI) water was used to wash the GCE and then was dried at room temperature. Subsequently, a solution of 5 mM phenol red was electropolymerized on cleaned GCE in 0.1 M PB (pH 7.0), sweeping the potential between 0 to 1.8 V vs. Ag/AgCl at a scan rate of 0.1 V s^{-1} (Fig. 2) for 30 consecutive cycles. After the preparation of a conducting layer of PPR on the GCE electrode surface (PPR/GCE), the electrode was washed through DI water and dried at room temperature.

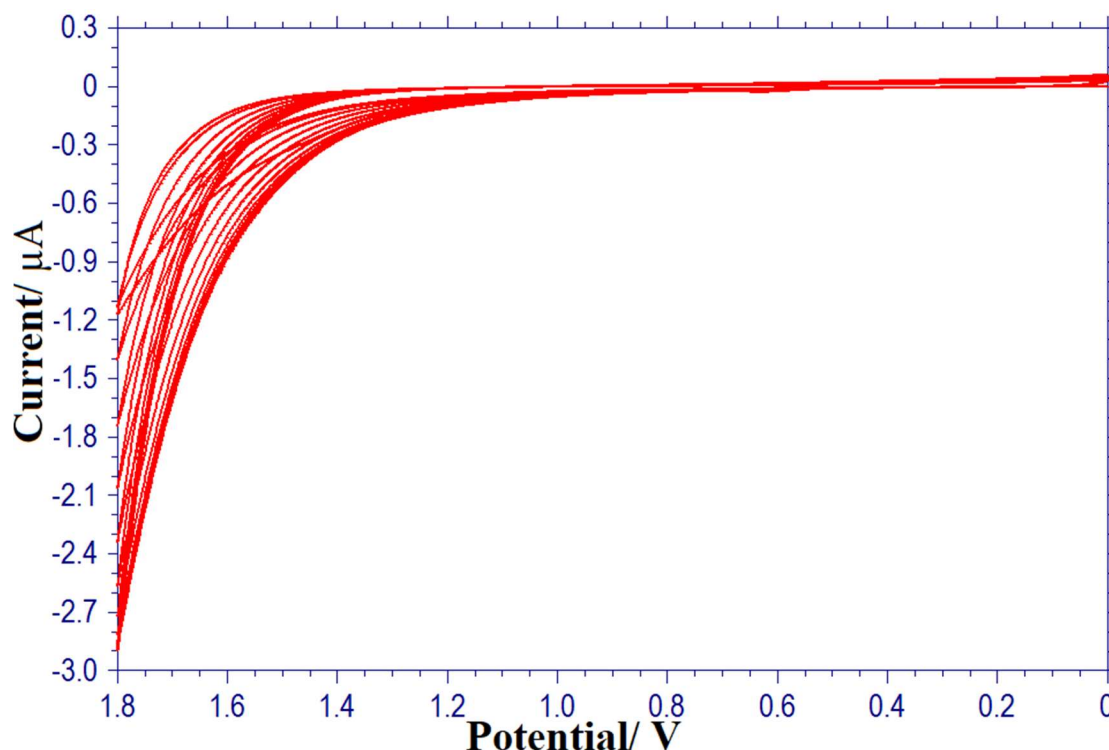


Figure. 2 Successive cyclic voltammograms during the polymerization of phenol red at surface of GCE.

2.4. Preparation of rGO/PPR/GCE

The GO suspension was prepared by dispersing 10 mg GO in 20 mL water and was sonicated for one hour at room temperature. The dispersed GO was then reduced with 10 μ L hydrazine hydrate and sonicated for 30 min to get the reduced graphene oxide (rGO). 1.5 mg of the rGO was dissolved in 2 mL of DI water and sonicated to form a uniform dispersion. 5 μ L of prepared rGO suspension was drop-casted on the PPR/GCE, followed by drying under the IR lamp for 20 minutes, annotated as rGO/PPR/GCE. The rGO/PPR/GCE was gently washed with water to remove the unbound rGO, further, used as the working electrode throughout the experiment.

2.5. Preparation of blood sample

The feasibility of the electrode was checked by the determination of Cfx in sheep blood serum samples. We are thankful to Dr. Thirumula Govenders lab at the University of KwaZulu-Natal, Westville, South Africa, for the sheep blood serum sample, which was used to carry out further studies. The sheep serum samples which were free from Cfx were diluted up to 10 times to reduce matrix effects and were then used for the detection of Cfx using rGO/PPR/GCE modified electrode.

The diluted sheep serum samples were spiked with 0 μML^{-1} , 0.002 μML^{-1} , 0.01 μML^{-1} , 0.1 μML^{-1} , 10 μML^{-1} , 100 μML^{-1} , and 400 μML^{-1} Cfx and differential pulse voltammetry (DPV) was carried out.

3. Results and discussion

3.1. FT-IR spectroscopic studies

The FTIR spectra (Fig. 3) of polymer shows a band at 3438 cm^{-1} corresponding to -OH stretching vibrations, the band at 1645 cm^{-1} is attributed to aromatic stretches of C=C in the polymeric structure, 1200-1100 cm^{-1} bands corresponds to the sulfone stretches and a band near 1600 cm^{-1} represents the C=O stretch of the active quinone group[34]. On the other hand, band at 1600 cm^{-1} for C=O stretch becomes broader, shifting towards a higher wavenumber, indicating the formation of C-O bond at alpha position of the carbonyl group in the ring of quinone methide after polymerization[35]. This confirms the electro-polymerization of phenol red on the electrode's surface. After the modification with rGO, two bands at 2357 cm^{-1} and 1041 cm^{-1} which can be attributed to carbon dioxide adsorbed on rGO and sulfone stretch of PPR respectively. All other peaks are diminished which confirms the successful deposition of rGO over PPR/GCE.

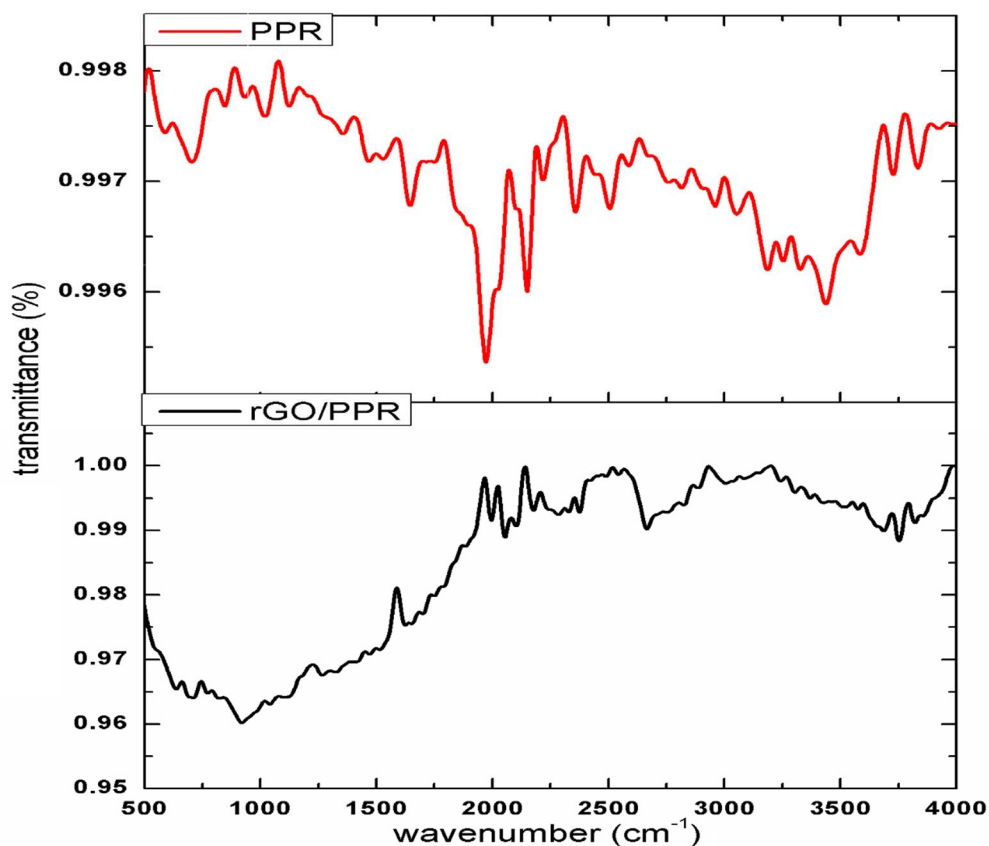


Figure. 3 ATR-FTIR results of the modified GCE electrodes by PPR and rGO/PPR.

3.2. FE-SEM Analysis

FE-SEM was used to study the morphological changes of rGO/PPR composite and PPR as illustrated in Fig. 4. The SEM image of PPR shows a sponge sheet-like structure with some corrugation in the structure of a sheet (Fig. 4a). The SEM image (Fig. 4b) of drop casted rGO over electrochemically synthesized PPR film, displaying their well exfoliated, wrinkled surface morphology of rGO [36]. The morphology of rGO/PPR composite shows that the spongy sheet-like structure was covered by wrinkled rGO nanosheets. These wrinkled rGO sheets increase the total surface area of the working electrode for better interactions with the analyte molecules. Roughness on the surface can be attributed to the point, edge, and line defects present on rGO's surface. These defects are a result of electrostatic interactions between unoxidized oxygen atoms and the conducting polymer.

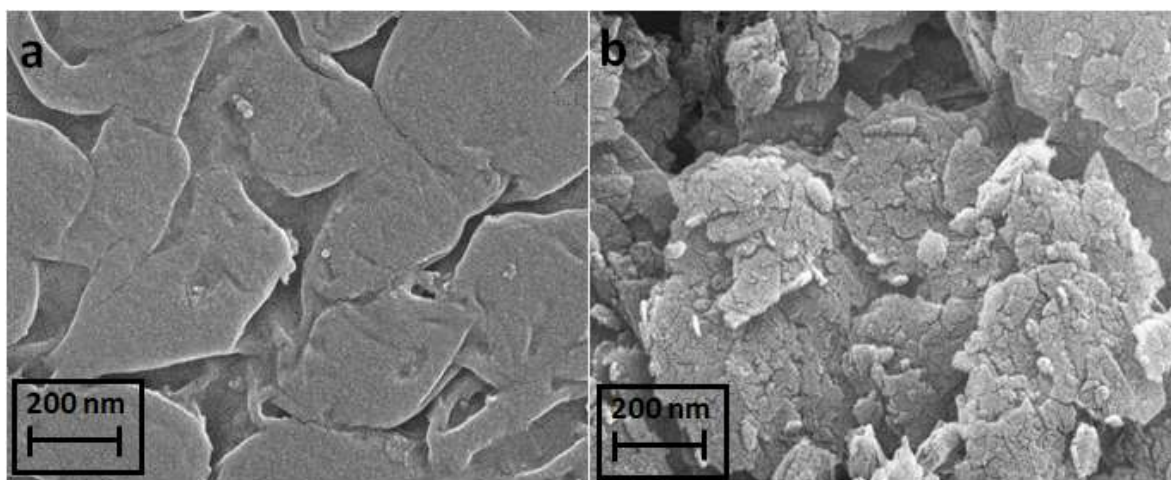


Figure. 4 (a) FE-SEM of PPR and (b) rGO/PPR composite

3.3. Electrochemical characterization of modified electrodes

The characterization of modified electrodes and bare GCE were carried out via cyclic voltammetry (CV) and electrochemical impedance spectroscopy (EIS). The redox behavior of the modified electrodes was carried out using cyclic voltammetry in 2.5 mM $[\text{Fe}(\text{CN})_6]^{3-/4-}$ in 1 M KCl. As shown in Fig. 5A, the current of cyclic voltammogram decreased for PPR/GCE electrode compared to the bare GCE electrode was due to the poor conductance caused by PPR modification of GCE. To overcome the challenge of poor conductivity, the electrode was modified with rGO. As a result, increased conductivity and higher surface area was obtained for rGO/PPR/GCE as represented in Figure 5A curve 'd'.

The CV response was used to calculate the effective area of the electrodes using the Randles-Sevcik [37] equation, The electrochemical active area was estimated from the peak current according to the following equation (1);

$$I_p = 2 \cdot 69 \times 10^5 A \sqrt{D} (\sqrt{n})^3 \sqrt{v} C_0 \quad (1)$$

where I_p - peak current (Amp), A - surface area of the electrode in cm^2 , n - number of electrons transferred (For $\text{K}_3[\text{Fe}(\text{CN})_6]$, $n=1$), v - scan rate (V s^{-1}), D is diffusion coefficient ($7.60 \times 10^{-6} \text{ cm}^2 \text{ s}^{-1}$ for $\text{K}_3[\text{Fe}(\text{CN})_6]$) and C_0 - concentration in mol cm^{-3} [37]. The surface area of rGO/PPR /GCE was calculated from the slope of the plot of I_{pa} vs $v^{1/2}$. The effective surface areas for GCE, PPR/GCE and Rg6O/GCE and rGO/PPR/GCE were calculated to be 0.022179 cm^2 , 0.018561 cm^2 , 0.025292 cm^2

0.02498 cm² respectively. As it show that the surface area and the current was reduced at PPR/GCE electrode, to enhance the surface area and conductivity of the electrode, the surface of PPR/GCE electrode was modified with rGO.

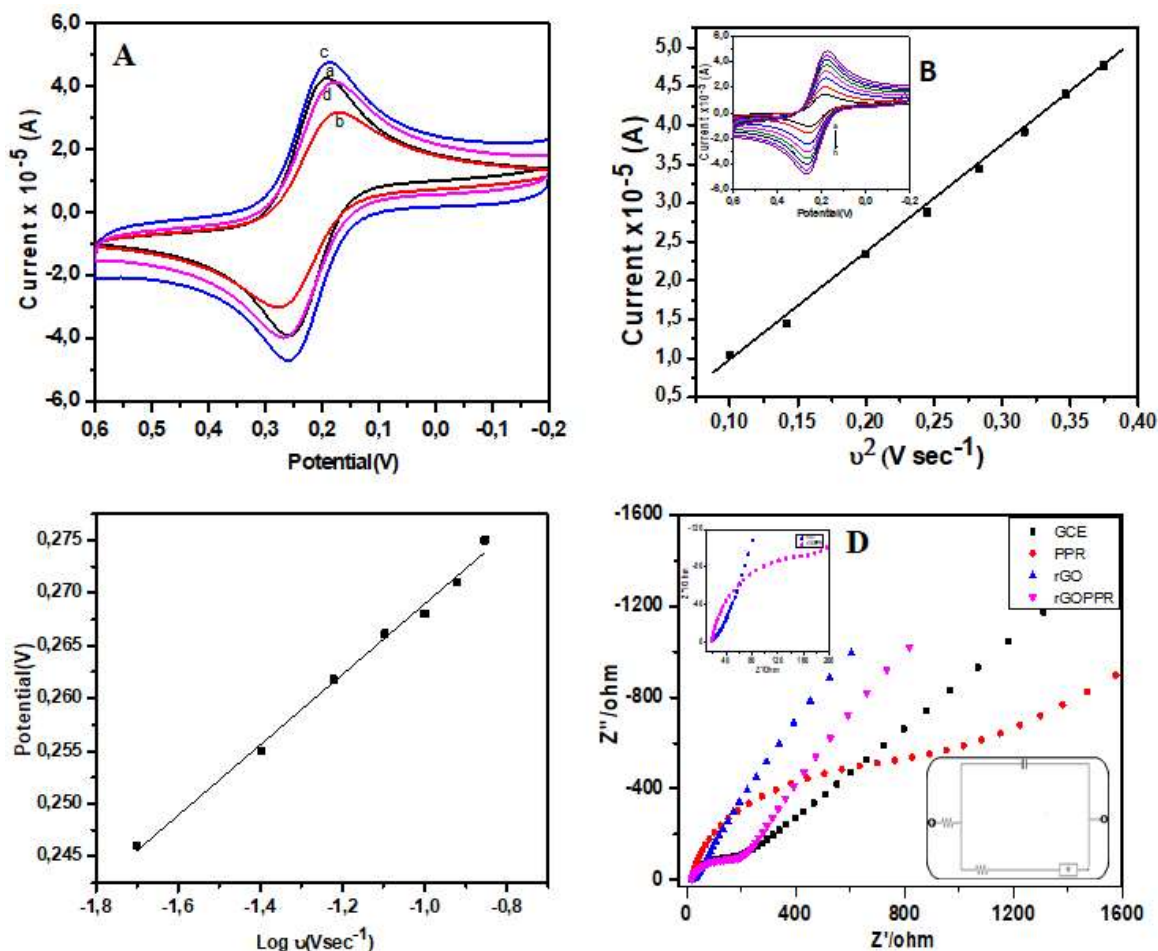


Figure 5. (A) Cyclic voltammograms of (a) GCE, (b) PPR/GCE, (c) rGO/GCE, (d) rGO/PPR/GCE (B) rGO/PPR/GCE show linear plot of the anodic peak current vs. square root of scan rate. (Inset- Cyclic voltammograms at various scan rates (0.01 to 0.14 V sec⁻¹) at 0.1 M KCl containing 2.5mM [Fe (CN)₆]^{3-/4-}. (C) linear plot of the peak potential vs. log scan rate (V sec⁻¹). (D) EIS spectra of 0.1 M KCl containing 2.5mM [Fe (CN)₆]^{3-/4-} at modified and bare GCEs. (Inset- Randles equivalent circuit model).

The effect of scan rate on modified rGO/PPR/GCE electrode was studied by varying the scan rate from 0.01 to 0.14 V sec⁻¹. A linear plot was obtained between peak current vs square root of scan rate (Vsec⁻¹) as illustrated in Fig. 5B, and the linear relationship between the potential and log scan rate (Vsec⁻¹) as illustrated in Figure 5C.

The EIS was carried out for studying the properties of interfacial electron transfer at the surface of the transducer. The spectral data obtained in 1 M KCl having 2.5 mM $[\text{Fe}(\text{CN})_6]^{3-/4-}$ as a redox couple was shown in Fig. 5D. The data shown in the form of Nyquist Plots for various electrodes, taking the starting potential at 0.243 V and the frequency choice ranging from 1 to 10^5 Hz. The Nyquist plot can be represented in the form of Randles equivalent circuit and its components are Warburg impedance (W), charge transfer resistance (R_{ct}), the resistance of the solution (R_s) and double layer capacitance (C_{dl}). The values of the components of the circuit equivalent to that of Nyquist plot are shown in Table 1. The R_{ct} value of the GCE was determined as 129.7 Ω , with a visible semi-circle with a small diameter signifying the impedance. However, in the case of PPR/GCE, the R_{ct} value 603.6 Ω , this might be due to the low conductivity of the polymer. The R_{ct} value of rGO/GCE was 0.001 Ω , with no semi-circle due to its exceptional conductivity. Therefore, when the rGO is coated over the PPR/GCE, the R_{ct} value is decreased to 89.12 Ω . This shows the study of charge transfer kinetics of rGO/PPR/GCE is consistent with the cyclic voltammetry studies performed.

Table 1: Components of randles equivalent circuit for GCE and Ag- β -CD/GCE

Electrode	R_s (Ω)	R_{ct} (Ω)	C_{dl} ($F\ g^{-1}$)	W ($\Omega\ s^{-1/2}$)
GCE	20.27	129.7	6.441×10^{-7}	0.0002294
PPR/GCE	18.89	603.7	2.492×10^{-6}	0.0001977
rGO/GCE	22.95	0.001	1.989×10^{-5}	0.0004271
rGO/PPR/GCE	18.78	89.12	2.527×10^{-6}	0.0004005

3.4 Electrochemical Detection of Cfx.

3.4.1 Effect of scan rate

To investigate the reaction mechanism of Cfx, the effect of scan rate from 0.01 to 0.14 $V\ s^{-1}$ on rGO/PPR/GCE electrode in 1mM ciprofloxacin (0.1 M PB at pH 5.5) was investigated as shown in Fig. 6. The peak current density varied linearly as the scan rates (v) ranged from 0.01 to 0.14 $V\ s^{-1}$ with the linear equation (2), which revealed that the oxidation of Cfx was an adsorption-controlled

process (Fig. 6 inset a). As there is formation of ionic bond between the Cfx and rGO/PPR/GCE surface via exchange of charge of electrons therefore oxidation of Cfx was a process of chemisorption.

$$\text{Current density } (\mu\text{Acm}^{-2}) = 127.40 + 21.97 \log v \text{ (mV sec}^{-1}\text{)} \quad (2)$$

As, on increasing the scan rate, the peak potential E_p shifted positively along with the increase of scan rate, showing a linear relationship with $\log v$, which was further constructed with the equation (3):

$$E_p \text{ (V)} = 1.28 + 0.0485 \log v \text{ (Vsec}^{-1}\text{)} \quad R^2 = 0.993 \quad (3)$$

This equation (3) can be described as follows[38, 39]:

$$E_p = A + \frac{2.303RT}{(1-\alpha)nF} \log v \quad (4)$$

A is a constant related to the formal electrode potential (E_0) and standard rate constant at E_0 ; α is the transfer coefficient characterizes the effect of electrochemical potential on activation energy of an electrochemical reaction; n is the number of electrons involved in the rate-controlling step; R , T and F are the gas constant, temperature and Faraday constant respectively. On the basis of the slope being equal to $2.303RT/(1-\alpha)nF$, the transferred electron is calculated to be 2.4, suggesting that two electrons were involved in the oxidation reaction.

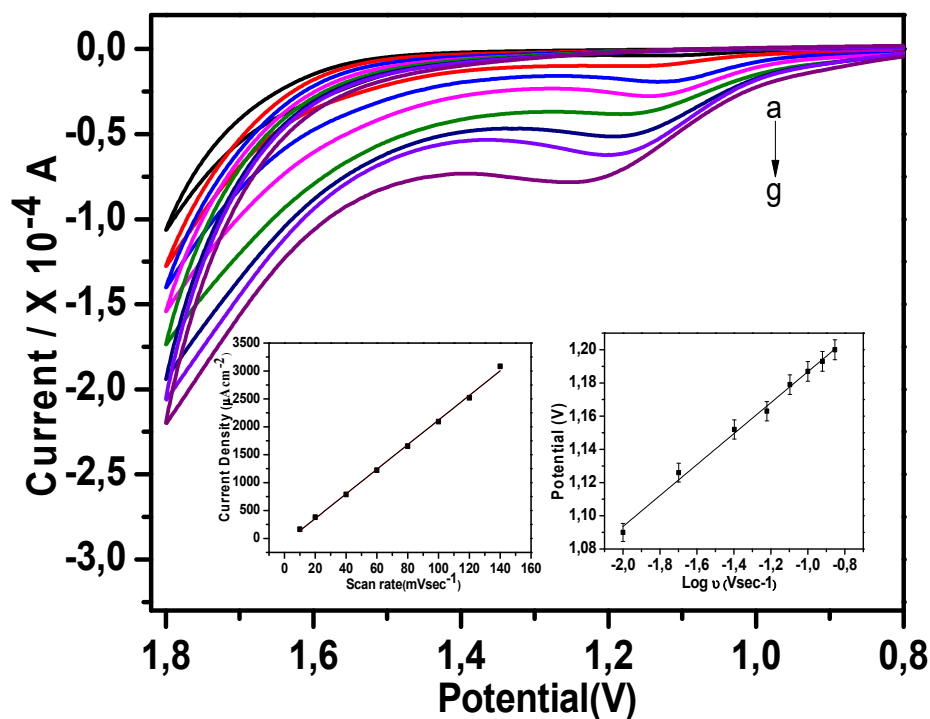


Figure 6. (a) Cyclic voltammograms at scan rates from A to K ($0.01\text{--}0.14\text{ V s}^{-1}$) of rGO/PPR/GCE electrode in 1mM ciprofloxacin (0.1 M PB at pH 5.5).inset (a) linear plot between peak current density and scan rate Vsec^{-1} inset (b) linear plot between potential vs log scan rate.

3.4.2 Effect of solution pH

To attain the best suitable conditions for the sensor, the pH of the electrolyte solution was altered from 2.5 to 7.5 and DPV was carried out in the presence of 1 mM ciprofloxacin in PB. With the increase of pH, the peak current was increased up to 5.5 pH, subsequently decreased at 6.5 and 7.5 pH, as shown in Fig. 7. The maximum peak current was observed at pH 5.5 and it was used for all further studies.

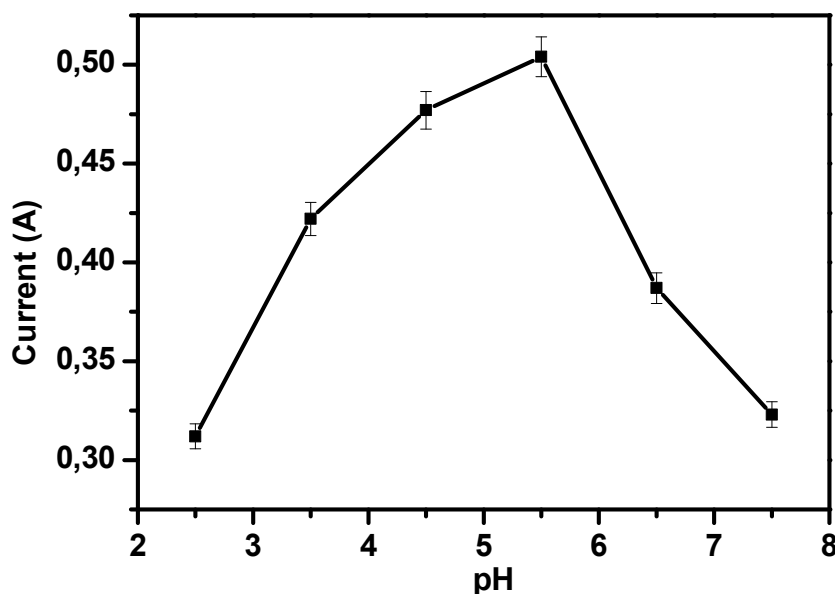


Figure 7. Plots of peak current I_p vs. pH from differential pulse voltammograms of 1mM solutions of ciprofloxacin at rGO/PPR/GCE electrode in different buffer electrolytes as a function of pH. Scan rate: 100mVsec^{-1} .

3.4.3 Electrochemical determination of ciprofloxacin

DPV has been employed for the effective determination of very low amount of drug molecules. To determine the activity of rGO/PPR/GCE electrode towards the analysis of Cfx, DPV were recorded under optimal conditions (sampling width: 0.0167 s, pulse width: 0.05 s, amplitude: 0.05 V and pulse period: 0.5 s) in 0.1M PB (pH 5.5) with varying concentrations of Cfx (Fig. 8). A sharp oxidation

peak for Cfx was observed at the potential of 1.08 V. At this oxidation potential peak current was increases as concentration of Cfx increases from 0.002 to 400 $\mu\text{M L}^{-1}$. After saturation of the electrode surface peak current get constant which shows the reaction is irreversible and chemisorption controlled. There are two linear calibration curves plotted between the varying concentration (0.002 – 0.5 and 0.5 – 400 μM) of ciprofloxacin and peak currents (Fig. 8B). The followings are the linear regression equations:

$$I_p(\text{A}) = 2.11 \times 10^{-6} + 1.291 \times 10^{-5} [\text{ciprofloxacin } (\mu\text{M})] \quad R^2=0.991 \quad (5)$$

$$I_p(\text{A}) = 3.88 \times 10^{-6} + 5.994 \times 10^{-9} [\text{ciprofloxacin } (\mu\text{M})] \quad R^2=0.998 \quad (6)$$

From the linear plots of 0.002– 0.5 μM and 0.5 – 400 μM range the obtained sensitivity was 516.41 $\mu\text{A} \mu\text{M}^{-1} \text{cm}^{-2}$ and 0.239 $\mu\text{A} \mu\text{M}^{-1} \text{cm}^{-2}$, respectively. The limit of detection (LOD) for the electrode was calculated using the relationship ($S/N=3$) with lower linear range (0.002-0.5 μM) and was found to be 2 nM, where ‘N’ is the slope of the calibration curve and ‘S’ is the standard deviation of blank responses. The electrochemical detection of Cfx based on the phenomenon of electrocatalytic behaviour of rGO/PPR matrix, where PPR behaves like a redox agent due to the presence of OH and $-\text{SO}_3\text{H}$, while rGO provides a high conductance to the matrix and higher surface area[40, 41]. The electrooxidation of Cfx was conducted via a secondary amine group – NH present in Cfx molecules. As scan rate study also suggested that electrochemical oxidation of ciprofloxacin involves two electrons and two protons. Consequently, the nanocomposite of rGO with PPR shows a synergistic effect towards the specific detection of ciprofloxacin. The rGO/PPR matrix achieved a broader linear range with lowest LOD (2nM) reported till date Table 2 shows the comparison with the other reported electrodes which proves the superiority of rGO/PPR matrix for the rapid and reliable detection of Cfx.

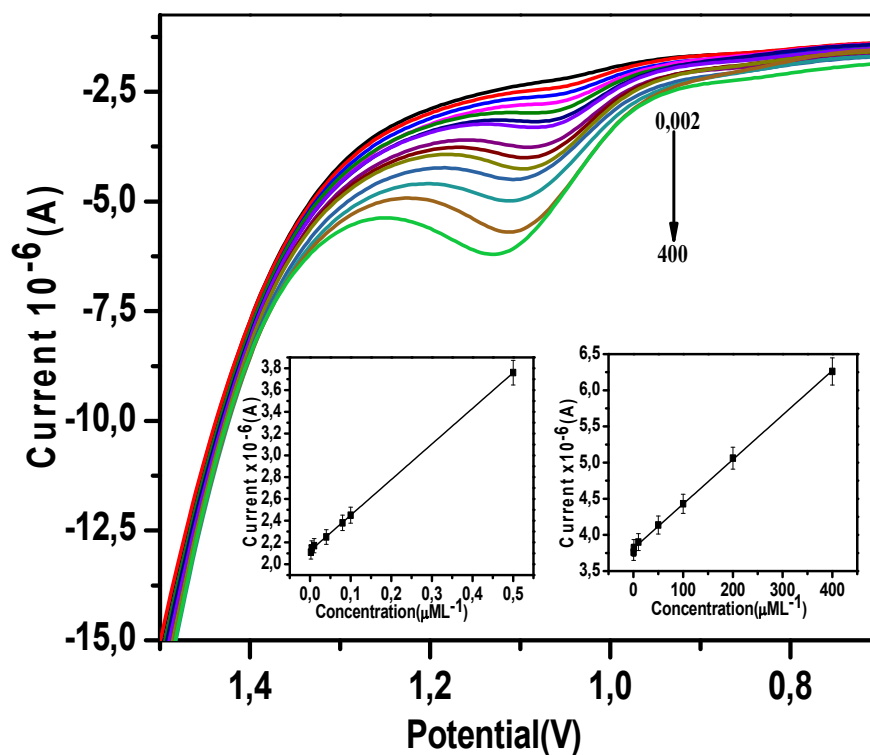


Figure. 8(a) Differential pulse voltammograms of ciprofloxacin with the different concentrations of ciprofloxacin in 0.1M PB of pH 5.5. Insets Calibration plot of I_{pa} vs different concentration of ciprofloxacin at pH 5.5 with a scan rate of 100 mV s^{-1} ; (a) for linear range $0.002\text{--}0.5 \mu\text{M}^{-1}$ (b) for linear range $0.5\text{--}400 \mu\text{M}^{-1}$

Table 2 : Comparison of previous modified electrodes for detection of ciprofloxacin

Modified Electrode	Technique	LOD(μM)	Matrices	References
COOH@MWCNT-MIP-QDs	fluorometry	0.066	chicken and milk	[25]
porous-Nafion-MWCNT/BDD	DPV	0.005	Natural waters and wastewater effluents.	[10]
MgFe ₂ O ₄ /MWCNTs	CV	0.01	Human urine, Plasma, tablet	[12]
β -cyclodextrin and l-arginine modified	DPV	0.01	Pharmaceutical formulations and	[13]

carbon paste electrode			human serum samples	
CdS QDs	Differential-pulse anodic stripping voltammetric (DPASV)	0.022	Urine sample	[14]
rGO/PPR/GCE	DPV	0.002	Animal serum	Present work

3.5. Interference study

One of the objectives of this work was to assess the ability of the sensor to quantify Cfx in biological samples (blood and urine). Different ions and compounds often coexist with Cfx in biological samples. Therefore, several non-target agents uric acid, ascorbic acid, D (+) glucose, L-glutamic acid, folic acid, and metal ions (Ca^{2+} , Na^{+} , Mg^{2+} and K^{+}) were tested with DPV analysis in different concentration of Cfx solution (0.1 M PB pH 7.0).

In the presence of 1 mM of the various non-target agents were studied. No interference was observed up to 10 times the original concentration of Cfx. The maximum error percentage was less than $\pm 5\%$. This was considered as the tolerance limit for the interfering substances. No interference in the voltammograms was observed as shown in Fig.9A, which confirmed excellent specificity of the electrode. The Cfx detection in the presence of all the non-target agents shows the linear equation as follows (7);

$$I_p = 2.14 \times 10^{-6} + 0.963 \times 10^{-5} \times [\text{conc. of Cfx } (\mu\text{M})] \quad R = 0.995 \quad (7)$$

Further, the capability of the sensor was also tested in presence of various drugs (norfloxacin, vancomycin). DPV was carried out to check the interference caused by other drugs to the ciprofloxacin response. For this ciprofloxacin solution (with different concentration) in 0.1 M phosphate buffer (1:9 by volume), 1 mL of 1 mM solution of each drug were tested out. After the addition, DPV was run in presence of ciprofloxacin, less than 3.4% deviation was observed for all concentration of ciprofloxacin, as shown in the Fig.9B. linear plot was obtained with the equation of (8);

$$I_p = 2.21 \times 10^{-6} + 1.14 \times 10^{-5} \times [\text{conc. of Cfx } (\mu\text{M})] \quad R = 0.992 \quad (8)$$

And the calculated LOD was 2.5nM for Cfx detection in the presence of other drugs. This indicated the high selectivity of rGO/PPR/GCE electrode towards Cfx.

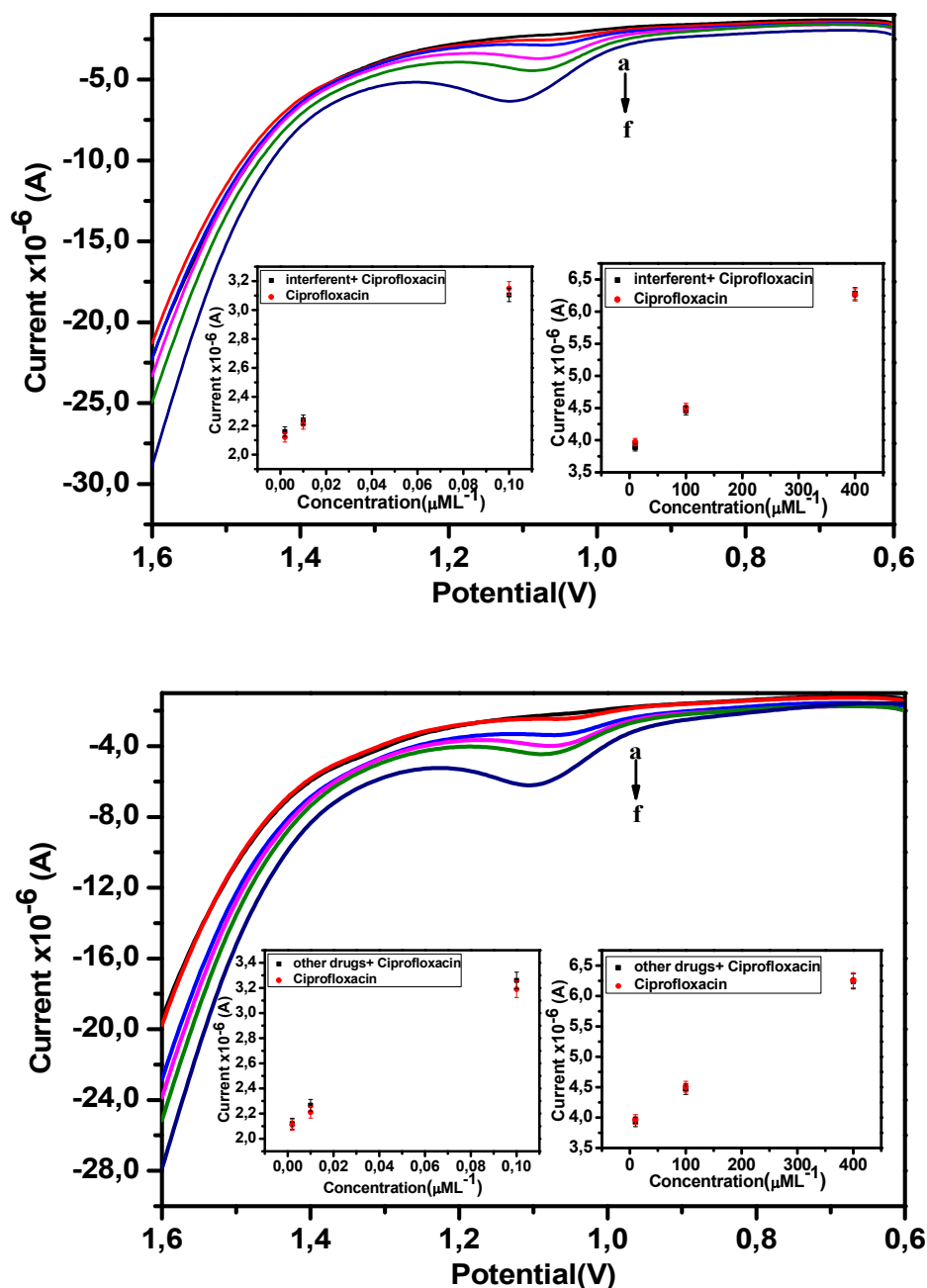


Figure. 9 (A) DPV at optimum conditions for interference studies of non-target agents in 0.1M PB buffer. (Inset – graph showing linear plots of peak current vs concentration of ciprofloxacin for lower and higher range 0.002-0.1 and 1-400 $\mu\text{M L}^{-1}$ respectively), (B) DPV at optimum conditions for interference studies of other drug in 0.1M PB buffer. (Inset – graph showing linear plots of peak

current vs concentration of ciprofloxacin for lower and higher range 0.002-0.1 and 1-400 μML^{-1} respectively

3.6. Reproducibility and Stability

The reproducibility of rGO/PPR/GCE electrode was also estimated in between multiple electrode preparations ($n=5$) by comparing the oxidation peak current of 1mM ciprofloxacin and the average peak current 4.501×10^{-6} A with the RSD of 4.2 %. It indicated that the modified electrode has good reproducibility. The stability of the proposed electrode was tested after every 24 hours using DPV in 0.1 mM Cfx in 0.1 M phosphate buffer. The peak current response was stable for five days. It was found that the peak current intensities decreased by only 6.6% after five days for Cfx detection, reflecting the excellent stability.

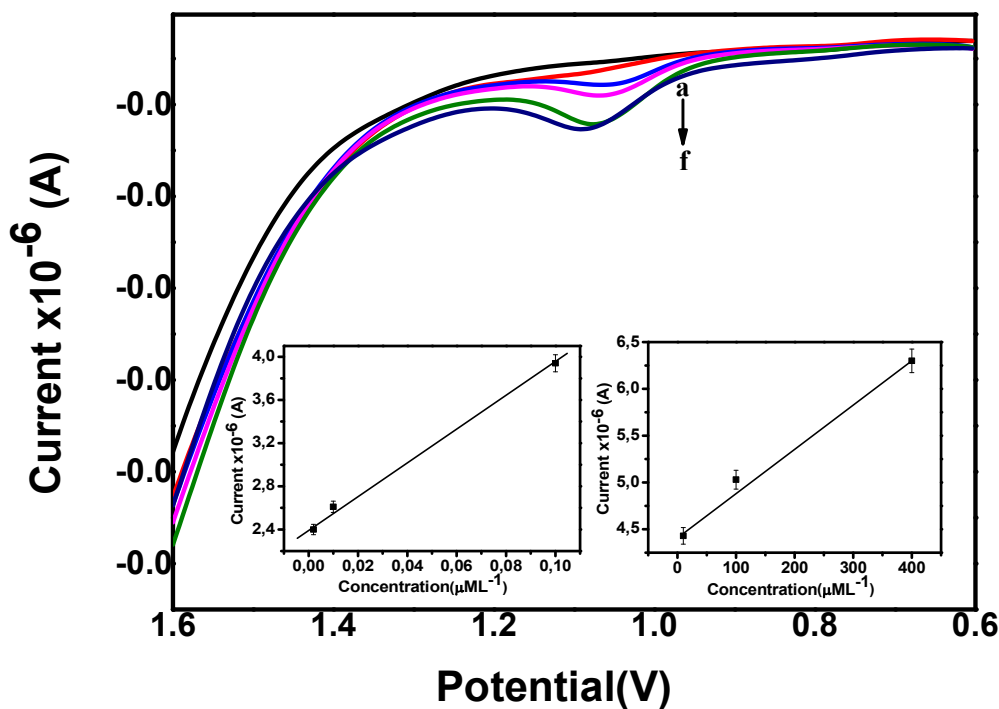


Figure. 10 DPV at optimum conditions for animal serum studies in 0.1M PB buffer. (Inset – graph showing linear plots of peak current vs concentration of ciprofloxacin for lower and higher range 0.002-0.1 and 1-400 μML^{-1} respectively

3.7. Real sample analysis

For practical applicability, the proposed sensor was evaluated against the sheep blood serum sample. Recovery studies were carried out at six concentration levels (0.002, 0.01, 0.1, 10, 100, and 400 μML^{-1}) for the unknown diluted (10 folds) blood serum and values obtained were compared with the calibration plot (Fig. 9 b). The linear plot (Fig.10) was obtained for the six different concentrations of spiked ciprofloxacin in diluted blood samples. The linear equation with the regression coefficient of 0.989 as;

$$I_p = 2.4 \times 10^{-6} + 1.53 \times 10^{-5} \times [\text{conc. of ciprofloxacin } (\mu\text{M})] \quad (9)$$

Two replicates were prepared at each concentration level, and each one was tested in triplicate. Absolute recoveries were calculated by comparing the relative peak current of the DPV procedure before and after the spiking of the serum sample. Recoveries higher than 96% were obtained in all cases with acceptable relative standard deviation (RSD). The results are shown in Table 3.

Table 3: Results of analysis of blood samples

Sample	Added concentration (μML^{-1})	Found concentration (μML^{-1})	Recovery %
1	0.002	0.0021 ± 0.001	105
2	0.01	0.0097 ± 0.0025	97
3	0.1	0.104 ± 0.028	104
4	10	10.107 ± 0.07	101.07
5	100	99.869 ± 0.8	99.86
6	400	398.948 ± 0.9	99.73

4. Conclusions

In summary, a facile and novel rGO/PPR/GCE electrode was synthesized via a drop cast method and used to detect ciprofloxacin with a LOD 2nM, using the DPV method. In this developed electrode, PPR exhibited high catalytic activity towards the oxidation of ciprofloxacin, while modification with

rGO led to enhance the sensitivity. The final modified electrode was able to detect Cfx with high selectivity and sensitivity, providing linear ranges from 0.002-0.5 μM and 0.5-400 μM . This novel electrode provided better linear range and sensitivity than other detection methods that have been employed. The sensor was able to detect Cfx in the presence of different interfering non-target agents (e.g., uric acid, ascorbic acid, D (+) glucose, L-glutamic acid, folic acid and metal ions (Ca^{2+} , Na^{+} , Mg^{2+} and K^{+})), and was also able to detect ciprofloxacin in animal serum with high sensitivity.

References

- [1] V.F. Samanidou, C.E. Demetriou, I.N. Papadoyannis, Direct determination of four fluoroquinolones, enoxacin, norfloxacin, ofloxacin, and ciprofloxacin, in pharmaceuticals and blood serum by HPLC, *Analytical and bioanalytical chemistry* 375(5) (2003) 623-9.
- [2] E.C. Regulation, laying down a Community procedure for the establishment of maximum residue limits of veterinary medicinal products in foodstuffs of animal origin, Council Regulation (EEC) No 2377/90 33 (1990) 0117.
- [3] E. Commission, implementing Council Directive 96/23/EC concerning the performance of analytical methods and the interpretation of results Official journal of the European Communities L221 (2002).
- [4] G. Carlucci, Analysis of fluoroquinolones in biological fluids by high-performance liquid chromatography, *J Chromatogr A* 812(1-2) (1998) 343-67.
- [5] J.D. Davis, L. Aarons, J.B. Houston, Simultaneous assay of fluoroquinolones and theophylline in plasma by high-performance liquid chromatography, *Journal of Chromatography B: Biomedical Sciences and Applications* 621(1) (1993) 105-109.
- [6] B.S. Nagaralli, J. Seetharamappa, M.B. Melwanki, Sensitive spectrophotometric methods for the determination of amoxycillin, ciprofloxacin and piroxicam in pure and pharmaceutical formulations, *J Pharm Biomed Anal* 29(5) (2002) 859-64.
- [7] M.I. Pascual-Reguera, G. Perez Parras, A. Molina Diaz, A single spectroscopic flow-through sensing device for determination of ciprofloxacin, *J Pharm Biomed Anal* 35(4) (2004) 689-95.
- [8] B. Liu, Y. Huang, Q. Shen, X. Zhu, Y. Hao, P. Qu, M. Xu, Turn-on fluorescence detection of ciprofloxacin in tablets based on lanthanide coordination polymer nanoparticles, *RSC Advances* 6(103) (2016) 100743-100747.
- [9] M. Varakneshin, M. Ebrahimi, Preconcentration and Determination of Ciprofloxacin with Solid-phase Microextraction and Silica-coated Magnetic Nanoparticles Modified with Salicylic Acid by UV-Vis Spectrophotometry, *Eurasian J Anal Chem* 13(3) (2018).

- [10] P. Gayen, B.P. Chaplin, Selective Electrochemical Detection of Ciprofloxacin with a Porous Nafion/Multiwalled Carbon Nanotube Composite Film Electrode, *ACS Applied Materials & Interfaces* 8(3) (2016) 1615-1626.
- [11] T.S.H. Pham, P.J. Mahon, G. Lai, A. Yu, Reduced Graphene Oxide Nanocomposite Modified Electrodes for Sensitive Detection of Ciprofloxacin, *Electroanalysis* 30(9) (2018) 2185-2194.
- [12] A.A. Ensafi, A.R. Allafchian, R. Mohammadzadeh, Characterization of MgFe₂O₄ nanoparticles as a novel electrochemical sensor: application for the voltammetric determination of ciprofloxacin, *Anal Sci* 28(7) (2012) 705-10.
- [13] F. Zhang, S. Gu, Y. Ding, Z. Zhang, L. Li, A novel sensor based on electropolymerization of β -cyclodextrin and L-arginine on carbon paste electrode for determination of fluoroquinolones, *Analytica Chimica Acta* 770 (2013) 53-61.
- [14] J. Shan, R. Li, K. Yan, Y. Zhu, J. Zhang, In situ anodic stripping of Cd(II) from CdS quantum dots for electrochemical sensing of ciprofloxacin, *Sensors and Actuators B: Chemical* 237 (2016) 75-80.
- [15] M. Heurich, M.K.A. Kadir, I.E. Tothill, An electrochemical sensor based on carboxymethylated dextran modified gold surface for ochratoxin A analysis, *Sensors and Actuators B: Chemical* 156(1) (2011) 162-168.
- [16] R. Liang, J. Qiu, P. Cai, A novel amperometric immunosensor based on three-dimensional sol-gel network and nanoparticle self-assemble technique, *Analytica Chimica Acta* 534(2) (2005) 223-229.
- [17] P.K. Brahman, N. Pandey, S.N. Topkaya, R. Singhai, Fullerene-C₆₀-MWCNT composite film based ultrasensitive electrochemical sensing platform for the trace analysis of pyruvic acid in biological fluids, *Talanta* 134 (2015) 554-559.
- [18] R.N. Goyal, V.K. Gupta, S. Chatterjee, Fullerene-C₆₀-modified edge plane pyrolytic graphite electrode for the determination of dexamethasone in pharmaceutical formulations and human biological fluids, *Biosensors and Bioelectronics* 24(6) (2009) 1649-1654.
- [19] H. Karimi-Maleh, P. Biparva, M. Hatami, A novel modified carbon paste electrode based on NiO/CNTs nanocomposite and (9, 10-dihydro-9, 10-ethanoanthracene-11, 12-dicarboximido)-4-ethylbenzene-1, 2-diol as a mediator for simultaneous determination of cysteamine, nicotinamide adenine dinucleotide and folic acid, *Biosensors and Bioelectronics* 48 (2013) 270-275.
- [20] S.Y. Ly, Detection of dopamine in the pharmacy with a carbon nanotube paste electrode using voltammetry, *Bioelectrochemistry* 68(2) (2006) 227-231.
- [21] J.A. Rather, K. De Wael, Fullerene-C₆₀ sensor for ultra-high sensitive detection of bisphenol-A and its treatment by green technology, *Sensors and Actuators B: Chemical* 176 (2013) 110-117.

- [22] P. Berenz, S. Tillmann, H. Massong, H. Baltruschat, Decoration of steps at Pt single crystal electrodes and its electrocatalytic effect, *Electrochimica Acta* 43(19) (1998) 3035-3043.
- [23] I. Danaee, M. Jafarian, F. Forouzandeh, F. Gobal, M.G. Mahjani, Electrocatalytic oxidation of methanol on Ni and NiCu alloy modified glassy carbon electrode, *International Journal of Hydrogen Energy* 33(16) (2008) 4367-4376.
- [24] A. Ramasubbu, A. Vanangamudi, S. Muthusubramanian, M. Shanmugam Ramachandran, S. Sivasubramanian, Electrocatalytic studies using silver–clay composite — a novel material, *Electrochemistry Communications* 2(1) (2000) 56-64.
- [25] N. Yuphintharakun, P. Nurerk, K. Chullasat, P. Kanatharana, F. Davis, D. Sooksawat, O. Bunkoed, A nanocomposite optosensor containing carboxylic functionalized multiwall carbon nanotubes and quantum dots incorporated into a molecularly imprinted polymer for highly selective and sensitive detection of ciprofloxacin, *Spectrochimica Acta Part A: Molecular and Biomolecular Spectroscopy* 201 (2018) 382-391.
- [26] K. Warriner, S. Higson, I. Christie, D. Ashworth, P. Vadgama, Electrochemical characteristics of two model electropolymerised films for enzyme electrodes, *Biosensors and Bioelectronics* 11(6) (1996) 615-623.
- [27] B. Shen, X. Wen, G.V. Korshin, Electrochemical oxidation of ciprofloxacin in two different processes: the electron transfer process on the anode surface and the indirect oxidation process in bulk solutions, *Environmental Science: Processes & Impacts* 20(6) (2018) 943-955.
- [28] W. Schuhmann, R. Lammert, M. Hämmerle, H.-L. Schmidt, Electrocatalytic properties of polypyrrole in amperometric electrodes, *Biosensors and Bioelectronics* 6(8) (1991) 689-697.
- [29] X. Wang, Y. Hu, J. Min, S. Li, X. Deng, S. Yuan, X. Zuo, Adsorption Characteristics of Phenolic Compounds on Graphene Oxide and Reduced Graphene Oxide: A Batch Experiment Combined Theory Calculation, *Applied Sciences* 8(10) (2018) 1950.
- [30] Z. Pei, L. Li, L. Sun, S. Zhang, X.-q. Shan, S. Yang, B. Wen, Adsorption characteristics of 1,2,4-trichlorobenzene, 2,4,6-trichlorophenol, 2-naphthol and naphthalene on graphene and graphene oxide, *Carbon* 51 (2013) 156-163.
- [31] H. Chang, L. Tang, Y. Wang, J. Jiang, J. Li, Graphene Fluorescence Resonance Energy Transfer Aptasensor for the Thrombin Detection, *Analytical Chemistry* 82(6) (2010) 2341-2346.
- [32] L. Wu, H.S. Chu, W.S. Koh, E.P. Li, Highly sensitive graphene biosensors based on surface plasmon resonance, *Opt Express* 18(14) (2010) 14395-400.
- [33] M. Zhou, Y. Zhai, S. Dong, Electrochemical Sensing and Biosensing Platform Based on Chemically Reduced Graphene Oxide, *Analytical Chemistry* 81(14) (2009) 5603-5613.

- [34] G. Yang, X. Qu, M. Shen, C. Wang, Q. Qu, X. Hu, Electrochemical behavior of lead(II) at poly(phenol red) modified glassy carbon electrode, and its trace determination by differential pulse anodic stripping voltammetry, *Microchimica Acta* 160(1) (2008) 275-281.
- [35] M.-T. Hsieh, T.-J. Whang, Mechanistic investigation on the electropolymerization of phenol red by cyclic voltammetry and the catalytic reactions toward acetaminophen and dopamine using poly(phenol red)-modified GCE, *Journal of Electroanalytical Chemistry* 795 (2017) 130-140.
- [36] S. Zhang, D. Zhang, V.I. Sysoev, O.V. Sedelnikova, I.P. Asanov, M.V. Katkov, H. Song, A.V. Okotrub, L.G. Bulusheva, X. Chen, Wrinkled reduced graphene oxide nanosheets for highly sensitive and easy recoverable NH₃ gas detector, *RSC Advances* 4(87) (2014) 46930-46933.
- [37] L.R.F. Allen J. Bard, *Electrochemical Methods: Fundamentals and Applications*, 2nd ed., Wiley, Hoboken, NJ, USA., 2000.
- [38] L. Fotouhi, Z. Atoofi, M.M. Heravi, Interaction of ciprofloxacin with DNA studied by spectroscopy and voltammetry at MWCNT/DNA modified glassy carbon electrode, *Talanta* 103 (2013) 194-200.
- [39] E. Laviron, General expression of the linear potential sweep voltammogram in the case of diffusionless electrochemical systems, *Journal of Electroanalytical Chemistry and Interfacial Electrochemistry* 101(1) (1979) 19-28.
- [40] A. Martín, A. Escarpa, Graphene: The cutting-edge interaction between chemistry and electrochemistry, *TrAC Trends in Analytical Chemistry* 56 (2014) 13-26.
- [41] X. Zhang, Y. Wei, Y. Ding, Electrocatalytic oxidation and voltammetric determination of ciprofloxacin employing poly(alizarin red)/graphene composite film in the presence of ascorbic acid, uric acid and dopamine, *Analytica chimica acta* 835 (2014) 29-36.

CHAPTER 7

1. Summary and Conclusion

MRSA is considered one of the most dangerous pathogenic bacteria which has created issues at both community and hospital levels. Due to the resistance to β -lactam antibiotics, the treatment of MRSA involves drugs such as vancomycin and daptomycin while restricting the use of certain drugs such as ciprofloxacin which can cause various side effects. However, these drugs are also known to cause various side effects if the quantity administered to the patients is not monitored properly. Further, the dumping of these drugs on surface waters and other water bodies has also led to the emergence of new bacterial strains which would increase the burden for public health centers. Therefore, it is necessary to develop rapid, cost effective and better analytical techniques to help the patients and health professionals for diagnostic purposes.

This thesis is based on the detection of MRSA bacteria and the drugs which should and should not be used for its treatment. In chapter 2 we present the literature review for the nanomaterials used for detection of MRSA using various techniques such as electrochemical, fluorescence and other novel techniques developed by researchers. Further, the drawbacks for these techniques have also been discussed in brief. The review also enlists the various biomarkers that are available that can be used to detect MRSA. Additionally, various conventional and commercial techniques presently used to detect MRSA have also been briefly discussed.

In chapter 3, a polyacrylic acid (PAA) modified copper benzene-1,3,5-tricarboxylate (BTC) metal-organic framework (MOF) is described for use in an electrochemical single shot assay for vancomycin detection. The MOF was synthesized via a single pot method resulting in enhanced solubility and dispersibility in water as compared to HKUST-1, but without altering its intrinsic crystalline and porous properties. The new MOF shows enhanced electro catalytic properties. This is assumed to be

due to the presence of a polyacrylic acid that forms a network between various HKUST-1 crystals through carboxylic acid dimer formation between BTC and PAA. This also led to better dispersion of the novel MOF as well as improved interactions between MOF and vancomycin. The characterization of the structural, spectral and electrochemical properties of the MOFs and their vancomycin complexes was carried out. A glassy carbon electrode was modified with the MOF for electrochemical determination (best at a working potential of 784 mV vs. Ag/AgCl) of vancomycin in spiked urine and serum samples. Response was linear from 1 - 500 nM vancomycin concentration range, and the lowest detectable concentration was 1 nM with a relative standard deviation of $\pm 4.27\%$. The presence of various potentially interfering analytes has no significant effect.

In chapter 4, we emphasize on electrochemical detection of ciprofloxacin in animal serum and run off water using silver nanoparticle modified β -cyclodextrin (Ag- β -CD) composite. The Ag- β -CD composite was synthesized via hydrothermal route which resulted in a high product yield. Morphological and spectral characterization of the Ag- β -CD composite was carried out. The Ag- β -CD composite was used to detect ciprofloxacin by employing differential pulse voltammetry (DPV) and cyclic voltammetry (CV). Ag- β -CD modified electrode displayed good specificity towards electro-oxidation of ciprofloxacin. Further, the sensor gave the best response towards electro-oxidation of ciprofloxacin near the physiological pH of 7.5. A linear response was obtained between the concentration range of 0.1 nM to 50 nM and limit of detection (LOD) at 0.028 nM with high sensitivity of $26,697.312 \mu\text{A mM}^{-1} \text{cm}^{-2}$ was achieved. Finally, the Ag- β -CD composite modified electrode was successful in detecting ciprofloxacin in spiked animal blood serum and domestic run off water samples.

In chapter 5, a novel porous nanocomposite was synthesized and used as a multipurpose platform for detection and antibacterial activity against pathogenic bacterial strain. The composite constituted of copper, β -cyclodextrin and graphene oxide which was functionalized with vancomycin (Van) as the

capture probe. The spectral and morphological characterization of the novel composite formed was carried out. The specificity towards gram-positive bacteria was provided by the Van molecule and was used to detect MRSA. Differential pulse voltammetry was used to carry out highly sensitive detection of MRSA and a low detection limit of 5 CFU mL^{-1} was achieved. Finally, the prepared composite was tested for antibacterial activity and MIC value of Van-Cu- β -CD-GO was achieved $2.23 \mu\text{g mL}^{-1}$ which was a result of the synergetic effect of copper and Van. Therefore, the current work provides a novel composite material for detection and inactivation of harmful pathogenic bacterial strains.

In chapter 6, we report a novel reduced graphene oxide/ poly (phenol red) fabricated sensor for highly selective and rapid detection of ciprofloxacin. A facile strategy was employed to fabricate the modified electrode by electro-polymerization of phenol red [poly (phenol red)] (PPR) followed by drop casting of reduced graphene oxide (rGO). The rGO/PPR/GCE electrode enhanced detection of ciprofloxacin due to selective adsorption, which was accomplished by a combination of electrostatic attraction at $-\text{SO}_3^-$ sites in the PPR film, and the formation of charge assisted hydrogen bonding between ciprofloxacin and rGO surface functional groups. The spectral and morphological studies of the novel nanocomposite were carried out using fourier transform infrared spectroscopy (FTIR) and field emission scanning electron microscopy (FE-SEM). The electrochemical characteristics of modified material were studied by cyclic voltammetry (CV) and electrical impedance spectroscopy (EIS). Differential pulse voltammetry (DPV) was performed to study the response of ciprofloxacin towards the modified electrode. The composite modified electrode displayed good electro-catalytic activity towards the oxidation of ciprofloxacin at pH 5.5 exhibited high sensitivity (detection limit 2 nM) and specificity towards ciprofloxacin. The practical applicability was also tested by quantitative analysis of ciprofloxacin in the animal blood sample. Recovery of analytes in spiked samples was $97 \pm 6\%$ over the range $0.002\text{--}400 \mu\text{M L}^{-1}$. It shows the developed electrode is a potential tool for a rapid, simple and sensitive detection of ciprofloxacin in blood sample.

2. Future prospects

The novel nanomaterials synthesized in the current thesis show a wide variety of applications in sensing, treatment and other related fields. The modified MOF (P-HKUST-1) can have various applications. It can be used for drug delivery of vancomycin which is shown to form complex with the drug. The inclusion of polyacrylic acid lowers the toxicity of the parent MOF (HKUST-1) and also makes it water soluble and easily dispersible. These parameters lead to further possibilities for the applicability of P-HKUST-1 for bioconjugation and using it as a biosensor. Further, P-HKUST-1 can also be used for the treatment of MRSA infections on skin. This is because of the vancomycin delivery and also because P-HKUST-1 can act as a reservoir of copper metal ions which aid in ablation of MRSA bacteria. Further, in chapter 4, Ag- β -CD composite was synthesized by a facile single step reaction and the changes in the solvent provided different colored Ag- β -CD composites, which can be applied for colorimetric detection or even for drug delivery purposes. Additionally, the synthesis technique can also be used to modify β -CD with various other metal nanoparticles to form novel nanocomposite for a variety of applications such as in electrochemistry, drug delivery and optical sensors. In chapter 5, a novel porous copper-based nanocomposite (Cu- β -CD-GO) was synthesized via hydrothermal route as a theranostic platform for MRSA detection and treatment. This novel nanocomposite exhibited good optical properties, mesoporous nature, high BET surface area and a good potential for future applications in the field of electrochemistry due to its electro-active nature, electrocatalytic properties, and storage devices such as capacitors and batteries. Finally, a novel electropolymerized film (PPR) was formed on the surface of glassy carbon electrode which possesses high stability and provides an economical option for synthesis of efficient electrodes to carry out highly selective detection.

Finally, an overall improvement in the practical applicability can be achieved by providing an on spot diagnostics method for detection of MRSA and the harmful drugs can be worked upon. To improve

the cost effectiveness of the product, custom electrodes using cheaper materials such as paper based or plastic can be used. The cost of these electrodes would be reduced significantly depending on the substrate of the electrode. However, further studies for sample diagnostics for clinical and large number of samples is needed to be carried out before the commercialization of these sensors. Then, these can be fabricated and a diagnostic kit can be provided at normal households and patients who are prone to the bacterial infections. This would lead to the lowering of burden on the public health centres and achieve faster treatment of the infected patients.

APPENDIX I

SUPPLEMENTARY INFORMATION CHAPTER 3

**Poly(acrylic acid) modified copper metal organic framework based single shot assay for
electrochemical detection of vancomycin**

Preliminary Molecular Dynamics Simulations study

Structure of HKUST-1 MOF was downloaded from the ChemTube3D [1] and single cluster was extracted from the whole structure (Fig. S2a). The structure of vancomycin was taken from the PDB id: 1QD8 (Fig. S2b) [2]. The PAA structure was taken from the PDB (ligand number TA8) (Fig. S2c). The universal force field (UFF) parameters were used for all three molecules. UFF parameters were generated using the OBGMX server, which have been tested for large number of MOFs [3]. Gasteiger partial charges, [4] were used for all these molecules, which are compatible with UFF [5] and generated using Open Babel software [6]. Three simulations systems were prepared, first one was HKUST-1 with vancomycin, second one was HKUST-1 with PAA and third one was PAA with vancomycin. All systems were solvated using the SPC water model [7]. The HUKST-1 with vancomycin system contains a total of 7999 water molecules, and HUKST-1 with PAA system contains 5698 water molecules and PAA with vancomycin system contains 5715 water molecules. All three systems were energy minimized using the steepest descent algorithm [8], and simulations were performed using NVT ensemble for 10 nanoseconds (ns) each. The Nose-hoover method [9] was used for temperature coupling with 1 ps time constant. The Particle Mesh Ewald (PME) method [10] was used to study long-range electrostatic interactions. Periodic boundary condition was employed in xyz dimension. The Leap-frog algorithm [11] used for the integration of Newton's equations of motion and simulation were performed at 298.15 K temperature using the GROMACS simulation package [12].

Centre of mass distance between molecules was calculated using in-house Tcl script and interaction energies were calculated using the g_mmpbsa [13] tool, which is used to calculate interaction energy in the vacuum.

Preliminary studies and synthesis

In our preliminary molecular dynamic (MD) simulations, interaction analysis was carried out between HKUST-1 molecule and vancomycin, HKUST-1 molecule and PAA and PAA molecule and vancomycin. Time evolution of center of mass (COM) distance (Fig. S3a, black line) between HKUST-1 and vancomycin revealed that the molecules came close to each other ~ 5.3 ns and formed the interaction, and molecules came further close to each other ~ 6.1 ns. However, during this time there were fluctuations in distance value, but from ~ 7.7 ns to 10 ns distance value remained very stable. Interaction energy value between HKUST-1 and vancomycin also followed to similar trend and were highest during ~ 7.7 ns to ~ 10 ns (Fig. S3b, black line), during this period interaction energy was between ~ 125 kJ.mol⁻¹ to ~ 145 kJ.mol⁻¹. Fig. 3a shows the representative images from HKUST-1 and vancomycin simulation. Time evolution of COM distance (Fig. S3a, red line) between Cu-BTC and PAA showed that molecules came to close each other ~ 5.8 ns and remained bound until end of the simulation time. But there were frequent fluctuations in distance value during the binding between these two molecules, interaction energy value (Fig. S3b, red line) showed the interaction energy between PAA and Cu-BTC was between ~ 35 kJ.mol⁻¹ to ~ 65 kJ.mol⁻¹. Fig. S4b shows the representative images from HKUST-1 and PAA simulation. Time evolution of COM distance between PAA and vancomycin (Fig. S3a, red line) showed that both molecules came close to each other ~ 0.33 ns and formed the first interaction and remained bound until end of the simulation. Interaction energy between PAA and vancomycin fluctuated between ~ 35 to ~ 85 kJ.mol⁻¹. From ~ 5.7 ns to 10 ns in interaction energy less fluctuations were observed and Fig. S4c shows representative images from PAA and vancomycin simulation. Overall this data suggested that these molecules can interact spontaneously and interaction between Cu-BTC and vancomycin is highly favorable followed by PAA and vancomycin and Cu-BTC and PAA. This suggested that the post synthetic modification of HKUST-1 with PAA was not a feasible reaction.

Therefore, to synthesize P-HKUST-1, a typical hydrothermal route was followed, similar to that of HKUST-1. Polyacrylic acid has been reported to form a chelating complex with copper ions [14, 15]. Therefore, PAA was introduced in the hydrothermal system along with other precursors. PAA has been known to improve the water solubility of various compounds. The resulting product (P-HKUST-1) demonstrated good solubility and dispersibility in water. The modification of MOF led to higher electro-activity of the linker molecule, which was attributed to the hydrogen bonding between the PAA and linker molecules [16]. This, in turn, resulted in faster and easier transport of electrons from the phenyl groups of the linker, as seen in the voltammogram (Fig. S5a). No significant rise in the electrochemical oxidation of copper ion cores was observed which may be due to PAA chelating with the copper cores and providing them the electrons required to keep them stable.

Characterization of P-HKUST-1

FTIR studies of HKUST-1 and P-HKUST-1 were carried out to confirm the formation of P-HKUST-1 (Fig. S6a). For HKUST-1, prominent vibrations observed at 1641 cm^{-1} attributed to C=C stretch and vibrations at 1583 cm^{-1} were accounted for carboxylate group, both of which represent characteristic peaks for linker molecule. The peaks at 1445 cm^{-1} and 1359 cm^{-1} may be attributed to symmetric stretching of the carboxylate group. The stretch at 760 cm^{-1} corresponds to the bending of the C-H present in linker. The bands near 930 cm^{-1} and the broad peak with a low intensity near 3300 cm^{-1} may be due to the O-H stretching frequencies which can be due to water molecules absorbed. These results were in accordance with the previously reported literature [17-19]. The FTIR of P-HKUST-1 has most of the peaks similar to that of HKUST-1, however an increase in intensity of peaks was observed. A few variations observed were the widening and increase in the intensity of peak around 3300 cm^{-1} attributed to O-H stretching which signifies the incorporation of PAA. The additional shift in the carboxylate group peak from 1359 cm^{-1} to 1254 cm^{-1} may be due to the

formation of carboxylic acid dimer between linker and PAA. Finally, the peak at 727 cm^{-1} is accounted for Cu–O stretching, which is found in both HKUST-1 and P-HKUST-1.

For morphological characteristics, FE-SEM and HR-TEM analysis were carried out displaying distinct octahedron and cuboid crystals of HKUST-1, as seen in Fig. S7a. Similarly, FE-SEM images of P-HKUST-1 illustrate HKUST-1 crystals covered with polymer threads, and HR-TEM images illustrated the formation of an interconnecting network between HKUST-1 crystals through PAA, as shown Fig. S7b. The polymer acts as a linker between HKUST-1 crystals leading to better solubility/dispersibility and electrochemical conductivity of newly formed P-HKUST-1. Further, the XRD analysis for HKUST-1 exhibited narrow and distinguished peaks highlighting its crystallinity [17-19], as shown in Fig. 5b. The XRD pattern of P-HKUST-1 (Fig. S6b) depicted no major change in the crystallinity of HKUST-1 on modification with PAA. Further, the BET surface area of P-HKUST-1 was found to be $395.998 \pm 11.1117\text{ m}^2.\text{g}^{-1}$, which can be accounted to the wrapping of HKUST-1 by the polymer. The pore volume for P-HKUST-1 was equivalent to $0.27\text{ cm}^3.\text{g}^{-1}$ providing a larger surface area than a previously employed method for HKUST-1 modification [20]. Finally, the adsorption and desorption isotherms obtained for P-HKUST-1 were analysed and they were found to be similar to that of mesoporous materials, as shown in Fig. S5b.

Characterization of vancomycin-MOF complexes

FTIR studies confirmed the formation of MOF-vancomycin complexes (Van-HKUST-1 and Van-P-HKUST-1), as shown in Fig. S6 b, c. A few changes were observed in vancomycin modified MOF structures. For Van-HKUST-1, firstly, there was an increase in the intensity of peak from $3200\text{--}3500\text{ cm}^{-1}$ that is attributed to N-H bending of the amide groups from vancomycin. Also, an increase in peak intensity is observed near 1580 cm^{-1} may be due to the C-Cl stretching. Additional peak diminishing at 876 cm^{-1} which is responsible for C-H bending of a trisubstituted carbon in an aromatic

ring is observed which depicts that vancomycin interacts with HKUST-1 at these particular sites. Further the peak at 664 cm^{-1} is no longer present which represents the out of plane -OH bending, which might also be due to the interaction with vancomycin molecules. In case of Van-P-HKUST-1, peaks at 1553 cm^{-1} and 1620 cm^{-1} are attributed to the N-O stretching and amide C=O stretch of vancomycin molecule, which confirms the incorporation of drug to P-HKUST-1. Additionally, the peak at 664 cm^{-1} is no longer present, which is similar as seen in van-HKUST-1.

When vancomycin interacts with HKUST-1, it undergoes a visible morphological change, as shown in FE-SEM image in Fig. S7. This is due to interaction of vancomycin with copper core of HKUST-1 leading to the impregnation of drug leading to the formation of irregular pores and cracks in HKUST-1. This can be further justified as no accessible copper sites were left for water to interact resulting in no swelling of the Van-HKUST-1 complex [21]. Further, small complexes of vancomycin with PAA and HKUST-1 crystals are seen in FE-SEM of Van-P-HKUST-1. The interaction of P-HKUST-1 with vancomycin does not bring any major change to the P-HKUST-1 crystal, which may be due to the formation of polyionic complexes of PAA with vancomycin [10]. BET surface area and pore volume of Van-HKUST-1 complex was $373.423\text{ m}^2.\text{g}^{-1}$ and $0.1757\text{ cm}^3.\text{g}^{-1}$, respectively, which further confirmed the reduction in surface area due to vancomycin incorporation. The variations in the crystallinity were confirmed using XRD diffraction patterns of van-complexes. Van-HKUST-1 illustrated a significant change (Fig. S8b) in the crystalline character which is seen between 10 degrees to 15 degrees resulting in the change in crystal structure as compared to HKUST-1, whereas no major change was observed for Van-P-HKUST-1 as compared to P-HKUST-1 which can majorly be attributed to polyacrylic acid and vancomycin interactions as observed in Fig S8c.

Electrochemical characterization of P-HKUST-1

The electrochemical characterization of the modified electrodes was carried out using 2.5 mM $[\text{Fe}(\text{CN})_6]^{3-/4-}$ in 1 M KCl as the electrolyte. The surface area calculations were carried out using cyclic voltammetry (CV) of the respective electrodes. The redox peaks observed between 0.7 V- 0.8 V were due to the redox active organic linker (BTC) of HKUST-1 and P-HKUST-1, as shown in the voltammograms (Fig. S5a). The response obtained from CV was used to calculate the effective surface area of the electrode by employing the Randles-Sevcik [22] equation:

$$I_p = 2 \cdot 69 \times 10^5 A \sqrt{D} (\sqrt{n})^3 \sqrt{v} C_0 \quad (1)$$

where I_p is the peak current (Amp), A is the surface area of the electrode in cm^2 , n is the number of electrons transferred (for $\text{K}_3[\text{Fe}(\text{CN})_6]$, $n=1$), v is the scan rate (V.s^{-1}), D is the diffusion coefficient ($7.60 \times 10^{-6} \text{ cm}^2.\text{s}^{-1}$ for $\text{K}_3[\text{Fe}(\text{CN})_6]$) and C_0 is the concentration in mol.cm^{-3} . The surface area of modified electrodes was calculated from the slope of the plot of I_{pa} vs $v^{1/2}$ in Fig. S9 (a) [Inset]. The effective surface areas for HKUST-1/GCE and P-HKUST-1/GCE were found to be 0.03808 cm^2 and 0.3778 cm^2 , respectively. High effective surface area of P-HKUST-1 is anticipated to be one of the factors responsible for the increase in peak current response. Additionally, voltammogram between current density and potential was plotted for HKUST-1 and P-HKUST-1 and higher current density is observed for P-HKUST-1 as shown in Fig. S9 (c)

Further, the electrochemical impedance spectroscopic (EIS) studies were carried out to study charge transfer characteristics of the modified electrodes (Fig. S9(b)). EIS measurements were recorded with open circuit potential as 0.68 V and range of frequency was set from 1 to 10^5 Hz. The data is represented as Nyquist Plot in the form of Randles equivalent circuit. The components of circuit are warburg impedance (W), charge transfer resistance (R_{ct}), the resistance of the solution (R_s) and double layer capacitance (C_{dl}). The value for each component of circuit is shown in Table S1. Lower R_{ct}

value of P-HKSUT-1 indicates that P-HKSUT-1 has superior conductivity than HKSUT-1 and hence possesses better charger transfer kinetics.

Electrochemical characterization of vancomycin-MOF complexes

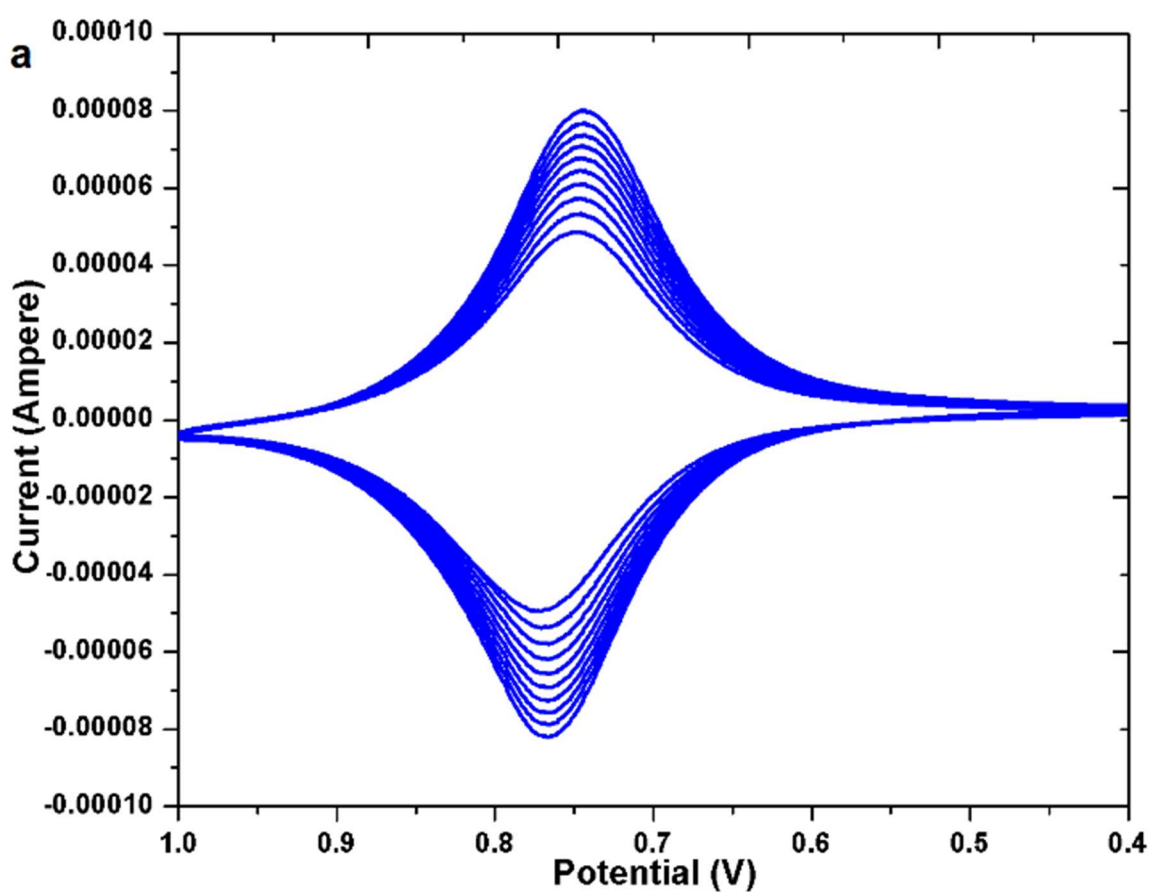
Electrochemical characterization via cyclic voltammetry was carried out using the same redox couple ($[\text{Fe}(\text{CN})_6]^{3-/4-}$ in 1 M KCl) to check the response of van-complexes. As depicted in Fig. 2a, van-HKUST-1/GCE did not show any noticeable variation in their redox peaks as compared to HKUST-1/GCE. On the other hand, a clear decrease in the redox peak was observed in case of van-P-HKUST-1/GCE as compared to P-HKUST-1/GCE. EIS studies were also carried out to validate the electrode response. Higher values of charge transfer resistance in the Randles equivalent circuit model of the van-complexes to their counter parts was obtained. All the components of the circuit are mentioned in Table S1.

UV spectroscopy Studies

Absorbance studies for the van-P-HKUST-1 complexes were carried out for confirming the complex formation of vancomycin with P-HKUST-1. Further, to check the amount of vancomycin interacting with P-HKUST-1, 1 mg.mL⁻¹ solution of vancomycin was added to 1 mg.mL⁻¹ solution of P-HKUST-1 and kept for 24 hours and centrifuged. The supernatant was used to check the free drug in the solution. Dilutions of vancomycin were prepared from 0.1 mg.mL⁻¹ to 2 mg.mL⁻¹ (0.1, 0.5, 1.0, 1.5, 2.0 mg.mL⁻¹) to create a calibration curve for achieving the amount of drug that was left in the supernatant. The calibration curve is shown in Fig. S10. The experiment was run in triplicate.

The spectrum of van-P-HKUST-1 (Fig. S11(a)) shows an increase in intensity of peak around 282 nm with a small shift (blue shift) is observed, which is due to vancomycin adsorbed with the copper metal sites, whereas a red shift is observed from 640 nm to 674 nm are due to vancomycin combining with the PAA of the P-HKUST-1. This leads to the removal of PAA from the Cu(II) sites increasing

the degeneracy in the d levels which leads to redshift. Further, the supernatant was also diagnosed to check for the unreacted drug in the solution. The absorbance of the unreacted came out to be 0.323 mg (Fig. S11(b)) and the remaining was incorporated with P-HKUST-1 which was equivalent to 0.677 mg per 1 mg of P-HKUST-1.



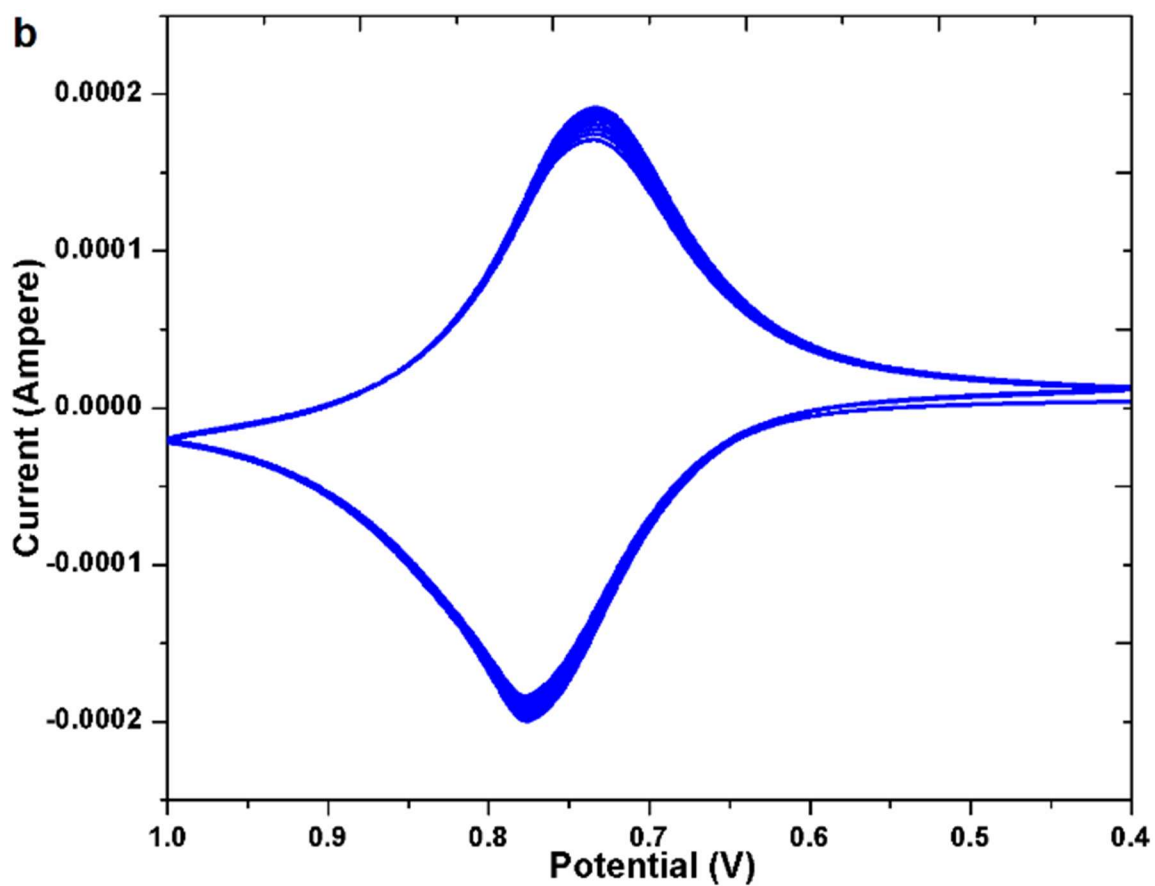


Fig. S1 (a) 10 sweeps run to achieve a constant current. (b) Finally another 16 sweeps to achieve complete stability of current with 10 folds increase from the initial value. CVs are carried out in 2.5 mM $[\text{Fe}(\text{CN})_6]^{3-/4-}$ in 1 M KCl at 0.1 V.s^{-1} scan rate.

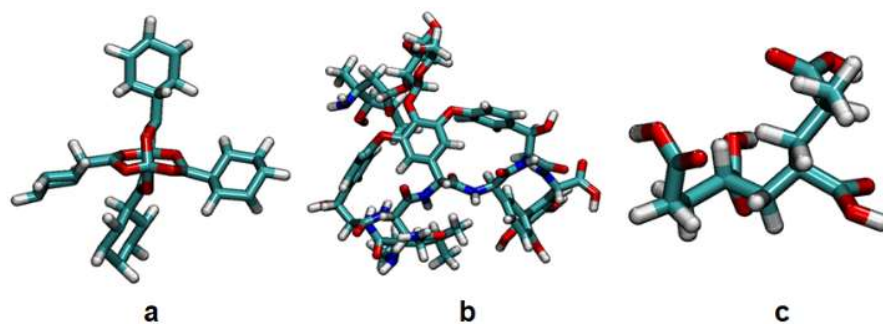


Fig. S2 (a) Structure of HKUST-1 cluster used in present simulation study. (b) Structure of Vancomycin. (c) Structure of PAA. All structures have been represented in the Licorice representation.

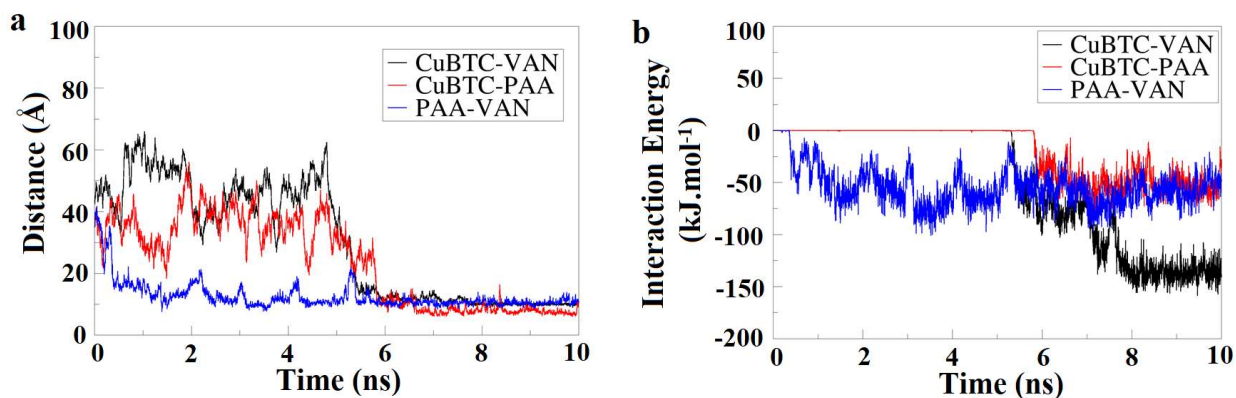


Fig. S3 (a) Shows time evolution of COM distance between CuBTC-VAN, CuBTC-PAA and PAA-VAN B) Show time evolution of interaction energy between CuBTC-VAN, CuBTC-PAA and PAA-VAN.

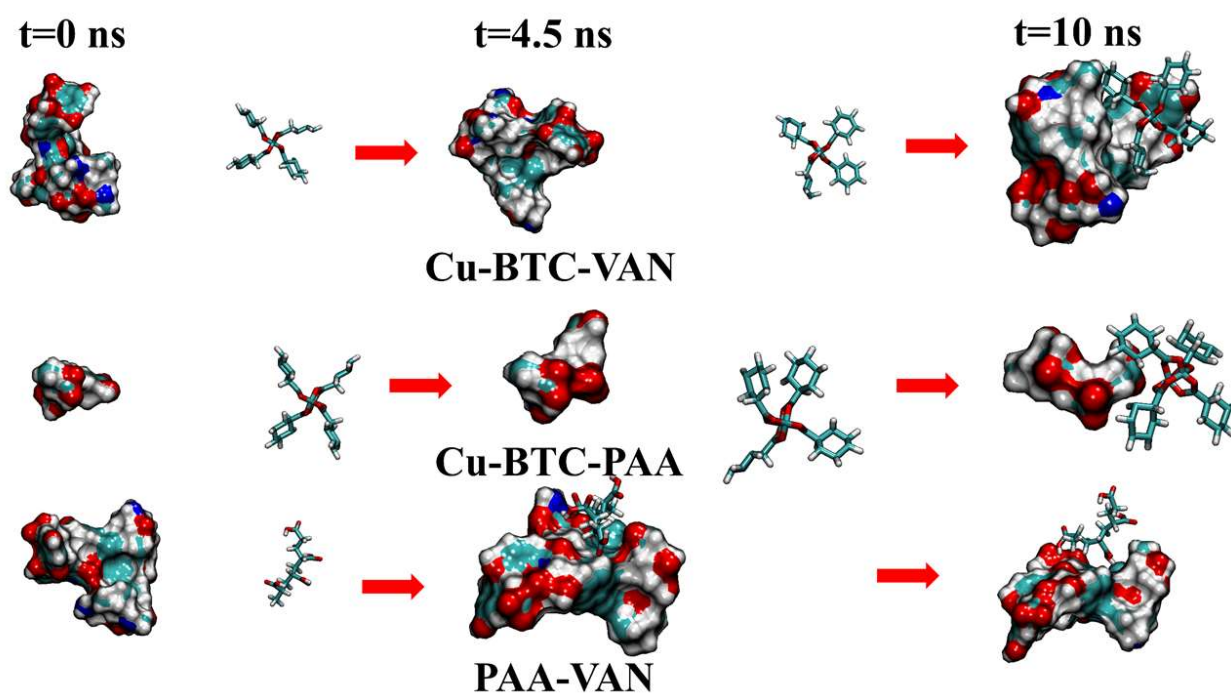
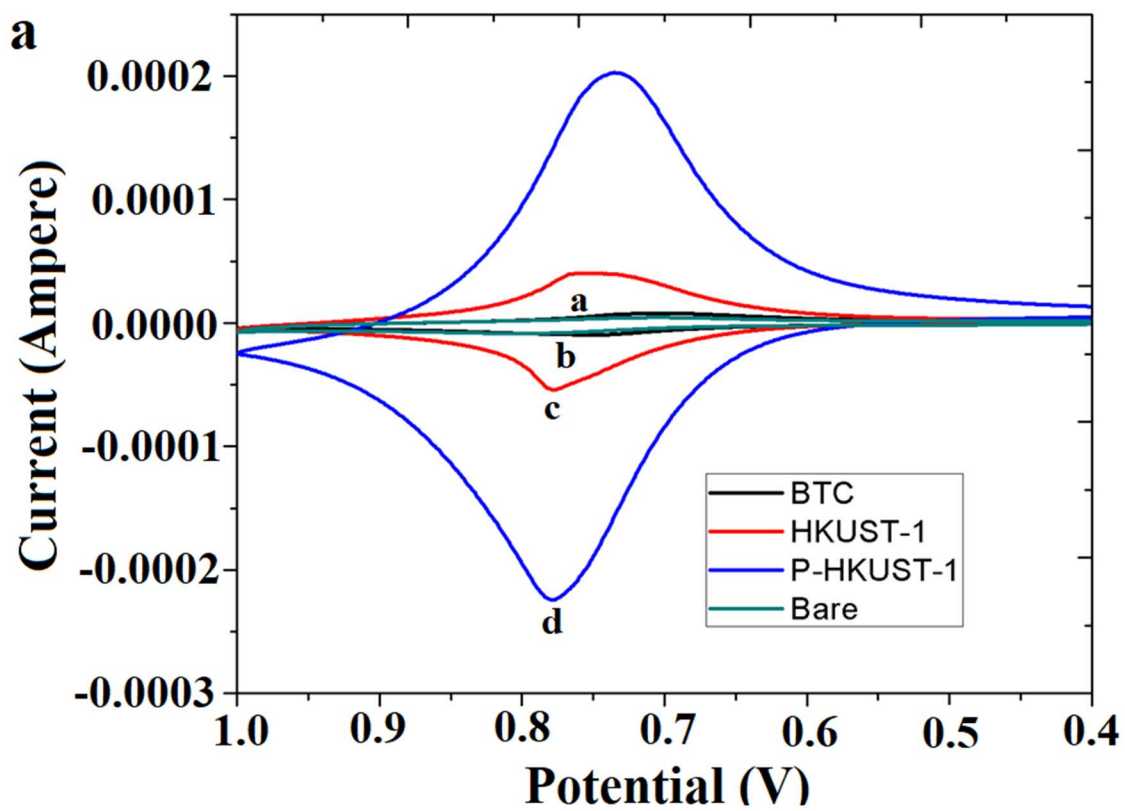


Fig. S4 Shows representative images of simulations a) Cu-BTC-VAN simulation b) Cu-BTC-PAA simulation, c) PAA-VAN simulation.



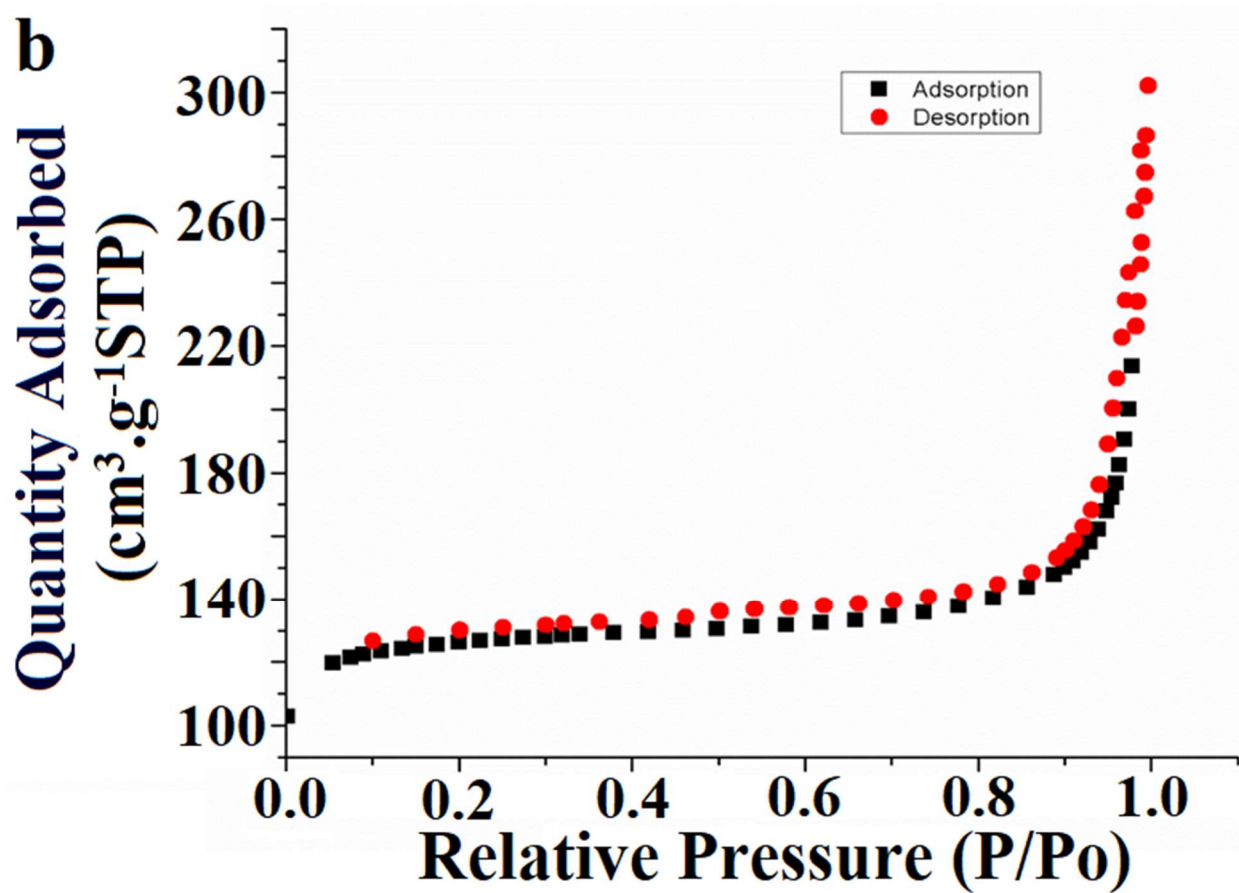
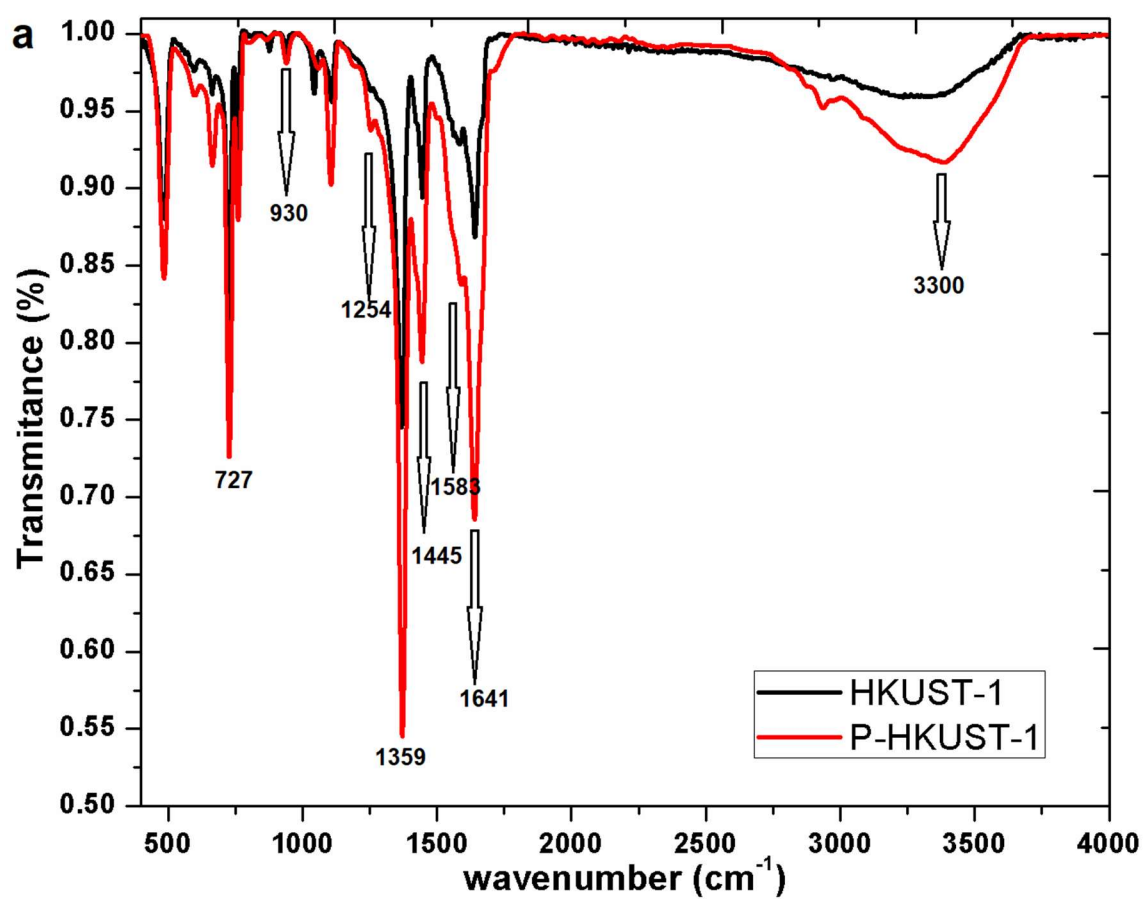
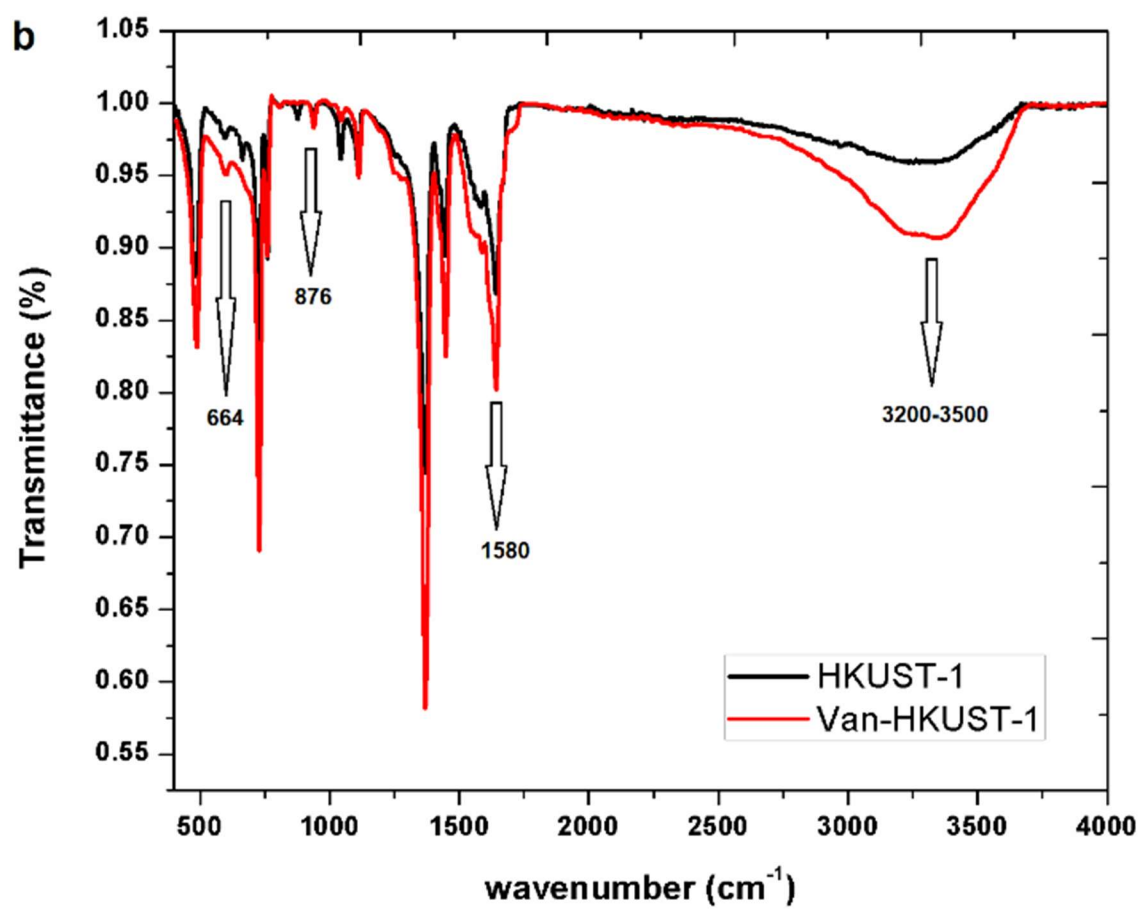


Fig. S5 (a) Cyclic voltammograms of bare (a) GCE, (b) BTC/GCE, (c) HKUST-1/GCE, (d) P-HKUST-1/GCE in 2.5 mM $[\text{Fe}(\text{CN})_6]^{3-/4-}$ in 1 M KCl (b) N_2 adsorption-desorption isotherm of P-HKUST-1.





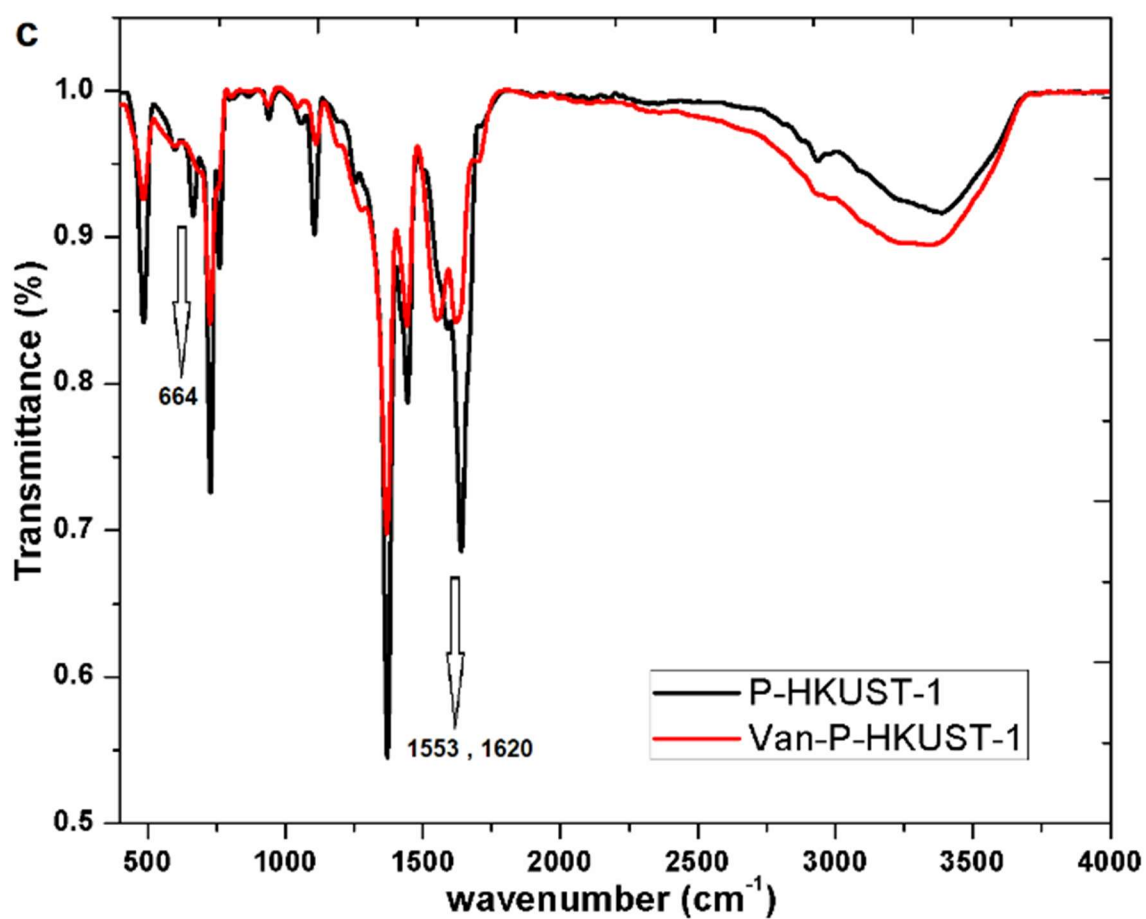


Fig. S6 FTIR spectras of (a) HKUST-1 and P-HKUST-1, (b) HKUST-1 and Van-HKUST-1, (c) P-HKUST-1 and Van-P-HKUST-1.

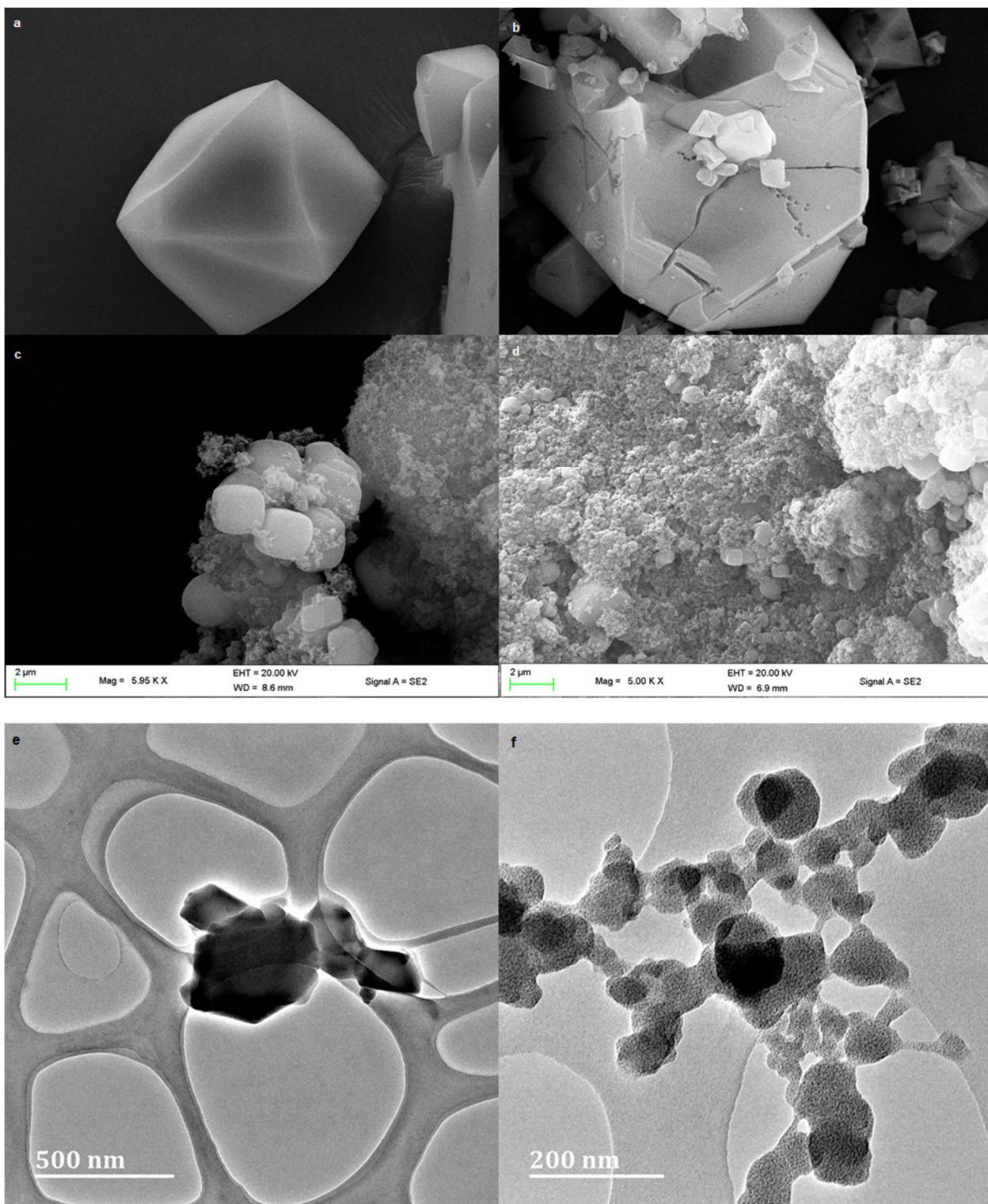
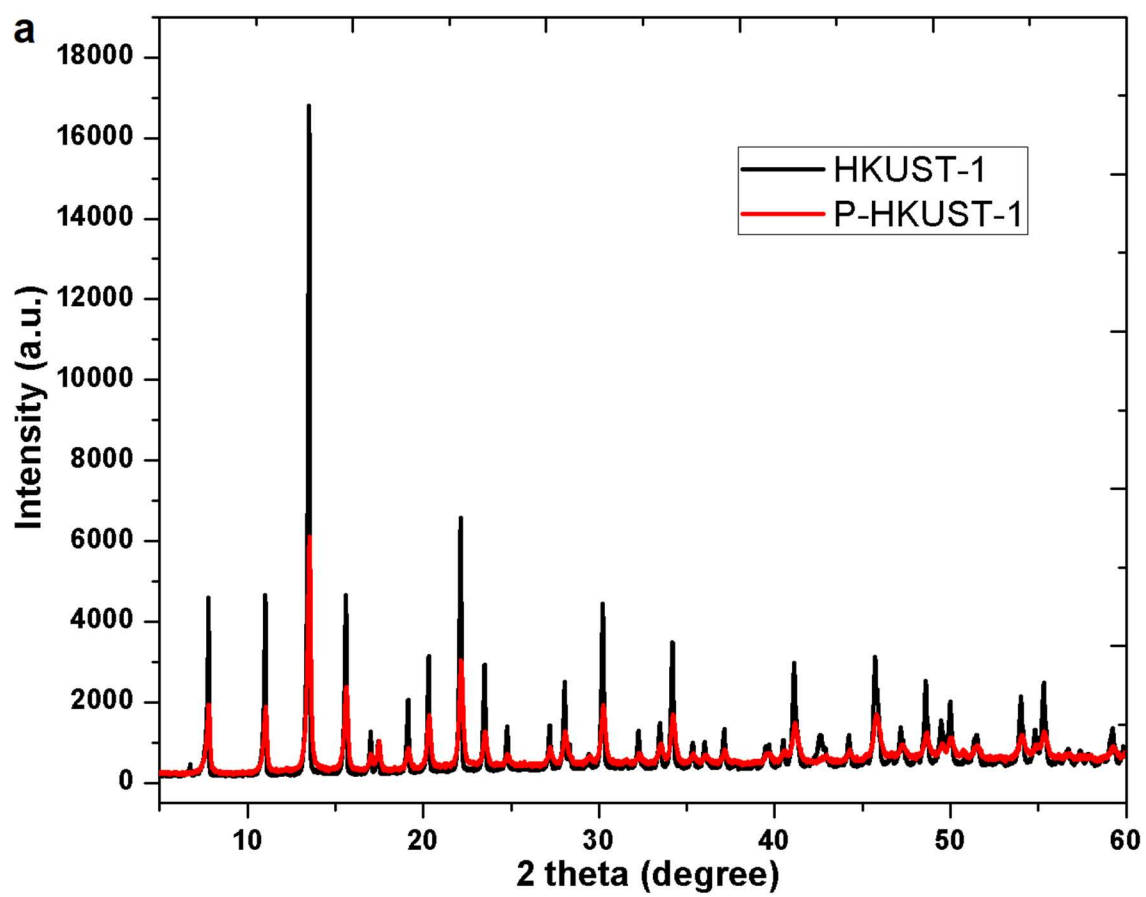
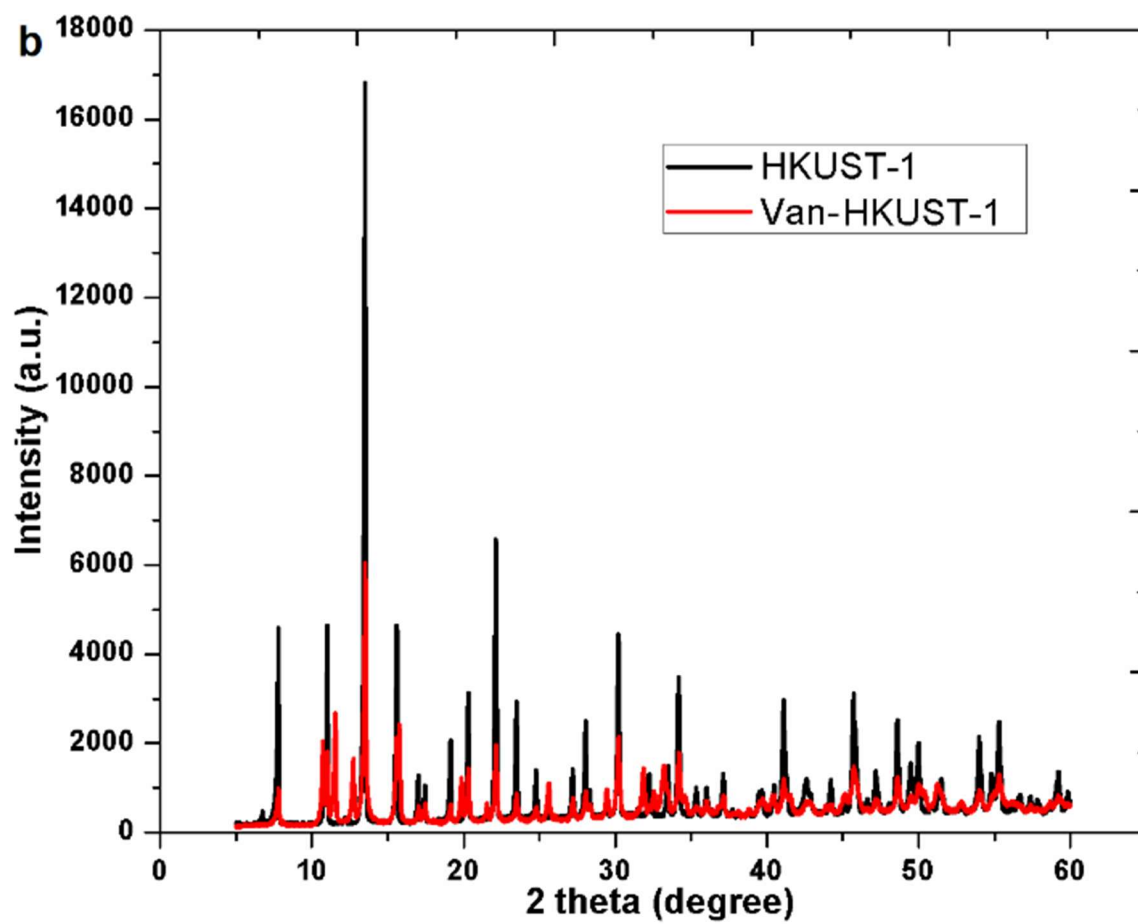


Fig. S7 FE-SEM of (a) HKUST-1 (b) Van-HKUST-1 complex (c) P-HKUST-1 (d) Van-P-HKUST-1. HR-TEM of (e) HKUST-1 (f) P-HKUST-1





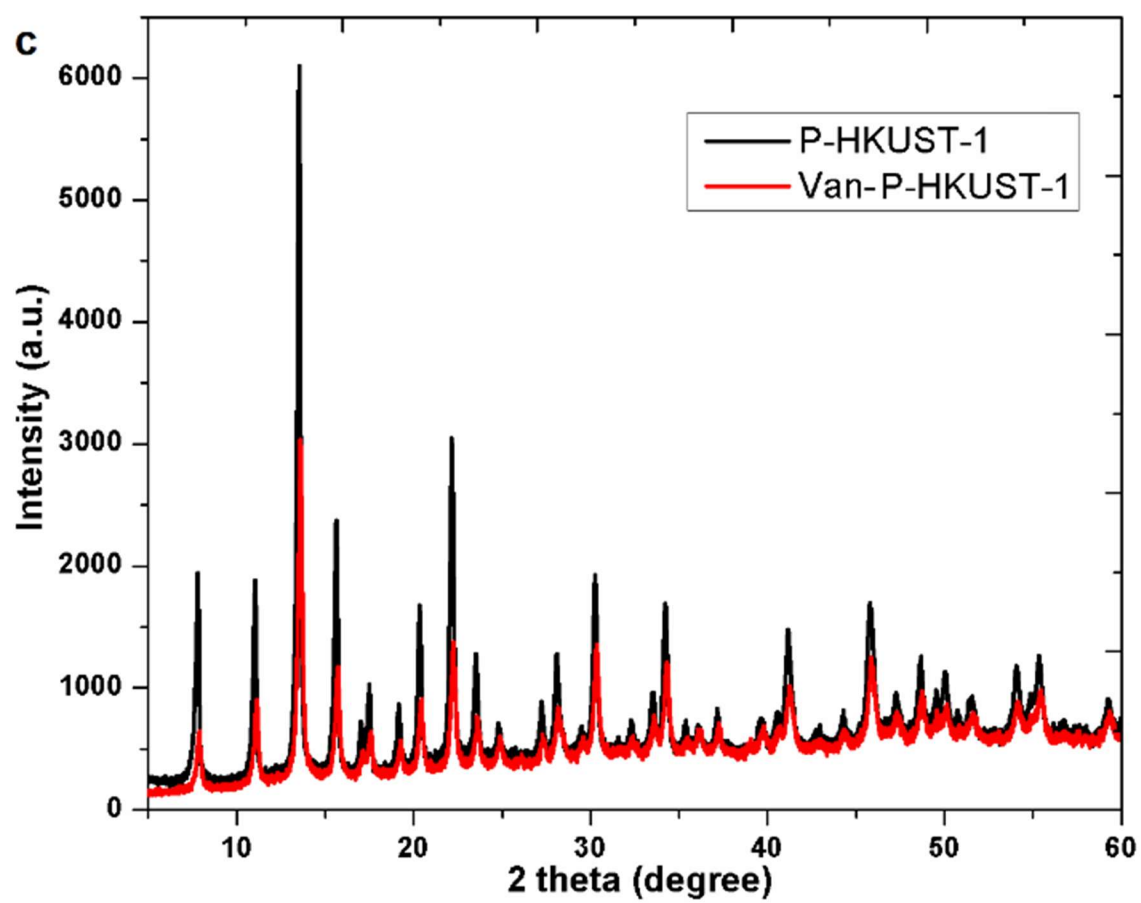
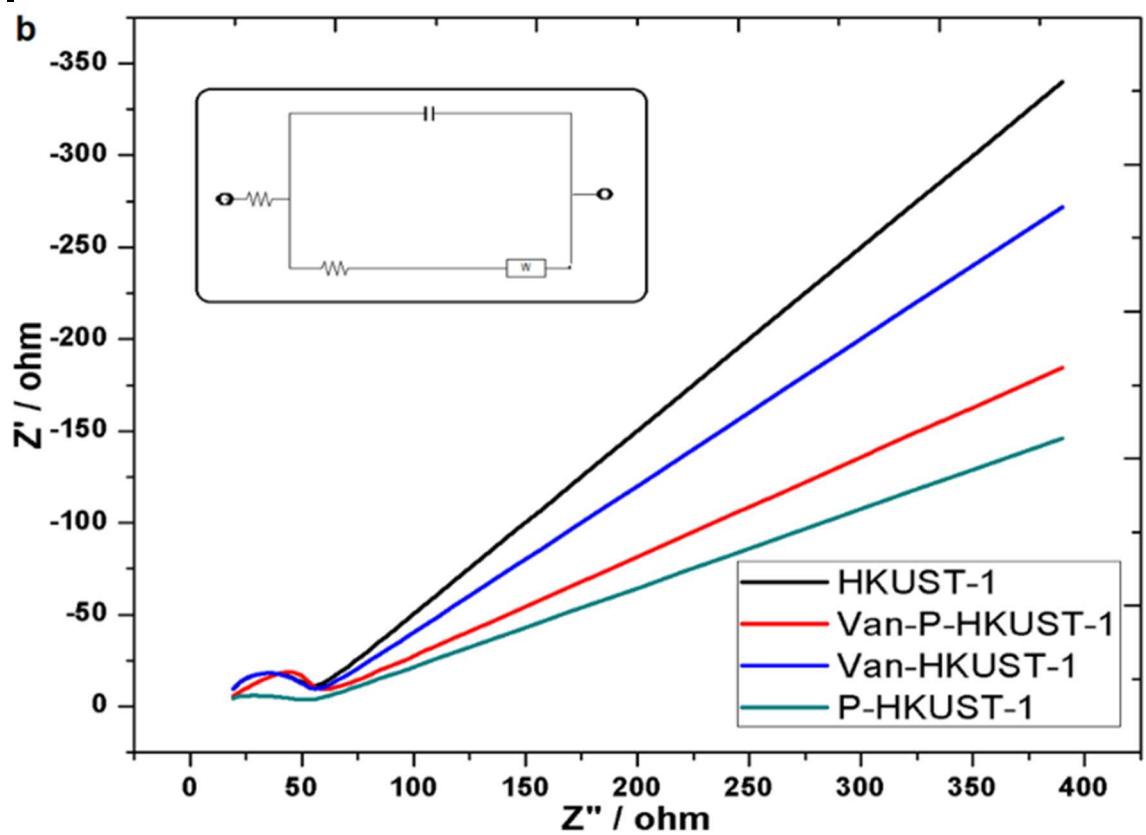
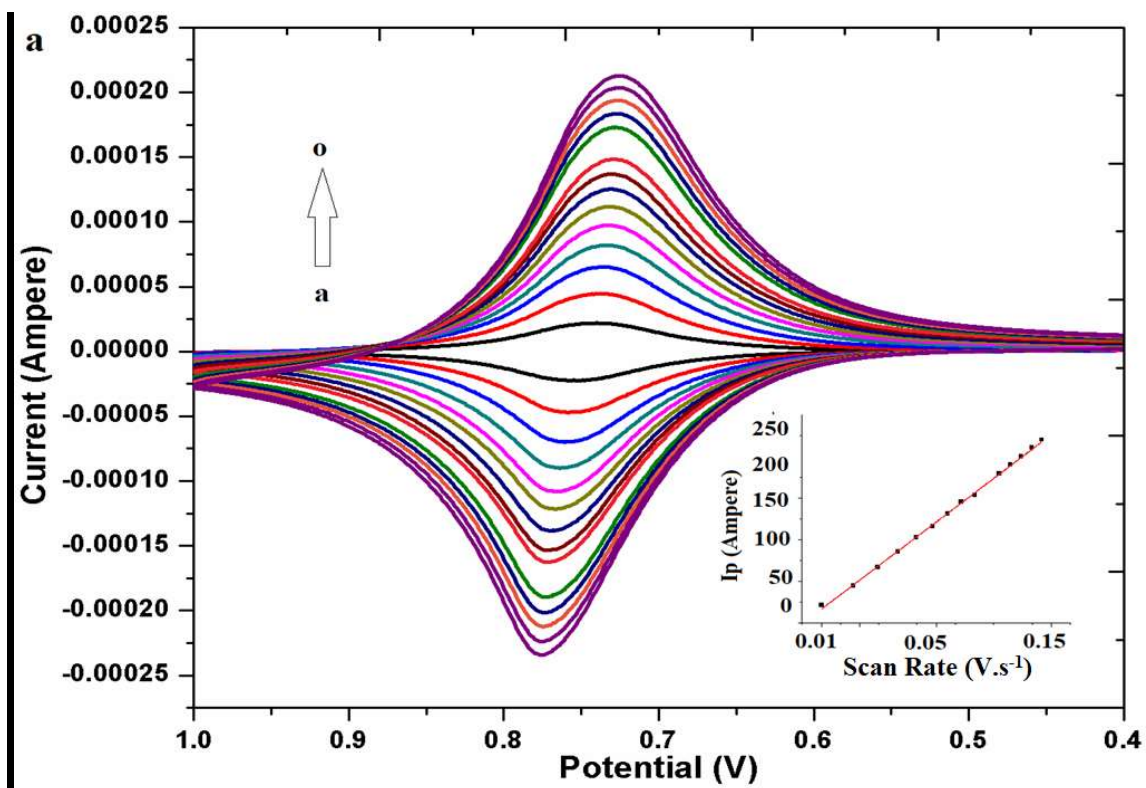


Fig. S8 XRD spectras of HKUST-1, P-HKUST-1 and their respective vancomycin complexes.



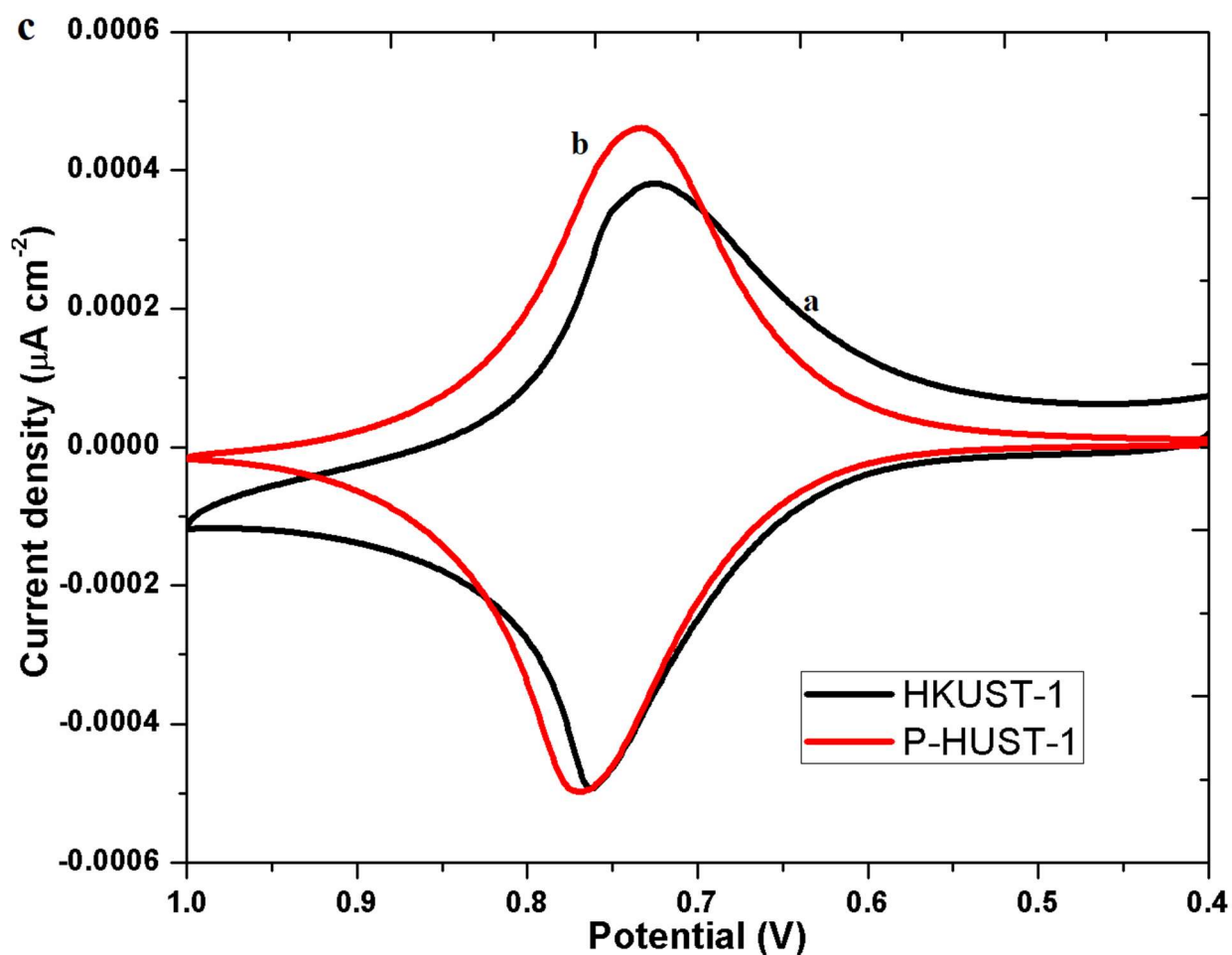


Fig. S9 (a) Scan rate studies of P-HKUST-1/GCE from “a” to “o” (0.01 to 0.15 V s⁻¹) carried out in 2.5 mM [Fe(CN)₆]^{3-/4-} in 1 M KCl, Inset- calibration plot for anodic peak current vs root of scan rate. **(b)** EIS spectra in 2.5 mM [Fe(CN)₆]^{3-/4-} in 1 M KCl at HKUST-1/GCE, Van-HKUST-1, P-HKUST-1 and Van-P-HKUST-1, Inset- Randles equivalent circuit model. **(c)** current density vs potential plotted for (a) HKUST-1 and (b) P-HKUST-1 at 0.1 V.s⁻¹ scan rate and in 2.5 mM [Fe(CN)₆]^{3-/4-} in 1 M KCl.

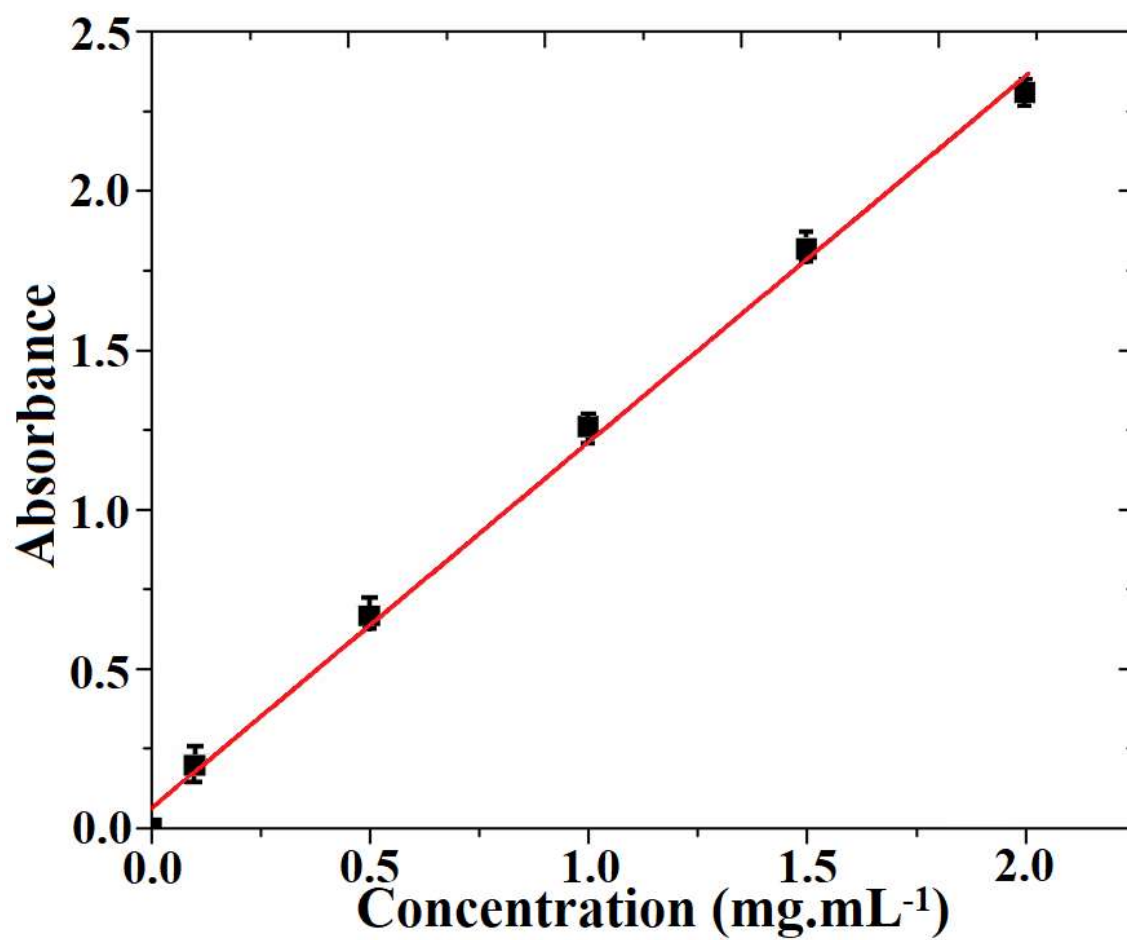
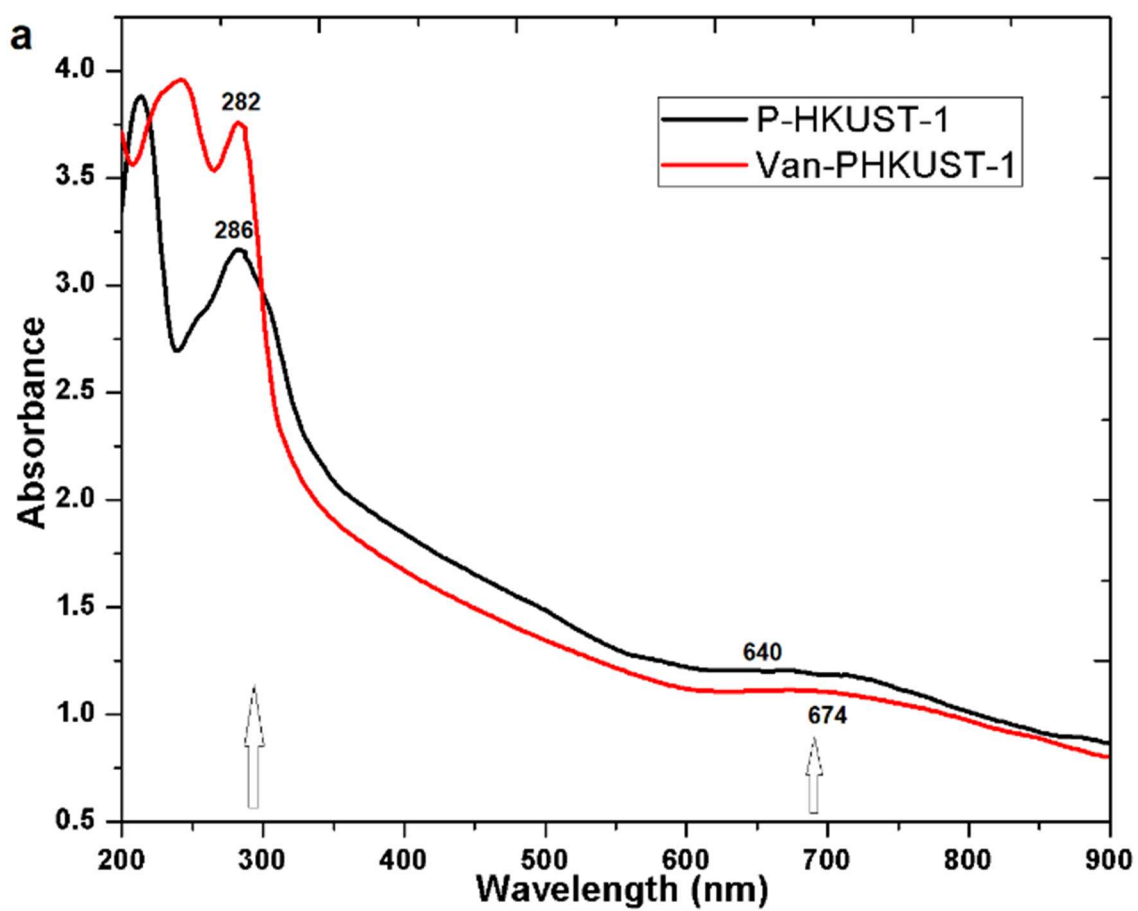


Fig. S10 Calibration curve for dilutions of vancomycin (0.1, 0.5, 1.0, 1.5, 2.0 mg.mL⁻¹) in methanol. Each absorbance values is recorded in triplicates.



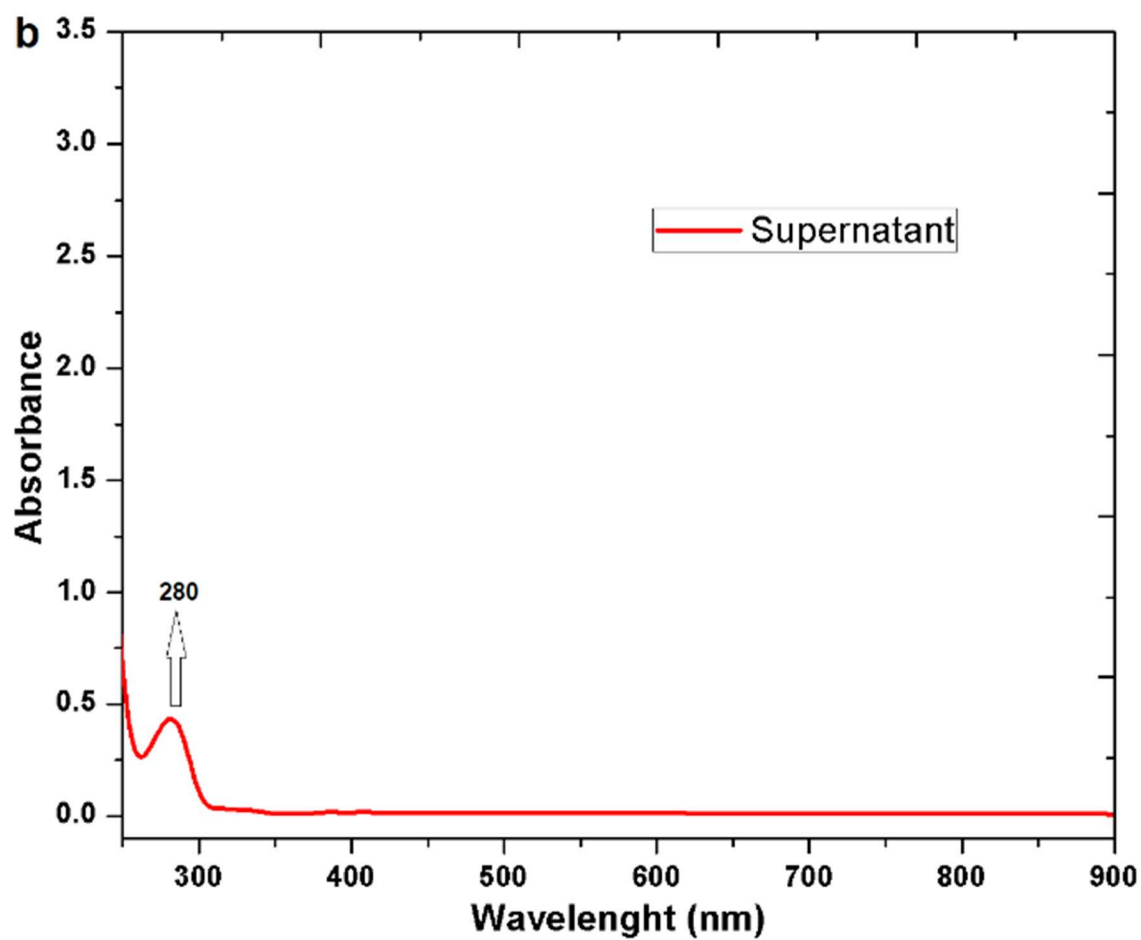
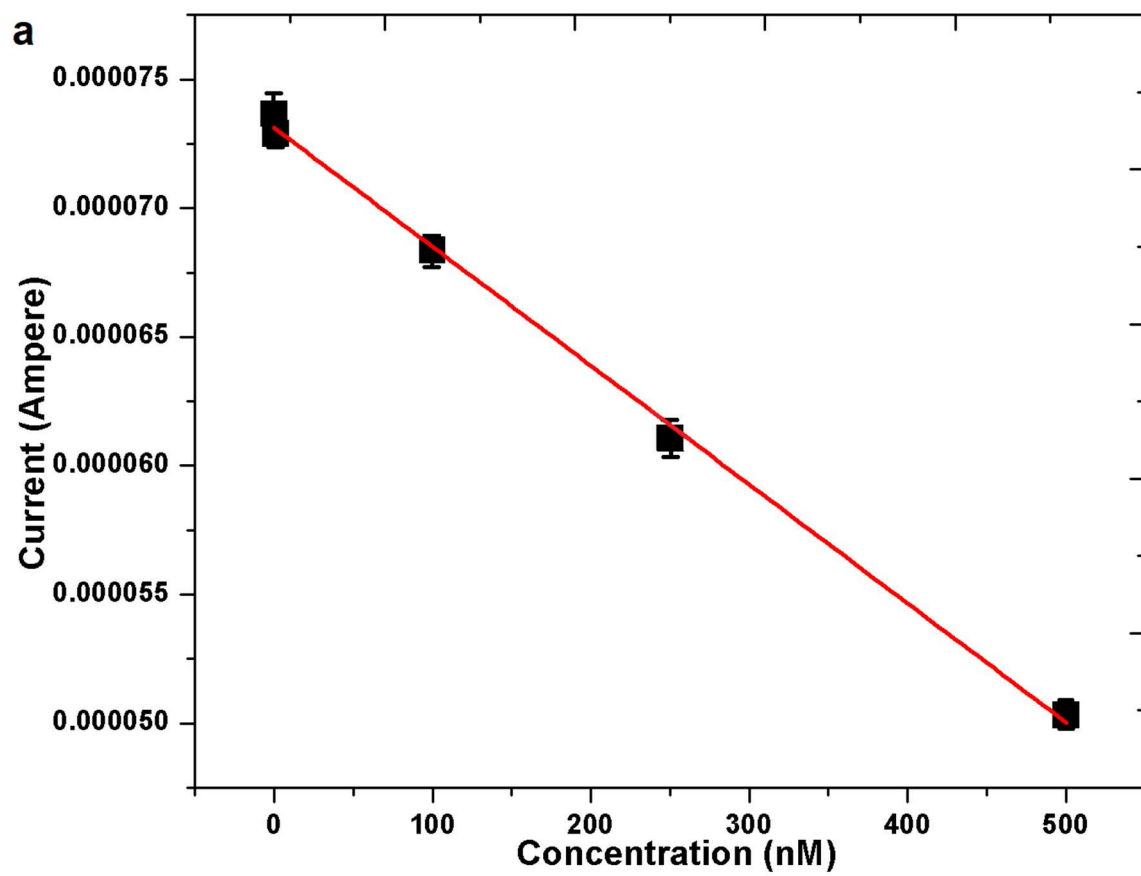


Fig. S11 (a) UV absorbance curve of P-HKUST-1 and Van-P-HKUST-1 in methanol. (b) UV absorbance of the supernatant of Van-P-HKUST-1 complex to check for unreacted drug.



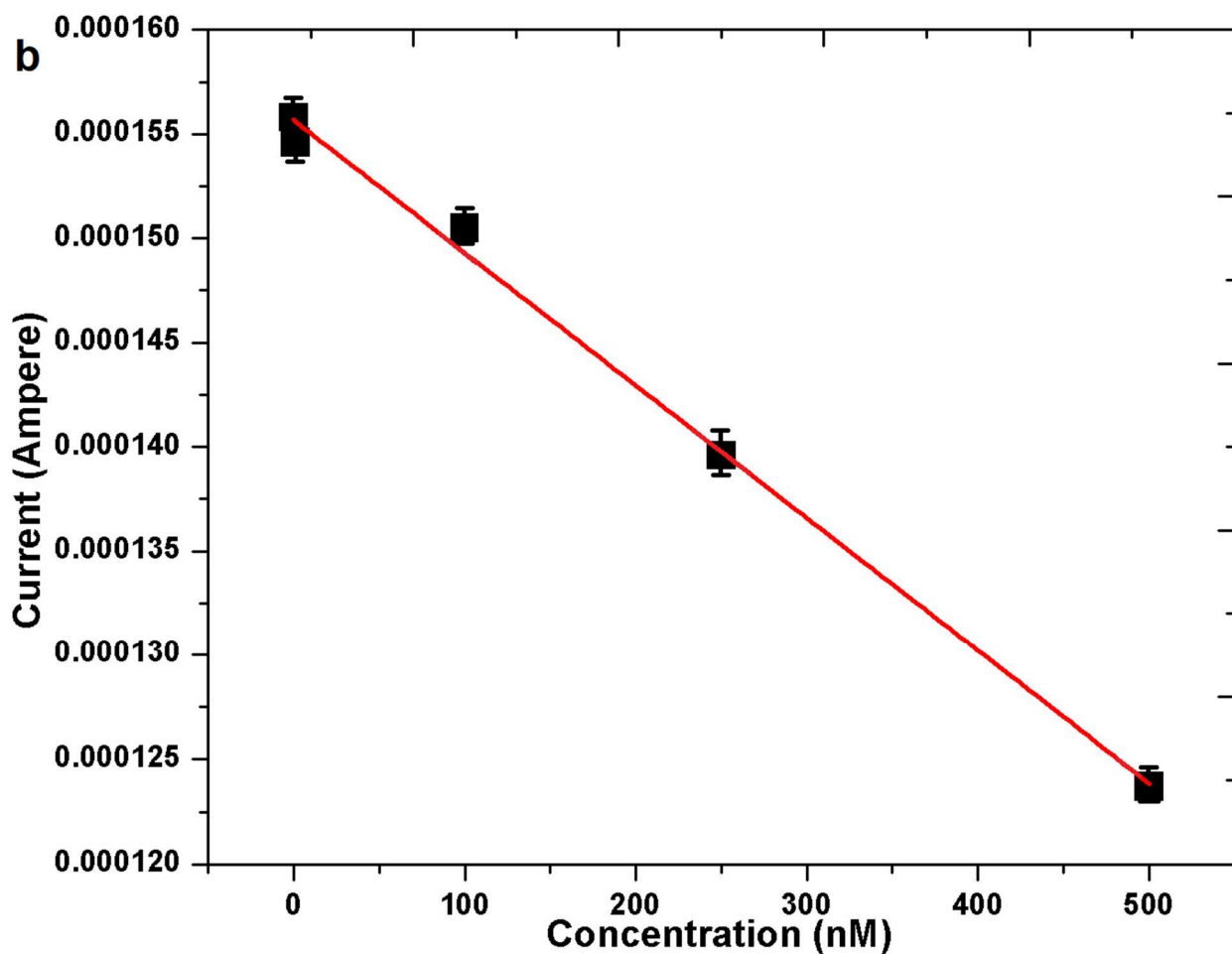
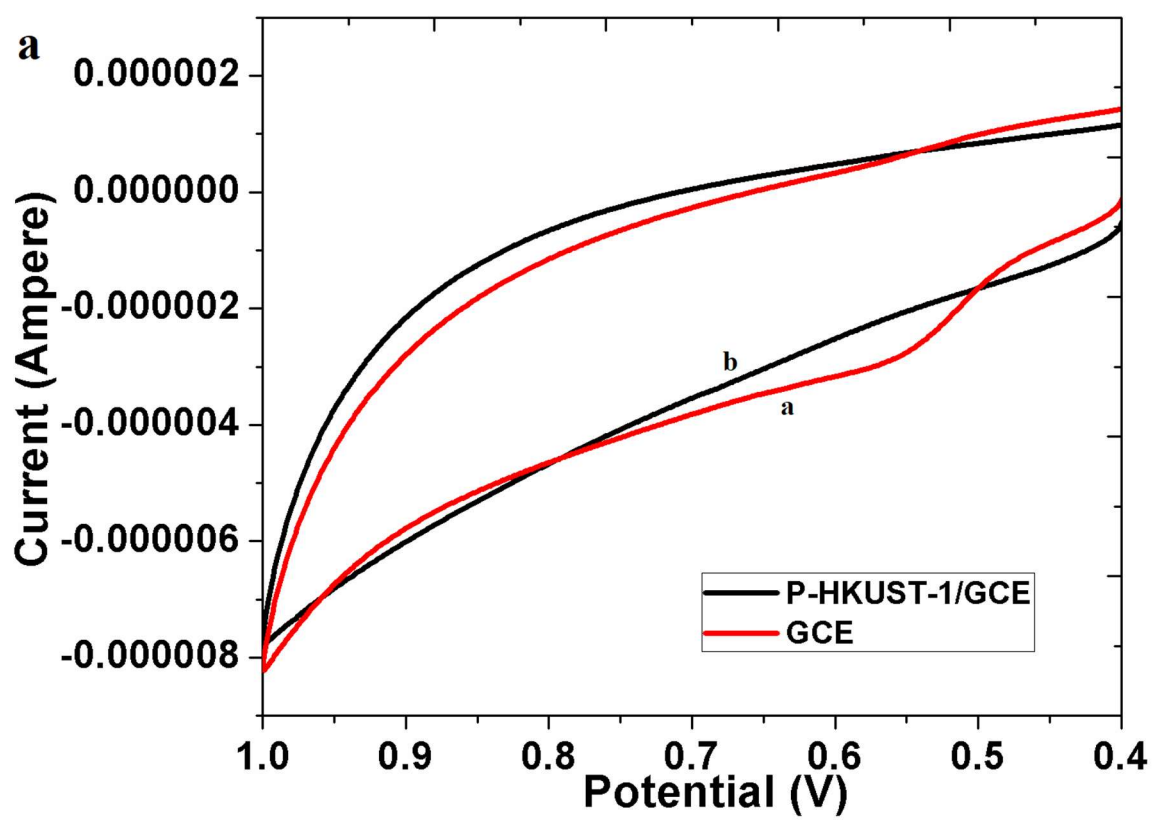
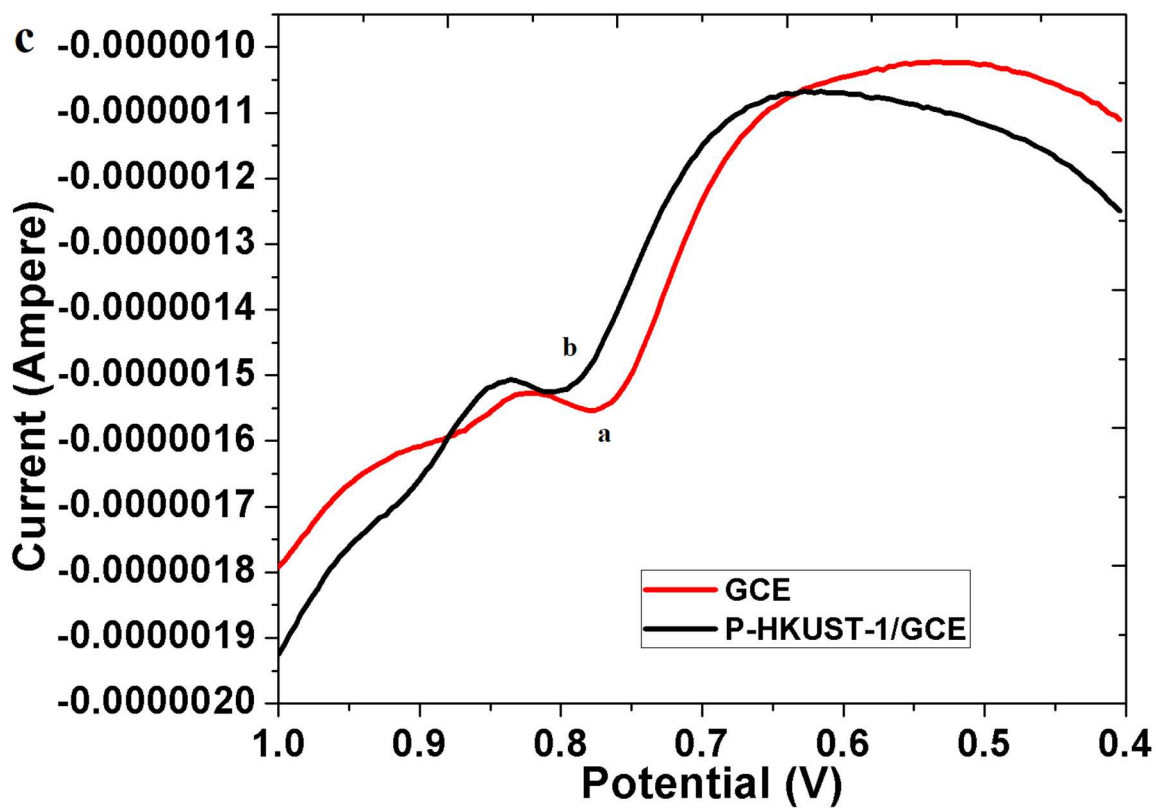
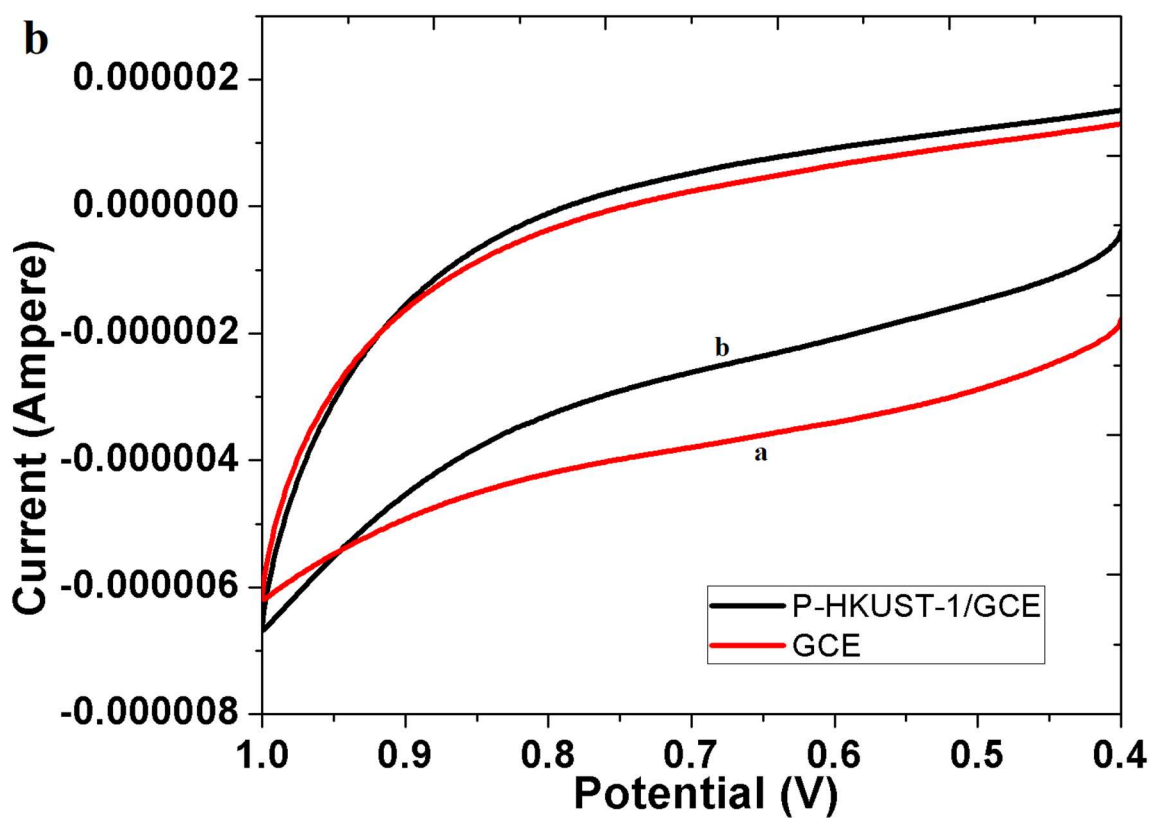
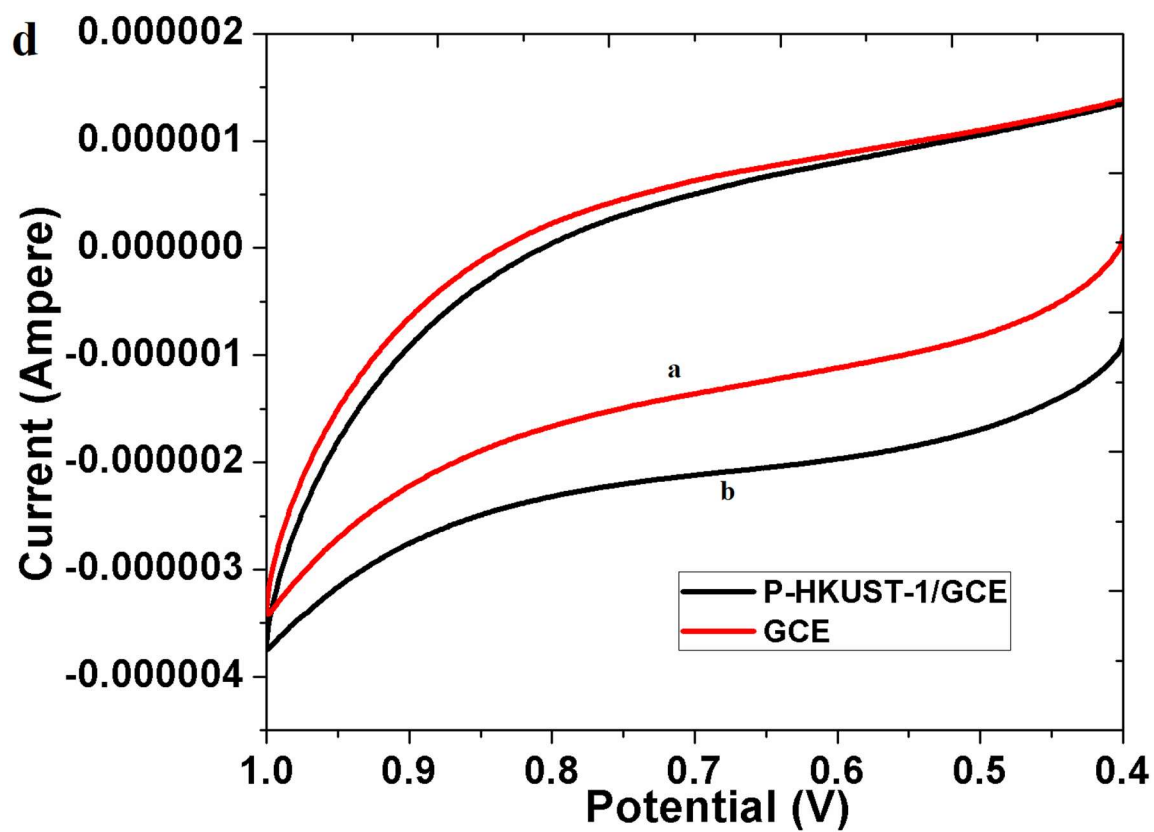


Fig. S12 Calibration curves for **(a)** P-HKUST-1 at different concentration spikes of vancomycin in presence of analogous drugs (ciprofloxacin and gentamicin) (0 nM, 1 nM, 100 nM, 250 nM, 500 nM) **(b)** In presence of metal ions (Vancomycin concentration: 0 nM, 1 nM, 100 nM, 250 nM, 500 nM). CV was carried out in 2.5 mM $[\text{Fe}(\text{CN})_6]^{3-/4-}$ (1 M KCl, at 0.1 V.s⁻¹).







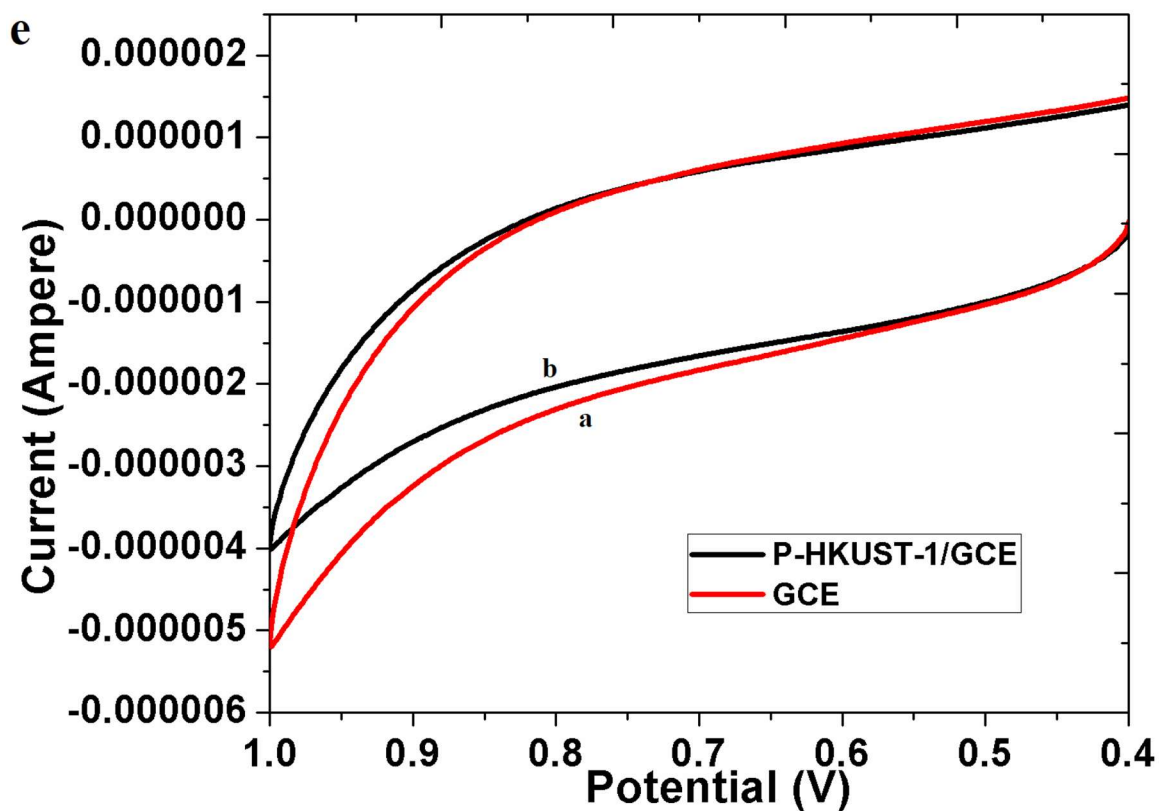
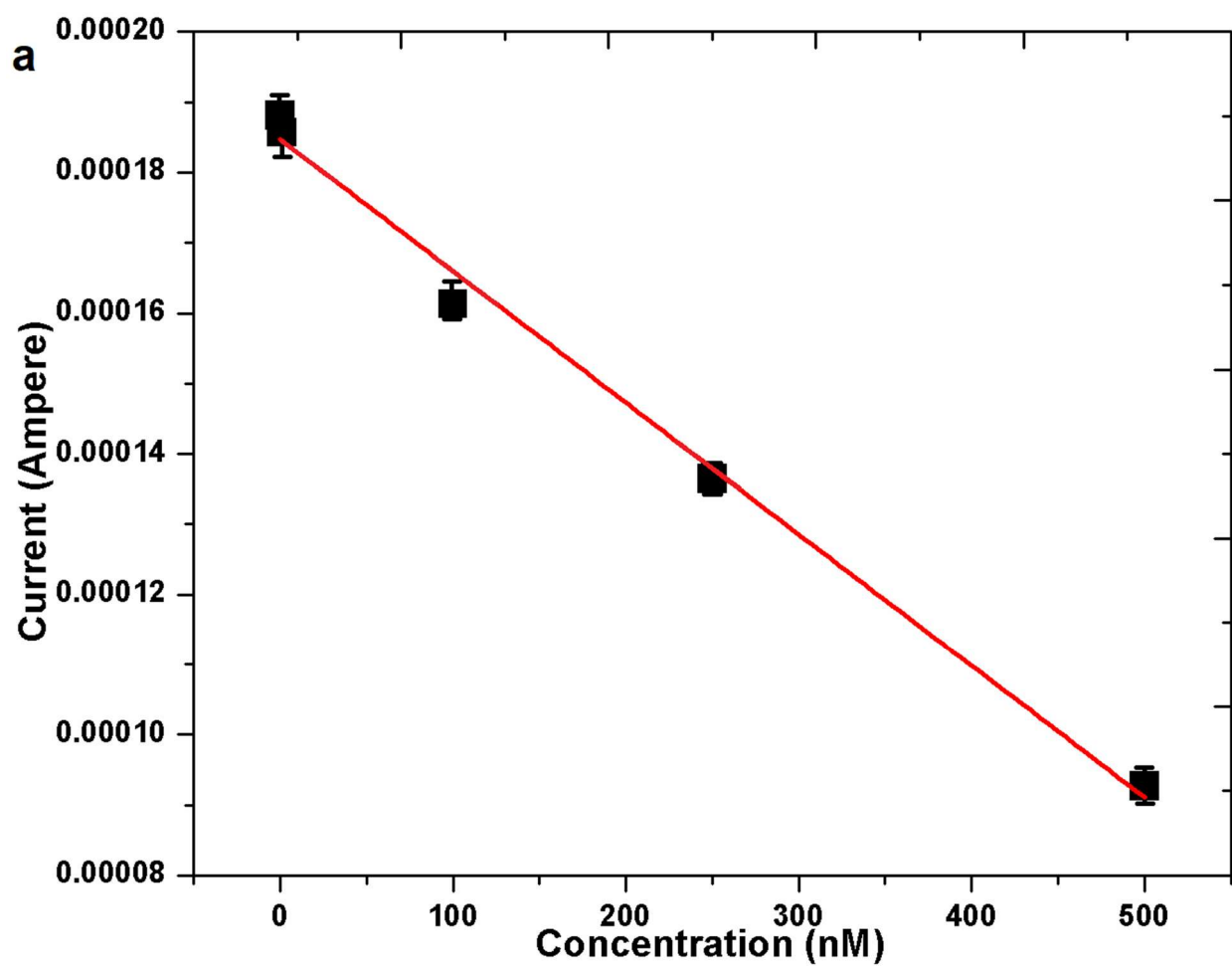


Fig. S13 Voltammograms at (a) GCE and (b) P-HKUST-1/GCE in different analytes **(a)** catechol (0.1 mM), **(b)** cystamine (0.1 mM) **(c)** folic acid (0.1 mM), **(d)** glutamic acid (0.1 mM), **(e)** mercury (0.1 mM) in 0.1 M phosphate buffer (pH = 7.0) at scan rate of 0.1 V.s⁻¹.



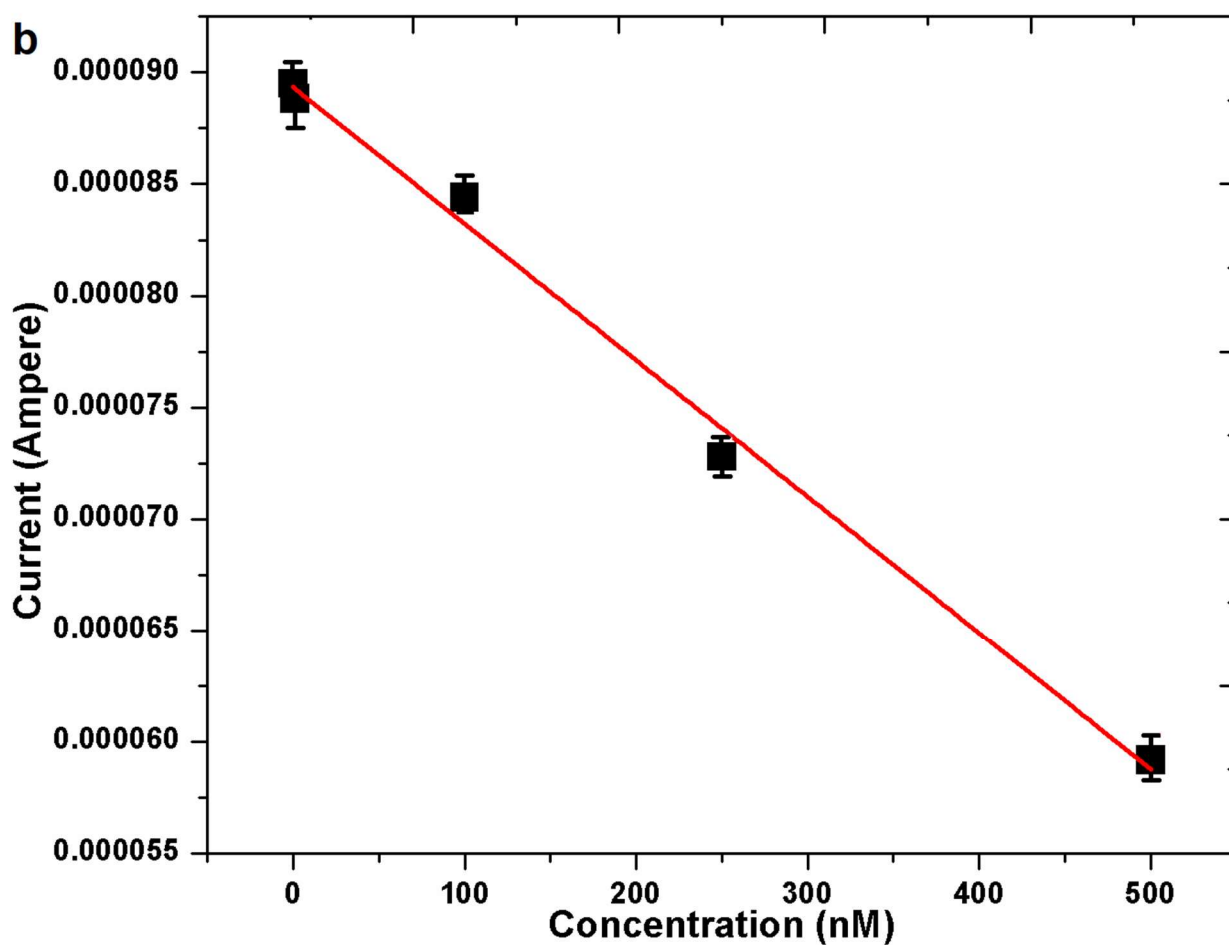


Fig. S14 Calibration curves for **(a)** P-HKUST-1 at different concentration spikes of vancomycin in human urine sample (0 nM, 1 nM, 100 nM, 250 nM, 500 nM) **(b)** CV curves in animal serum sample (Vancomycin concentration: 0 nM, 1 nM, 100 nM, 250 nM, 500 nM). CV was carried out in 2.5 mM $[\text{Fe}(\text{CN})_6]^{3-/4-}$ (1 M KCl, at 0.1 V.s⁻¹).

Tables

Table S1 Values of components of Randles equivalent circuit for bare and modified electrodes

Material	$R_s (\Omega)$	$R_{ct} (\Omega)$	$C_{dl} (F\ g^{-1})$	$W (\Omega\ s^{-1/2})$
GCE	20.27	129.7	$6.441\ e^{-7}$	0.0002294
HKUST-1	16.5	33.87	$1.92\ e^{-7}$	0.0008298
Van-HKUST-1	7.983	34.67	$1.896\ e^{-7}$	0.0001037
P-HKUST-1	17.96	10.93	$3.671\ e^{-7}$	0.0001932
Van-P-HKUST-1	17.1	35.77	$3.553\ e^{-7}$	0.0001529

Table S2 Data for Vancomycin detection in presence of various interfering agents and different matrices.

Interferences/ Matrices	Lowest Detection Concentration	Linear range	Sensitivity
Ions	1 nM	1-500 nM	Intercept: $1.5567e^{-4} \pm 5.5e^{-7}$, $R^2 = 0.9967$. Slope: $-6.362e^{-8} \pm 2.16e^{-9}$ Sensitivity: 168.395 $\mu A \cdot \mu M^{-1} \cdot cm^{-2}$
Drugs	1 nM	1-500 nM	Intercept: $7.377e^{-5} \pm 2.4e^{-7}$, $R^2 = 0.995$. Slope: $-4.623e^{-8} \pm 3.25e^{-9}$ Sensitivity: 122.366 $\mu A \cdot \mu M^{-1} \cdot cm^{-2}$

Urine	1 nM	1-500 nM	Intercept: $1.847\text{e}^{-4} \pm 2.2\text{e}^{-6}$, $R^2 = 0.9916$. Slope: $-1.87\text{e}^{-7} \pm 8.606\text{e}^{-9}$ Sensitivity: 484.971 $\mu\text{A} \cdot \mu\text{M}^{-1} \cdot \text{cm}^{-2}$
Blood serum	1 nM	1-500 nM	Intercept: $8.934\text{e}^{-5} \pm 6.4\text{e}^{-7}$, $R^2 = 0.993$. Slope: $-6.114\text{e}^{-8} \pm 2.53\text{e}^{-9}$ Sensitivity: 161.858 $\mu\text{A} \cdot \mu\text{M}^{-1} \cdot \text{cm}^{-2}$

References

- [1] Greeves N (2010) ChemTube3D
- [2] Loll PJ, Kaplan J, Selinsky BS, Axelsen PH (1999) Vancomycin binding to low-affinity ligands: delineating a minimum set of interactions necessary for high-affinity binding. *Journal of medicinal chemistry* 42 (22): 4714-4719
- [3] Garberoglio G (2012) OBGMX: A web-based generator of GROMACS topologies for molecular and periodic systems using the universal force field. *Journal of computational chemistry* 33 (27): 2204-2208
- [4] Gasteiger J, Marsili M (1980) Iterative partial equalization of orbital electronegativity—a rapid access to atomic charges. *Tetrahedron* 36 (22): 3219-3228.
- [5] Hamad S, Balestra SRG, Bueno-Perez R, Calero S, Ruiz-Salvador AR (2015) Atomic charges for modeling metal–organic frameworks: Why and how. *Journal of Solid State Chemistry* 223: 144-151.
- [6] O'Boyle NM, Banck M, James CA, Morley C, Vandermeersch T, Hutchison GR (2011) Open Babel: An open chemical toolbox. *Journal of cheminformatics* 3 (1): 33.

- [7] Mark P, Nilsson L (2001) Structure and dynamics of the TIP3P, SPC, and SPC/E water models at 298 K. *The Journal of Physical Chemistry A* 105 (43): 9954-9960.
- [8] Bixon M, Lifson S, (1967) Potential functions and conformations in cycloalkanes. *Tetrahedron* 23 (2): 769-784.
- [9] Evans DJ, Holian BL (1985) The nose–hoover thermostat. *The Journal of chemical physics* 83 (8): 4069-4074.
- [10] Darden T, York D, Pedersen L (1993) Particle mesh Ewald: An $N \cdot \log(N)$ method for Ewald sums in large systems. *The Journal of chemical physics* 98 (12): 10089-10092.
- [11] Van Gunsteren WF, Berendsen H (1988) A leap-frog algorithm for stochastic dynamics. *Molecular Simulation* 1 (3): 173-185.
- [12] Abraham MJ, Murtola T, Schulz R, Páll S, Smith JC, Hess B, Lindahl E (2015) GROMACS: High performance molecular simulations through multi-level parallelism from laptops to supercomputers. *SoftwareX*, 1: 19-25.
- [13] Kumari R, Kumar R, Consortium OSDD, Lynn A g_mmpbsa (2014) A GROMACS tool for high-throughput MM-PBSA calculations. *Journal of chemical information and modeling* 54 (7): 1951-1962.
- [14] Wall FT, Gill SJ (1954) Interaction of cupric ions with polyacrylic acid. *J. Phys. Chem.* 58 (12):1128–1130.DOI: 10.1021/j150522a017
- [15] Rivas BL, Quilodra'n B, Quiroz E (2005) Metal Ion Retention Properties of Poly(acrylic acid) and Poly[N-3-(dimethylamino)propyl acrylamide-co-acrylic acid. *Journal of Applied Polymer Science* 97: 1385–1394 DOI 10.1002/app.21836

- [16] Florio GM, Zwier TS, Myshakin EM, Jordan KD, Sibert EL. (2003) Theoretical modeling of the OH stretch infrared spectrum of carboxylic acid dimers based on first-principles anharmonic couplings. *J. Chem. Phys.* 118: 1735 doi: 10.1063/1.1530573
- [17] Li Q, Jiang S, Ji S, Shi D, Yan J, Huo Y, Zhang Q (2014) Magnetically Recyclable Cu-BTC@SiO₂@Fe₃O₄ Catalysts and Their Catalytic Performance for the Pechmann Reaction. *Ind. Eng. Chem. Res.* 53: 14948–14955.
- [18] Li ZQ, Wang A, Guo CY, Tai YF, Qiu LG (2013) One-Pot Synthesis of Metal–Organic Framework@SiO₂ Core–Shell Nanoparticles with Enhanced Visible-Light Photoactivity. *Dalton Trans* 42: 13948–13954.
- [19] Stavila V, Volponi J, Katzenmeyer AM, Dixon MC, Allendorf MD (2012) Kinetics and Mechanism of Metal–Organic Framework Thin Film Growth: Systematic Investigation of HKUST-1 Deposition on QCM Electrodes. *Chem. Sci.* 3: 1531–1540.
- [20] Bhardwaj SK, Bhardwaj N, Mohanta GC, Kumar P, Sharma AL, Kim KH, Akash Deep (2015) Immunosensing of Atrazine with Antibody-Functionalized Cu-MOF Conducting Thin Films. *ACS Appl. Mater. Interfaces* 7 (47):26124–26130. DOI: 10.1021/acsami.5b07692
- [21] Burtch NC, Jasuja H, Walton KS (2014) Water Stability and Adsorption in Metal–Organic Frameworks. *Chem. Rev.* 114: 10575–10612. dx.doi.org/10.1021/cr5002589.
- [22] L.R. F, A.J. Bard, (2001) *Electrochemical Methods: Fundamentals and Applications*, John Wiley, New York.